The AdS/CFT spectrum via integrability-based algorithms

Christian Marboe
School of Mathematics, Trinity College Dublin
College Green, Dublin 2, Ireland

Trinity College Dublin
Coláiste na Tríonóide, Baile Átha Cliath
The University of Dublin

Submitted to The University of Dublin for the degree of
Doctor in Philosophy

Academic advisor: Dr. Dmytro Volin

November 2017

Declaration

I declare that this thesis has not been submitted as an exercise for a degree at this or any other university and it is entirely my own work.

I agree to deposit this thesis in the University's open access institutional repository or allow the Library to do so on my behalf, subject to Irish Copyright Legislation and Trinity College Library conditions of use and acknowledgement.

Christian Marboe	Date

Summary

The AdS/CFT correspondence has given rise to new tools that enable both perturbative and non-perturbative calculations of unseen precision in four-dimensional quantum field theories. The topic of this thesis is the spectral problem of the $\mathrm{AdS}_5/\mathrm{CFT}_4$ correspondence in the planar limit, which from the point of view of the CFT, $\mathcal{N} = 4$ super Yang-Mills theory, amounts to determining the spectrum of anomalous dimensions of single-trace operators.

There is substantial evidence that the spectral problem is integrable in the planar limit. This surprising asset makes the problem exactly solvable, and allows the application of sophisticated techniques to reformulate it. The Quantum Spectral Curve formulates the problem in terms of a relatively simple Riemann-Hilbert problem. To produce physical results from the Quantum Spectral Curve, one needs to solve it explicitly. There is one solution for each symmetry multiplet of single-trace operators. The main goal of this thesis is the development of efficient algorithms to find perturbative solutions for arbitrary multiplets. The two main steps of this process are, first, to find leading solutions and, second, to generate perturbative corrections.

To classify symmetry multiplets of single-trace operators, the relevant aspects of representation theory of non-compact super Lie algebras is revisited. It is argued that a generalisation of Young diagrams provides a convenient classification and leads to an intuitive way to count the multiplets.

The leading solution to the Quantum Spectral Curve is traditionally found by solving Bethe equations. These equations are hard to solve in practice, and the number of solutions exceeds the expectation from representation theory. To overcome these issues, a stronger criterion on the solutions is formulated, and an efficient algorithm to enforce this criterion is introduced. The result is a conceptually simple algorithm that is not only significantly more efficient than the solution of Bethe equations, but also yields exactly the expected number of solutions.

The perturbative corrections to the leading solutions are controlled by the analytic structure imposed by the Quantum Spectral Curve. Different strategies to recursively generate these corrections are discussed, and the ultimate approach is argued to be a concise algorithm to solve the $\mathbf{P}\mu$-system for general states. This opens the door to a vast range of new spectral data, including 10-loop anomalous dimensions for a variety of multiplets. This data is furthermore used to reconstruct the six- and seven-loop contributions to the anomalous dimension of twist-2 operators with arbitrary spin.

Finally, an attempt to apply the Quantum Spectral Curve on the operatorial level is initiated. In particular, a general strategy to evaluate matrix elements of Q-operators for non-compact super spin chains is outlined.

List of publications

The thesis is based on the author's research presented in the publications

[1] **Quantum spectral curve as a tool for a perturbative quantum field theory**
with D. Volin, *Nucl.Phys. B899 (2015) 810-847*, [arXiv:1411.4758].

[2] **Six-loop anomalous dimension of twist-two operators in planar $\mathcal{N} = 4$ SYM theory**
with D. Volin and V. Velizhanin, *JHEP 1507 (2015) 084*, [arXiv:1412.4762].

[3] **Twist-2 at seven loops in planar $\mathcal{N}$=4 SYM theory: Full result and analytic properties**
with V. Velizhanin, *JHEP 1611 (2016) 013*, [arXiv:1607.06047].

[4] **Fast analytic solver of rational Bethe equations**
with D. Volin, *J.Phys. A50 (2017) no.20, 204002*, [arXiv:1608.06504].

[5] **The full spectrum of AdS5/CFT4 I: Representation theory and one-loop Q-system**
with D. Volin, [arXiv:1701.03704].

[6] **Evaluation of the operatorial Q-system for non-compact super spin chains**
with R. Frassek and D. Meidinger, *JHEP 1709 (2017) 018*, [arXiv:1706.02320].

Furthermore, a substantial part of the thesis is based on yet unpublished work that will appear in

[7] **The full spectrum of AdS5/CFT4 II**
with D. Volin, *work in progress*.

Contents

Introduction

Quantum field theory is by far the most successful framework for describing the nature of elementary particles. The guiding principle for model building within this framework is symmetry. The fundamental objects in the theory, the fields, represent this symmetry choice. This starting point is however obscured by the quantum mechanical nature of the interactions between the fields. In consequence, quantum field theory is mainly a perturbative tool: we have to start from the limit of no interactions, and then gradually turn on the coupling. Many fundamental questions, such as the confining properties of quarks, cannot be described in this way. Furthermore, perturbative quantum field theory is an immensely complicated procedure. Not only do the combinatorics grow so rapidly that supercomputers quickly come to terms. One also has to go through the tedious mathematical procedures of regularisation and renormalisation for each individual process contributing to the result under study. In contrast, the results of these lengthy calculations often turn out to be strikingly simple. Sometimes just simple integer numbers. One naturally starts to wonder whether there is a simpler structure behind.

There exists a quantum field theory in four spacetime dimensions where such underlying mathematical structures have been discovered. Again, symmetry was the guiding principle that led theoretical physicists towards it: the theory has the maximal amount of supersymmetry that can be put into a four-dimensional quantum field theory. The mathematical structures appearing in this theory allow not only efficient perturbation theory, but also give rise to non-perturbative tools allowing explicit results at any interaction strength.

This thesis is a contribution to the effort of understanding the appearance and use of these structures. It is devoted to the use of a particular structure as a super-efficient perturbative tool. Before explaining the precise goals that are pursued, we take a brief look at the theory that is under investigation.

The remarkable features of $\mathcal{N} = 4$ super Yang-Mills theory

$\mathcal{N} = 4$ super Yang-Mills theory [8], or $\mathcal{N} = 4$ SYM for short, is a theory with many particular properties. On one hand, these properties mean that the theory is certainly not

an adequate description of Nature, but on the other hand, they make the theory easier to analyse. It is of course important to ask to what degree the found structures have a generalisation in more realistic theories or if they are specific to $\mathcal{N} = 4$ SYM. In this thesis we are not that ambitious: the goal is simply to demonstrate that there is something about this theory that is worth trying to generalise.

Yang-Mills theory is the type of quantum field theory on which the Standard Model of particle physics is built. It is based on the invariance of physical observables under local transformations belonging to a Lie group, in our case $SU(N)$. "$\mathcal{N} = 4$" refers to the amount of supersymmetry, and this is the maximal amount in a four-dimensional theory with fields of spin no higher than one. This has profound consequences.

Superconformal symmetry

The field content in $\mathcal{N} = 4$ SYM is six real scalars, four Weyl fermions, and a single gauge boson, all transforming in the adjoint representation of the $SU(N)$ gauge group, and forming one big $\mathcal{N} = 4$ supermultiplet. The Lagrangian of the theory is invariant under conformal transformations, which is not unusual. It is however unusual that the conformal invariance is not spoiled by quantum corrections. The single coupling constant appearing in the theory, g_{YM}, is not subject to renormalisation, i.e. the β-function is zero [9]. The generators of conformal symmetry combine with the supersymmetry generators to the larger superconformal algebra, which is isomorphic to the graded super Lie algebra $\mathfrak{psu}(2,2|4)$, including also the additional bosonic R-symmetry.

Correlation functions are the basic objects to study in quantum field theory, and conformal symmetry constrains the structure of these functions significantly, see e.g. [10]. The key object to study in a conformal field theory is the spectrum of the *dilatation operator* D, i.e. the generator of dilatations $x^\mu \to c\, x^\mu$. This eigenproblem reads

$$D\,\mathcal{O}(0) = \Delta\,\mathcal{O}(0)\,, \tag{1}$$

where $\mathcal{O}(x)$ is a local operator and Δ is its *conformal dimension*. In general, all quantities in this equation are subject to quantum corrections and acquire a dependence on the coupling g. The coupling-dependent part of the conformal dimension is referred to as the *anomalous dimension* γ,

$$\Delta(g) = \Delta_0 + \gamma(g)\,, \tag{2}$$

where $\Delta_0 \equiv \Delta(0)$ is referred to as the *classical dimension*. The conformal dimensions completely determine two-point functions, which for scalar operators with suitable normalisation are given by

$$\langle \mathcal{O}_i(x_1)\mathcal{O}_j(x_2)\rangle = \frac{\delta_{ij}}{|x_1 - x_2|^{2\Delta_i}}\,. \tag{3}$$

Together with the *structure constants* C_{ijk}, the conformal dimensions also determine three-point functions to be

$$\langle \mathcal{O}_i(x_1)\mathcal{O}_j(x_2)\mathcal{O}_k(x_3)\rangle = \frac{C_{ijk}}{|x_1-x_2|^{\Delta_1+\Delta_2-\Delta_3}|x_2-x_3|^{\Delta_2+\Delta_3-\Delta_1}|x_1-x_3|^{\Delta_1+\Delta_3-\Delta_2}}\,. \quad (4)$$

Higher-point functions are, in principle, also given by the conformal data $\{\Delta_i, C_{ijk}\}$ through operator product expansions.

Importantly, as the anomalous part of the dilatation operator commutes with the generators of the superconformal algebra, all operators related by symmetry transformations have the same anomalous dimension, see e.g. [11].

The AdS/CFT correspondence

According to the conjectured AdS/CFT correspondence [12], $\mathcal{N}=4$ SYM and type IIB superstring theory on $\mathrm{AdS}_5\times S^5$ are equivalent theories. In particular, local gauge-invariant operators in $\mathcal{N}=4$ SYM correspond to string states, and the conformal dimensions of the former are dual to the energies of the latter. The first hint of an equivalence is seen by matching the symmetries: the isometries of AdS_5 and S^5 fit with the bosonic subalgebras $\mathfrak{su}(2,2)$ and $\mathfrak{su}(4)$ of the superconformal symmetry.

One of the reasons why the AdS/CFT correspondence is exciting is that in certain limits it relates strongly coupled gauge theory to weakly coupled string theory or simply supergravity. This opens the door to non-perturbative studies of quantum field theory.

Integrability in the planar limit

In this thesis, we will consider the AdS/CFT correspondence in the *'t Hooft limit* where the coupling g_{YM} is sent to zero, while the rank N of the $SU(N)$ gauge group is sent to infinity. The product $\lambda = g_{\mathrm{YM}}^2 N$ is kept finite. We will usually redefine this *'t Hooft coupling* by

$$g \equiv \frac{\sqrt{\lambda}}{4\pi}\,. \quad (5)$$

The limit $N\to\infty$ suppresses non-planar interactions, and it is thus called the *planar limit*. In this limit, the theory displays yet another remarkable property: there is strong evidence that at least certain aspects of the theory become *integrable*. Integrability is the presence of an infinite set of conserved charges, and in some sense this makes the theory *exactly solvable*.

The first sign of integrability was the discovery that the one-loop correction to the dilatation operator of $\mathcal{N}=4$ SYM acts like the Hamiltonian of an integrable spin chain [13]. This initiated more than a decade of intense study, which, using additional information from the AdS/CFT correspondence, has led to a beautiful mathematical structure that is

believed to encode the spectrum of anomalous dimensions at any value of the coupling: the *Quantum Spectral Curve* [14, 15].

The Quantum Spectral Curve as a perturbative tool

The Quantum Spectral Curve (QSC) is a unique discovery in the study of four-dimensional quantum field theories: it is a rather simple mathematical structure that can be solved to obtain explicit results at any value of the coupling. With such a framework at hand, we should understand how to exploit it – both to demonstrate its power, but also to test its scope and validity. The main goal of this thesis is to master this framework as a perturbative tool.

We first need to understand the objects under study: local gauge-invariant operators built by a single trace over fundamental fields. These objects have already been studied thoroughly in the literature, but we need to rephrase their classification in a language relevant for the QSC. Solving the QSC perturbatively has two main steps: finding the leading solution and perturbing around it. The problem of finding the leading solution is equivalent to solving Bethe equations for a certain type of spin chain. Again, the literature contains several approaches to doing this, but none which have the practical power that we are looking for. This thesis presents a new approach to this task, and the result is a method that is useful not only for the QSC, but for spin chains in more generality. Perturbative corrections can be generated through a recursive procedure repeating a small set of closed operations. However, the complexity of the appearing expressions grows rapidly, and the presented algorithms are the result of several cycles of implementation and optimisation. The final result is an automatisation of the procedure that gives access to a much wider range of explicit data than in previous studies.

The philosophy of the thesis is that new insights often appear through explicit computations. The enhanced data accessibility opens the possibility to look for patterns in the results that may hide even deeper structures. One such structure is the analytic continuation of the anomalous dimension of twist-2 operators, and we exploit the new data to add two new perturbative orders to this result. Finally, we initiate the study of what the QSC tells us about the whole eigenproblem of the dilatation operator, and not just the eigenvalues. In particular, the framework has the potential to produce perturbative corrections to Q-operators, which are so far only understood at the leading order. This could shed light on the still mysterious nature of AdS/CFT integrability, and how it fits into the framework of the algebraic Bethe ansatz.

Structure of the thesis

In an attempt to make a distinction between review and original work, the thesis has two main parts. The connection between the chapters is summarised in figure 1.

Part I: ***The spectral problem in AdS/CFT integrability*** is mainly a review and contains four chapters:

1 ***Single-trace operators in*** $\mathcal{N} = 4$ ***SYM*** revisits the representation theory relevant for classifying symmetry multiplets of single-trace operators in $\mathcal{N} = 4$ SYM. It contains a few new ideas, in particular the concept of extended Young diagrams, which have been presented in [5].

2 ***Spin chains and integrability*** introduces the key concepts of integrability – coordinate and algebraic Bethe ansatz – in a simple setting, the Heisenberg spin chain. The generalisation to models with higher rank symmetry is briefly discussed.

3 ***AdS/CFT integrability*** gives a brief review of the appearance of integrability in the spectral problem of the AdS/CFT correspondence. The basic ideas behind the techniques to bootstrap the spectrum by assuming integrability – the asymptotic and thermodynamic Bethe ansatz – are summarised.

4 ***Quantum Spectral Curve*** presents the QSC in an axiomatic form and discusses all technical details that are needed for using it as a perturbative tool.

Part II: ***The explicit spectrum*** presents the original research on which the thesis is based, and it also contains four chapters:

5 ***The 1-loop Q-system*** is based on [4] and [5] and explains a new powerful method to solve Bethe equations for rational spin chains, of which the leading solution to the QSC is a special example.

6 ***Perturbative algorithms*** is based on [1] and the yet unpublished work [7]. It explains first a strategy to solve the QSC perturbatively for multiplets belonging

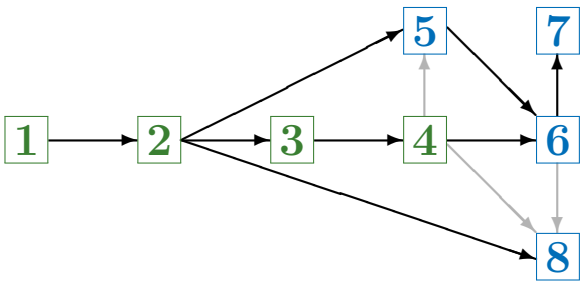

Figure 1: Connection between chapters.

to the $\mathfrak{sl}(2)$ subsector and then a completely general algorithm, before presenting a sample of results.

7 ***Twist-2 operators*** is based on [2] and [3] and summarises how the produced data can be used to reconstruct six- and seven-loop contributions to the analytically continued anomalous dimension for the infinite series of twist-2 operators.

8 ***QSC with Q-operators?*** is based on [6] and outlines a general strategy to evaluate matrix elements of Q-operators for non-compact super spin chains. This provides a starting point for using the QSC on the operatorial level.

Part I

The spectral problem in AdS/CFT integrability

Chapter 1

Single-trace operators in $\mathcal{N} = 4$ SYM

The goal of this thesis is to study anomalous dimension of local gauge-invariant operators made out of the fundamental fields in $\mathcal{N} = 4$ SYM. The fields are all in the adjoint representation of the $SU(N)$ gauge symmetry, but as we ensure gauge-invariance by tracing over the colour indices, the colour structure is completely absent in our treatment. The fields constitute a representation of the global symmetry of the theory, generated by the superconformal algebra, which is isomorphic to the graded super Lie algebra $\mathfrak{psu}(2,2|4)$. Composite local operators with several field insertions can then be thought of as tensor products, and they will form more general irreducible representations of the symmetry. All operators within such a multiplet have the same anomalous dimension $\gamma(g)$, and we can restrict our attention to single-trace operators, since they do not mix with operators containing multiple traces in the planar limit, see e.g. [11].

To classify the multiplets of single-trace operators, this chapter reviews the relevant aspects of representation theory of graded super Lie algebras before specialising to the case of $\mathcal{N} = 4$ SYM. The goal is to find a convenient way to classify the multiplets and understand the multiplet content of $\mathcal{N} = 4$ SYM quantitatively.

1.1 Representations of graded super Lie algebras

In the following we will consider graded super Lie algebras that are real forms of $\mathfrak{gl}(N+M|K)$ and their unitary representations. The treatment will be informal, and the notation will not distinguish abstract Lie algebra generators from their realisation as explicit endomorphisms of representation modules. Likewise, we will always understand the abstract Lie algebra bracket as an (anti-)commutator.

1.1.1 Definitions

Let us start by introducing the basic nomenclature. The generators, E_{mn}, of $\mathfrak{gl}(N+M|K)$ satisfy the (anti-)commutation relation

$$E_{mn}E_{kl} - (-1)^{(p_m+p_n)(p_k+p_l)}E_{kl}E_{mn} \quad = \quad \delta_{nk}E_{ml} - (-1)^{(p_m+p_n)(p_k+p_l)}\delta_{ml}E_{kn}\,, \tag{1.1}$$

where $m = 1, ..., N+M+K$. We introduce two gradings, p_m and c_m, taking the values

m	$1, ..., N$	$N+1, ..., N+M$	$N+M+1, ..., N+M+K$
p_m	0	0	1
c_m	1	0	0

. (1.2)

The real form $\mathfrak{u}(N, M|K)$ is obtained by imposing the conjugation property

$$E_{mn}^{\dagger} = (-1)^{c_m+c_n}E_{nm}\,. \tag{1.3}$$

Note that we will use the non-standard notation $\mathfrak{u}(N, |K)$ when $M = 0$.

$\mathfrak{su}(N, M|K)$ is the subalgebra of super-traceless elements in $\mathfrak{u}(N, M|K)$. The projective subalgebra $\mathfrak{psu}(N, M|K)$ can effectively be defined by furthermore imposing that the central charge vanishes,

$$C = \sum_n E_{nn} = 0\,. \tag{1.4}$$

Representations

By a *representation* of a Lie algebra, we will refer to a vector space on which the generators act linearly. The map from the abstract generators to linear transformations on the vector space should preserve the (anti-)commutation relation defining the Lie algebra, e.g. (1.1) for $\mathfrak{gl}(N+M|K)$. If the vector space is finite-dimensional, then the generators can be represented by square matrices. The dimension of the representation is the dimension of the vector space.

An *irreducible* representation, or just *irrep*, is a representation that has no non-trivial invariant subspaces. For finite-dimensional representations, this means that the individual generators cannot simultaneously be written in a block-diagonal form. We will interchangeably refer to irreducible representations as *multiplets*.

Fundamental weights

Each vector, or state, $|\Omega\rangle$, can be characterised by its eigenvalues of the diagonal generators E_{nn}. For $gl(N|K)$ we will denote these numbers by ν_i and λ_a according to

$$E_{ii}|\Omega\rangle = \nu_i|\Omega\rangle \qquad i = 1, ..., N \tag{1.5a}$$

$$E_{(N+a)(N+a)}|\Omega\rangle = \lambda_a|\Omega\rangle \qquad a = 1, ..., K\,. \tag{1.5b}$$

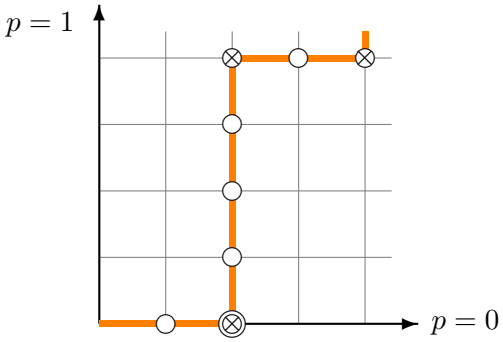

Figure 1.1: Depiction of the grading as a path on a lattice. The n'th segment is vertical if p_n=1 and horizontal if $p_n = 0$. The nodes correspond to those of the Dynkin diagram associated to the Lie algebra. A cross inside the n'th node denotes a change in the p-grading [16], i.e. that $p_n \neq p_{n+1}$, while a double circle denotes a change in the c-grading. Dynkin diagrams as paths on a two-dimensional lattice came into use after [17]. The shown path is denoted by $12\hat{1}\hat{2}\hat{3}\hat{4}34\hat{5}$... in the notation introduced below.

Highest weight states

The irreducible representations that we want to consider are of highest weight type, which means that they contain a *highest weight state* (HWS), which we can define as the state that is annihilated by all generators above the diagonal,

$$E_{mn}|\text{HWS}\rangle = 0 \quad \text{for } m < n\,. \tag{1.6}$$

The fundamental weights of the HWS then characterise the whole multiplet.

Gradings

One has the freedom to relabel the indices of the generators. With the above definition, it simply corresponds to (possibly) changing the HWS within multiplets. We can shuffle the indices, and thus the values of p_n and c_n, as we want. For $\mathfrak{gl}(N+M|K)$, it is convenient to depict the choice of p-grading as a path on an $(N+M)\times K$ lattice and associate it to a Dynkin diagram, see figure 1.1.

To denote the order in the p-grading, we will follow [15] and use a sequence of numbers either with or without a hat. A number without a hat signifies $p = 0$, while a number with a hat signifies $p = 1$. The number itself denotes the number of preceding indices with that value of p. For example, $1\hat{1}\hat{2}234\hat{3}$... means that $p_1 = 0$, $p_2 = 1$, etc. Note that one could just as well use the values of p_n themselves, e.g. 0110001..., but we will nonetheless use the slightly redundant notation for clarity.

All changes in grading can be built from exchanges of two neighbouring indices. Exchanges that permute labels with the same p- and c-grading only change the HWS up to a relabelling of indices, while exchanges that permute indices with the same p- but different c-grading simply obscure the definition of the HWS. We will thus mainly be concerned with permutations of indices with different p-grading.

Consider the exchange of the order of two indices m and n with different p-grading, i.e. $p_m + p_n = 1$. For the $\mathfrak{gl}(1|1)$ subalgebra formed by the generators with these two indices, this corresponds to the change

$$\begin{pmatrix} E_{mm} & E_{mn} \\ E_{nm} & E_{nn} \end{pmatrix} \leftrightarrow \begin{pmatrix} E_{nn} & E_{nm} \\ E_{mn} & E_{mm} \end{pmatrix} . \tag{1.7}$$

E_{mn} and E_{nm} are fermionic in the sense that they are related by an anti-commutation relation (1.1). The procedure (1.7) is referred to as *fermionic duality transformation* [18]. Consider a HWS, denoted $|\Omega\rangle$, with respect to the first grading in (1.7). It satisfies $E_{mn}|\Omega\rangle = 0$. As $E_{nm}^2 = 0$, we can maximally act once with E_{nm} on $|\Omega\rangle$. Denote the weights of the state by $E_{kk}|\Omega\rangle = e_k|\Omega\rangle$. The case where $E_{nm}|\Omega\rangle = 0$ occurs only when $e_m + e_n = 0$ (one e is a λ, one is a ν). Indeed,

$$E_{mn}E_{nm}|\Omega\rangle = \{E_{mn}, E_{nm}\}|\Omega\rangle = (E_{mm} + E_{nn})|\Omega\rangle = (e_m + e_n)|\Omega\rangle . \tag{1.8}$$

Long representations. When $e_m + e_n \neq 0$ the HWS is $E_{nm}|\Omega\rangle$ with respect to the second grading. The weights of this new HWS can be changed in two ways. If $p_m = 1$, we can denote the weights of the state $|\Omega\rangle$ by $e_{mm} = \lambda$ and $e_{nn} = \nu$. The new HWS $E_{nm}|\Omega\rangle$ will then have the weights $e_{mm} = \lambda + 1$ and $e_{nn} = \nu - 1$. All other weights remain unchanged. On the other hand, if $p_m = 0$, the new HWS will have the weights $\lambda - 1$ and $\nu + 1$, while the rest are unchanged.

Short representations. If $e_m + e_n = 0$ then $E_{mn}E_{nm}|\Omega\rangle = 0$, which implies $E_{nm}|\Omega\rangle = 0$ since otherwise the representation would be reducible indecomposable which is impossible for a unitary representation. Therefore $|\Omega\rangle$ is the HWS for both choices of grading, so λ and ν remain unchanged under the duality transformation. The effect of fermionic duality transformations is summarised in figure 1.2.

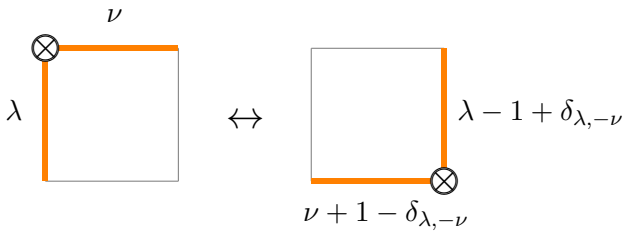

Figure 1.2: Fermionic duality transformation. When $\lambda + \nu = 0$, the weights are unchanged.

1.1.2 Unitarity constraints

We wish to consider unitary representations, meaning that all states have positive norm, $\langle\Omega|\Omega\rangle > 0$. Consider a HWS, $|\Omega\rangle$, and again denote its weights by $E_{kk}|\Omega\rangle = e_k|\Omega\rangle$. For

any two indices $m<n$ we have

$$\langle\Omega|[E_{mn},E_{nm}\}|\Omega\rangle=\langle\Omega|(E_{mm}-(-1)^{(p_m+p_n)^2}E_{nn})|\Omega\rangle=(e_m-(-1)^{p_m+p_n}e_n)\langle\Omega|\Omega\rangle\,, \tag{1.9}$$

i.e. the inner product is given in terms of the weights. At the same time $E_{mn}|\Omega\rangle=0$ and $E_{mn}^\dagger=(-1)^{c_m+c_n}E_{nm}$, so

$$\langle\Omega|[E_{mn},E_{nm}\}|\Omega\rangle=\langle\Omega|E_{mn}E_{nm}|\Omega\rangle=(-1)^{c_m+c_n}\langle\Omega|E_{mn}E_{mn}^\dagger|\Omega\rangle\,. \tag{1.10}$$

Unitarity demands that the inner products $\langle\Omega|\Omega\rangle$ and $\langle\Omega|E_{mn}E_{mn}^\dagger|\Omega\rangle$ are positive real numbers, which by combining (1.9) and (1.10) means that

$$(-1)^{c_m+c_n}\big(e_m-(-1)^{p_m+p_n}e_n\big)\geq 0\,. \tag{1.11}$$

For $\mathfrak{u}(N,M|K)$ this means that the weights (1.5) must satisfy

$$\begin{aligned}
\lambda_a-\lambda_{a+1} &\geq 0 && \text{(1.12a)}\\
\nu_{N+j}\geq\nu_{N+j+1} &\geq \nu_k\geq\nu_{k+1} && \text{(1.12b)}\\
\lambda_a+\nu_k &\leq 0 && \text{(1.12c)}\\
\lambda_a+\nu_{N+j} &\geq 0\,, && \text{(1.12d)}
\end{aligned}$$

where $j=1,...,M$ and $k=1,...,N$. These constraints should be satisfied by all members of a multiplet. Note that if (1.12a) and (1.12b) hold, then

$$\begin{aligned}
\lambda_1+\nu_1 &\leq 0 && \text{(1.13a)}\\
\lambda_K+\nu_{N+M} &\geq 0 && \text{(1.13b)}
\end{aligned}$$

ensure that (1.12c) and (1.12d) are satisfied. Note that the saturation of (1.12c) and (1.12d) corresponds exactly to the case where shortening happens. We will refer to (1.13) as *shortening conditions* in the following.

1.1.3 Oscillator formalism

We want to study unitary representations with integer weights, and then it is convenient to parametrise the generators in terms of Jordan-Schwinger oscillators,

$$E_{mn}=\bar{\boldsymbol{\chi}}_m\boldsymbol{\chi}_n\,. \tag{1.14}$$

The usage of such oscillators in superconformal algebras goes back to [19], and they have featured heavily in the study of the AdS/CFT spectrum, see e.g. [20, 21].

Let us return to the nicely ordered gradings (1.2). Three different oscillator representations of $\mathfrak{gl}(n)$,

$$\begin{aligned}
E_{\dot\alpha\dot\beta}&=-\mathbf{b}_{\dot\alpha}\mathbf{b}_{\dot\beta}^\dagger\,, && [\mathbf{b}_{\dot\alpha},\mathbf{b}_{\dot\beta}^\dagger]=\delta_{\dot\alpha\dot\beta}\,, && \dot\alpha,\dot\beta\in\{1,...,N\}\,, && \text{(1.15a)}\\
E_{(N+\alpha)(N+\beta)}&=\mathbf{a}_\alpha^\dagger\mathbf{a}_\beta\,, && [\mathbf{a}_\alpha,\mathbf{a}_\beta^\dagger]=\delta_{\alpha\beta}\,, && \alpha,\beta\in\{1,...,M\}\,, && \text{(1.15b)}\\
E_{(N+M+a)(N+M+b)}&=\mathbf{f}_a^\dagger\mathbf{f}_b\,, && \{\mathbf{f}_a,\mathbf{f}_b^\dagger\}=\delta_{ab}\,, && a,b\in\{1,...,K\}\,, && \text{(1.15c)}
\end{aligned}$$

can be used to parametrise the bosonic generators of $\mathfrak{u}(N,M|K)$. In the notation (1.14) this corresponds to $\bar{\boldsymbol{\chi}}_m = \{-\mathbf{b}_{\dot{\alpha}}, \mathbf{a}^\dagger_\alpha, \mathbf{f}^\dagger_a\}$ and $\boldsymbol{\chi}_m = \{\mathbf{b}^\dagger_{\dot{\alpha}}, \mathbf{a}_\alpha, \mathbf{f}_a\}$. The fermionic generators are then parametrised by other bilinear combinations of the oscillators $\mathbf{a}$, $\mathbf{b}$ and $\mathbf{f}$. The full set of generators are

$$E_{mn} = \begin{pmatrix} -\mathbf{b}_{\dot{\alpha}}\mathbf{b}^\dagger_{\dot{\beta}} & -\mathbf{b}_{\dot{\alpha}}\mathbf{a}_\beta & -\mathbf{b}_{\dot{\alpha}}\mathbf{f}_\mathbf{b} \\ \mathbf{a}^\dagger_\alpha\mathbf{b}^\dagger_{\dot{\beta}} & \mathbf{a}^\dagger_\alpha\mathbf{a}_\beta & \mathbf{a}^\dagger_\alpha\mathbf{f}_b \\ \mathbf{f}^\dagger_a\mathbf{b}^\dagger_{\dot{\beta}} & \mathbf{f}^\dagger_a\mathbf{a}_\beta & \mathbf{f}^\dagger_a\mathbf{f}_b \end{pmatrix} . \tag{1.16}$$

In terms of oscillators, the central charge (1.4) is

$$C = -N - n_\mathbf{b} + n_\mathbf{f} + n_\mathbf{a} \,, \tag{1.17}$$

where n are number operators, e.g. $n_{\mathbf{f}_a} \equiv \mathbf{f}^\dagger_a\mathbf{f}_a$, and $n_\mathbf{f} \equiv \sum_{a=1}^K n_{\mathbf{f}_a}$.

States

To construct representations we define a Fock vacuum $|0\rangle$ by

$$\mathbf{a}_\alpha|0\rangle = \mathbf{b}_{\dot{\alpha}}|0\rangle = \mathbf{f}_a|0\rangle = 0 \,. \tag{1.18}$$

Each irreducible representation has a fixed central charge (1.17). Specifying this central charge, we can construct the space of states of that type. Note that unless $C = -N$, the Fock vacuum $|0\rangle$ does not belong to the vector space. When both $N \neq 0$ and $M \neq 0$, generators of the type $\mathbf{a}^\dagger\mathbf{b}^\dagger$ are present. These generators are bosonic and can be applied an unlimited number of times without annihilating a state. This makes the representations infinite-dimensional, reflecting the non-compact nature of unitary representations of $\mathfrak{u}(N,M|K)$. When either $N = 0$ or $M = 0$, all generators can only act a finite number of times on a state before annihilating it, corresponding to the compact nature of $\mathfrak{u}(M|K) \cong \mathfrak{u}(M,|K)$.

As a simple example, consider $\mathfrak{u}(1|1)$, i.e. $N = 0$ and $M = K = 1$, with $C = 2$. The possible states are then $\mathbf{f}^\dagger_1\mathbf{a}^\dagger_1|0\rangle$ and $(\mathbf{a}^\dagger_1)^2|0\rangle$, and they are related by the action of $\mathbf{a}^\dagger_1\mathbf{f}_1$ and its conjugate, so these states form a two-dimensional representation.

Tensor products

We can now consider tensor products of Jordan-Schwinger type representations. Throughout the thesis, our interest will be tensor products of L representations of the same type. Tensor product representations are in general not irreducible.

As an example, consider the tensor product representation of two $C = 2$ representations of $\mathfrak{u}(1|1)$ as considered above. The corresponding vector space is four-dimensional and spanned by the states

$$\mathbf{f}^\dagger_1\mathbf{a}^\dagger_1|0\rangle \otimes \mathbf{f}^\dagger_1\mathbf{a}^\dagger_1|0\rangle \qquad \mathbf{f}^\dagger_1\mathbf{a}^\dagger_1|0\rangle \otimes (\mathbf{a}^\dagger_1)^2|0\rangle \qquad (\mathbf{a}^\dagger_1)^2|0\rangle \otimes \mathbf{f}^\dagger_1\mathbf{a}^\dagger_1|0\rangle \qquad (\mathbf{a}^\dagger_1)^2|0\rangle \otimes (\mathbf{a}^\dagger_1)^2|0\rangle \,. \tag{1.19}$$

The symmetry acts on a tensor product via the chain rule, but one should be careful with signs due to the fermionic oscillators. The tensor product space (1.19) splits into two irreps, both of dimension two:

$$\begin{aligned} \mathbf{f}_1^\dagger \mathbf{a}_1^\dagger|0\rangle^{\otimes 2} \quad &\rightleftharpoons \quad \mathbf{f}_1^\dagger \mathbf{a}_1^\dagger|0\rangle \otimes (\mathbf{a}_1^\dagger)^2|0\rangle - (\mathbf{a}_1^\dagger)^2|0\rangle \otimes \mathbf{f}_1^\dagger \mathbf{a}_1^\dagger|0\rangle \\ \mathbf{f}_1^\dagger \mathbf{a}_1^\dagger|0\rangle \otimes (\mathbf{a}_1^\dagger)^2|0\rangle + (\mathbf{a}_1^\dagger)^2|0\rangle \otimes \mathbf{f}_1^\dagger \mathbf{a}_1^\dagger|0\rangle \quad &\rightleftharpoons \quad (\mathbf{a}_1^\dagger)^2|0\rangle^{\otimes 2}\,, \end{aligned} \tag{1.20}$$

where the arrows denote the action of the off-diagonal generators $\mathbf{a}_1^\dagger \mathbf{f}_1$ and its conjugate.

In terms of oscillator number operators, the total central charge for a tensor product state is

$$C_{\text{total}} = L\,C = -N\,L - n_{\mathbf{b}} + n_{\mathbf{f}} + n_{\mathbf{a}}\,. \tag{1.21}$$

We will often characterise multiplets by the oscillator content of their HWS, using the notation $n = [n_{\mathbf{b}_{\dot\alpha}}|n_{\mathbf{f}_a}|n_{\mathbf{a}_\alpha}]$. Note that this only makes sense if the grading is specified, since the HWS changes under the fermionic duality transformations. In the example (1.20), the multiplets can be denoted by two numbers $n = [n_{\mathbf{f}_1}|n_{\mathbf{a}_1}]$. In the grading $1\hat{1}$, where the HWS is annihilated by $E_{12} = \mathbf{a}_1^\dagger \mathbf{f}_1$, the two multiplets are then denoted $n = [1|3]$ and $n = [0|4]$, respectively. In the grading $\hat{1}1$, where $E_{12} = \mathbf{f}_1^\dagger \mathbf{a}_1$, they are instead denoted $n = [2|2]$ and $n = [1|3]$.

We will now introduce a tool from representation theory that allows a classification of irreps in which the ambiguity related to the choice of grading is absent.

1.2 Young diagrams

Young diagrams were first introduced in representation theory of finite groups, where they can be used to construct representations of the symmetric group S_N. Due to the Schur-Weyl duality [22] they simultaneously classify irreducible representations of both S_N and $\mathfrak{gl}(N)$.

The following treatment of Young diagrams as a classification of irreducible representations of $\mathfrak{gl}$-type algebras will be rather informal, and we will only introduce the concepts necessary for our applications. A more complete treatment can be found in most modern books on representation theory, see e.g. [23]. For simplicity, we begin with the compact case.

1.2.1 Compact Young diagrams

As discussed, unitary representations of $\mathfrak{u}(M|K)$ are finite-dimensional. They can be characterised by the $(M+K)$-partition $\{\nu_1, ..., \nu_M|\lambda_1, ..., \lambda_K\}$ given by the fundamental weights of the HWS in the chosen grading. For representations of Jordan-Schwinger type,

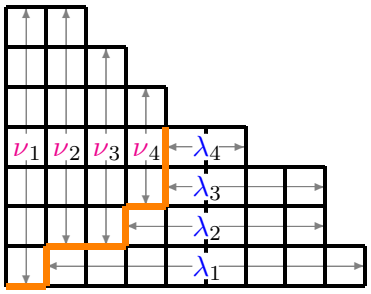

Figure 1.3: Definition of compact Young diagram in terms of a grading and a partition $\{\nu|\lambda\}$. Note that we use the "French notation" for Young diagrams.

these weights are equivalent to the oscillator numbers $n_{\mathbf{a}_\alpha}$ and $n_{\mathbf{f}_a}$. As discussed above, the grading defines a two-dimensional path. The Young diagram is constructed by drawing ν_j boxes above the j'th horizontal line, and λ_a boxes to the right of the a'th vertical line, see figure 1.3. From this definition it is clear that a representation of $\mathfrak{u}(M|K)$ is characterised by a Young diagram that fits within an L-shaped hook of the form shown in figure 1.4.

Unitarity constraints

Notice that due to the nature of the fermionic duality transformations, the Young diagram is independent of the chosen path. The unitarity constraints (1.12) should hold no matter which grading is chosen. This means that the Young diagrams have to be shaped as a ladder, i.e. the width of the rows have to decrease or remain the same as one goes from below.

Shortening has a very natural interpretation on the level of Young diagrams. A representation is short if it does not touch the point (M, K) at the corner of the L-hook. See figure 1.4 for an example.

Young diagrams as algebra-independent objects

We can just as well describe a Young diagram entirely by the width of its rows, i.e. by a partition $\lambda' = \{\lambda'_1, ..., \lambda'_H\}$ where H is the height of the first column in the diagram, see figure 1.5. It is clearly not necessary to specify an algebra in order to define the Young

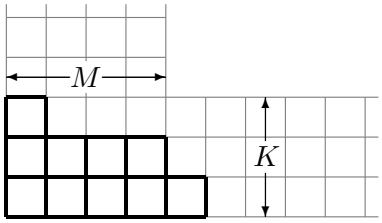

Figure 1.4: L-hook for $\mathfrak{u}(M|K)$ with $M = 4$ and $K = 3$. The Young diagram specifies a short representation of $\mathfrak{u}(4|3)$ since it does not touch the point $(4, 3)$.

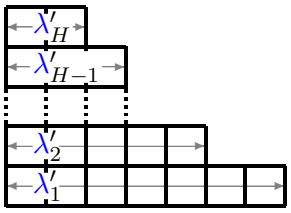

Figure 1.5: Young diagram as a partition $\lambda' = \{\lambda'_1, ..., \lambda'_H\}$.

diagram. In fact, a diagram characterises an irreducible representation of any $\mathfrak{u}(M|K)$ algebra for which it fits inside the corresponding L-hook.

Tensor products and trivial extension

The discussion so far has been for abstract representations. If we want to interpret the vector spaces of the representations as tensor products, we need to specify another number: the length L of the tensor product or, equivalently, the central charge C for the individual components in the tensor product. The length and central charge are related to the weights by

$$L\,C = \sum_{k=1}^{M} \nu_k + \sum_{k=1}^{K} \lambda_k = \sum_{k=1}^{H} \lambda'_k\,. \tag{1.22}$$

Let us restrict to the Jordan-Schwinger type representations. As the oscillators $\mathbf{f}_a$ are fermionic, they can act only once on the vacuum $|0\rangle$. This means that the allowed representations for the individual components in a tensor product are given by Young diagrams with a single column whose height equals the central charge, see figure 1.6.

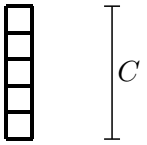

Figure 1.6: The representation at each site in the tensor product is given by the central charge C.

Consider a tensor product where each component is a $\mathfrak{u}(M|K)$ representation with central charge C. By introducing an additional oscillator $\mathbf{f}_0$ and redefining our Fock vacuum as $|0\rangle = \mathbf{f}_0^\dagger|\tilde{0}\rangle$, we can think of this as a tensor product of $\mathfrak{u}(M|K{+}1)$ representations with central charge $C{+}1$. We embed the original $\mathfrak{u}(M|K)$ representation in a larger $\mathfrak{u}(M|K{+}1)$ representation. The corresponding Young diagram obtains an additional row of length L at the bottom and the partition becomes $\{\nu_1, ..., \nu_M|L, \lambda_1, ..., \lambda_K\}$. Alternatively, we can extend the algebra to $\mathfrak{u}(M|K{+}1)$ by adding an extra weight with value 0 corresponding to the partition $\{\nu_1, ..., \nu_M|\lambda_1, ..., \lambda_K, 0\}$. This corresponds to extending the algebra by an oscillator $\mathbf{f}_{K+1}$, but without modifying the $\mathfrak{u}(M|K)$ subspace or the central charge. The Young diagram is then unchanged. We can do arbitrarily many of these extensions, and

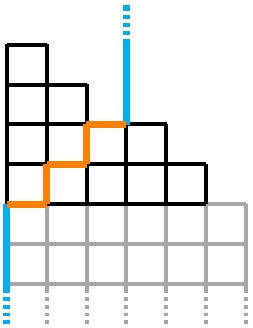

Figure 1.7: Extension of a compact Young diagram. The extension depends on the specification of a central charge C, which defines the length through (1.22). The orange path corresponds to the original grading, while the blue path is the extension. The extension can be arbitrarily big and will have weights $\{\nu_1, ..., \nu_M | L, ..., L, \lambda_1, ..., \lambda_K, 0, ..., 0\}$. In the depicted example, the $\mathfrak{u}(3|2)$ partition $\{4, 2, 0|4, 2\}_{1\hat{1}\hat{2}\hat{2}3}$ is interpreted as a tensor product with central charge $C = 2$ and thus length $L = 6$. We call the grey part the *trivial extension*.

we will refer to this process as *trivial extensions*. The process is depicted in figure 1.7, and it will play a key role in the following.

1.2.2 Non-compact Young diagrams

Young diagrams are a standard tool in the analysis of compact representations. In the AdS/CFT integrability context, non-compact representations have previously been classified by diagrams within a T-hook [24, 25, 26]. In the yet unpublished work on classifications of unitary representations of $\mathfrak{u}(N, M|K)$ [27], a generalisation of Young diagrams to the non-compact case will be introduced. As a special case of that approach, we now define Young diagrams for a restricted class of irreducible representations. In particular, we want to consider representations that are realised as tensor products of Jordan-Schwinger type representations with integer weights. It is convenient to characterise these representations by the oscillator numbers $n_{\mathbf{a}}$, $n_{\mathbf{b}}$ and $n_{\mathbf{f}}$ rather than their fundamental weights ν and λ. We will discuss the ambiguity in using the fundamental weights after defining non-compact Young diagrams in terms of Jordan-Schwinger oscillators.

Definition in terms of Jordan-Schwinger oscillators

An irreducible representation of $\mathfrak{u}(N, M|K)$ is characterised by a Young diagram within a grid of the form shown in figure 1.8, which we will refer to as a χ-hook. Figure 1.8 also shows the definition of the Young diagram in terms of the oscillator numbers. Note that it is necessary to specify the central charge C, or, equivalently, the length L. Again, C and L are related through (1.21).

To draw the diagram, the starting point is the Dynkin path, cf. figure 1.1, which consists of N+M+K segments. For the first N horizontal segments, draw $n_{\mathbf{b}_{\dot{\alpha}}}$ boxes below

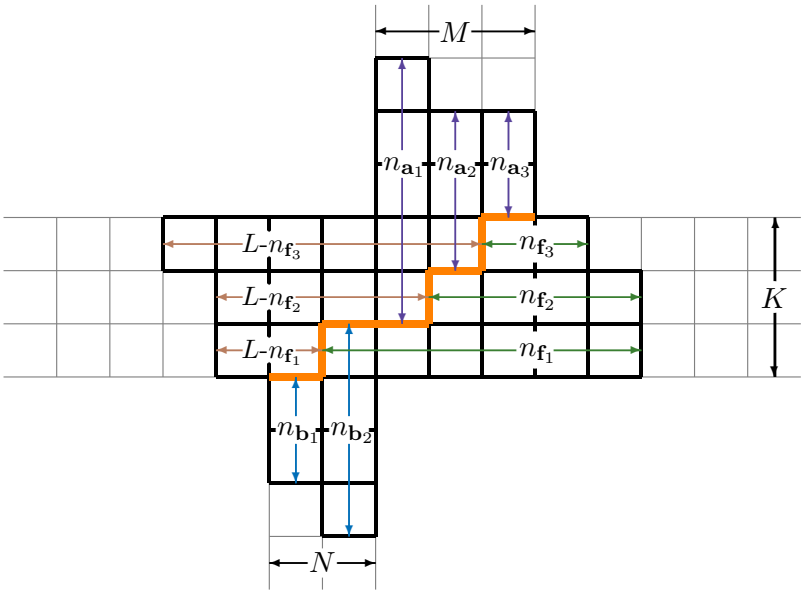

Figure 1.8: Young diagram corresponding to the oscillator numbers $n_{\mathbf{a}}$, $n_{\mathbf{f}}$, $n_{\mathbf{b}}$ with respect to a given grading and a specified central charge C that defines L through (1.21). The example here corresponds to an $\mathfrak{u}(2,3|3)$ representation with $n^{1\hat{1}23\hat{2}4\hat{3}5} = [2,4|6,4,2|5,3,2]$ and $C=0$. Consequently, $L=8$.

the $\dot{\alpha}$'th segment. For the last M horizontal segments, draw $n_{\mathbf{a}_\alpha}$ above the $(N+\alpha)$'th segment. For the a'th vertical segments, draw $n_{\mathbf{f}_a}$ boxes to the right and $L-n_{\mathbf{f}_a}$ boxes to the left.

It is important to note that the above prescription is not valid in all gradings if the representation in question is short. For long representations, the Young diagram touches the start- and end-point of the Dynkin path, which we denote $(0,0)$ and $(N+M,K)$. For short representations, the prescription always yields the correct diagram if one chooses the path

$$1\,2\,\ldots\,(N{-}1)\,N \quad \hat{1}\,\hat{2}\,\ldots\,\widehat{K{-}1}\,\hat{K} \quad (N{+}1)\,(N{+}2)\,\ldots\,(N{+}M)\,,$$

corresponding to ordering the oscillators such that all $\mathbf{b}$ oscillators come before all $\mathbf{f}$ oscillators followed by all $\mathbf{a}$ oscillators, i.e. $\mathfrak{u}(N,|K|M)$.

Why the fundamental weights are ambiguous

The above definition of Young diagrams depends on the $N+M+K$ oscillator numbers, but also on the central charge C, or, equivalently, the length L.

Why not use the fundamental weights λ and ν? In the following, our focus will be on projective algebras of $\mathfrak{pu}$-type, where the central charge is zero. The issue is that when $C=0$, the length L drops out of (1.22), so the weights do not determine L. In contrast, we get L for free through (1.21) by using oscillator numbers. We will see examples of this in the $\mathcal{N}=4$ SYM context below.

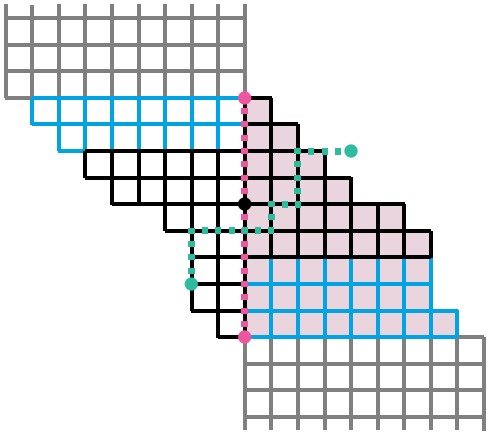

Figure 1.9: Extension of a Young diagram that was originally defined for $\mathfrak{u}(2,2|4)$ and $C = 0$ ($n^{12\hat{1}\hat{2}\hat{3}\hat{4}34} = [2,3|7,6,4,3|2,1]$). The *non-trivial extension* is marked in blue, while the *trivial extension* is marked in grey. The trivial part continues infinitely in the vertical direction without any horizontal shifts. The central point is marked with a black circle. The two red points correspond to the algebra $\mathfrak{u}(9)$, and the shaded boxes show the corresponding $\mathfrak{u}(9)$ Young diagram with $C = 5$. The two green points correspond to the algebra $\mathfrak{u}(2,4|5)$ with $C = 1$. As one of the points is outside the diagram, the corresponding multiplet is short.

Extension and map to $\mathfrak{u}(N')$

In analogy with the compact case, we would like to think of the non-compact Young diagram as independent of the algebra. Similarly to the compact discussion, we can embed a representation in representations of algebras of higher rank, by extending the set of oscillators and through redefinitions of the Fock vacuum and central charge.

In this procedure, we first extend all rows to have length L. In the upper part of the diagram, we extend the rows towards the left, and in the lower part towards the right. We call this the *non-trivial extension*. Above and below this diagram, we place an infinite column of rows that are completely aligned with central vertical line in the diagram. In the upper part, this infinite column is on the left side, while it is on the right side in the lower part. We call this the *trivial extension*. See figure 1.9.

The diagram now corresponds to an irreducible representation of any $\mathfrak{u}(N,M|K)$ algebra for which it fits inside the χ-hook. An algebra is specified by choosing two points on the $\mathbb{Z}^2$ lattice such that the extended Young diagram is between them and that the right point is not lower than the left point. The relative position of these points to one another and to the central vertical line specify the algebra, and the Young diagram then defines an irrep of this algebra. If both points are on the boundary of the extended diagram then this representation is a long multiplet, otherwise it is a short multiplet.

We interpret the irrep defined by a Young diagram as a subspace of a tensor product of L copies of a simpler representation with a given central charge. The point on the central

vertical line where the number of boxes that are placed *to the left and below* the point equals the number of boxes *to the right and above* the point defines the central charge for each component in the tensor product. For $\mathfrak{u}(N,M|K)$ this point is $(N,C+N)$, since the equality of the number of boxes southwest and northeast of the point,

$$n_{\mathbf{b}} + \sum_{a=1}^{N+C} (L - n_{\mathbf{f}_a}) = n_{\mathbf{a}} + \sum_{a=N+C+1}^{K} n_{\mathbf{f}_a} \,, \tag{1.23}$$

is identical to the central charge constraint (1.21), and we refer to it as the *central point* or simply *center* of the diagram. Later, we will also refer to it as the *momentum-carrying node*. Note further that the central vertical line splits the diagram into two halves that are shaped as extended compact diagrams. We call them the *left* and *right compact diagrams*. This gives a way to map $\mathfrak{u}(N,M|K)$ representations to $\mathfrak{u}(N')$ representations, which we will now exploit.

1.3 Characters and counting

Having introduced a way to classify representations, either through the specification of a partition or a Young diagram plus a central charge, we are ready to study the decomposition of tensor product representations into irreps. Representation theory provides a convenient tool in terms of *characters*.

Character theory for compact representations is described in most textbooks on representation theory, see e.g. [23]. The generalisation to supersymmetry and non-compactness is less well-studied, and the author is unaware of a treatment combining both features. As proposed in [5], we will use the concept of extended Young diagrams to map $\mathfrak{u}(N,M|K)$ representations to representations of $\mathfrak{u}(N')$, and thus circumvent the complications arising from supersymmetry and non-compactness. The trade-off is that the rank N' is unbounded.

1.3.1 $\mathfrak{gl}(N)$ characters

The character of an irrep of $\mathfrak{gl}(N)$ with weights $\lambda = \{\lambda_1, ..., \lambda_N\}$ is given by the Schur polynomial

$$\chi_\lambda = \frac{\det_{1\leq i,j\leq N} x_i^{\lambda_j+N-j}}{\det_{1\leq i,j\leq N} x_i^{N-j}} \equiv \frac{W_\lambda}{\Delta_V} \,, \tag{1.24}$$

where the denominator $\Delta_V = \prod_{i<j}(x_i - x_j)$ is the Vandermonde determinant.

We are particularly interested in tensor products of such irreps. A tensor product representation is *reducible*, and it can be written as a direct sum of irreps,

$$\lambda \otimes \tilde{\lambda} = \bigoplus_i \lambda_i \,. \tag{1.25}$$

The character of the tensor product representation is simply the product of the characters of its factors, i.e. $\chi_{\lambda^{\otimes L}} = \chi_\lambda^L$. At the same time, the character of a reducible representation is a sum of characters of irreps:

$$\chi_{\text{reducible}} = \sum_\lambda c_\lambda \, \chi_\lambda \,, \tag{1.26}$$

and the integer multiplicities c_λ are uniquely determined. In the case of the L'th tensor product of an irrep λ, we get

$$\chi_\lambda^L = \sum_{\lambda'} c_{\lambda'} \chi_{\lambda'} \,. \tag{1.27}$$

Actually, the polynomial $W_\lambda = \Delta_V \cdot \chi_\lambda$ is more convenient to work with. For a given representation λ, W_λ will contain a term of the kind

$$x_1^{\lambda_1+N-1} x_2^{\lambda_2+N-2} \cdots x_{N-1}^{\lambda_{N-1}+1} x_N^{\lambda_N} \,, \tag{1.28}$$

which we will call the *dominant term*. The advantage of W compared to χ is that the dominant terms are unique to W_λ, i.e. they do not appear in $W_{\lambda'}$ if $\lambda \neq \lambda'$. We can then effectively decompose into irreps by reading off the coefficient of the dominant terms in the expression

$$\Delta_V \cdot \chi_{\text{reducible}} = \sum_\lambda c_\lambda W_\lambda \,. \tag{1.29}$$

1.3.2 Polya theory

The tensor product character (1.27) can be seen as a sum of all the states in the spectrum with length L. In the next section, we will want to interpret single-trace operators in $\mathcal{N} = 4$ SYM as tensor product states. The trace is cyclic, which means that tensor product states that are related by cyclic permutations, i.e. by the cyclic group $\mathbb{Z}_L$, are considered to be equivalent. This effectively reduces the size of the vector space of states. The above analysis does not take this property into account.

The *Polya theorem* [28][1] provides a way to account for equivalence relations between tensor product states, in our case cyclic permutations. According to the Polya theorem, the tensor product character (1.27) should be replaced by the reduced sum of states Z_L given by

$$Z_L = \sum_{d|L} \frac{\phi(d)}{L} \chi_1(x_1^d, ..., x_N^d)^{\frac{L}{d}} \,. \tag{1.30}$$

Here $d|L$ denotes all divisors of L, while $\phi(d)$ is the Euler totient function given by the number of integers between 1 and d that are mutually prime with d. χ_1 is the character of the representation that each component of the tensor product is in.

[1] See [29] for a detailed explanation relevant for our purposes.

The practical usage of characters is demonstrated in appendix A.2, both in simple examples and to understand the multiplet content in $\mathcal{N}=4$ SYM, towards which we now turn our focus.

1.4 The $\mathcal{N}=4$ SYM spectrum

Our goal is to classify the symmetry multiplets formed by single-trace operators in $\mathcal{N}=4$ SYM. Such a classification was first done in [30] and further investigations made in [31].

The superconformal algebra is isomorphic to $\mathfrak{psu}(2,2|4)$. The generators of the symmetry can be realised as differential operators on the fundamental fields that constitute local operators, and as such, they act via the chain rule. This fits well with the action of abstract symmetry generators on a tensor product, and thus we can interpret the composite operators as tensor products.

At zero coupling, i.e. $g \to 0$, the symmetry is in fact enhanced to $\mathfrak{pu}(2,2|4)\oplus\mathfrak{u}(1)$, where the extra $\mathfrak{u}(1)$ corresponds to the fixed length L. This section reviews how multiplets of single-trace operators are affected by this transition in symmetry induced by turning on the coupling.

1.4.1 Field interpretation of states

The states satisfying the central charge constraint $C=0$ and their interpretation in terms of fields in $\mathcal{N}=4$ SYM are summarised in table 1.1. The fields correspond to an infinite-dimensional representation reflecting the possibility of acting with an arbitrary number of covariant derivatives on each field. The corresponding $\mathfrak{pu}(2,2|4)$ Young diagram is depicted in figure 1.10. The fields are assigned a classical conformal dimension, Δ_0, given

Field interpretation		Content	Δ_0	Components
scalar	Φ_{ab}	$\mathbf{f}_a^\dagger \mathbf{f}_b^\dagger \lvert 0\rangle$	1	6
fermion	$\Psi_{a\alpha}$	$\mathbf{f}_a^\dagger \mathbf{a}_\alpha^\dagger \lvert 0\rangle$	$\frac{3}{2}$	8
	$\bar{\Psi}_{a\dot{\alpha}}$	$\epsilon_{abcd}\mathbf{f}_b^\dagger \mathbf{f}_c^\dagger \mathbf{f}_d^\dagger \mathbf{b}_{\dot{\alpha}}^\dagger \lvert 0\rangle$	$\frac{3}{2}$	8
field strength	$\mathcal{F}_{\alpha\beta}$	$\mathbf{a}_\alpha^\dagger \mathbf{a}_\beta^\dagger \lvert 0\rangle$	2	3
	$\bar{\mathcal{F}}_{\dot{\alpha}\dot{\beta}}$	$\mathbf{f}_1^\dagger \mathbf{f}_2^\dagger \mathbf{f}_3^\dagger \mathbf{f}_4^\dagger \mathbf{b}_{\dot{\alpha}}^\dagger \mathbf{b}_{\dot{\beta}}^\dagger \lvert 0\rangle$	2	3
covariant derivative	$\mathcal{D}_{\alpha\dot{\alpha}}$	$\mathbf{a}_\alpha^\dagger \mathbf{b}_{\dot{\alpha}}^\dagger$	1	4

Table 1.1: States satisfying the central charge constraint. Note that $\Phi_{ab} = -\Phi_{ba}$, i.e. there are six independent scalars. We denote them by $\mathcal{Z} \equiv \mathbf{f}_1^\dagger \mathbf{f}_2^\dagger|0\rangle$, $\mathcal{X} \equiv \mathbf{f}_1^\dagger \mathbf{f}_3^\dagger|0\rangle$, $\mathcal{Y} \equiv \mathbf{f}_1^\dagger \mathbf{f}_4^\dagger|0\rangle$, $\bar{\mathcal{Y}} \equiv \mathbf{f}_2^\dagger \mathbf{f}_3^\dagger|0\rangle$, $\bar{\mathcal{X}} \equiv \mathbf{f}_2^\dagger \mathbf{f}_4^\dagger|0\rangle$, $\bar{\mathcal{Z}} \equiv \mathbf{f}_3^\dagger \mathbf{f}_4^\dagger|0\rangle$. Note also that $\mathcal{F}_{\alpha\beta} = \mathcal{F}_{\beta\alpha}$ and $\bar{\mathcal{F}}_{\dot{\alpha}\dot{\beta}} = \bar{\mathcal{F}}_{\dot{\beta}\dot{\alpha}}$. A state can contain one of the fundamental fields and an unlimited number of covariant derivatives.

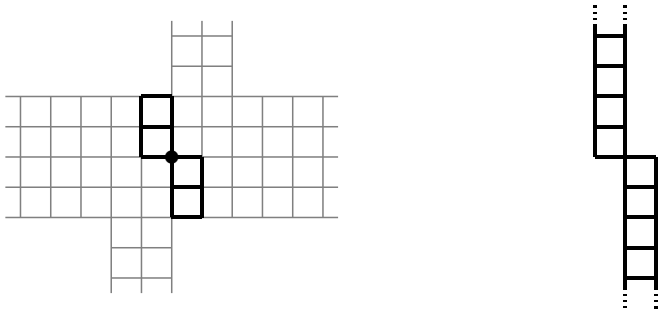

Figure 1.10: (left) The χ-hook and the Young diagram corresponding to the single-field representation in $\mathcal{N} = 4$ SYM. The central point is marked. (right) The extended Young diagram corresponding to the single-field representation.

by

$$\Delta_0 = \frac{n_{\mathbf{f}}}{2} + n_{\mathbf{a}} \,. \tag{1.31}$$

Composite operators made of L fields are interpreted as tensor products of L vectors from the above representation. As an example, consider the $L = 3$ state

$$\mathrm{Tr}[\, \mathcal{Z}\ \mathcal{D}_{12}\Psi_{11}\ \mathcal{F}_{12}\,] = \mathbf{f}_1^\dagger \mathbf{f}_2^\dagger |0\rangle \otimes (\mathbf{a}_1^\dagger)^2 \mathbf{b}_2^\dagger \mathbf{f}_1^\dagger |0\rangle \otimes \mathbf{a}_1^\dagger \mathbf{a}_2^\dagger |0\rangle \,. \tag{1.32}$$

For simplicity, we will often leave out the Tr[...] symbol. Cyclicity of the trace means that two states are equivalent if they are related by cyclic permutations, e.g. $\mathcal{Z}\mathcal{X} = \mathcal{X}\mathcal{Z}$. As fermions anti-commute, this also means that some states involving fermions vanish, e.g. $\Psi_{a\alpha}\Psi_{a\alpha} = -\Psi_{a\alpha}\Psi_{a\alpha} = 0$. The central charge constraint for a tensor product state is

$$n_{\mathbf{a}} - n_{\mathbf{b}} + n_{\mathbf{f}} = 2L \,, \tag{1.33}$$

and this defines L through the oscillator numbers.

$\mathfrak{pu}(2,2|4)$ Young diagrams

The Young diagrams of the irreps of $\mathfrak{pu}(2,2|4)$ are drawn within the χ-hook shown in figure 1.10. We will refer to the point $(2,2)$ as the *central point*. It splits the diagram into four quadrants. The central charge constraint $C = 0$ manifests itself as the demand that the number of boxes in the upper-right and lower-left quadrants must be equal, see figure 1.11. Furthermore, the left and right half of the diagram should be of ladder shape [27]. The unitarity constraints (1.12) only demands this for the four middle rows, but it turns out that diagrams which are not of ladder-shape correspond to operators that are set to zero by the equations of motions. An example is the diagram on the right in figure 1.11 ($n^{\lrcorner} = [1,1|1,1,1,1|1,1]$ in the notation introduced below), which corresponds to a HWS of the form $\epsilon^{abcd}\Phi_{ab}\Box\Phi_{cd}$. The equations of motion are realised in the oscillator language as $\Box = \epsilon_{\alpha\beta}\epsilon_{\dot\alpha\dot\beta}\mathcal{D}_{\alpha\dot\alpha}\mathcal{D}_{\beta\dot\beta} = \det_{1\le\alpha,\dot\alpha\le 2} \mathbf{a}_\alpha^\dagger \mathbf{b}_{\dot\alpha}^\dagger = 0$, and consequently this operator vanishes.

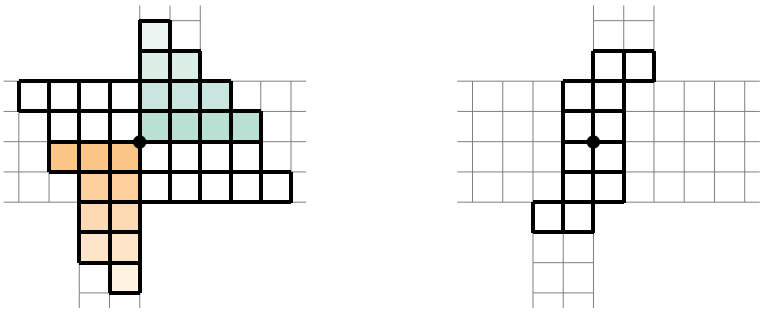

Figure 1.11: (left) An example of a $\mathfrak{pu}(2,2|4)$ diagram having the same number of boxes in the lower-left and upper-right quadrant. (right) A Young diagram that is not ladder-shaped and allowed by the $\mathfrak{pu}(2,2|4)$ unitarity constraints (1.12), but corresponds to an operator that is zero due to the equations of motion.

1.4.2 Quantum numbers and finite g

At zero coupling, the multiplets of operators are representations of $\mathfrak{pu}(2,2|4) \oplus \mathfrak{u}(1)$. As such, we need eight numbers to classify the representations. As mentioned, we will prefer to use the oscillator numbers to classify representations. We will do this in the notation

$$n^{\text{grading}} = [\, n_{\mathbf{b}_1}, n_{\mathbf{b}_2} \,|\, n_{\mathbf{f}_1}, n_{\mathbf{f}_2}, n_{\mathbf{f}_3}, n_{\mathbf{f}_4} \,|\, n_{\mathbf{a}_1}, n_{\mathbf{a}_2} \,], \tag{1.34}$$

where the oscillator numbers are those of the HWS with respect to the specified grading. Our preferred choice of grading will be $12\hat{1}\hat{2}\hat{3}\hat{4}34$, also known as the *compact beauty* grading [32], for which we will use the symbol $\lrcorner\!\!\lceil$ as a short-hand notation referring to its Dynkin path. This choice is convenient since it minimises the classical conformal dimension (1.31).

Turning on g

The above use of Jordan-Schwinger oscillators is only an adequate description of $\mathcal{N}=4$ SYM at $g=0$. The Jordan-Schwinger-type representations have integer weights, and this is no longer true when $g \neq 0$. Understanding the nature of the representations formed by single-trace operators at finite coupling is still an unsolved, and very interesting, problem.

The global symmetry of $\mathcal{N}=4$ SYM has the two bosonic subalgebras $\mathfrak{su}(4)$ and $\mathfrak{su}(2,2)$. The $\mathfrak{su}(4)$ part corresponds to the R-symmetry and is related to the S^5 part of the dual geometry. The corresponding weights λ_a do not run with the coupling and remain integers at any coupling. The $\mathfrak{su}(2,2)$ part, related to the conformal symmetry and the AdS_5 part of the dual geometry, is not as simple. The conformal symmetry includes the dilatation operator, and as it is renormalised, the weights of this part of the symmetry, ν_i, run with the coupling since they contain the anomalous dimension. The behaviour is

$$\nu_i \;=\; \nu_i|_{g=0} + \frac{\gamma}{2}\{-1,-1,1,1\}_i\,. \tag{1.35}$$

$n^{\lrcorner}$	L	Field content example	λ_a	ν_j
$[1,1\|2,2,2,2\|1,1]$	4	$\Psi_{11}\Psi_{12}\bar{\Psi}_{11}\bar{\Psi}_{12}$	$\{2,2,2,2\}$	$\{-5,-5,1,1\}$
$[0,0\|2,2,2,2\|1,1]$	5	$\Psi_{11}\Psi_{12}\bar{\mathcal{Z}}\bar{\mathcal{X}}\bar{\mathcal{Y}}$	$\{2,2,2,2\}$	$\{-5,-5,1,1\}$
$[1,1\|3,3,3,3\|0,0]$	5	$\bar{\Psi}_{11}\bar{\Psi}_{12}\mathcal{Z}\mathcal{X}\mathcal{Y}$	$\{3,3,3,3\}$	$\{-6,-6,0,0\}$

Table 1.2: Three types of operators with differing oscillator content and length that have the same $\mathfrak{psu}(2,2|4)$ quantum numbers: $\lambda_a-\lambda_{a+1}=\{0,0,0\}$ and $\nu_j-\nu_{j+1}=\{0,-6,0\}$.

At finite coupling, the multiplets organise themselves in representations of $\mathfrak{psu}(2,2|4)$. Such representations are characterised by just six numbers. A choice is the differences of the fundamental weights $\lambda_a-\lambda_{a+1}$ and $\nu_j-\nu_{j+1}$. Note that the weights $\{\lambda,\nu\}$ and $\{\lambda+\Lambda,\nu-\Lambda\}$ define isomorphic irreps of $\mathfrak{psu}(2,2|4)$.

The relation between oscillator numbers and other conventionally used parametrisations of the $\mathfrak{psu}(2,2|4)$ quantum numbers are given in appendix A.1. Despite the obscured interpretation at finite coupling, we will prefer to label multiplets by the HWS oscillator content (1.34) that they flow towards as $g\to 0$, since this classification contains the complete information, and since our main objective is perturbative calculations.

Length mixing

At finite coupling, the notion of a length breaks down. In general, the eigenstates of the dilatation operator is a mix of any operator with the same $\mathfrak{psu}(2,2|4)$ quantum numbers [33]. On the level of level of oscillators, the length can be changed by two transformations that leave the differences $\lambda_a-\lambda_{a+1}$ and $\nu_j-\nu_{j+1}$ invariant:

$$\{L,\, n_{\mathbf{b}_{\dot\alpha}}\} \quad\leftrightarrow\quad \{L-1,\, n_{\mathbf{b}_{\dot\alpha}}+1\}\,, \tag{1.36a}$$

$$\{L,\, n_{\mathbf{f}_a},\, n_{\mathbf{a}_\alpha}\} \quad\leftrightarrow\quad \{L-1,\, n_{\mathbf{f}_a}-1, n_{\mathbf{a}_\alpha}+1\} \tag{1.36b}$$

Note that (1.36a) leaves λ and ν invariant, while (1.36b) takes $\lambda_a\leftrightarrow\lambda_a-1$ and $\nu_i\leftrightarrow\nu_i+1$. An example of operators related by these transformations and consequently able to mix at higher loops is given in table 1.2.

1.4.3 Shortening and joining

As discussed, shortening happens whenever $\lambda_a+\nu_j=0$. At $g=0$ this happens for all multiplets that correspond to diagrams not touching the edges of the χ-hook. This means that some fermionic duality transformations do not alter the HWS.

At $g\neq 0$ the situation is different. Generically, the shortening conditions are not satisfied due to the running of ν_j. In consequence, all unprotected multiplets of operators should be long representations of the symmetry with distinct highest weight states for all

70 possible Dynkin paths on the 4|4 lattice. The only explanation of this phenomenon is that the short $\mathfrak{pu}(2,2|4) \oplus \mathfrak{u}(1)$ multiplets must combine into larger $\mathfrak{psu}(2,2|4)$ multiplets.

Protected operators: the BMN vacuum

There is one type of multiplet that is not subject to joining: the multiplets containing the states $\mathrm{Tr}\, \mathcal{Z}^L$. The oscillator numbers are

$$n^{\ulcorner} = [0,0|L,L,0,0|0,0]\,. \tag{1.37}$$

Due to the fact that they are annihilated by half the supercharges, these operators are protected from quantum corrections and have vanishing anomalous dimension, see e.g. [11].

Shortening conditions

The non-trivial unitarity bounds are

$$\lambda_1 + \nu_1 \;\leq\; 0\,, \tag{1.38a}$$

$$\lambda_4 + \nu_4 \;\geq\; 0\,. \tag{1.38b}$$

These bounds must be satisfied by any member of a multiplet. For this, we need to require that (1.38a) holds for gradings of the type $\{1\hat{1}\}$..., and that (1.38b) holds for gradings of the type ...$\{4\hat{4}\}$. Here the notation $\{ab\}$ means that a and b can be in either order.

Shortening happens when one or both bounds are saturated, i.e. when

$$\lambda_1 + \nu_1 \;=\; n_{\mathbf{f}_1} - L - n_{\mathbf{b}_1} \;=\; 0\,, \tag{1.39a}$$

$$\lambda_4 + \nu_4 \;=\; n_{\mathbf{f}_4} + n_{\mathbf{a}_2} \;=\; 0\,, \tag{1.39b}$$

which we refer to as *shortening conditions*. On the level of oscillators, the condition (1.39a) can only happen if $n_{\mathbf{f}_1} = L$ and $n_{\mathbf{b}_1} = 0$. Similarly, (1.39b) implies $n_{\mathbf{f}_4} = n_{\mathbf{a}_2} = 0$. Shortenings rule out the possibility of the length-changing replacements (1.36). In particular, (1.39a) rules out (1.36a) and (1.39b) rules out (1.36b).

Joining

Let us take a short multiplet and reconsider what happens during fermionic duality transformations that leave the HWS unchanged.

Consider a multiplet subject to the shortening (1.39a). The oscillator content in a grading of the type $1\hat{1}$... must be of the form

$$[0, n_{\mathbf{b}_2}|L, \bullet, \bullet, \bullet|\bullet, \bullet]^L_{1\hat{1}\ldots}\,, \tag{1.40a}$$

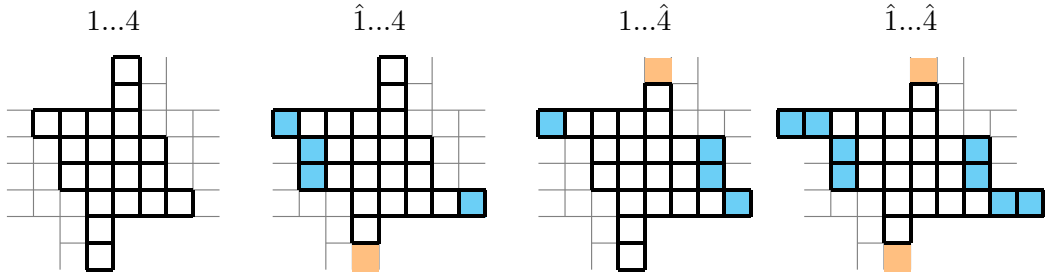

Figure 1.12: Example of four different Young diagrams for short multiplets that join into one at finite coupling. The changes with respect to the diagram on the left are highlighted.

where the length and grading is specified in super- and subscript. If the multiplet was long, the effect of the duality transformation to the $\hat{1}1...$ grading would be $\{\lambda_1, \nu_1\} \to \{\lambda_1 + 1, \nu_1 - 1\}$, which seems to give the inadmissible oscillator content $[1, n_{\mathbf{b}_2}|L+1, \bullet, \bullet, \bullet|\bullet, 0]^L_{\hat{1}1...}$. However, this can be cured by the length-changing replacement (1.36a). The resulting oscillator numbers are

$$[0, n_{\mathbf{b}_2} - 1|L+1, \bullet, \bullet, \bullet|\bullet, \bullet]^{L+1}_{\hat{1}1...}\,. \tag{1.40b}$$

This is how joining works: short $\mathfrak{pu}(2,2|4)\oplus\mathfrak{u}(1)$ multiplets of different lengths join into one $\mathfrak{psu}(2,2|4)$ multiplet. A similar treatment reveals that multiplets subject to the shortening (1.39b) combine as

$$[\bullet, \bullet|\bullet, \bullet, \bullet, 0|n_{\mathbf{a}_1}, 0]^L_{...\hat{4}4}\,, \tag{1.41a}$$

$$[\bullet, \bullet|\,\bullet+1, \bullet+1, \bullet+1, 0|n_{\mathbf{a}_1} - 1, 0]^{L+1}_{...4\hat{4}}\,. \tag{1.41b}$$

If both shortenings (1.39) happen, the four multiplets

$$\begin{aligned}
&[0, \bullet|L, \bullet, \bullet, 0|\bullet, 0]^L_{1...4}\,,\\
&[0, \bullet-1|L+1, \bullet, \bullet, 0|\bullet, 0]^{L+1}_{\hat{1}...4}\,,\\
&[0, \bullet|L+1, \bullet+1, \bullet+1, 0|\,\bullet-1, 0]^{L+1}_{1...\hat{4}}\,,\\
&[0, \bullet-1|L+2, \bullet+1, \bullet+1, 0|\,\bullet-1, 0]^{L+2}_{\hat{1}...\hat{4}}\,,
\end{aligned} \tag{1.42}$$

join into one.

In table 1.3 we give examples of the different members of the short Konishi multiplet. We also display the joining on the level of Young diagrams in figure 1.12. Note that two identical Young diagrams can appear in different types of long multiplets as they can describe the HWS in different gradings.

Stronger shortenings

We could also encounter an operator with $n_{\mathbf{f}_1} = L$ and $n_{\mathbf{b}_1} = n_{\mathbf{b}_2} = 0$, which would satisfy also the shortening $\lambda_1 + \nu_2 = 0$. To make the joining (1.40) possible, it would have to

Grading	n	Possible field content	L	Δ_0	Young diagram
$1\{2\hat{1}\hat{2}\hat{3}\hat{4}3\}4$	$[0,0\|1,1,1,1\|0,0]$	$\mathcal{Z}\bar{\mathcal{Z}}$, $\mathcal{X}\bar{\mathcal{X}}$, $\mathcal{Y}\bar{\mathcal{Y}}$	2	2	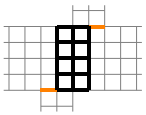
$1\{\hat{1}2\hat{2}\hat{3}\hat{4}3\}4$	$[0,1\|2,1,1,1\|0,0]$	$\mathcal{Z}\bar{\Psi}_{2,2}$, $\mathcal{X}\bar{\Psi}_{32}$, $\mathcal{Y}\bar{\Psi}_{42}$	2	$\frac{5}{2}$	
$1\{\hat{1}\hat{2}23\hat{3}\hat{4}\}4$	$[0,2\|2,2,0,0\|2,0]$	$\mathcal{D}_{12}^2\mathcal{Z}^2$	2	4	
$\hat{1}\{12\hat{2}\hat{3}\hat{4}3\}4$	$[0,0\|3,1,1,1\|0,0]$	$\mathcal{Z}\mathcal{X}\mathcal{Y}$	3	3	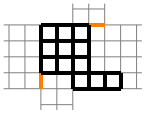
$\hat{1}\{12\hat{2}3\hat{3}\hat{4}\}4$	$[0,0\|3,1,0,0\|2,0]$	$\mathcal{Z}\Psi_{11}^2$	3	4	
$\hat{2}\hat{3}\hat{4}123$	$[3,3\|3,3,3,3\|0,0]$	$\bar{\mathcal{F}}_{12}^3$, $\bar{\mathcal{F}}_{11}\bar{\mathcal{F}}_{12}\bar{\mathcal{F}}_{21}$	3	6	
$1\{2\hat{1}\hat{2}\hat{3}34\}\hat{4}$	$[0,0\|2,2,2,0\|0,0]$	$\mathcal{Z}\mathcal{X}\bar{\mathcal{Y}}$	3	3	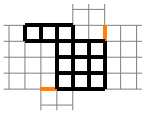
$1\{\hat{1}2\hat{2}3\hat{3}4\}\hat{4}$	$[0,2\|3,3,2,0\|0,0]$	$\mathcal{Z}\bar{\Psi}_{42}^2$	3	4	
$234\hat{1}\hat{2}\hat{3}$	$[0,0\|0,0,0,0\|3,3]$	$\mathcal{F}_{12}^3$, $\mathcal{F}_{11}\mathcal{F}_{12}\mathcal{F}_{21}$	3	6	
$\hat{1}\{12\hat{2}\hat{3}34\}\hat{4}$	$[0,0\|4,2,2,0\|0,0]$	$\mathcal{Z}^2\mathcal{X}^2$	4	4	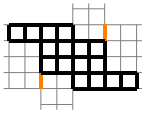
$\hat{2}12343\}\hat{4}$	$[1,1\|4,4,0,0\|1,1]$	$\mathcal{D}_{11}\mathcal{D}_{22}\mathcal{Z}^4$, $\mathcal{D}_{12}\mathcal{D}_{21}\mathcal{Z}^4$	4	6	
$\hat{2}\hat{3}1234$	$[2,2\|4,4,4,0\|0,0]$	$\bar{\Psi}_{41}^2\bar{\Psi}_{42}^2$	4	6	

Table 1.3: Selected components of the Konishi multiplet, which splits into four short multiplets at $g=0$.

be a HWS in the grading $\hat{1}12...$ at finite coupling. Similarly, the case $n_{\mathbf{f}_1}=n_{\mathbf{f}_2}=L$ and $n_{\mathbf{b}_1}=0$ implies the $1\hat{1}\hat{2}...$ grading. If (1.39b) is supplemented by $n_{\mathbf{a}_2}=0$ it implies the grading $...34\hat{4}$, and if supplemented by $n_{\mathbf{f}_3}=0$ it implies $...\hat{3}\hat{4}4$ at finite coupling.

There is one scenario that the joining mechanism cannot handle: if both $n_{\mathbf{b}_2}=0$ in the $\{1\hat{1}2\}...$ gradings and $n_{\mathbf{f}_2}=L$ in the $\{1\hat{1}\hat{2}\}...$ gradings. The only multiplets in the $\mathcal{N}=4$ spectrum with this property are the protected BMN vacua discussed above which remain short at finite coupling.

1.4.4 Sectors

Shortening is crucial in understanding the appearance of closed sectors of operators. By a *closed sector*, we refer to operators with restricted field content that do not mix with operators with different field content, i.e. the eigenstates of the dilatation operator will be a linear combination of single-trace operators of only this kind at any coupling. This is the case when the $\mathfrak{psu}(2,2|4)$ quantum numbers, i.e. the six numbers $\lambda_a-\lambda_{a+1}$ and $\nu_j-\nu_{j+1}$, can only be used to construct certain fields.

In a closed sector, some oscillators are passive in the sense that they are either saturated (e.g. $n_{\mathbf{f}_1}=L$) or not excited at all (e.g. $n_{\mathbf{f}_4}=0$), while some oscillators are excited and form a set of non-trivial raising operators. Furthermore, the length-changing transformations (1.36a) and (1.36b) do not excite the passive oscillators.

The six different possibilities of shortening are summarised in table 1.4. All closed sectors can be understood in terms of combinations of these shortenings. For example,

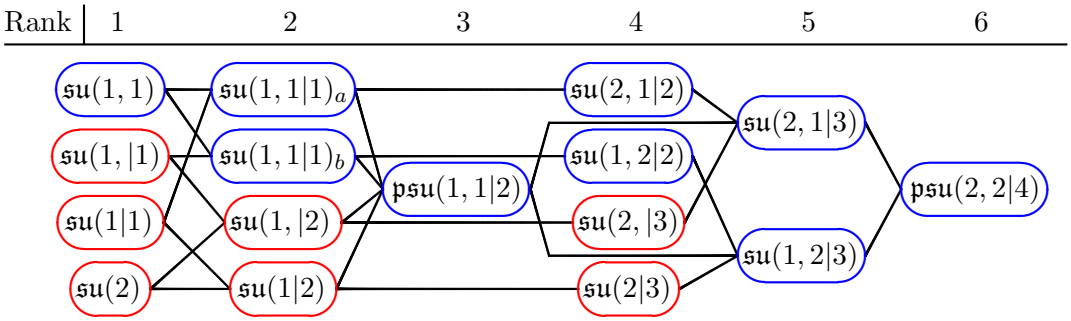

Figure 1.13: Closed sectors. ●compact ●non-compact.

the $\mathfrak{su}(1,1) = \mathfrak{sl}(2)$ sector combines the fourth and sixth type: $[0, \bullet|L, L, 0, 0|\bullet, 0]$, while the $\mathfrak{su}(2,1|3)$ sector is of the second type: $[\bullet, \bullet|\bullet, \bullet, \bullet, 0|\bullet, 0]$. All closed sectors are listed in table 1.5. The rank of the sector is one lower than the number of active oscillators. The sectors of low rank are subsectors of those of higher rank, and the relationship between sectors is summarised in figure 1.13.

Note that in sectors where only one of the shortening conditions (1.39) is satisfied, one of the length changing transformations (1.36) is allowed and results in an operator with the same $\mathfrak{psu}(2,2|4)$ quantum numbers, but with a different length. As discussed, this means that at higher loops the eigenstates of the dilatation operator can mix operators of different length.

Figure 1.14 shows the Young diagrams for multiplets containing operators in the $\mathfrak{sl}(2)$ and $\mathfrak{su}(2)$ sectors. Note that the multiplets $n^{\lceil} = [0, 0|L-1, L-1, 1, 1|0, 0]$ contain operators from all sectors.

$[n_b\|n_f\|n_a]$	Grading
$[0, \bullet\|L, \bullet, \bullet, \bullet\|\bullet, \bullet]$	$\{1\hat{1}\}...$
$[\bullet, \bullet\|\bullet, \bullet, \bullet, 0\|\bullet, 0]$	$...\{4\hat{4}\}$
$[0, 0\|L, \bullet, \bullet, \bullet\|\bullet, \bullet]$	$\hat{1}12...$
$[0, \bullet\|L, L, \bullet, \bullet\|\bullet, \bullet]$	$1\hat{1}\hat{2}...$
$[\bullet, \bullet\|\bullet, \bullet, \bullet, 0\|0, 0]$	$...34\hat{4}$
$[\bullet, \bullet\|\bullet, \bullet, 0, 0\|\bullet, 0]$	$...\hat{3}\hat{4}4$

Table 1.4: Types of shortening and resulting grading for the state that remains a HWS at finite coupling. Brackets {} denote interchangeable gradings.

1.4.5 Counting multiplets

In the AdS_5/CFT_4 context the counting of multiplets was done in [29, 34] by engineering $\mathfrak{so}(N)$ characters to account for supersymmetry and non-compactness. As proposed in [5], we will take another approach. In section 1.2.2, we saw how to map a non-compact representation to an $\mathfrak{u}(N)$ representation via the extended Young diagram. All $\mathfrak{pu}(2,2|4)$

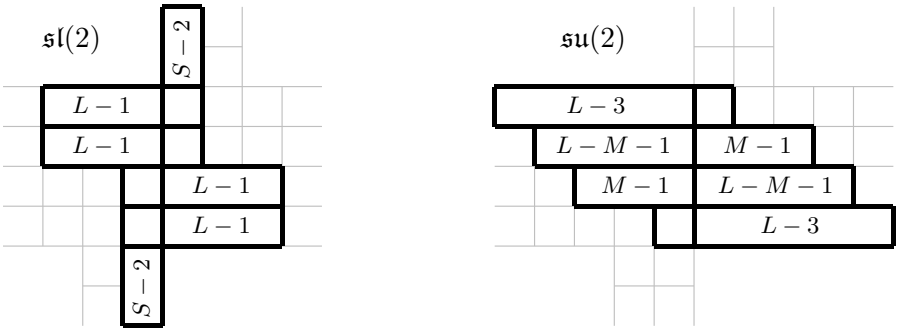

Figure 1.14: Young diagrams (of $\ulcorner$ HWS) for multiplets containing $\mathfrak{sl}(2)$, $\mathcal{D}_{12}^{S}\mathcal{Z}^{L}$, and $\mathfrak{su}(2)$, $\mathcal{Z}^{L-M}\mathcal{X}^{M}$, operators.

diagrams can in fact be seen as representations of $\mathfrak{u}(4+n_{\mathbf{b}_2}^{\ulcorner}+n_{\mathbf{a}_1}^{\ulcorner})$ with central charge $C=2+n_{\mathbf{b}_2}^{\ulcorner}$. We can exploit this to apply the tools of section 1.3 to count the multiplets in $\mathcal{N}=4$ SYM. An important point is that it is possible to make a cut-off in the classical dimension given by (1.31). To account for all multiplets up to a maximal classical dimension $\Delta_{0,\max}^{\ulcorner}$ of the HWS in the $\ulcorner$ grading, it is sufficient to consider $\mathfrak{u}(2\Delta_{0,\max}^{\ulcorner})$ representations where the tensor product components are in representations with central charge $C=\Delta_{0,\max}^{\ulcorner}$, cf. (1.30). Details of such calculations are given in appendix A.2. Table 1.6 gives an overview of the multiplets with $\Delta_0^{\ulcorner}\leq 5.5$. See appendix A.3 for a list of all multiplets with $\Delta_0^{\ulcorner}\leq 8$.

Subconclusion

In this chapter, we have seen how to construct and classify Jordan-Schwinger type representations of $\mathfrak{u}(N,M|K)$ in terms of oscillators and Young diagrams. By introducing the idea of extended Young diagrams, we have seen how to use standard Schur polynomials to decompose tensor products of non-compact representations into irreps, also taking cyclic equivalence into account. We then applied this framework to the global symmetry of $\mathcal{N}=4$ SYM in the limit $g\to 0$. We saw how its representations quite magically glue together at finite coupling to form long $\mathfrak{psu}(2,2|4)$ multiplets.

With a clear picture of the content of multiplets of single-trace operators in $\mathcal{N}=4$ SYM, we are ready to start our search for the anomalous dimensions that characterise each of these multiplets. The dilatation operator, of which the anomalous dimensions are eigenvalues, turns out to have the remarkable property that it acts like the Hamiltonian of an integrable system. Integrable models have a rich underlying mathematical structure, which can be formulated in terms of a Q-system, and these structures will be the topic of the next chapter. For now, the introduction of extended Young diagrams gave us an intuitive way to classify and count irreps. Their true usefulness will be revealed in chapter 5, where they will serve as skeletons for Q-systems.

Rank	Sector	Field content	$[n_{\mathbf{b}}\|n_{\mathbf{f}}\|n_{\mathbf{a}}]$	Grading(s)
1	$\mathfrak{su}(1,1)$	$\mathcal{D}_{12}^{S}\mathcal{Z}^{L}$	$[0\,,\,S\,\vert\,L\,,\,L\,,\,0\,,\,0\,\vert\,S\,,\,0]$	$1\hat{1}\hat{2}23\hat{3}\hat{4}4$
	$\mathfrak{su}(1,\vert 1)$	$\mathcal{Z}^{L-N}\bar{\Psi}_{42}^{N}$	$[0\,,\,N\,\vert\,L\,,\,L\,,\,N\,,\,0\,\vert\,0\,,\,0]$	$1\hat{1}\hat{2}[2\hat{3}]34\hat{4}$
	$\mathfrak{su}(1\vert 1)$	$\mathcal{Z}^{L-N}\Psi_{11}^{N}$	$[0\,,\,0\,\vert\,L\,,\,L{-}N\,,\,0\,,\,0\,\vert\,N\,,\,0]$	$\hat{1}12[3\hat{2}]\hat{3}\hat{4}4$
	$\mathfrak{su}(2)$	$\mathcal{Z}^{L-M}\mathcal{X}^{M}$	$[0\,,\,0\,\vert\,L\,,\,L{-}M\,,\,M\,,\,0\,\vert\,0\,,\,0]$	$\hat{1}12\hat{2}\hat{3}34\hat{4}$
2	$\mathfrak{su}(1,1\vert 1)_a$	$\mathcal{D}_{12}^{S}\mathcal{Z}^{L-N}\Psi_{11}^{N}$	$[0,S\,\vert\,L\,,\,L{-}N\,,\,0\,,\,0\,\vert\,S{+}N,0]$	$\{1\hat{1}\}[23\hat{2}]\hat{3}\hat{4}4$
	$\mathfrak{su}(1,1\vert 1)_b$	$\mathcal{D}_{12}^{S}\mathcal{Z}^{L-N}\bar{\Psi}_{42}^{N}$	$[0,S{+}N\,\vert\,L\,,\,L\,,\,N\,,\,0\,\vert\,S,0]$	$1\hat{1}\hat{2}[23\hat{3}]\{4\hat{4}\}$
	$\mathfrak{su}(1,\vert 2)$	$\mathcal{Z}^{L-M-N}\mathcal{X}^{M}\bar{\Psi}_{42}^{N}$	$[0,N\,\vert\,L,L{-}M,M{+}N,0\,\vert\,0,0]$	$\{1\hat{1}\}[2\hat{2}\hat{3}]34\hat{4}$
	$\mathfrak{su}(1\vert 2)$	$\mathcal{Z}^{L-M-N}\mathcal{X}^{M}\Psi_{11}^{N}$	$[0,0\,\vert\,L,L{-}M{-}N,M,0\,\vert\,N,0]$	$\hat{1}12[3\hat{2}\hat{3}]\{4\hat{4}\}$
3	$\mathfrak{psu}(1,1\vert 2)$	$\mathcal{D}_{12}^{S}\mathcal{Z}^{L-M-N_1-N_2+S}$ $\mathcal{X}^{M+S}\Psi_{11}^{N_1-S}\bar{\Psi}_{42}^{N_2-S}$	$[0\,,\,N_2\,\vert\,L\,,\,L{-}M{-}N_1\,,$ $M{+}N_2\,,\,0\,\vert\,N_1\,,\,0]$	$\{1\hat{1}\}[23\hat{2}\hat{3}]\{4\hat{4}\}$
4	$\mathfrak{su}(2,1\vert 2)$	$\mathcal{D}_{11}^{S_1}\mathcal{D}_{12}^{S_2}\mathcal{Z}^{L-N_1-N_2+n}$ $\Psi_{11}^{N_1-n}\Psi_{21}^{N_2-n}\mathcal{F}_{11}^{n}$	$[\,S_1\,,\,S_2\,\vert\,L{-}N_2\,,\,L{-}N_1\,,$ $0\,,\,0\,\vert\,N_1{+}N_2{+}S_1{+}S_2\,,\,0\,]$	$[123\hat{1}\hat{2}]\hat{3}\hat{4}4$
	$\mathfrak{su}(2,\vert 3)$	$\mathcal{Z}^{L-M_1-M_2-N_1-N_2}$ $\mathcal{X}^{M_1}\bar{\mathcal{Y}}^{M_2}\bar{\Psi}_{42}^{N_1}\bar{\Psi}_{41}^{N_2}$	$[\,N_2\,,\,N_1\,\vert\,L{-}M_2\,,\,L{-}M_1\,,$ $M_1{+}M_2{+}N_1{+}N_2\,,\,0\,\vert\,0\,,\,0\,]$	$[12\hat{1}\hat{2}\hat{3}]34\hat{4}$
	$\mathfrak{su}(1,2\vert 2)$	$\mathcal{D}_{12}^{S_1}\mathcal{D}_{22}^{S_2}\mathcal{Z}^{L-N_1-N_2+n}$ $\bar{\Psi}_{42}^{N_1-n}\bar{\Psi}_{32}^{N_2-n}\bar{\mathcal{F}}_{22}^{n}$	$[\,0\,,\,S_1{+}S_2{+}N_1{+}N_2\,\vert\,L\,,\,L\,,$ $N_1\,,\,N_2\,\vert\,S_1\,,\,S_2\,]$	$1\hat{1}\hat{2}[234\hat{3}\hat{4}]$
	$\mathfrak{su}(2\vert 3)$	$\mathcal{Z}^{L-M_1-M_2-N_1-N_2}$ $\mathcal{X}^{M_1}\mathcal{Y}^{M_2}\Psi_{11}^{N_1}\Psi_{12}^{N_2}$	$[\,0,0\,\vert\,L,L{-}M_1{-}M_2{-}N_1{-}N_2\,,$ $M_1\,,\,M_2\,\vert\,N_1\,,\,N_2\,]$	$\hat{1}12[34\hat{2}\hat{3}\hat{4}]$
5	$\mathfrak{su}(1,2\vert 3)$	$\mathcal{D}_{12}^{\bullet}\mathcal{D}_{22}^{\bullet}\mathcal{X}^{\bullet}\mathcal{Y}^{\bullet}\mathcal{Z}^{\bullet}$ $\Psi_{11}^{\bullet}\Psi_{12}^{\bullet}\bar{\Psi}_{42}^{\bullet}\bar{\Psi}_{32}^{\bullet}\bar{\Psi}_{22}^{\bullet}\bar{\mathcal{F}}_{22}^{\bullet}$	$[0,\bullet\vert L,\bullet,\bullet,\bullet\vert\bullet,\bullet]$	$[123\hat{1}\hat{2}\hat{3}]\{4\hat{4}\}$
	$\mathfrak{su}(2,1\vert 3)$	$\mathcal{D}_{11}^{\bullet}\mathcal{D}_{12}^{\bullet}\mathcal{X}^{\bullet}\bar{\mathcal{Y}}^{\bullet}\mathcal{Z}^{\bullet}$ $\bar{\Psi}_{42}^{\bullet}\bar{\Psi}_{41}^{\bullet}\Psi_{11}^{\bullet}\Psi_{21}^{\bullet}\Psi_{31}^{\bullet}\mathcal{F}_{11}^{\bullet}$	$[\bullet,\bullet\vert\bullet,\bullet,\bullet,0\vert\bullet,0]$	$\{1\hat{1}\}[234\hat{2}\hat{3}\hat{4}]$

Table 1.5: Closed sectors. Passive oscillators are marked in grey. A bracket [] denotes duality transformations that shuffle active oscillators and change the HWS within the sector while preserving the length. A bracket {} denotes a duality transformation that shuffles passive oscillators and changes the HWS within the sector while changing L. Note that the field content in the $\mathfrak{psu}(1,1|2)$, $\mathfrak{su}(2,1|2)$, $\mathfrak{su}(1,2|2)$, $\mathfrak{su}(2,1|3)$ and $\mathfrak{su}(1,2|3)$ sectors is not completely fixed by the oscillator numbers, but they can still be considered sectors as only a restricted field content can appear.

$\Delta_0^{\ulcorner}$	L	$[\,n_{\mathbf{b}}\,\vert\,n_{\mathbf{f}}\,\vert\,n_{\mathbf{a}}\,]^{\urcorner}$	S_1	S_2	Sector	Multiplicity
2	2-4	$[0,0\vert1,1,1,1\vert0,0]$	✔	✔	all	1
3	3-5	$[0,0\vert2,2,1,1\vert0,0]$	✔	✔	all	1
4	4-6	$[0,0\vert3,3,1,1\vert0,0]$	✔	✔	all	2
	3-5	$[0,1\vert2,2,1,1\vert1,0]$	✔	✔	$\mathfrak{sl}(2)$	2
	2-4	$[0,2\vert1,1,1,1\vert2,0]$	✔	✔	$\mathfrak{sl}(2)$	1
	4-6	$[0,0\vert3,2,2,1\vert0,0]$	✔	✔	$\mathfrak{su}(2)$	1
	3-4	$[0,0\vert1,1,1,1\vert2,0]$	✘	✔	$\mathfrak{su}(2,1\vert2)$	1
		$[0,2\vert2,2,2,2\vert0,0]$	✔	✘	$\mathfrak{su}(1,2\vert2)$	1
	4	$[0,0\vert2,2,2,2\vert0,0]$	✘	✘	$\mathfrak{psu}(2,2\vert4)$	2
5	5-7	$[0,0\vert4,4,1,1\vert0,0]$	✔	✔	all	2
	4-6	$[0,1\vert3,3,1,1\vert1,0]$	✔	✔	$\mathfrak{sl}(2)$	2
	3-5	$[0,2\vert2,2,1,1\vert2,0]$	✔	✔	$\mathfrak{sl}(2)$	1
	5-7	$[0,0\vert4,3,2,1\vert0,0]$	✔	✔	$\mathfrak{su}(2)$	2
	4-6	$[0,0\vert3,1,1,1\vert2,0]$	✔	✔	$\mathfrak{su}(1\vert1)$	1
		$[0,2\vert3,3,3,1\vert0,0]$			$\mathfrak{su}(1,\vert1)$	1
	4-6	$[0,1\vert3,2,2,1\vert1,0]$	✔	✔	$\mathfrak{psu}(1,1\vert2)$	4
	5-6	$[0,0\vert3,3,3,1\vert0,0]$	✘	✔	$\mathfrak{su}(2,\vert3)$	2
		$[0,0\vert4,2,2,2\vert0,0]$	✔	✘	$\mathfrak{su}(2\vert3)$	2
	4-5	$[0,0\vert2,2,1,1\vert2,0]$	✘	✔	$\mathfrak{su}(2,1\vert2)$	2
		$[0,2\vert3,3,2,2\vert0,0]$	✔	✘	$\mathfrak{su}(1,2\vert2)$	2
	5	$[0,0\vert3,3,2,2\vert0,0]$	✘	✘	$\mathfrak{psu}(2,2\vert4)$	4
	4	$[0,1\vert2,2,2,2\vert1,0]$	✘	✘	$\mathfrak{psu}(2,2\vert4)$	2
$\frac{11}{2}$	5-7	$[0,0\vert4,3,1,1\vert1,0]$	✔	✔	$\mathfrak{su}(1\vert1)$	2
		$[0,1\vert4,4,2,1\vert0,0]$			$\mathfrak{su}(1,\vert1)$	2
	4-6	$[0,1\vert3,2,1,1\vert2,0]$	✔	✔	$\mathfrak{su}(1,1\vert1)_a$	2
		$[0,2\vert3,3,2,1\vert1,0]$			$\mathfrak{su}(1,1\vert1)_b$	2
	3-5	$[0,2\vert2,1,1,1\vert3,0]$	✔	✔	$\mathfrak{su}(1,1\vert1)_a$	2
		$[0,3\vert2,2,2,1\vert2,0]$			$\mathfrak{su}(1,1\vert1)_b$	2
	5-6	$[0,0\vert3,3,2,1\vert1,0]$	✘	✔	$\mathfrak{su}(2,1\vert3)$	4
		$[0,1\vert4,3,2,2\vert0,0]$	✔	✘	$\mathfrak{su}(1,2\vert3)$	4
	4-5	$[0,1\vert2,2,2,1\vert2,0]$	✘	✔	$\mathfrak{su}(2,1\vert3)$	4
		$[0,2\vert3,2,2,2\vert1,0]$	✔	✘	$\mathfrak{su}(1,2\vert3)$	4
	5	$[0,0\vert3,2,2,2\vert1,0]$	✘	✘	$\mathfrak{psu}(2,2\vert4)$	4
		$[0,1\vert3,3,3,2\vert0,0]$				4

Table 1.6: All unprotected multiplets for which $\Delta_0^{\ulcorner} \leq \frac{11}{2}$. The columns S_1 and S_2 denote whether the two shortening conditions (1.38a) and (1.38b), are saturated, respectively.

Chapter 2

Spin chains and integrability

We call a model *quantum integrable* if it falls within the framework of Bethe ansatz techniques, where the Yang-Baxter equation is the basic prerequisite. This chapter gives a practical and informal review of these frameworks, and the discussion will progress through explicit examples. To avoid getting lost in tedious notation, we will introduce the techniques in a model with $\mathfrak{su}(2)$ symmetry, the Heisenberg spin chain, and comment on the generalisation to higher rank symmetry at the end of the chapter. The main goal is to introduce the concept of a Q-system, which plays a central role throughout the thesis.

2.1 The Heisenberg spin chain and coordinate Bethe ansatz

The Heisenberg spin chain is not only a convenient toy model on which the tools of integrability can be demonstrated, it also describes the one-loop spectrum of the $\mathfrak{su}(2)$ sector in $\mathcal{N} = 4$ SYM.

2.1.1 The closed Heisenberg spin chain

Consider a one-dimensional model of L spins, which are all in the same representation of some Lie algebra, with periodic boundary conditions, see figure 2.1. In the Heisenberg spin chain, these spins belong to the two-dimensional fundamental representation of $\mathfrak{su}(2)$, and we denote the states *spin up* $\uparrow$ and *spin down* $\downarrow$. The model is specified by the Hamiltonian

$$H = \sum_{k=1}^{L} (\mathbb{I} - \mathbb{P}_{k,k+1}) \,, \tag{2.1}$$

where $\mathbb{P}_{i,j}$ is the permutation operator that interchanges the spins at position i and j. As the chain is closed, we identify the k'th and the $(L+k)$'th site, i.e. $\mathbb{P}_{L,L+1} = \mathbb{P}_{L,1}$. Notice that the Hamiltonian only contains interactions between neighbouring spins.

Through the permutation operator, we can define a *shift operator* U that shifts all

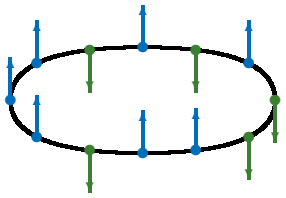

Figure 2.1: A closed Heisenberg spin chain.

spins by one site towards the left:

$$U = \mathbb{P}_{L-1,L} \cdots \mathbb{P}_{2,3}\mathbb{P}_{1,2} \,. \tag{2.2}$$

For example, $U \cdot \uparrow\uparrow\downarrow = \uparrow\downarrow\uparrow$. By using the properties $\mathbb{P}_{i,j} = \mathbb{P}_{j,i}$ and $\mathbb{P}_{i,j}\mathbb{P}_{j,k} = \mathbb{P}_{i,k}\mathbb{P}_{i,j}$, one can show that the shift operator commutes with the Hamiltonian (2.1).

We can furthermore define a spin-flip operator, $S_\uparrow$, that flips a down spin to an up spin and annihilates the state if it acts on an up spin. It acts via the chain rule, e.g.

$$S_\uparrow \cdot \downarrow\uparrow\downarrow \;=\; \uparrow\uparrow\downarrow + \;0\; + \downarrow\uparrow\uparrow \,. \tag{2.3}$$

We can define the opposite spin-flip operator $S_\downarrow$ similarly[1]. The spin-flip operators also commute with H.

The Hamiltonian acts linearly on the vector space of spin chain configurations. It only relates spin chain configurations with the same length, and the same number of up and down spins. We call these subspaces *magnon blocks*. We denote the length of the chain by L, and the number of down spins (magnons) by M. The Hamiltonian can be represented by a matrix that is block diagonal on each magnon block. We are interested in its eigenstates and eigenvalues.

Example: $L = 3$, $M = 1$

As an example, consider chains of length three. There are eight spin chain configurations forming four magnon blocks:

$$\uparrow\uparrow\uparrow \qquad \uparrow\uparrow\downarrow \quad \uparrow\downarrow\uparrow \quad \downarrow\uparrow\uparrow \qquad \uparrow\downarrow\downarrow \quad \downarrow\uparrow\downarrow \quad \downarrow\downarrow\uparrow \qquad \downarrow\downarrow\downarrow$$

Let us consider the magnon block corresponding to $M = 1$ and denote the spin chain configurations by the vectors

$$\uparrow\uparrow\downarrow \;\equiv \begin{pmatrix} 1 \\ 0 \\ 0 \end{pmatrix} , \qquad \uparrow\downarrow\uparrow \;\equiv \begin{pmatrix} 0 \\ 1 \\ 0 \end{pmatrix} , \qquad \downarrow\uparrow\uparrow \;\equiv \begin{pmatrix} 0 \\ 0 \\ 1 \end{pmatrix} . \tag{2.4}$$

[1] In terms of the Jordan-Schwinger oscillators introduced in section 1.1.3 our states are $\uparrow \;= \mathbf{a}_1^\dagger|0\rangle$ and $\downarrow \;= \mathbf{a}_2^\dagger|0\rangle$. A spin chain configuration is a tensor product, e.g. $\downarrow\uparrow\downarrow \;= \mathbf{a}_2^\dagger|0\rangle \otimes \mathbf{a}_1^\dagger|0\rangle \otimes \mathbf{a}_2^\dagger|0\rangle$. The spin-flip operators on a single site are the symmetry generators $S_\uparrow = \mathbf{a}_1^\dagger\mathbf{a}_2$ and $S_\downarrow = \mathbf{a}_2^\dagger\mathbf{a}_1$. On tensor products they act like $S_\uparrow = \mathbf{a}_1^\dagger\mathbf{a}_2 \otimes 1^{\otimes L-1} + 1 \otimes \mathbf{a}_1^\dagger\mathbf{a}_2 \otimes 1^{\otimes L-2} + \ldots + 1^{\otimes L-1} \otimes \mathbf{a}_1^\dagger\mathbf{a}_2$.

On this subspace the Hamiltonian is

$$H = \begin{pmatrix} 2 & -1 & -1 \\ -1 & 2 & -1 \\ -1 & -1 & 2 \end{pmatrix} . \tag{2.5}$$

This matrix can easily be diagonalised yielding the eigenvalues and -states ($H\psi = E\psi$)

$$\begin{aligned} E_0 = 0 \qquad & \psi_0 = \begin{pmatrix} 1 \\ 1 \\ 1 \end{pmatrix} = \uparrow\uparrow\downarrow + \uparrow\downarrow\uparrow + \downarrow\uparrow\uparrow \\ E_\pm = 3 \qquad & \mathrm{span}\{\psi_+, \psi_-\} = \mathrm{span}\{ \begin{pmatrix} -1 \\ 1 \\ 0 \end{pmatrix} , \begin{pmatrix} -1 \\ 0 \\ 1 \end{pmatrix} \} . \end{aligned} \tag{2.6}$$

The shift operator is

$$U = \begin{pmatrix} 0 & 0 & 1 \\ 1 & 0 & 0 \\ 0 & 1 & 0 \end{pmatrix} , \tag{2.7}$$

with eigenvalues and -vectors[2] ($U\phi = \upsilon\phi$)

$$\begin{aligned} \upsilon_0 = 1 \qquad & \phi_0 = \begin{pmatrix} 1 \\ 1 \\ 1 \end{pmatrix} = \uparrow\uparrow\downarrow + \uparrow\downarrow\uparrow + \downarrow\uparrow\uparrow \\ \upsilon_\pm = \frac{-1 \pm \mathrm{i}\sqrt{3}}{2} = e^{\pm\frac{2\mathrm{i}\pi}{3}} \qquad & \phi_\pm = \begin{pmatrix} e^{\mp\frac{2\mathrm{i}\pi}{3}} \\ e^{\pm\frac{2\mathrm{i}\pi}{3}} \\ 1 \end{pmatrix} = e^{\mp\frac{2\mathrm{i}\pi}{3}}\uparrow\uparrow\downarrow + e^{\pm\frac{2\mathrm{i}\pi}{3}}\uparrow\downarrow\uparrow + \downarrow\uparrow\uparrow . \end{aligned} \tag{2.8}$$

We thus have a set of non-degenerate eigenvectors, $\psi_0 = \phi_0$ and $\phi_\pm$ that are simultaneous eigenstates of the Hamiltonian and the shift operator.

The whole space of length-three states form irreps of the $\mathfrak{su}(2)$ symmetry, for which the spin-flip operators play the role of raising and lowering operators. One multiplet is four-dimensional while the other two are two-dimensional[3], see figure 2.2. As H commutes with the spin-flip operators, we know that all states within a multiplet have the same energy.

We learned another lesson here: the Hamiltonian has simple, rational-valued entries, while its eigenvalues are more general algebraic numbers arising from the diagonalisation.

[2] The trained representation theorist might notice that U is just a representation of the permutation $(12...L)$ belonging to the cyclic group $\mathbb{Z}_L$. Its eigenvalues are simply the character of the one-dimensional irreps formed by the corresponding eigenstate on the group element $(12...L)$.

[3] On the level of Young diagrams, this is the statement $\square^{\otimes 3} = \square\square\square \oplus 2\,\begin{smallmatrix}\square\square\\\square\end{smallmatrix}$ which is easily verified using characters.

$$\uparrow\uparrow\uparrow \quad \rightleftharpoons \quad \uparrow\uparrow\downarrow + \uparrow\downarrow\uparrow + \downarrow\uparrow\uparrow \quad \rightleftharpoons \quad \uparrow\downarrow\downarrow + \downarrow\uparrow\downarrow + \downarrow\downarrow\uparrow \quad \rightleftharpoons \quad \downarrow\downarrow\downarrow$$

$$e^{\mp\frac{2\mathrm{i}\pi}{3}}\uparrow\uparrow\downarrow + e^{\pm\frac{2\mathrm{i}\pi}{3}}\uparrow\downarrow\uparrow + \downarrow\uparrow\uparrow \quad \rightleftharpoons \quad e^{\pm\frac{\mathrm{i}\pi}{3}}\downarrow\downarrow\uparrow + e^{\mp\frac{\mathrm{i}\pi}{3}}\downarrow\uparrow\downarrow - \uparrow\downarrow\downarrow$$

Figure 2.2: The $\mathfrak{su}(2)$ irreps formed by length-three spin chains.

2.1.2 The coordinate Bethe ansatz

We can proceed as above to find the energy spectrum of the Heisenberg spin chain. However, the matrices quickly grow in size, and the diagonalisation soon becomes practically impossible. A more sophisticated technique, the *coordinate Bethe ansatz*, was proposed by Hans Bethe in 1931 [35].

Ansatz for the eigenstates

Consider a spin chain of length L with M magnons. Bethe's approach is to write a plane-wave ansatz for the eigenfunctions of the Hamiltonian:

$$\Psi(p_1, p_2, ..., p_M) = \sum_{\sigma \in S_M} A_\sigma \; \psi(p_{\sigma(1)}, p_{\sigma(2)}, \dots, p_{\sigma(M)}) \,, \tag{2.9}$$

where the sum is over all $M!$ permutations in the permutation group S_M, and where ψ is the plane wave

$$\psi(p_1, p_2, ..., p_M) = \sum_{1 \le k_1 < k_2 < ... < k_M \le L} e^{\mathrm{i}\sum_{j=1}^{M} p_j k_j} \phi_{k_1,...,k_M} \,, \tag{2.10}$$

with $\phi_{k_1,...,k_M}$ being the spin chain configuration with magnons at the sites k_j, e.g. $\phi_{2,5} = \uparrow\downarrow\uparrow\uparrow\downarrow$ for $L = 5$. We can always choose a normalisation such that $A_{\mathrm{Id}} = 1$.

Periodicity of the chain is realised as the equivalence between labelling the last site in the chain as 0 or L, i.e.

$$\phi_{k_1,...,k_{M-1},L} = \phi_{0,k_1,...,k_{M-1}} \,. \tag{2.11}$$

One magnon

For a single magnon, $M = 1$, the ansatz (2.9) is quite simple:

$$\Psi(p) = e^{\mathrm{i}p}\phi_1 + e^{2\mathrm{i}p}\phi_2 + \ldots + e^{L\mathrm{i}p}\phi_L \,. \tag{2.12}$$

Periodicity (2.11) means that we could have replaced the last term by $e^{0\cdot\mathrm{i}p}\phi_0$. This results in a quantisation condition,

$$e^{\mathrm{i}pL} = 1 \,. \tag{2.13}$$

We can interpret p as a momentum of the magnon. Indeed, applying the shift operator is a discrete analog of a translation, and on the one-magnon state it gives

$$U\,\Psi(p) = e^{\mathbb{i}p}\,\Psi(p)\,, \tag{2.14}$$

by using the quantisation (2.13).

Applying the Hamiltonian to the wavefunction (2.12) reveals that it is exactly an eigenstate when the momentum quantisation (2.13) is satisfied. Its eigenvalue is given by

$$H\,\Psi(p) \;\;=\;\; \big(2-2\cos(p)\big)\,\Psi(p)\,. \tag{2.15}$$

Two magnons

For more magnons, we need to fix the amplitudes A_σ. Consider the case of two magnons. The plane wave $\psi(p_1,p_2)$ is not an eigenstate of H, but it turns out that the choice[4]

$$A_{(12)} = -\frac{1-2e^{\mathbb{i}p_2}+e^{\mathbb{i}(p_1+p_2)}}{1-2e^{\mathbb{i}p_1}+e^{\mathbb{i}(p_1+p_2)}} \tag{2.16}$$

takes care of the off-diagonal terms and ensures that $\Psi(p_1,p_2)$ is an eigenstate with eigenvalue $E(p_1)+E(p_2)$, where $E(p)\equiv 2-2\cos(p)$ as in (2.15). At this stage, it is convenient to make a change of variables from p to a rapidity u defined through

$$u = \frac{1}{2}\cot\left(\frac{p}{2}\right) \quad\Leftrightarrow\quad e^{\mathbb{i}p} = \frac{u+\frac{\mathbb{i}}{2}}{u-\frac{\mathbb{i}}{2}}\,. \tag{2.17}$$

In terms of u the amplitude $A_{(12)}$ takes a simple form. In fact, we will rename it $\mathcal{S}_{12}\equiv A_{(12)}$ and let it define a function $\mathcal{S}_{ab}$, through

$$\mathcal{S}_{ab} = \frac{u_a-u_b-\mathbb{i}}{u_a-u_b+\mathbb{i}}\,. \tag{2.18}$$

Note the property $\mathcal{S}_{ab}\mathcal{S}_{ba}=1$. We will refer to $\mathcal{S}$ as a *scattering matrix* or *S-matrix*. Imposing periodicity (2.11) on the wavefunction $\Psi(p_1,p_2)$ leads to the constraints

$$e^{\mathbb{i}p_1L} = \mathcal{S}_{12}\,, \qquad e^{\mathbb{i}p_2L} = \mathcal{S}_{21}\,. \tag{2.19}$$

M magnons

Any element of the symmetric group S_M can be split into elementary permutations of neighbouring labels, e.g. $(123)=[13][12]$. For arbitrary magnon number, the amplitudes in (2.9) turn out to have the factorised form

$$A_\sigma = A_{[a_1b_1][a_2b_2]\ldots[a_nb_n]} = \prod_{j=1}^{n}\mathcal{S}_{a_jb_j}\,. \tag{2.20}$$

[4] We here use the standard cycle notation to label permutations, see e.g. [23], where a permutation $\begin{pmatrix}1 & 2 & \ldots & n\\ \sigma(1) & \sigma(2) & \ldots & \sigma(n)\end{pmatrix}$ is written in terms of its closed cycles e.g. $\begin{pmatrix}1&2&3&4&5&6\\3&6&4&1&5&2\end{pmatrix}=(134)(26)$.

The energies of the states are simply $E = \sum_{j=1}^{M} E(p_j)$. An important point here is that the decomposition of a permutation into elementary permutations is ambiguous. The first appearance arises in the three-magnon wavefunction, where $A_{(13)}$ can be written in two ways, since $(13) = [12][13][23] = [23][13][12]$. In order for the amplitudes (2.20) in the Bethe wavefunction to be unambiguous, $\mathcal{S}_{ab}$ must satisfy the *Yang-Baxter equation*,

$$\mathcal{S}_{12}\mathcal{S}_{13}\mathcal{S}_{23} = \mathcal{S}_{23}\mathcal{S}_{13}\mathcal{S}_{12}\,, \tag{2.21}$$

and (2.18) trivially does.

Periodicity of the wavefunction (2.9) in general leads to M constraints of the form

$$e^{\mathrm{i}p_j L} = \prod_{k=1,\, k\neq j}^{M} S_{kj}\,, \tag{2.22}$$

which in terms of u read

$$\left(\frac{u_j + \frac{\mathrm{i}}{2}}{u_j - \frac{\mathrm{i}}{2}}\right)^L = -\prod_{k=1}^{M} \frac{u_j - u_k + \mathrm{i}}{u_j - u_k - \mathrm{i}}\,. \tag{2.23}$$

These are the famous $\mathfrak{su}(2)$ *Bethe equations*. In practice, these algebraic equations are rather hard to solve, but for now we will accept them as a beautiful solution to the spectral problem of the Heisenberg spin chain. The *Bethe roots* u_j determine the momentum and energy eigenvalues through

$$e^{\mathrm{i}p_{\text{total}}} = \sum_{j=1}^{M} \frac{u_j + \frac{\mathrm{i}}{2}}{u_j - \frac{\mathrm{i}}{2}}\,, \qquad E = \sum_{j=1}^{M} 2 - 2\cos(p_j) = \sum_{j=1}^{M} \frac{1}{u_j^2 + \frac{1}{4}}\,. \tag{2.24}$$

Example: $L = 3$, $M = 1$

Consider again the example $L = 3$ and $M = 1$. There is just one Bethe equation (2.23) on a single root, $(u + \frac{\mathrm{i}}{2})^3 = (u - \frac{\mathrm{i}}{2})^3$. This quadratic equation has the two solutions $u = \pm\frac{1}{2\sqrt{3}}$, both corresponding to $E = 3$ via (2.24). This matches two of the eigenstates (2.8) but what happened to the eigenstate with $E = 0$? Recall that this state was part of a four-dimensional multiplet, and that it was not a HWS (the corresponding HWS is either $\uparrow\uparrow\uparrow$ or $\downarrow\downarrow\downarrow$ depending on definition). It is clear from (2.24) that $E = 0$ corresponds to $u = \infty$. This is a general feature of descendants: their Bethe roots diverge. A regular solution will appear only in the Bethe equations where M correspond to the HWS in the multiplet.

2.2 Algebraic Bethe ansatz

We have seen how to reduce the problem of finding the energy spectrum of the Heisenberg spin chain to solving a set of algebraic equations, but why do we call it integrable? The

Heisenberg spin chain belongs to a family of models that fit into the framework of the *quantum inverse scattering method* or *algebraic Bethe ansatz*. The classic reference on this topic is [36]. A clear and basic review is given in [37]. The review [38] gives a nice overview with emphasis on the aspects relevant to the discussion here.

The algebraic Bethe ansatz deals with models where the configuration space is a tensor product, $\mathcal{H} = \mathcal{H}_1 \otimes \cdots \otimes \mathcal{H}_L$. For the Heisenberg spin chain, each site is a two-dimensional vector space $\mathcal{H}_j = \mathbb{C}^2$, so a spin chain of length L corresponds to $\mathcal{H} = (\mathbb{C}^2)^{\otimes L}$. We will refer to this vector space as *physical space*. In addition, we will introduce a number of *auxiliary spaces*, $\mathcal{A}_j$. The algebraic Bethe ansatz involves a variety of operators that act on these spaces, see table 2.1.

Name	Symbol	Acts (non-trivially) in
Transfer matrix	$\mathcal{T}$	$\mathcal{H}$
Monodromy matrix	$\mathcal{M}_j$	$\mathcal{H} \otimes \mathcal{A}_j$
R-matrix	$\mathcal{R}_{jk}$	$\mathcal{A}_j \otimes \mathcal{A}_k$
Lax operator	$\mathcal{L}_{j,k}$	$\mathcal{H}_j \otimes \mathcal{A}_k$

Table 2.1: Overview of operators in the algebraic Bethe ansatz.

The transfer and monodromy matrix

The key feature of an integrable model is an infinite set of commuting operators $\mathcal{O}_n$, including the Hamiltonian. The idea of the algebraic Bethe ansatz is to package these operators into a generating function, the *transfer matrix*,

$$\mathcal{T}(u) = e^{\sum_{n=0}^{\infty} \frac{(u-\frac{\mathrm{i}}{2})^n}{n!} \mathcal{O}_n}\,, \qquad \mathcal{O}_n = \frac{\mathrm{d}^n}{\mathrm{d}u^n} \ln \mathcal{T}(u)\bigg|_{u=\frac{\mathrm{i}}{2}}\,. \tag{2.25}$$

The transfer matrix is a function of a *spectral parameter* u, and it acts on the whole physical space $\mathcal{H}$.

The transfer matrix is related to a *monodromy matrix* that likewise acts in the whole physical space, but also in one auxiliary space. The transfer matrix is the trace of the monodromy matrix over this auxiliary space:

$$\mathcal{T}(u) = \mathrm{Tr}_{\mathcal{A}_j}\, \mathcal{M}_j(u)\,. \tag{2.26}$$

The R-matrix and the Yang-Baxter equation

From the definition of the transfer matrix, it is a requirement that it commutes with itself at arbitrary values of the spectral parameter, i.e.

$$[\mathcal{T}(u), \mathcal{T}(v)] = 0\,. \tag{2.27}$$

Consider now the tensor product of the physical space and a number of auxiliary spaces, $\mathcal{H} \otimes \mathcal{A}_1 \otimes \mathcal{A}_2 \otimes \mathcal{A}_3 \otimes \cdots$. Due to the cyclicity of the trace, we should then have

$$\mathrm{Tr}_{\mathcal{A}_1 \otimes \mathcal{A}_2} \left(\mathcal{M}_1(u) \mathcal{M}_2(v) \right) = \mathrm{Tr}_{\mathcal{A}_1 \otimes \mathcal{A}_2} \left(\mathcal{M}_2(v) \mathcal{M}_1(u) \right) \tag{2.28}$$

which is true if the arguments of the traces are related by a similarity transformation in the auxiliary spaces $\mathcal{A}_1 \otimes \mathcal{A}_2$ given by some invertible matrix $\mathcal{R}_{12}$:

$$\mathcal{R}_{12}(u,v) \mathcal{M}_1(u) \mathcal{M}_2(v) = \mathcal{M}_2(v) \mathcal{M}_1(u) \mathcal{R}_{12}(u,v) \,. \tag{2.29}$$

This *R-matrix* should have some nice properties. If we try to use $\mathcal{R}$ to relate the product $\mathcal{M}_1(u)\mathcal{M}_2(v)\mathcal{M}_3(w)$ to $\mathcal{M}_3(w)\mathcal{M}_2(v)\mathcal{M}_1(u)$, we see that there are two ways to do it[5]. A sufficient condition for the equivalence of the two possibilities is that $\mathcal{R}$ satisfies the Yang-Baxter equation

$$\mathcal{R}_{23}(v,w) \mathcal{R}_{13}(v,w) \mathcal{R}_{12}(u,v) = \mathcal{R}_{12}(u,v) \mathcal{R}_{13}(v,w) \mathcal{R}_{23}(v,w) \,. \tag{2.30}$$

It is possible to choose $\mathcal{R}$ such that

$$\mathcal{R}_{12}(u,v) \mathcal{R}_{21}(v,u) = 1 \,. \tag{2.31}$$

We will look at R-matrices with these properties.

The R-matrix as the building block

The R-matrix is the fundamental object in the algebraic Bethe ansatz, and it encodes the information about the model.

For simplicity[6], let the auxiliary space be $\mathcal{A} = \mathbb{C}^2$. On $\mathcal{A}$ the monodromy matrix is then a 2×2 matrix which we can write as

$$\mathcal{M}(u) \equiv \begin{pmatrix} A(u) & B(u) \\ C(u) & D(u) \end{pmatrix} , \tag{2.32}$$

where A, B, C and D are operators acting on $\mathcal{H}$. By (2.26) the transfer matrix is $\mathcal{T}(u) = A(u) + D(u)$.

The R-matrix is a 4×4 matrix on $\mathcal{A}^{\otimes 2}$. We can now start looking for solutions that satisfy (2.30). The structure of the R-matrix can be constrained by the symmetry which

[5] In the same way that we had two ways to decompose the permutation (13) in section 2.1.2.

[6] We could equally well have chosen a different representation in the auxiliary space. This would lead to a different transfer matrix, but generating the same information about the model. It turns out that the family of such transfer matrices satisfy a set of functional relations referred to as a T-system. We will encounter this system in chapter 3.

we want it to respect. For instance, if we want to preserve the magnon number and not give a preference to one type of spin, then the most general ansatz for $\mathcal{R}$ has the form

$$\mathcal{R}_{jk}(u,v) = \begin{pmatrix} \alpha(u,v) & 0 & 0 & 0 \\ 0 & \beta(u,v) & \gamma(u,v) & 0 \\ 0 & \gamma(u,v) & \beta(u,v) & 0 \\ 0 & 0 & 0 & \alpha(u,v) \end{pmatrix}, \tag{2.33}$$

on the basis $e_i = \{\uparrow\uparrow, \uparrow\downarrow, \downarrow\uparrow, \downarrow\downarrow\}_i$. If we plug such an ansatz into (2.31) and (2.30) we get constraints on its entries. Likewise, the relation (2.29) would result in bilinear relations between A, B, C and D with the entries of $\mathcal{R}$ as coefficients.

Eigenstates of the transfer matrix and Bethe equations

Our goal is to study the eigenstates of $\mathcal{T} = A + D$. Assume that $\mathcal{H}$ contains a state $|0\rangle$ that is annihilated by C and is a simultaneous eigenstate of A and D, i.e.

$$A(u)|0\rangle = a(u)|0\rangle\,, \quad D(u)|0\rangle = d(u)|0\rangle\,, \quad C(u)|0\rangle = 0\,. \tag{2.34}$$

Acting with B creates further states

$$\left(\prod_{j=1}^{M} B(u_j)\right)|0\rangle \equiv |u_1, u_2, \ldots, u_M\rangle\,. \tag{2.35}$$

We would like these states to also be eigenstates of $\mathcal{T} = A + D$. If we act on the states by A and D, we can use the bilinear relations derived from (2.29) to commute A and D through the B's. This will produce cross-terms different from (2.35) unless the eigenvalues $a(u)$ and $d(u)$ satisfy very particular constraints that are strongly dependent on the entries of the R-matrix. These are a generalised version of Bethe equations.

2.2.1 The Heisenberg spin chain

To go any further, we need to specify the R-matrix and also the monodromy matrix. We will now axiomatically state these constructions for the Heisenberg spin chain and demonstrate that they reproduce the wanted model.

The R-matrix, $\mathcal{R}(u,v) = \mathcal{R}(u-v)$, acting on $\mathcal{A}_j \otimes \mathcal{A}_k$ is given by

$$\mathcal{R}_{jk}(u) = u\,\mathbb{I}_{jk} + \mathbb{i}\,\mathbb{P}_{jk} = u \begin{pmatrix} 1 & 0 & 0 & 0 \\ 0 & 1 & 0 & 0 \\ 0 & 0 & 1 & 0 \\ 0 & 0 & 0 & 1 \end{pmatrix} + \mathbb{i} \begin{pmatrix} 1 & 0 & 0 & 0 \\ 0 & 0 & 1 & 0 \\ 0 & 1 & 0 & 0 \\ 0 & 0 & 0 & 1 \end{pmatrix}, \tag{2.36}$$

where $\mathbb{P}_{jk}$ permutes the two auxiliary spaces. Recall the construction of $\mathfrak{su}(2)$ generators in terms of two Jordan-Schwinger oscillators $\mathbf{a}_1$ and $\mathbf{a}_2$ in section 1.1.3. Each space $\mathbb{C}^2$ is

spanned by $\mathbf{a}_1^\dagger|0\rangle$ and $\mathbf{a}_2^\dagger|0\rangle$. We can write the R-matrix (2.36) as

$$\mathcal{R}_{jk}(u) = u + \mathbb{i}\left(\mathbf{a}^\dagger_{1,j}\mathbf{a}_{1,j}\mathbf{a}^\dagger_{1,k}\mathbf{a}_{1,k} + \mathbf{a}^\dagger_{1,j}\mathbf{a}_{2,j}\mathbf{a}^\dagger_{2,k}\mathbf{a}_{1,k} + \mathbf{a}^\dagger_{2,j}\mathbf{a}_{1,j}\mathbf{a}^\dagger_{1,k}\mathbf{a}_{2,k} + \mathbf{a}^\dagger_{2,j}\mathbf{a}_{2,j}\mathbf{a}^\dagger_{2,k}\mathbf{a}_{2,k}\right), \tag{2.37}$$

where the extra subscript denotes which space the oscillator acts in. We can also write this as a 2×2 matrix on one of the spaces[7]

$$\mathcal{R}_{jk}(u) = \begin{pmatrix} u + \mathbb{i}\,\mathbf{a}^\dagger_{1,j}\mathbf{a}_{1,j} & \mathbb{i}\,\mathbf{a}^\dagger_{2,j}\mathbf{a}_{1,j} \\ \mathbb{i}\,\mathbf{a}^\dagger_{1,j}\mathbf{a}_{2,j} & u + \mathbb{i}\,\mathbf{a}^\dagger_{2,j}\mathbf{a}_{2,j} \end{pmatrix}_{(k)} = (j \leftrightarrow k)\,. \tag{2.38}$$

Note that this can be written even more compactly as e.g. $(\mathcal{R}_{jk})_{ab} = u\,1_{ab} + \mathbb{i}\,E^\dagger_{ab,j}$, where E_{ab} are the $\mathfrak{u}(2)$ generators as in (1.16).

The monodromy matrix is constructed via the introduction of a Lax matrix $\mathcal{L}_{j,k}$ that, up to a shift $u \to u - \frac{\mathbb{i}}{2}$, is really just the R-matrix acting on one physical space $\mathcal{H}_j$ and one auxiliary space $\mathcal{A}_k$,

$$\mathcal{L}_{j,k}(u) = \begin{pmatrix} u - \frac{\mathbb{i}}{2} + \mathbb{i}\,\mathbf{a}^\dagger_{1,j}\mathbf{a}_{1,j} & \mathbb{i}\,\mathbf{a}^\dagger_{2,j}\mathbf{a}_{1,j} \\ \mathbb{i}\,\mathbf{a}^\dagger_{1,j}\mathbf{a}_{2,j} & u - \frac{\mathbb{i}}{2} + \mathbb{i}\,\mathbf{a}^\dagger_{2,j}\mathbf{a}_{2,j} \end{pmatrix}_{(k)}. \tag{2.39}$$

A monodromy matrix satisfying (2.29) can then be built as

$$\mathcal{M}_j(u) = \mathcal{L}_{1,j}(u)\mathcal{L}_{2,j}(u)\cdots\mathcal{L}_{L-1,j}(u)\mathcal{L}_{L,j}(u)\,. \tag{2.40}$$

As argued above, the transfer matrix constructed from (2.36) and (2.40) generates an infinite family of commuting operators, cf. (2.25), of which the shift operator (2.2) and the Hamiltonian (2.1) can be constructed as linear combinations. The shift operator is

$$U \propto \mathcal{T}(\tfrac{\mathbb{i}}{2})\,, \tag{2.41}$$

and the Hamiltonian is

$$H \propto L\,\mathbb{I} - \mathbb{i}\,\frac{\mathrm{d}}{\mathrm{d}u}\ln\mathcal{T}(u)\Big|_{u=\frac{\mathbb{i}}{2}} = L\,\mathbb{I} - \mathbb{i}\,\mathcal{T}(u)^{-1}\frac{\mathrm{d}}{\mathrm{d}u}\mathcal{T}(u)\Big|_{u=\frac{\mathbb{i}}{2}}. \tag{2.42}$$

The derivation is elementary, but a bit tedious unless one uses a graphical notation, and we refer to [36] for the details. Instead we demonstrate the construction on a simple example.

Example: $L = 3$**,** $M = 1$

For length three, i.e. $\mathcal{H} = (\mathbb{C}^2)^{\otimes 3}$, the transfer matrix is

$$\begin{aligned}\mathcal{T}(u) &= \mathrm{Tr}_{\mathcal{A}_k}(\mathcal{M}_k) = \mathrm{Tr}_{\mathcal{A}_k}(\mathcal{L}_{1,k}\mathcal{L}_{2,k}\mathcal{L}_{3,k}) \\ &= \langle 0|\mathbf{a}_{1,k}\,\mathcal{M}_k\,\mathbf{a}^\dagger_{1,k}|0\rangle + \langle 0|\mathbf{a}_{2,k}\,\mathcal{M}_k\,\mathbf{a}^\dagger_{2,k}|0\rangle\,.\end{aligned} \tag{2.43}$$

[7] We use basis vectors $\begin{pmatrix}1\\0\end{pmatrix}_k = \mathbf{a}^\dagger_{1,k}|0\rangle_k$ and $\begin{pmatrix}0\\1\end{pmatrix}_k = \mathbf{a}^\dagger_{2,k}|0\rangle_k$.

Explicitly, the transfer matrix is

$$\begin{aligned}
\mathcal{T}(u) &= \begin{pmatrix}1 & 0\end{pmatrix} \prod_{j\in\{3,2,1\}} \begin{pmatrix} u-\frac{\mathbb{i}}{2}+\mathbb{i}\, n_{\mathbf{a}_{1,j}} & \mathbb{i}\, \mathbf{a}^\dagger_{2,j}\mathbf{a}_{1,j} \\ \mathbb{i}\, \mathbf{a}^\dagger_{1,j}\mathbf{a}_{2,j} & u-\frac{\mathbb{i}}{2}+\mathbb{i}\, n_{\mathbf{a}_{2,j}} \end{pmatrix} \begin{pmatrix}1\\0\end{pmatrix} \\
&\quad + \begin{pmatrix}0 & 1\end{pmatrix} \prod_{j\in\{3,2,1\}} \begin{pmatrix} u-\frac{\mathbb{i}}{2}+\mathbb{i}\, n_{\mathbf{a}_{1,j}} & \mathbb{i}\, \mathbf{a}^\dagger_{2,j}\mathbf{a}_{1,j} \\ \mathbb{i}\, \mathbf{a}^\dagger_{1,j}\mathbf{a}_{2,j} & u+\frac{\mathbb{i}}{2}-\mathbb{i}\, n_{\mathbf{a}_{2,j}} \end{pmatrix} \begin{pmatrix}0\\1\end{pmatrix} \\
&= 2u^3 - 3\mathbb{i}u^2 - \frac{3}{2}u + \frac{\mathbb{i}}{4} + \left(\mathbb{i}u^2 + u - \frac{\mathbb{i}}{4}\right) \sum_{\alpha=1}^{2}\sum_{j=1}^{3} n_{\mathbf{a}_{\alpha,j}} \\
&\quad - \left(u-\frac{\mathbb{i}}{2}\right) \sum_{\alpha=1}^{2} \sum_{1\le j<k\le 3} n_{\mathbf{a}_{\alpha,j}} n_{\mathbf{a}_{\alpha,k}} - \left(u-\frac{\mathbb{i}}{2}\right) \sum_{\substack{j,\,k=1\\ j\neq k}}^{3} \mathbf{a}^\dagger_{1,j}\mathbf{a}_{2,j}\mathbf{a}^\dagger_{2,k}\mathbf{a}_{1,k} \\
&\quad - \mathbb{i} \sum_{\alpha=1}^{2} n_{\mathbf{a}_{\alpha,1}} n_{\mathbf{a}_{\alpha,2}} n_{\mathbf{a}_{\alpha,3}} - \mathbb{i} \sum_{\alpha=1}^{2} \sum_{\sigma\in\mathbb{Z}_3} n_{\mathbf{a}_{\alpha,\sigma(1)}} \mathbf{a}^\dagger_{\alpha,\sigma(2)}\mathbf{a}_{\bar\alpha,\sigma(2)}\mathbf{a}^\dagger_{\bar\alpha,\sigma(3)}\mathbf{a}_{\alpha,\sigma(3)}\,,
\end{aligned} \tag{2.44}$$

where $\bar\alpha$ means the complement, e.g. $\bar 1 = 2$. Note that it is a polynomial of degree $L = 3$ in u. On the subspace

$$\begin{pmatrix}1\\0\\0\end{pmatrix} = \uparrow\uparrow\downarrow = \mathbf{a}^\dagger_{1,1}\mathbf{a}^\dagger_{1,2}\mathbf{a}^\dagger_{2,3}|0\rangle^{\otimes 3} \qquad \begin{pmatrix}0\\1\\0\end{pmatrix} = \uparrow\downarrow\uparrow \qquad \begin{pmatrix}0\\0\\1\end{pmatrix} = \downarrow\uparrow\uparrow \tag{2.45}$$

the transfer matrix is

$$\mathcal{T}(u) = \begin{pmatrix} 2u^3+\frac{u}{2} & -u+\frac{\mathbb{i}}{2} & -u-\frac{\mathbb{i}}{2} \\ -u-\frac{\mathbb{i}}{2} & 2u^3+\frac{u}{2} & -u+\frac{\mathbb{i}}{2} \\ -u+\frac{\mathbb{i}}{2} & -u-\frac{\mathbb{i}}{2} & 2u^3+\frac{u}{2} \end{pmatrix}. \tag{2.46}$$

Around $u = \frac{\mathbb{i}}{2}$ it behaves like

$$\mathcal{T}(u+\tfrac{\mathbb{i}}{2}) = -\begin{pmatrix}0&0&\mathbb{i}\\ \mathbb{i}&0&0\\0&\mathbb{i}&0\end{pmatrix} + u\begin{pmatrix}-1&-1&-1\\-1&-1&-1\\-1&-1&-1\end{pmatrix} + \mathcal{O}(u^2)\,, \tag{2.47}$$

and through (2.41) and (2.42) we get

$$U = \mathbb{i}\,\mathcal{T}(\tfrac{\mathbb{i}}{2}) = \begin{pmatrix}0&0&1\\1&0&0\\0&1&0\end{pmatrix} \tag{2.48}$$

$$H = L\,\mathbb{I} - \mathbb{i}\mathcal{T}^{-1}(\tfrac{\mathbb{i}}{2})\mathcal{T}'(\tfrac{\mathbb{i}}{2}) = 3\begin{pmatrix}1&0&0\\0&1&0\\0&0&1\end{pmatrix} - \mathbb{i}\begin{pmatrix}0&\mathbb{i}&0\\0&0&\mathbb{i}\\\mathbb{i}&0&0\end{pmatrix}\begin{pmatrix}-1&-1&-1\\-1&-1&-1\\-1&-1&-1\end{pmatrix} = \begin{pmatrix}2&-1&-1\\-1&2&-1\\-1&-1&2\end{pmatrix},$$

which coincides with the Hamiltonian (2.5) and shift operator (2.7).

2.3 Q-operators

We have now seen three ways of finding the spectrum of the Heisenberg spin chain, each one going one layer deeper in the underlying mathematical structure. We will now try to go even a step further. The idea is roughly to factorise the Lax operator (2.39) and use the factors as building blocks for transfer matrix-like objects called Q-operators. Q-operators were first introduced for the eight-vertex model [39], and only recently constructed for the Heisenberg spin chain [40]. In constrast to the eight-vertex model, the construction of Q-operators for the Heisenberg spin chain requires the introduction of a regulator.

2.3.1 Introducing a twist

We can introduce a *twist*, which is a parameter that breaks the off-diagonal symmetries, cf. (1.16), of the spin chain model. In the Heisenberg spin chain, we can do this by modifying the periodicity condition (2.11) to

$$\phi_{k_1,\dots,k_{M-1},L} = \mathsf{x}^2\, \phi_{0,k_1,\dots,k_{M-1}}\,. \tag{2.49}$$

where $\mathsf{x} = e^{\mathbb{i}\Phi}$ is a pure phase. In turn, this modifies the Bethe equations (2.23) to

$$\left(\frac{u_j + \frac{\mathbb{i}}{2}}{u_j - \frac{\mathbb{i}}{2}}\right)^L = -\frac{1}{\mathsf{x}^2}\prod_{k=1}^{M}\frac{u_j - u_k + \mathbb{i}}{u_j - u_k - \mathbb{i}}\,. \tag{2.50}$$

In contrast to the untwisted case, all eigenstates will appear as regular solutions of these equations. We have broken the symmetry, so there are no descendants. For $L = 3$ and $M = 1$ we now have a cubic equation with solutions

$$u = -\frac{\mathbb{i}}{2} + \frac{\mathbb{i}}{1 - e^{\frac{2\pi\mathbb{i}n}{3}}\mathsf{x}^{\frac{1}{3}}}\,, \qquad n = 0, 1, 2\,. \tag{2.51}$$

Note that in the limit $\mathsf{x} \to 1$ we recover the roots $u = \pm\frac{1}{2\sqrt{3}}$ and $u \to \infty$.

In the algebraic Bethe ansatz set-up, the twist appears in the monodromy matrix (2.40) which is modified to

$$\mathcal{M}_j(u) = \begin{pmatrix} \mathsf{x} & 0 \\ 0 & \frac{1}{\mathsf{x}} \end{pmatrix}_j \mathcal{L}_{1,j}(u)\mathcal{L}_{2,j}(u)\cdots\mathcal{L}_{L-1,j}(u)\mathcal{L}_{L,j}(u)\,. \tag{2.52}$$

2.3.2 The construction

The construction of Q-operators for the Heisenberg spin chain [40] is analogous to the construction of transfer matrices. The Q-operators are built from Lax operators that are in some sense factorisations of the Lax operators of a generalised version of the transfer matrix, see [40]. The important difference is that for the Q-operators, the auxiliary space is infinite-dimensional. An overview of the operators appearing in the construction is given in table 2.2.

Name	Symbol	Acts in
Q-operator	$\mathcal{Q}_J$	$\mathcal{H}$
Lax operator	$\mathcal{L}_J^{(j)}$	$\mathcal{H}_j \otimes \mathcal{A}$

Table 2.2: Overview of operators in the Q-operator construction.

The auxiliary space

The auxiliary space is not a representation of the $\mathfrak{su}(2)$ symmetry algebra, as it was the case for transfer matrices, but instead a Fock space generated by a set of oscillators $\boldsymbol{\xi}_{a\bar{a}}$ with $a \neq \bar{a} \in \{1,2\}$ satisfying the algebra

$$[\boldsymbol{\xi}_{a\bar{a}}, \bar{\boldsymbol{\xi}}_{b\bar{b}}] = \delta_{ab}\delta_{\bar{a}\bar{b}}\,. \tag{2.53}$$

$\bar{\boldsymbol{\xi}}_{a\bar{a}}$ and $\boldsymbol{\xi}_{a\bar{a}}$ form a set of raising and lowering operators acting in a separate space $\mathcal{A}_{a\bar{a}}$ with vacuum $\boldsymbol{\xi}_{a\bar{a}}|0\rangle_{a\bar{a}} = 0$. The auxiliary space is formed by a tensor product of these individual oscillator spaces,

$$\langle k_1, k_2| \equiv \frac{1}{\sqrt{k_1!k_2!}}{}_{12}\langle 0|\boldsymbol{\xi}_{12}^{k_1} \otimes {}_{21}\langle 0|\boldsymbol{\xi}_{21}^{k_2}\,, \qquad |k_1, k_2\rangle \equiv \frac{1}{\sqrt{k_1!k_2!}}\bar{\boldsymbol{\xi}}_{12}^{k_1}|0\rangle_{12} \otimes \bar{\boldsymbol{\xi}}_{21}^{k_2}|0\rangle_{21}\,. \tag{2.54}$$

A trace over this space is then formally the sum

$$\mathrm{Tr}_{\mathcal{A}}(f) = \sum_{k_1,k_2=0}^{\infty} \langle k_1, k_2|f|k_1, k_2\rangle\,. \tag{2.55}$$

As we will see below, the twist is needed in order to make such sums convergent. We denote number operators on the individual spaces $|0\rangle_{a\bar{a}}$ by $\mathbf{N}_{a\bar{a}} \equiv \bar{\boldsymbol{\xi}}_{a\bar{a}}\boldsymbol{\xi}_{a\bar{a}}$.

Lax operators

We introduce a set of Lax operators labelled by a set $J \subset \{1,2\}$, i.e. four in total: $\mathcal{L}_\emptyset$, $\mathcal{L}_{\{1\}}$, $\mathcal{L}_{\{2\}}$ and $\mathcal{L}_{\{1,2\}}$. With a particular choice of normalisation, they can be written as [40]

$$\mathcal{L}_J(u) = e^{\sum_{j\in J,\bar{\jmath}\in\bar{J}} \bar{\boldsymbol{\xi}}_{j\bar{\jmath}}\mathbf{a}_j^\dagger\mathbf{a}_j} \left[\mathbb{i}u - \tfrac{|J|}{2}\right]_{\sum_{\bar{\jmath}\in\bar{J}} n_{\mathbf{a}_{\bar{\jmath}}}} e^{-\sum_{j\in J,\bar{\jmath}\in\bar{J}} \boldsymbol{\xi}_{j\bar{\jmath}}\mathbf{a}_j^\dagger\mathbf{a}_{\bar{\jmath}}}\,, \tag{2.56}$$

where the oscillators $\mathbf{a}$ act in the physical space which is in the fundamental representation of $\mathfrak{su}(2)$, $|J|$ is the numbers of elements in the set J, and where we introduced the Pochhammer symbol

$$[n]_m = n(n+1)\cdots(n+m-1) = \frac{\Gamma(n+m)}{\Gamma(n)}\,. \tag{2.57}$$

Using that $n_{\mathbf{a}_1} + n_{\mathbf{a}_2} = C = 1$ for the fundamental representation of $\mathfrak{su}(2)$, the four explicit Lax operators are

$$\mathcal{L}_{\emptyset} = u \tag{2.58a}$$
$$\mathcal{L}_{\{1\}} = e^{\bar{\boldsymbol{\xi}}_{12}\mathbf{a}_2^\dagger\mathbf{a}_1}\left[\mathbb{i}u - \tfrac{1}{2}\right]_{n_{\mathbf{a}_2}} e^{-\boldsymbol{\xi}_{12}\mathbf{a}_1^\dagger\mathbf{a}_2} \tag{2.58b}$$
$$\mathcal{L}_{\{2\}} = e^{\bar{\boldsymbol{\xi}}_{21}\mathbf{a}_1^\dagger\mathbf{a}_2}\left[\mathbb{i}u - \tfrac{1}{2}\right]_{n_{\mathbf{a}_1}} e^{-\boldsymbol{\xi}_{21}\mathbf{a}_2^\dagger\mathbf{a}_1} \tag{2.58c}$$
$$\mathcal{L}_{\{1,2\}} = 1\,. \tag{2.58d}$$

Constructing the Q-operators

The Q-operators are defined by [40]

$$\mathcal{Q}_J(u) = \left(\prod_{j\in J} \mathsf{x}_j^{-\mathbb{i}\,u}\right) \widehat{\mathrm{Tr}}_{\mathcal{A}}\left(\mathcal{L}_J^{(1)}\cdots\mathcal{L}_J^{(L)}\right), \tag{2.59}$$

where $\mathsf{x}_1 = \mathsf{x}$ and $\mathsf{x}_2 = \frac{1}{\mathsf{x}}$, $\mathcal{L}_J^{(j)}$ acts on $\mathcal{H}_j$, and where $\widehat{\mathrm{Tr}}_{\mathcal{A}}$ denotes the normalised trace

$$\widehat{\mathrm{Tr}}_{\mathcal{A}}(f) = \frac{\mathrm{Tr}_{\mathcal{A}}\left(\mathsf{x}^{2\,\mathbf{N}_{12}}\mathsf{x}^{-2\,\mathbf{N}_{21}} f\right)}{\mathrm{Tr}_{\mathcal{A}}\left(\mathsf{x}^{2\,\mathbf{N}_{12}}\mathsf{x}^{-2\,\mathbf{N}_{21}}\right)}\,. \tag{2.60}$$

The normalisation is

$$\mathrm{Tr}_{\mathcal{A}}\left(\mathsf{x}^{2\,\mathbf{N}_{12}}\mathsf{x}^{-2\,\mathbf{N}_{21}}\right) = \sum_{k_1=0}^{\infty}\mathsf{x}^{2\,k_1}\sum_{k_2=0}^{\infty}\mathsf{x}^{-2\,k_2} = \frac{1}{1-\mathsf{x}^2}\frac{1}{1-\mathsf{x}^{-2}} = \frac{1}{2-\mathsf{x}^2-\mathsf{x}^{-2}}\,. \tag{2.61}$$

Note that we have to regularise the sums by setting $\mathsf{x} = e^{\mathbb{i}\Phi-\epsilon}$ such that $|\mathsf{x}| < 1$, see the discussion in [41].

Functional relations

It can be shown [40] that the Q-operators satisfy the QQ-relation[8]

$$\mathcal{Q}_{\emptyset}(u)\mathcal{Q}_{\{1,2\}}(u) \propto \mathcal{Q}_{\{1\}}(u+\tfrac{\mathbb{i}}{2})\mathcal{Q}_{\{2\}}(u-\tfrac{\mathbb{i}}{2}) - \mathcal{Q}_{\{1\}}(u-\tfrac{\mathbb{i}}{2})\mathcal{Q}_{\{2\}}(u+\tfrac{\mathbb{i}}{2})\,. \tag{2.62}$$

They can furthermore be used to construct the transfer matrix, defined as the trace of the twisted monodromy matrix (2.52) over $\mathcal{A} = \mathbb{C}^2$, through

$$\mathcal{T}(u) \propto \mathcal{Q}_{\{1\}}(u+\mathbb{i})\mathcal{Q}_{\{2\}}(u-\mathbb{i}) - \mathcal{Q}_{\{1\}}(u-\mathbb{i})\mathcal{Q}_{\{2\}}(u+\mathbb{i})\,, \tag{2.63}$$

and as a consequence, they satisfy the *Baxter equation* [39],

$$\mathcal{T}(u)\mathcal{Q}_{\{j\}}(u) = \left(u+\tfrac{\mathbb{i}}{2}\right)^L \mathcal{Q}_{\{j\}}(u-\mathbb{i}) + \left(u-\tfrac{\mathbb{i}}{2}\right)^L \mathcal{Q}_{\{j\}}(u+\mathbb{i})\,. \tag{2.64}$$

[8] Note that we could equally well have defined power-like Q-operators without the exponential prefactor in (2.59). The QQ-relation (2.62) would then be modified by factors of the twist-parameter x.

Q-operators and Bethe roots

From the above construction, it is clear that, up to an overall exponential prefactor, the Q-operators are polynomial in u. Denote an eigenvalue of a Q-operator $\mathcal{Q}_J$ by Q_J. The zeros of these polynomials turn out to coincide with Bethe roots, i.e. the solutions of the Bethe equations (2.50). More concretely,

$$Q_{\{1\}}(u) \propto \mathsf{x}^{-\mathbb{i}u} \prod_{j=1}^{M} (u - u_j)\,, \tag{2.65}$$

while also $Q_{\{2\}} \propto \mathsf{x}^{+\mathbb{i}u} \prod_{j=1}^{L-M} (u - v_j)$, where v_j is another set of roots of a Bethe equation (2.50) with $\mathsf{x} \to \frac{1}{\mathsf{x}}$. The Bethe equation (2.50) can be derived by considering the QQ-relation (2.62) at zeros of $Q_{\{1\}}$. Let us see that this is indeed the case in our usual example.

2.3.3 Example: $L = 3$, $M = 1$

We want to evaluate the matrix elements of Q-operators on the subspace of states with $L = 3$ and $M = 1$. So we have to evaluate the trace over the auxiliary space and consider the action on our basis in the physical space. But we can in fact do it in the reverse order, since the Lax operators all act on different factors of the physical space.

Magnon block matrix elements of Lax operators

As before, each physical space is a two-dimensional representation formed by $\binom{1}{0}_j = \mathbf{a}_1^\dagger|0\rangle_j = |\uparrow\rangle$ and $\binom{0}{1}_j = \mathbf{a}_2^\dagger|0\rangle_j = |\downarrow\rangle$. On this basis, the Lax operators (2.58) act as

$$\begin{aligned}
\mathcal{L}^{(j)}_{\emptyset} &= \begin{pmatrix} \mathbb{i}u & 0 \\ 0 & \mathbb{i}u \end{pmatrix}_j & \mathcal{L}^{(j)}_{\{1\}} &= \begin{pmatrix} 1 & -\boldsymbol{\xi}_{12} \\ \bar{\boldsymbol{\xi}}_{12} & \mathbb{i}u - \frac{1}{2} - \mathbf{N}_{12} \end{pmatrix}_j \\
\mathcal{L}^{(j)}_{\{2\}} &= \begin{pmatrix} \mathbb{i}u - \frac{1}{2} - \mathbf{N}_{21} & \bar{\boldsymbol{\xi}}_{21} \\ -\boldsymbol{\xi}_{21} & 1 \end{pmatrix}_j & \mathcal{L}^{(j)}_{\{1,2\}} &= \begin{pmatrix} 1 & 0 \\ 0 & 1 \end{pmatrix}_j .
\end{aligned} \tag{2.66}$$

Note that the exponentials, e.g. $e^{-\boldsymbol{\xi}_{21}\mathbf{a}_2^\dagger\mathbf{a}_1} = \sum_{n=0}^{\infty} \frac{1}{n!}(-\boldsymbol{\xi}_{21}\mathbf{a}_2^\dagger\mathbf{a}_1)^n$, immediately truncate due to the compactness of the space.

Tracing over the auxiliary space

Next, we have to evaluate the trace over the auxiliary space. We again work in the basis (2.45). We first pick the relevant terms from (2.66) and then take the trace, e.g.

$$\langle\uparrow\downarrow\uparrow|\mathcal{Q}_J|\uparrow\uparrow\downarrow\rangle = \left(\prod_{j\in J} \mathsf{x}_j^{-\mathbb{i}\,u}\right) \widehat{\mathrm{Tr}}_{\mathcal{A}} \left(\langle\uparrow|\mathcal{L}_J^{(1)}|\uparrow\rangle\langle\downarrow|\mathcal{L}_J^{(2)}|\uparrow\rangle\langle\uparrow|\mathcal{L}_J^{(3)}|\downarrow\rangle\right) . \tag{2.67}$$

We thus immediately get

$$\mathcal{Q}_{\emptyset} = \begin{pmatrix} -\mathbb{i}u^3 & 0 & 0 \\ 0 & -\mathbb{i}u^3 & 0 \\ 0 & 0 & -\mathbb{i}u^3 \end{pmatrix}, \qquad \mathcal{Q}_{\{1,2\}} = \begin{pmatrix} 1 & 0 & 0 \\ 0 & 1 & 0 \\ 0 & 0 & 1 \end{pmatrix}. \tag{2.68}$$

For the two non-trivial Q-operators, we have e.g.

$$\begin{aligned} \langle\uparrow\downarrow\uparrow|\mathcal{Q}_{\{2\}}|\uparrow\uparrow\downarrow\rangle &= \mathsf{x}^{\mathbb{i}\,u}\,\widehat{\mathrm{Tr}}_{\mathcal{A}}\Big((\mathbb{i}u - \tfrac{1}{2} - \mathbf{N}_{21})(-\boldsymbol{\xi}_{21})\bar{\boldsymbol{\xi}}_{21}\Big) \\ &= \mathsf{x}^{\mathbb{i}\,u}\,\widehat{\mathrm{Tr}}_{\mathcal{A}}\Big(\mathbf{N}_{21}^2 + (\tfrac{3}{2} - \mathbb{i}u)\mathbf{N}_{21} - \mathbb{i}u + \tfrac{1}{2}\Big). \end{aligned} \tag{2.69}$$

Consequently, we have to evaluate terms of the kind $\widehat{\mathrm{Tr}}_{\mathcal{A}}(\mathbf{N}_{ab}^k)$ which will contain a sum of the form

$$\sum_{j=0}^{\infty} \mathsf{x}^{2j} j^k = \Phi(\mathsf{x}^2, -k, 0) = \frac{\sum_{j=0}^{k} \left\langle {k \atop j} \right\rangle \mathsf{x}^{2(j+1)}}{(1-\mathsf{x}^2)^{k+1}}, \qquad \left\langle {k \atop j} \right\rangle = \sum_{n=0}^{j+1} (-1)^n \binom{k+1}{n} (j-n+1)^k, \tag{2.70}$$

where we again had to regularise by setting $|\mathsf{x}| < 1$, and Φ is the *Hurwitz-Lerch transcendent*. $\left\langle {k \atop j} \right\rangle$ are the *Eulerian numbers*. Resultingly,

$$\widehat{\mathrm{Tr}}_{\mathcal{A}}(\mathbf{N}_{ab}^k) = \frac{\sum_{j=0}^{k} \left\langle {k \atop j} \right\rangle \left(\frac{\mathsf{x}_a}{\mathsf{x}_b}\right)^{j+1}}{\left(1 - \frac{\mathsf{x}_a}{\mathsf{x}_b}\right)^k}, \tag{2.71}$$

so (2.69) evaluates to

$$\langle\uparrow\downarrow\uparrow|\mathcal{Q}_{\{2\}}|\uparrow\uparrow\downarrow\rangle = \mathsf{x}^{\mathbb{i}u}\left(\frac{\mathbb{i}\mathsf{x}^2}{1-\mathsf{x}^2}u + \frac{\mathsf{x}^2(3+\mathsf{x}^2)}{2(\mathsf{x}^2-1)^2}\right). \tag{2.72}$$

We can proceed in this way for each matrix element to obtain

$$\mathcal{Q}_{\{1\}} = \mathsf{x}^{-\mathbb{i}u}\begin{pmatrix} \mathbb{i}u - \frac{1}{2} + \frac{\mathsf{x}^2}{\mathsf{x}^2-1} & \frac{1}{\mathsf{x}^2-1} & \frac{1}{\mathsf{x}^2-1} \\ \frac{\mathsf{x}^2}{\mathsf{x}^2-1} & \mathbb{i}u - \frac{1}{2} + \frac{\mathsf{x}^2}{\mathsf{x}^2-1} & \frac{1}{\mathsf{x}^2-1} \\ \frac{\mathsf{x}^2}{\mathsf{x}^2-1} & \frac{\mathsf{x}^2}{\mathsf{x}^2-1} & \mathbb{i}u - \frac{1}{2} + \frac{\mathsf{x}^2}{\mathsf{x}^2-1} \end{pmatrix}, \tag{2.73}$$

$$\mathcal{Q}_{\{2\}} = \mathsf{x}^{\mathbb{i}u}\begin{pmatrix} -u^2 + \mathbb{i}\frac{\mathsf{x}^2+1}{\mathsf{x}^2-1}u + \frac{1+6\mathsf{x}^2+\mathsf{x}^4}{4(\mathsf{x}^2-1)^2} & \frac{\mathbb{i}}{\mathsf{x}^2-1}u + \frac{1+3\mathsf{x}^2)}{2(\mathsf{x}^2-1)^2} & \frac{\mathbb{i}\mathsf{x}^2}{1-\mathsf{x}^2}u + \frac{\mathsf{x}^2(3+\mathsf{x}^2)}{2(\mathsf{x}^2-1)^2} \\ \frac{\mathbb{i}}{\mathsf{x}^2-1}u + \frac{3+\mathsf{x}^2)}{2(\mathsf{x}^2-1)^2} & -u^2 + \mathbb{i}\frac{\mathsf{x}^2+1}{\mathsf{x}^2-1}u + \frac{1+6\mathsf{x}^2+\mathsf{x}^4}{4(\mathsf{x}^2-1)^2} & \frac{\mathbb{i}}{\mathsf{x}^2-1}u + \frac{1+3\mathsf{x}^2)}{2(\mathsf{x}^2-1)^2} \\ \frac{\mathbb{i}\mathsf{x}^2}{1-\mathsf{x}^2}u + \frac{\mathsf{x}^2(1+3\mathsf{x}^2)}{2(\mathsf{x}^2-1)^2} & \frac{\mathbb{i}\mathsf{x}^2}{1-\mathsf{x}^2}u + \frac{\mathsf{x}^2(3+\mathsf{x}^2)}{2(\mathsf{x}^2-1)^2} & -u^2 + \mathbb{i}\frac{\mathsf{x}^2+1}{\mathsf{x}^2-1}u + \frac{1+6\mathsf{x}^2+\mathsf{x}^4}{4(\mathsf{x}^2-1)^2} \end{pmatrix}. \tag{2.73}$$

Functional relations and Bethe roots

We can plug (2.73) into (2.62) and see that indeed

$$\mathcal{Q}_{\{1\}}(u+\tfrac{\mathbb{i}}{2})\mathcal{Q}_{\{2\}}(u-\tfrac{\mathbb{i}}{2}) - \mathcal{Q}_{\{1\}}(u-\tfrac{\mathbb{i}}{2})\mathcal{Q}_{\{2\}}(u+\tfrac{\mathbb{i}}{2}) \propto u^3 \mathbb{I}_{3\times 3}. \tag{2.74}$$

We can also diagonalise the Q-operators. The eigenvalues, which we in general refer to as *Q-functions*, of $\mathcal{Q}_{\{1\}}$ turn out to be

$$Q_{\{1\}} = \mathsf{x}^{-\mathbb{i}u}\left(\mathbb{i}u + \frac{1}{2} + \frac{1}{e^{\frac{2\pi\mathbb{i}n}{3}}\mathsf{x}^{\frac{1}{3}} - 1}\right), \qquad n = 0, 1, 2, \tag{2.75}$$

which fits nicely with the Bethe roots (2.51).

Removing the twist

What if we are interested in the model with no twist? From the explicit Q-operators (2.73) it is obvious that the limit $\mathsf{x} \to 1$ is not regular. However for some quantities the limit is completely smooth. For example, two of the eigenvalues (2.75) become simply $Q = \mathbb{i} u \pm \frac{\mathbb{i}}{2\sqrt{3}}$. It is easy to check that the Baxter TQ-equation (2.64) is satisfied by these eigenvalues, where $\mathcal{T}$ is replaced by the corresponding eigenvalue of (2.46).

The quantities that do diverge are related to symmetries that are being restored. First of all, Q-functions that correspond to eigenstates that become descendants when the symmetry is restored will diverge. For eigenstates that remain highest weight states, only one of the Q-functions has a smooth limit. One can indeed see from the QQ-relation (2.62) that as the exponential prefactors disappear in the $\mathsf{x} \to 1$ limit, the leading polynomial power on the right hand side vanishes. To balance this, the polynomial degree of the other Q-function must increase.

On the eigenvalue level, we can deal with this by normalising before taking the untwisting limit [42]. For the $L = 3$, $M = 1$ example, one of the eigenstates corresponds to Q-functions with untwisting limits

$$-\mathbb{i} \lim_{\mathsf{x}\to 1} Q_{\{1\}} \;=\; 2\mathbb{i} \lim_{\mathsf{x}\to 1} (\mathsf{x}-1) Q_{\{2\}} \;=\; u - \frac{1}{2\sqrt{3}} \;\equiv\; Q_1 \,. \tag{2.76}$$

What happens is that both Q-functions tend to the same value, which would make the right hand side of the QQ-relation (2.62) vanish. We can instead consider a linear combination where this leading term vanishes. Let us first set $\mathsf{x} = 1 + \epsilon$ and examine the expansion of the Q-functions in ϵ, which in our case yields

$$\begin{aligned} -\mathbb{i} Q_{\{1\}} &= Q_1 + q_2 \epsilon + q_3 \epsilon^2 + \mathcal{O}(\epsilon^3) \\ 2\mathbb{i}(\mathsf{x}-1) Q_{\{2\}} &= Q_1 + (q_2 + c\, Q_1)\, \epsilon + \tilde{q}_3 \epsilon^2 + \mathcal{O}(\epsilon^3) \,, \end{aligned} \tag{2.77}$$

where q_2 is a quadratic polynomial, q_3 and $\tilde{q}_3$ are distinct cubic polynomials, and $c = \frac{1}{2} - \frac{2\mathbb{i}}{\sqrt{3}}$. We can then construct a linear combination which does not untwist to Q_1:

$$\begin{aligned} Q_2 &= \lim_{\mathsf{x}\to 1} \frac{\mathbb{i}\left(1 + (\mathsf{x}-1)c + (\mathsf{x}-1)^2 d\right) Q_{\{1\}} + 2\mathbb{i}(\mathsf{x}-1) Q_{\{2\}}}{(\mathsf{x}-1)^2} \\ &= \tilde{q}_3 - q_3 - c q_2 - d\, Q_1 \qquad (2.78) \\ &= 2u^3 + \sqrt{3} u^2 + \frac{1}{\sqrt{3}} + \tilde{d}\, Q_1 \qquad (2.79) \end{aligned}$$

where we made the freedom to add Q_1 explicit by including the term containing the constant d. From the construction, it is clear that Q_1 and Q_2 will satisfy a QQ-relation identical to (2.74):

$$Q_1^+ Q_2^- - Q_1^+ Q_2^- \;\propto\; u^3 \;\equiv\; Q_\emptyset Q_{12} \,. \tag{2.80}$$

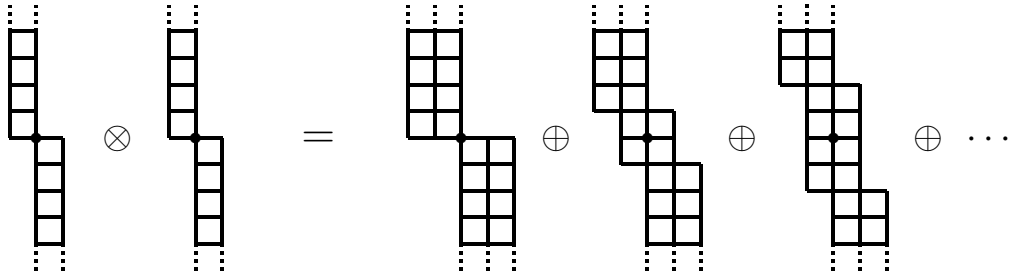

Figure 2.3: The tensor product of two single-field representations is the direct sum of all possible length-2 representations. We denote the latter by $\mathcal{V}_j$, $j = 0, 1, 2, ...$, where j is the number of boxes above and to the right of the central node in the diagram.

In conclusion, the Q-operators are obscured by the restoration of symmetry caused by the removal of the twist. However, their eigenvalues live on unaffected in the untwisted theory, and satisfy the same functional relations.

2.4 Generalisation to higher rank symmetry

The above discussion served to introduce some of the important concepts in integrable models. This was done by considering models with compact rank one symmetry, in order to not get lost in technicalities. We will soon direct our focus towards models with higher rank symmetry, so it is appropriate to have a brief look at the generalisations of the above story to non-compact super algebras of higher rank.

2.4.1 The XXX spin chain

The Heisenberg spin chain is based on a Hilbert space formed by tensor products of fundamental representations of $\mathfrak{su}(2)$. It belongs to a more general family of integrable spin chains that we will refer to as *XXX* or *rational* spin chains, where the Hilbert space is the tensor product of more general representations of a given Lie algebra. The name *rational* refers to the specific structure of the universal R-matrix which, when being evaluated on compact representations becomes a rational function of the spectral parameter. Note however that it is not a rational function for non-compact representations.

We restrict to the case of homogeneous chains where the Hamiltonian can be written as a sum of nearest-neighbour interactions. When the spin chain is not in the fundamental representation of $\mathfrak{su}(2)$, there are other possible interactions than simple permutations. The Hamiltonian of the XXX spin chain with $\mathfrak{psu}(2,2|4)$ symmetry can be written very compactly in terms of *projectors*. All nodes in the chain are in the non-compact single-field representation described in chapter 1. The tensor product of two such representations is the infinite direct sum of all length-2 representations, see figure 2.3. We denote these representations by $\mathcal{V}_j$. The projector $\mathbf{P}_{k,k+1}(j)$ considers two neighbouring nodes and

projects[9] this subchain to the representation $\mathcal{V}_j$. The XXX Hamiltonian then has the form [32]

$$H = \sum_{k=1}^{L} \sum_{j=0}^{\infty} h(j) \mathbf{P}_{k,k+1}(j) \,, \tag{2.81}$$

where $h(j) = \sum_{n=1}^{j} \frac{1}{n}$ are the harmonic numbers. A more practically useful, but maybe less aesthetic, representation of the Hamiltonian is given in terms of Jordan-Schwinger oscillators by the so-called *harmonic action*, see [32].

2.4.2 Nested Bethe equations

One can carry out a generalised version of the Bethe ansatz techniques for the higher rank cases. This results in *nested* Bethe equations satisfied by different types of Bethe roots. The Bethe equations for the $\mathfrak{gl}(N)$ case were formulated in [43], the $\mathfrak{gl}(N|K)$ version was introduced in [44], and further studies were done in [18, 45] to include arbitrary choices of representations at each spin chain node.

The obtained Bethe equations depend on the Dynkin diagram that corresponds to the grading of the Lie algebra in question, cf. figure 1.1. For $\mathfrak{gl}(N|K)$ there will be $N+K-1$ sets of equations on $N+K-1$ sets of Bethe roots. Let us label these roots by $u_j^{(a)}$ where $a = 1, ..., N+K-1$ denotes the node in the Dynkin diagram. For simplicity, let us write down the $\mathfrak{u}(N|K)$ Bethe equations. If a is a bosonic node, i.e. if $p_a = p_{a+1}$, the roots $u_j^{(a)}$ satisfy the equations

$$\prod_{k=1}^{m_a} \frac{u_j^{(a)} - u_k^{(a)} + \mathrm{i}}{u_j^{(a)} - u_k^{(a)} - \mathrm{i}} \prod_{k=1}^{m_{a-1}} \frac{u_j^{(a)} - u_k^{(a-1)} - \frac{\mathrm{i}}{2}}{u_j^{(a)} - u_k^{(a-1)} + \frac{\mathrm{i}}{2}} \prod_{k=1}^{m_{a+1}} \frac{u_j^{(a)} - u_k^{(a+1)} - \frac{\mathrm{i}}{2}}{u_j^{(a)} - u_k^{(a+1)} + \frac{\mathrm{i}}{2}} = -1 \,, \tag{2.82a}$$

while if a is a fermionic node, $p_a \neq p_{a+1}$, they satisfy

$$\prod_{k=1}^{m_{a-1}} \frac{u_j^{(a)} - u_k^{(a-1)} + \frac{\mathrm{i}}{2}}{u_j^{(a)} - u_k^{(a-1)} - \frac{\mathrm{i}}{2}} \prod_{k=1}^{m_{a+1}} \frac{u_j^{(a)} - u_k^{(a+1)} - \frac{\mathrm{i}}{2}}{u_j^{(a)} - u_k^{(a+1)} + \frac{\mathrm{i}}{2}} = 1 \,. \tag{2.82b}$$

The number of roots m_a are related to the weights of the representation. The roots $u_j^{(0)}$ and $u_j^{(N+K)}$ are fixed trivial roots. The non-compact case is similar, but certain equations

[9] A simple way to understand how projectors work in practice is to consider the tensor product of two fundamental representations of $\mathfrak{su}(2)$, which decomposes into a three-dimensional $\{\uparrow\uparrow, \uparrow\downarrow + \downarrow\uparrow, \downarrow\downarrow\}$ and a one-dimensional irrep $\{\uparrow\downarrow - \downarrow\uparrow\}$. Denote the projectors to these representations by $\mathbf{P}^{\{1,1\}}$ and $\mathbf{P}^{\{2\}}$, respectively. On the basis $\{\uparrow\uparrow, \uparrow\downarrow + \downarrow\uparrow, \downarrow\downarrow, \uparrow\downarrow - \downarrow\uparrow\}$, the projectors have the form

$$\mathbf{P}^{\{1,1\}} = \begin{pmatrix} 1 & 0 & 0 & 0 \\ 0 & 1 & 0 & 0 \\ 0 & 0 & 1 & 0 \\ 0 & 0 & 0 & 0 \end{pmatrix} , \qquad \mathbf{P}^{\{1,1\}} = \begin{pmatrix} 0 & 0 & 0 & 0 \\ 0 & 0 & 0 & 0 \\ 0 & 0 & 0 & 0 \\ 0 & 0 & 0 & 1 \end{pmatrix} .$$

One needs to understand the precise vector spaces of the irreps to use the projectors in practice.

will contain additional factors of $u_j^{(a)\pm L}$. We return to these equations and their explicit solution in chapter 5.

The energy and momentum are encoded in the Bethe roots at the *momentum carrying* node through (2.24). For $\mathfrak{u}(N,M|K)$ and central charge C, this node is identified as the one at the central point of the corresponding Young diagram, see the discussion in section 1.2 and the later discussion in chapter 5. In the $\sqcap$ grading, this is the node $a = 2N + C$.

2.4.3 Q-operators

The algebraic Bethe ansatz has a natural generalisation to higher rank symmetry. In order to have a cleaner notation, we introduce a redefined spectral parameter z through

$$z \equiv \mathbb{i}u - \tfrac{1}{2}\,. \tag{2.83}$$

The Q-operator construction for rational spin chains has been developed recently in [40, 41, 46, 47, 48]. The Lax operators that are building blocks for $\mathfrak{u}(N,M|K)$ Q-operators can be written as [47, 49]

$$\mathcal{L}_J(z) \;=\; e^{\sum (\text{-}1)^{p_j+p_j p_{\bar{j}}}\boldsymbol{\xi}_{j\bar{j}}\bar{\boldsymbol{\chi}}_{\bar{j}}\boldsymbol{\chi}_j}\left[z+1-\frac{C}{2}-\frac{\sum(\text{-}1)^{p_j}}{2}\right]_{\sum\bar{\boldsymbol{\chi}}_{\bar{j}}\boldsymbol{\chi}_{\bar{j}}} e^{-\sum(\text{-}1)^{p_j+p_{\bar{j}}+p_j p_{\bar{j}}}\boldsymbol{\xi}_{j\bar{j}}\bar{\boldsymbol{\chi}}_j\boldsymbol{\chi}_{\bar{j}}}\,, \tag{2.84}$$

where the sums are over the indices $j \in J$ and $\bar{j} \in \bar{J}$, and p_j is the p-grading (1.2). The physical space oscillators are given by $\bar{\boldsymbol{\chi}} = \{\text{-}\mathbf{b}_{\dot{\alpha}}, \mathbf{a}_\alpha^\dagger, \mathbf{f}_a^\dagger\}$ and $\boldsymbol{\chi} = \{\mathbf{b}_{\dot{\alpha}}^\dagger, \mathbf{a}_\alpha, \mathbf{f}_a\}$ as in (1.14), and the oscillators $\boldsymbol{\xi}$ act in an auxiliary space of the same kind as discussed in section 2.3.2. We will allow the subscript of the Pochhammer symbol to take negative values and in that case define it through

$$[k]_{-n} = \frac{\Gamma(k-n)}{\Gamma(k)} = \frac{1}{[k-n]_n} = \frac{(\text{-}1)^n}{[1-k]_n}\,. \tag{2.85}$$

Note that for $J = \emptyset$, the Lax operator is simply

$$\mathcal{L}_\emptyset(z) = \left[z+1-\frac{C}{2}\right]_C = \prod_{j=1}^{|C|}\left(z-\frac{|C|}{2}+j\right)^{\mathrm{sign}(C)} \propto \prod_{j=\frac{1-|C|}{2}}^{\frac{|C|-1}{2}}(u+\mathbb{i}j)^{\mathrm{sign}(C)}\,, \tag{2.86}$$

and also that for the full set $J = \bar{\emptyset}$ we always have $\mathcal{L}_{\bar{\emptyset}} = 1$.

The Q-operators are defined by

$$\mathcal{Q}_J(z) = \left(\prod_{j\in J}\mathsf{x}_j^{(\text{-}1)^{p_j+1}z}\right)\,\widehat{\mathrm{str}}_{\mathcal{A}}\left(\mathcal{L}_J^{(1)}\cdots\mathcal{L}_J^{(L)}\right)\,. \tag{2.87}$$

where $\widehat{\mathrm{str}}$ is a normalised supertrace defined by

$$\widehat{\mathrm{str}}_{\mathcal{A}}(f) = \frac{\mathrm{str}_{\mathcal{A}}\left(\prod_{j,k=1,j\neq k}^{N+M+K}\left(\frac{\mathsf{x}_j}{\mathsf{x}_k}\right)^{\mathbf{N}_{jk}}f\right)}{\mathrm{str}_{\mathcal{A}}\left(\prod_{j,k=1,j\neq k}^{N+M+K}\left(\frac{\mathsf{x}_j}{\mathsf{x}_k}\right)^{\mathbf{N}_{jk}}\right)}\,. \tag{2.88}$$

Note that the twists should satisfy $\prod_{j=1}^{N+M+K} \varkappa_j = 1$.

The $\mathfrak{gl}(N|K)$ Q-system

One can show [46] that the $\mathfrak{gl}(N|K)$ Q-operators will satisfy two types of QQ-relations depending on the p-grading:

$$\begin{aligned} \mathcal{Q}_{J\cup\{i,j\}}(z)\mathcal{Q}_J(z) &\propto \mathcal{Q}_{J\cup\{i\}}(z+\tfrac{1}{2})\mathcal{Q}_{J\cup\{j\}}(z-\tfrac{1}{2}) - \mathcal{Q}_{J\cup\{i\}}(z-\tfrac{1}{2})\mathcal{Q}_{J\cup\{j\}}(z+\tfrac{1}{2}) \qquad p_i = p_j \\ \mathcal{Q}_{J\cup\{i\}}(z)\mathcal{Q}_{J\cup\{j\}}(z) &\propto \mathcal{Q}_{J\cup\{i,j\}}(z+\tfrac{1}{2})\mathcal{Q}_J(z-\tfrac{1}{2}) - \mathcal{Q}_{J\cup\{i,j\}}(z-\tfrac{1}{2})\mathcal{Q}_J(z+\tfrac{1}{2}) \qquad p_i \neq p_j \end{aligned} \tag{2.89}$$

It is possible to introduce a notation that makes the p-grading more transparent. One can label the Q-operators by two separate ordered multi-indices, $\mathcal{Q}_{A|J}$, where A and J keep track of indices with $p = 0$ and $p = 1$, respectively.

Matrix elements of non-compact Q-operators

We can try to proceed along the same lines as in the $\mathfrak{su}(2)$ case to evaluate matrix elements of the Q-operators on magnon blocks. However, for non-compact algebras we quickly face a new challenge: when evaluating matrix elements of the Lax operators, i.e. when taking inner products of states in the physical space, the exponential terms in the Lax operators (2.84) do not truncate.

This is evident already for $\mathfrak{sl}(2)$, corresponding to $\boldsymbol{\chi} = \{\mathbf{b}^\dagger, \mathbf{a}\}$ and $\bar{\boldsymbol{\chi}} = \{-\mathbf{b}, \mathbf{a}\}$, where $\mathcal{L}_{\{2\}}$ takes the form

$$\mathcal{L}_{\{2\}} = e^{-\bar{\boldsymbol{\xi}}_{21}\mathbf{ab}}\,[z+1]_{-1-n_\mathbf{b}}\,e^{-\boldsymbol{\xi}_{21}\mathbf{a}^\dagger\mathbf{b}^\dagger}\,. \tag{2.90}$$

If we try to evaluate a matrix element, we see that there are infinitely terms that contribute because $(\mathbf{a}^\dagger\mathbf{b}^\dagger)^n$ never annihilates the state in question. For higher rank, there can even be more than one of these non-compact directions, so evaluating matrix elements would involve multiple infinite sums. In the $\mathcal{N} = 4$ SYM field interpretation of section 1.4.1 this corresponds to the possibility of acting an arbitrary number of times with covariant derivatives.

Prior to [6] this feature has not been studied in detail, and we will present a way to overcome this challenge in chapter 8. The seemingly non-truncating Lax operator matrix elements will in fact turn out to be rational expressions in both z and the auxiliary space oscillators $\boldsymbol{\xi}$.

Subconclusion

In this chapter, we introduced the notion of integrable models as those that fall under the framework of the Algebraic Bethe Ansatz. This framework provides a systematic way of

constructing the infinite family of conserved quantities in such models.

The deepest structure we reached was the system of Q-operators. However, we had to introduce a regulating twist in order to construct these quantities. On the operatorial level, the removal of the twist obscures the Q-operators, but we saw that their eigenvalues remain well-defined quantities that satisfy the same functional relations as the operators. The Q-system will play a key role for us. For now, and throughout the main part of thesis, we will focus our attention on the eigenvalue level. Only in the chapter 8 will we return to the operatorial formalism.

It is now time to see how integrable models appear in four-dimensional quantum field theory, more precisely in the planar limit of the AdS/CFT correspondence. After quite a detour, this will again lead us to a Q-system.

Chapter 3

AdS/CFT integrability

The $\mathrm{AdS}_5/\mathrm{CFT}_4$ correspondence has two sides: on one hand the four-dimensional quantum field theory $\mathcal{N} = 4$ SYM, and on the other Type IIB string theory on $\mathrm{AdS}_5 \times S^5$. This chapter gives a brief review of the appearance of integrability in the spectral problem within the two sides of the AdS/CFT correspondence in the planar limit.

By assuming that the spectral problem is integrable at any coupling, one can derive beautiful mathematical structures that characterise the spectrum. We give a summary of the ideas behind the asymptotic and thermodynamic Bethe ansatz which capture the asymptotic and exact spectrum, respectively.

No attempt is made to give a full account of these rich topics, and this chapter is at best a historical and superficial overview of the progress that eventually led to the Quantum Spectral Curve, which is described in detail in chapter 4. For a thorough review of AdS/CFT integrability and a complete list of references see [50].

3.1 Integrability in $\mathcal{N} = 4$ super Yang-Mills theory

Integrability was first discovered on the gauge theory side of the correspondence. The following is a brief summary of the appearance of integrable structures in perturbative $\mathcal{N} = 4$ SYM.

3.1.1 The one-loop dilatation operator

The study of AdS/CFT integrability was initiated by the discovery [13] that the first perturbative correction to the dilatation operator in planar $\mathcal{N} = 4$ SYM behaves as the Hamiltonian of an integrable spin chain when acting on single-trace operators. Similar phenomena had previously been observed in QCD [51, 52, 53]. The single-trace operators can be interpreted as closed spin chain configurations. We saw in the previous chapters how both composite operators and spin chain configurations have natural interpretations as tensor product spaces.

Figure 3.1: Field contractions that contribute to the two-point correlation function of composite local operators in the planar limit. The horizontal lines represent the composite operators, with the nodes corresponding to single fields. The vertical lines correspond to contractions. The left diagram contributes at tree level while the right diagram contributes at one-loop.

As mentioned, the two-point correlation function in a conformal field theory is given by

$$\langle \mathcal{O}(x)\mathcal{O}(y)\rangle = \frac{1}{|x-y|^{2\Delta}}\,. \tag{3.1}$$

At tree level, the conformal dimension Δ is simply the bare dimension Δ_0. Due to quantum corrections, the operators are however subject to renormalisation, and only particular linear combinations of single-trace operators have a well-defined anomalous dimension. We can characterise this mixing by a renormalisation factor Z acting on the bare operators $\mathcal{O}_0$,

$$\mathcal{O}^i_{\text{ren}} = Z^i_j\,\mathcal{O}^j_0\,. \tag{3.2}$$

Z depends on the coupling constant g and a UV cutoff scale Λ, and it is related to the anomalous part of the dilatation operator, which we denote by Γ, through

$$\Gamma = \frac{\mathrm{d}\,Z}{\mathrm{d}\ln\Lambda}Z^{-1}\,. \tag{3.3}$$

In [13] a diagrammatic computation of planar contributions to the two-point correlation function (3.1), see figure 3.1, revealed that the one-loop contribution to Γ takes the form of a spin chain Hamiltonian with nearest-neighbour interactions. The argument was made for the $\mathfrak{so}(6)$, or $\mathfrak{su}(4)$, subspace of operators formed by the scalar fields, which in the language of chapter 1 are the states $\Phi_{ab} \equiv \mathbf{f}^\dagger_a\mathbf{f}^\dagger_b|0\rangle$. Importantly, it was shown that this Hamiltonian belongs to a family of commuting operators generated from the algebraic Bethe ansatz starting from a rational R-matrix solving the Yang-Baxter equation.

An expression for the one-loop dilatation operator of the full theory was derived in [20]. It was argued that it likewise corresponds to an integrable spin chain with $\mathfrak{psu}(2,2|4)$ symmetry in [32], again by demonstrating its origins from a rational R-matrix in the algebraic Bethe ansatz framework.

3.1.2 The dilatation operator at higher loops

With the discovery of one-loop integrability, it was natural to look for similar structures at higher loop orders. In [54] the two-loop dilatation operator in the $\mathfrak{su}(2)$ sector was derived.

It was argued to correspond to an integrable spin chain Hamiltonian in the planar limit, up to higher-order terms, by also considering corrections to other conserved charges in the integrable one-loop spin chain. It was then conjectured that *to any loop order* and *in all sectors* the dilatation operator coincides with an integrable spin chain Hamiltonian in the planar limit. At the n'th loop, a node in this spin chain interacts with its n nearest neighbouring sites. At a given loop order, the charges of the model commute up to the considered order in g. For example, the two-loop dilatation operator in the $\mathfrak{su}(2)$ sector corresponds to a spin chain Hamiltonian of the form $H = g^2 H_1 + g^4 H_2$, where H_1 is the Hamiltonian of the Heisenberg spin chain (2.1) and H_2 has the form [54]

$$H_2 \;\propto\; \sum_{k=1}^{L} \left(-4\,\mathbb{I} + 6\,\mathbb{P}_{k,k+1} - \mathbb{P}_{k,k+1}\mathbb{P}_{k+1,k+2} - \mathbb{P}_{k+1,k+2}\mathbb{P}_{k,k+1}\right) . \tag{3.4}$$

A three-loop computation of the dilatation operator in the $\mathfrak{su}(2)$ sector was carried out in [55], the length-mixing $\mathfrak{su}(2|3)$ sector dilatation operator was studied in [33], and the two-loop dilatation operator in the non-compact $\mathfrak{psu}(1,1|2)$ sector was studied in [56]. However, the explicit structure of the full $\mathfrak{psu}(2,2|4)$ two-loop dilatation operator is still unknown.

3.1.3 Explicit results from perturbative QFT calculations

Perturbative quantum field theory calculations quickly become enormously complicated. For the Konishi multiplet, the simplest multiplet not protected from quantum corrections, the four-loop anomalous dimension has been determined from Feynman diagram-based calculations in [57], while the five-loop result was obtained with the help of other arguments in [58]. The result is

$$\begin{aligned} \gamma \;=\; & 12g^2 - 48g^4 + 336g^6 + g^8\big(-2496 + 576\,\zeta_3 - 1440\,\zeta_5\big) \\ & + g^{10}\big(15168 + 6912\,\zeta_3 - 5184\,\zeta_3^2 - 8640\,\zeta_5 + 30240\,\zeta_7\big)\,, \end{aligned} \tag{3.5}$$

and the fact that it coincides with the results coming from the integrability-assuming techniques described in the following is a very important and non-trivial check of the integrability of the spectral problem.

3.2 Integrability in type IIB string theory

In this section we briefly discuss the appearance of integrability on the string theory side of the AdS/CFT correspondence. Strings are one-dimensional objects in space, which means that in spacetime, they span a two-dimensional surface, the *worldsheet*. Sigma models live on these worldsheets, and for Type IIB String theory on $\mathrm{AdS}_5 \times S^5$ the corresponding sigma model [59] turns out to be integrable, in the sense that one can construct infinitely

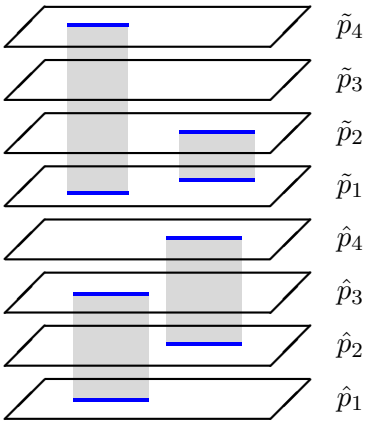

Figure 3.2: Schematic depiction of the AdS/CFT spectral curve, an eight-sheeted Riemann surface formed by the quasi-momenta. The blue lines denote branch cuts connecting the sheets.

many conserved charges at the classical level [60]. The spectrum of string energies is nicely characterised by the elegant framework of *spectral curves*.

3.2.1 The spectral curve

The use of spectral curves in the AdS/CFT context was first proposed in [61] and subsequently developed in [62]. A nice review is given in [63].

For an integrable sigma model, the equations of motion can be reformulated as a flatness condition on a so-called *Lax connection*,

$$\partial_\alpha \mathcal{L}_\beta - \partial_\beta \mathcal{L}_\alpha - [\mathcal{L}_\alpha, \mathcal{L}_\beta] \quad = \quad 0 \tag{3.6}$$

where α and β are worldsheet coordinates. The Lax connection $\mathcal{L}(u)$ takes values in the Lie algebra associated to the symmetry group of the sigma model. It is a function of a spectral parameter u and (3.6) should hold for any value of this parameter. One can construct a *monodromy matrix* taking values in the corresponding Lie group through the path-ordered exponential

$$\mathcal{M}(u) = \mathcal{P}\mathrm{exp}\left(\int_0^{2\pi} \mathrm{d}\sigma\, \mathcal{L}_\sigma(u)\right) , \tag{3.7}$$

where σ is the compact spacelike direction on the worldsheet. The eigenvalues λ_i of the monodromy matrix satisfy the characteristic equation

$$\det(\mathcal{M} - \lambda) = 0\,. \tag{3.8}$$

They are usually parametrised by a set of *quasi-momenta* p_i through $\lambda_i \equiv e^{\mathrm{i}\, p_i}$.

In the AdS/CFT case, the quasi-momenta solving the characteristic equation form an eight-sheeted Riemann surface in the spectral parameter. The quasi-momenta are usually denoted $\hat{p}_i$ and $\tilde{p}_a$ to mark their relation to the AdS_5 and S^5 parts of the symmetry. See

figure 3.2 for a schematic illustration. This Riemann surface is what is referred to as the *spectral curve*. Explicit solutions to this spectral curve have asymptotics specified by the weights of the global symmetry, including the string energy. The spectral curve thus provides a convenient approach to solving the classical equations of motion in order to obtain the classical string energies. Note that it is also possible to consider fluctuations around the classical solutions, and in this way obtain the first perturbative quantum corrections to the string energies, see e.g. [64].

As explained in [15], the Quantum Spectral Curve, towards which we will soon turn our attention, can be thought of as a quantisation of the classical spectral curve described here.

3.3 The asymptotic Bethe ansatz

With the clear hints of integrability of the spectral problem in the planar limit of the AdS/CFT correspondence, it is tempting to ask what we can achieve by assuming integrability at any value of the coupling g. The *asymptotic Bethe ansatz* refers to a technique which makes this assumption and considers the limit of infinitely long operators.

3.3.1 The S-matrix

The key quantity to understand is the S-matrix of the integrable model [65]. In section 2.1.2 we encountered the S-matrix for the Heisenberg spin chain, and in this section we review how to *bootstrap* the analog of this quantity for the exact AdS/CFT spectrum. It turns out that it is possible to fix the S-matrix by imposing integrability and by requiring that it has certain symmetries.

The idea is to consider the protected operator $\mathrm{Tr}(\mathcal{Z}^L)$ as a vacuum and study other field insertions as excitations. We consider operators of the type

$$\mathrm{Tr}(\mathcal{Z}\mathcal{Z}...\mathcal{Z}\Phi_1\mathcal{Z}...\mathcal{Z}\Phi_2\mathcal{Z}...\mathcal{Z}\Phi_M\mathcal{Z}...\mathcal{Z})\,, \tag{3.9}$$

where Φ_i denote fields different from $\mathcal{Z}$. We can denote the position of the field Φ_i in the composite operator by n_i. We will consider the limit of very long operators, but also with a large separation between the excitations, i.e. $1 \ll |n_i - n_j| < L$.

S-matrix bootstrap

Consider a theory in one spatial dimension, where only $2 \to 2$ scattering processes are possible. Each excitation in the theory can be characterised by a momentum p_i. For the theory to be integrable, it should have an infinite number of conserved charges Q_n, with momentum and energy usually corresponding to $n = 1, 2$. For all charges to be

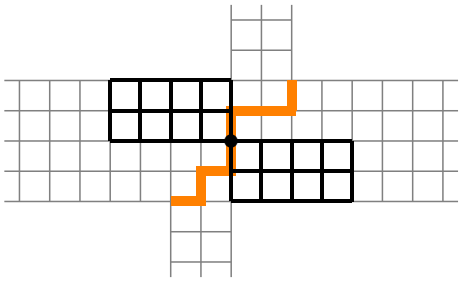

Figure 3.3: The Young diagram for the multiplet containing $\mathrm{Tr}(\mathcal{Z}^4)$ and an example of a Dynkin path that goes through the central node of the diagram. Any Dynkin path that goes through the central node corresponds to a grading where $\mathrm{Tr}(\mathcal{Z}^L)$ is the highest weight state, but duality transformations that move the path from the central node will result in a different highest weight state. In this way we see that the operator $\mathrm{Tr}(\mathcal{Z}^L)$ is invariant under two copies of $\mathfrak{su}(2|2)$, but not under the full $\mathfrak{psu}(2,2|4)$ symmetry.

conserved in scattering processes, the only thing that can happen in such a process is that the momenta are exchanged, see [66] for a nice discussion.

Consider two excitations characterised by momenta p_1 and p_2. We can describe a scattering process between the two by an S-matrix $\mathcal{S}(p_1, p_2)$. Each excitation corresponds to a vector belonging to the representation $\mathcal{V}$ that the fields are in. In that sense the S-matrix acts in the tensor product of two such representations, $\mathcal{S} : \mathcal{V} \otimes \mathcal{V} \to \mathcal{V} \otimes \mathcal{V}$. As a basic example, consider $\mathcal{V}$ to be the two-dimensional fundamental representation of $\mathfrak{su}(2)$. Then $\mathcal{S}$ would act in the direct sum of a singlet and a triplet. We can denote this by $\{1\} \otimes \{1\} = \{2\} \oplus \{1,1\}$ according to the partitions $\lambda = \{\lambda_1, \lambda_2, ...\}$ specifying the representations in question. As $\mathcal{S}$ should commute with the symmetry of the theory, it should act similarly on vectors within the same irreducible representation, and it should thus have the form

$$\mathcal{S}(p_1, p_2) = f_1(p_1, p_2)\mathbf{P}_{\{2\}} + f_2(p_1, p_2)\mathbf{P}_{\{1,1\}} = \sigma(p_1, p_2)\left(\mathbf{P}_{\{2\}} + f(p_1, p_2)\mathbf{P}_{\{1,1\}}\right) \quad (3.10)$$

where $\mathbf{P}_\lambda$ is the projector onto the representation λ. The function σ is referred to as the *dressing factor*. The function f is usually determined from the constraint that $\mathcal{S}$ satisfies the Yang-Baxter equation. The dressing factor is in general not fixed by the continuous symmetries of the problem, but rather by discrete symmetries as proposed in [65] for relativistic theories. This leads to so-called *crossing equations* that fix the dressing factor.

The AdS/CFT S-matrix

The S-matrix bootstrap was first applied to the AdS/CFT spectrum in [67]. An important point is that the BMN vacuum $\mathrm{Tr}(\mathcal{Z}^L)$ is not invariant under the full $\mathfrak{psu}(2,2|4)$ symmetry, but only under two copies of $\mathfrak{su}(2|2)$ [21]. See figure 3.3 for a sketchy argument on the level of Young diagrams. Consequently, the S-matrix factorises into a tensor product of two

$\mathfrak{su}(2|2)$ S-matrices. Importantly, the $\mathfrak{su}(2|2)$ symmetry is extended by two central charges and its action is described by a non-trivial co-product [68, 69, 70].

The fundamental representation of $\mathfrak{su}(2|2)$ is four-dimensional, and the tensor product of two such representations is thus 16 dimensional. For the centrally extended symmetry that appears in the AdS/CFT context, this tensor product representation turns out to also be irreducible, which means that the S-matrix is fixed up to the dressing factor, cf. (3.10), and automatically satisfies the Yang-Baxter equation.

One can study the action of the symmetry generators on plane wave states with a single excitation,

$$|\Phi(p)\rangle \equiv \sum_{n=1}^{L} e^{\mathrm{i}\, p\, n} \operatorname{Tr}(\mathcal{Z}...\mathcal{Z} \underbrace{\Phi}_{\text{pos. } n} \mathcal{Z}...\mathcal{Z}) \,, \tag{3.11}$$

and it turns out that the actions are given in terms of two parameters: the momentum p and another parameter that can be identified with the coupling constant g by comparison to other data [71]. In particular, the standard $\mathfrak{su}(2|2)$ central charge, which can be identified with the magnon energy through $E = 2C - 1$, is given by

$$C = \frac{1}{2}\sqrt{1 + 16g^2 \sin^2\left(\frac{p}{2}\right)} \,. \tag{3.12}$$

Expanding this expression in the coupling, we see that the g^2 contribution to the energy matches that of the XXX spin chain (2.24). It turns out to be convenient to parametrise the momentum as $e^{\mathrm{i}p} = \frac{x^+}{x^-}$, where x is related to a spectral parameter u through the Zhukowsky map

$$x + \frac{1}{x} = \frac{u}{g} \,, \qquad x^{\pm} = x(u \pm \tfrac{\mathrm{i}}{2}). \tag{3.13}$$

We will often encounter the Zhukowsky variable x in this thesis, and it is discussed in more detail in appendix A.4.1. Note that we always choose the branch $|x(u)| > 1$. In the limit $g \to 0$ the parameter u corresponds to the rapidity of the XXX spin chain discussed in chapter 2. In terms of the Zhukowsky variable x, the energy of the one-magnon state (3.11) takes the form

$$E(p) = 2\mathrm{i}g\left(\frac{1}{x^+} - \frac{1}{x^-}\right) . \tag{3.14}$$

The structure of the $\mathfrak{su}(2|2)$ S-matrix is determined up to a dressing factor by requiring that it commutes with the symmetry generators. The structure is rather complicated, and we refer to [68] for the details. The question of determining the dressing factor by using crossing symmetry was first addressed in [72]. The strong coupling expansion of the dressing factor was found in [73] and its exact structure proposed in [74]. The solution to the crossing equation and its analytic properties were investigated further in [75]. A nice review of the dressing factor problem is given in [76].

3.3.2 Asymptotic Bethe equations

With the S-matrix at hand, one can use the coordinate Bethe ansatz philosophy described in section 2.1.2 to derive periodicity constraints on the values of the magnon momenta p_i for the energy eigenstates. In fact, a proposal for these *asymptotic Bethe equations* was made already before the precise S-matrix was known [77]. After understanding the S-matrix, it was derived more rigorously by using the the coordinate Bethe ansatz in [69].

The resulting asymptotic Bethe equations are so beautiful that it is worth repeating them, despite the fact that we will not use them much in this thesis. In the non-compact ABA grading, $1\hat{1}\hat{2}23\hat{3}\hat{4}4$, see figure 3.4, they take the form [77]

$$1 = \prod_{j=1}^{K_2} \frac{u_{1,k}-u_{2,j}-\frac{\mathrm{i}}{2}}{u_{1,k}-u_{2,j}+\frac{\mathrm{i}}{2}} \prod_{j=1}^{K_4} \frac{1-\frac{1}{2x_{1,k}x^-_{4,j}}}{1-\frac{1}{2x_{1,k}x^+_{4,j}}} \tag{3.15a}$$

$$-1 = \prod_{j=1}^{K_2} \frac{u_{2,k}-u_{2,j}+\mathrm{i}}{u_{2,k}-u_{2,j}-\mathrm{i}} \prod_{j=1}^{K_1} \frac{u_{2,k}-u_{1,j}-\frac{\mathrm{i}}{2}}{u_{2,k}-u_{1,j}+\frac{\mathrm{i}}{2}} \prod_{j=1}^{K_3} \frac{u_{2,k}-u_{3,j}-\frac{\mathrm{i}}{2}}{u_{2,k}-u_{3,j}+\frac{\mathrm{i}}{2}} \tag{3.15b}$$

$$1 = \prod_{j=1}^{K_2} \frac{u_{3,k}-u_{2,j}-\frac{\mathrm{i}}{2}}{u_{3,k}-u_{2,j}+\frac{\mathrm{i}}{2}} \prod_{j=1}^{K_4} \frac{x_{3,k}-x^-_{4,j}}{x_{3,k}-x^+_{4,j}} \tag{3.15c}$$

$$\begin{aligned} -1 = {} & \left(\frac{x^-_{4,k}}{x^+_{4,k}}\right)^L \prod_{j=1}^{K_4} \frac{x^-_{4,k}-x^+_{4,j}}{x^+_{4,k}-x^-_{4,j}} \frac{1-\frac{1}{2x^+_{4,k}x^-_{4,j}}}{1-\frac{1}{2x^-_{4,k}x^+_{4,j}}} \sigma^2(u_{4,k},u_{4,j}) \\ & \times \prod_{j=1}^{K_1} \frac{1-\frac{1}{2x^+_{4,k}x_{1,j}}}{1-\frac{1}{2x^-_{4,k}x_{1,j}}} \prod_{j=1}^{K_7} \frac{1-\frac{1}{2x^+_{4,k}x_{7,j}}}{1-\frac{1}{2x^-_{4,k}x_{7,j}}} \prod_{j=1}^{K_3} \frac{x^+_{4,k}-x_{3,j}}{x^-_{4,k}-x_{3,j}} \prod_{j=1}^{K_5} \frac{x^+_{4,k}-x_{5,j}}{x^-_{4,k}-x_{5,j}} \end{aligned} \tag{3.15d}$$

$$1 = \prod_{j=1}^{K_6} \frac{u_{5,k}-u_{6,j}-\frac{\mathrm{i}}{2}}{u_{5,k}-u_{6,j}+\frac{\mathrm{i}}{2}} \prod_{j=1}^{K_4} \frac{x_{5,k}-x^-_{4,j}}{x_{5,k}-x^+_{4,j}} \tag{3.15e}$$

$$-1 = \prod_{j=1}^{K_6} \frac{u_{6,k}-u_{6,j}+\mathrm{i}}{u_{6,k}-u_{6,j}-\mathrm{i}} \prod_{j=1}^{K_7} \frac{u_{6,k}-u_{7,j}-\frac{\mathrm{i}}{2}}{u_{6,k}-u_{7,j}+\frac{\mathrm{i}}{2}} \prod_{j=1}^{K_5} \frac{u_{6,k}-u_{5,j}-\frac{\mathrm{i}}{2}}{u_{6,k}-u_{5,j}+\frac{\mathrm{i}}{2}} \tag{3.15f}$$

$$1 = \prod_{j=1}^{K_6} \frac{u_{7,k}-u_{6,j}-\frac{\mathrm{i}}{2}}{u_{7,k}-u_{6,j}+\frac{\mathrm{i}}{2}} \prod_{j=1}^{K_4} \frac{1-\frac{1}{2x_{7,k}x^-_{4,j}}}{1-\frac{1}{2x_{7,k}x^+_{4,j}}}\,, \tag{3.15g}$$

and the form of the dressing factor σ can be found in [74]. Cyclicity of single-trace operators means that they correspond to spin chain configurations that are translationally invariant, and this imposes the additional zero-momentum condition

$$\prod_{j=1}^{K_4} \frac{x^+_{4,k}}{x^-_{4,k}} = 1\,. \tag{3.16}$$

The number of roots K_n are given in terms of the weights of the representation in question, and the correspondence will be made precise in chapter 5. The anomalous dimension is

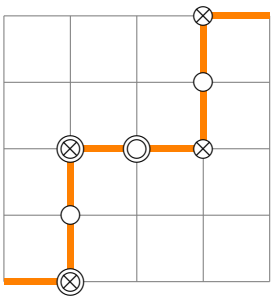

Figure 3.4: The Dynkin path, cf. figure 1.1, corresponding to the grading $1\hat{1}\hat{2}23\hat{3}\hat{4}4$ in which the asymptotic Bethe equations (3.15) are written.

identified with the energy (3.14) and is given by

$$\gamma_{\text{ABA}}(g) = 2\,\mathrm{i}\,g \sum_{k=1}^{K_4} \left(\frac{1}{x^+_{4,k}} - \frac{1}{x^-_{4,k}} \right) . \tag{3.17}$$

Perturbative solution

For comparison with the perturbative frameworks that will be described in chapter 6, it is worth mentioning how the asymptotic Bethe equations are solved perturbatively. The strategy is to expand the Bethe roots in g^2 according to

$$u_{n,k}(g) = u^{(1)}_{n,k} + g^2 u^{(2)}_{n,k} + g^4 u^{(3)}_{n,k} + \dots \tag{3.18}$$

The Zhukowsky variable should be reexpressed in terms of u and expanded in g yielding

$$x = \frac{u}{g} - \frac{g}{u} - \frac{g^3}{u^3} - \frac{2g^5}{u^5} + \mathcal{O}(g^7) . \tag{3.19}$$

Generically, the dressing factor is trivial until the fourth order, i.e. $\sigma^2 = 1 + \mathcal{O}(g^6)$, where it will start to contribute [74]. This contribution contains transcendental numbers, more precisely ζ-values, which we will also encounter later in the thesis.

Finding the leading solutions turns out to be rather hard in practice, and moreover the equations allow additional solutions that are not in correspondence with single-trace operators or spin chain states. Curing these issues is the topic of chapter 5. Once the leading solution is known, generating perturbative solutions is quite simple. One simply takes the contribution to the equation at a given order, plugs in the lower-order contributions to the roots, and demands that the equations hold.

A nice property of the asymptotic Bethe equations is that only a subset of the equations are needed when considering sectors where some nodes are not excited. For example, in the $\mathfrak{sl}(2)$ sector it is sufficient to consider only the central equation (3.15d), and the problem can be formulated as simply as

$$-\left(\frac{x^+_k}{x^-_k}\right)^L = \prod_{j=1}^{S} \frac{x^-_k - x^+_j}{x^+_k - x^-_j} \frac{1 - \frac{1}{x^+_k x^-_j}}{1 - \frac{1}{x^-_k x^+_j}} \sigma^2(u_k, u_j), \qquad \prod_{k=1}^{S} \frac{x^+_k}{x^-_k} = 1 , \tag{3.20}$$

where we made the identification $u_k = u_{4,k}$ and $S = K_4$. We will use this equation in chapter 7, where will need to generate a large number of explicit results.

The asymptotic Bethe equations give an exact description of the AdS/CFT spectrum for loop orders lower than the length of the spin chain L. It does not account for the self-interactions that occur when the range of the interactions wraps all the way around the closed chain. Note that for $\mathfrak{sl}(2)$ operators, the result is actually exact up to $L+1$ loops since these operators belong to multiplets containing operators that have a length increased by two. This feature means that, for any multiplet, the asymptotic Bethe equations are exact up to at least three loops. For the Konishi multiplet, the four-loop result is

$$\Delta_{L=S=2} = 4 + 12g^2 - 48g^4 + 336g^6 + g^8(-2820 - 288\zeta_3) + \mathcal{O}(g^{10})\,, \tag{3.21}$$

and we see that the first three orders match the field theory result (3.5), while the fourth does not. We now turn towards frameworks that capture also these finite-size corrections.

3.3.3 Lüscher corrections

A way to capture the finite-size effects as corrections to the asymptotic result is given by so-called *Lüscher formulae*, which is a method to describe the exponentially suppressed finite-size correction to the energy of a single particle on a large cylinder in a relativistic QFT [78]. The effect stems from virtual particles travelling around the cylinder. The corrections are again related to the S-matrix of the theory.

Wrapping corrections were first discussed in [79] for the AdS/CFT case. Lüscher formulae were used to calculate the four-loop [80] and five-loop [81] anomalous dimension of the Konishi multiplet in agreement with the result (3.5). Twist-2 operators were also considered more generally at four [82] and five loops [83]. Impressively, the six- and seven-loop results for the Konishi multiplet, i.e. all single-wrapping contributions, were derived in [84]. Even though Lüscher formulae for double-wrapping effects can potentially be obtained [85], it is desirable to find a framework that does not make the distinction between contributions from wrapping and short-range effects. We now turn towards such a framework.

3.4 The thermodynamic Bethe ansatz

The asymptotic Bethe ansatz is a powerful and convenient tool, but one should of course strive to describe the finite-size spectrum in a more complete way. This was achieved by using the *thermodynamic Bethe ansatz* philosophy, originally developed in [86]. The method [87] provides an ingenious trick to determine the ground state energy of an integrable theory in finite volume from its infinite volume S-matrix, but also excited states can be studied via analytic continuation [88]. See [89, 90] for nice reviews of the approach.

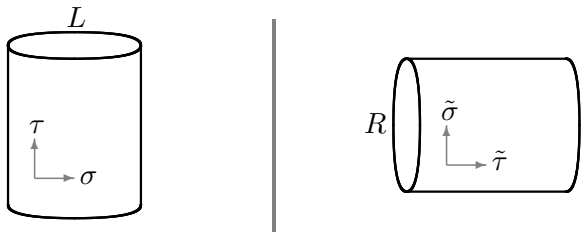

Figure 3.5: The mirror trick: (left) the original theory, (right) the mirror theory.

The TBA approach

Consider a theory in one compact spatial dimension plus a timelike dimension, i.e. a cylinder, which we can parametrise by two coordinates (σ, τ). The main trick in the TBA is to do a double Wick rotation by introducing new coordinates $(\tilde{\sigma}, \tilde{\tau})$ through $\tau = \mathrm{i}\tilde{\sigma}$ and $\sigma = \mathrm{i}\tilde{\tau}$.

To study the ground state energy in the original theory in a finite volume L, we consider its partition function which in the zero-temperature limit, $\beta \to \infty$, is dominated by the ground state,

$$Z(\beta, L) \;=\; \sum_n e^{-\beta\, E_n(L)} \;\xrightarrow{\beta\to\infty}\; e^{-\beta\, E_0(L)}\,. \tag{3.22}$$

By doing a single Wick rotation, $t = \mathrm{i}\tilde{\sigma}$, we get an Euclidean theory on a torus where the direction parametrised by $\tilde{\sigma}$ has circumference $R = \beta$. Doing the second Wick rotation $\sigma = \mathrm{i}\tilde{\tau}$ puts the theory on a cylinder of circumference R, see figure 3.5. The partition function of this mirror theory is then

$$\tilde{Z}(L, R) = \sum_n e^{-L\,\tilde{E}_n(R)}\,. \tag{3.23}$$

The partition functions (3.22) and (3.23) should be equivalent descriptions of the same system. The zero-temperature limit in the original theory, $R \to \infty$, corresponds to infinite volume, but finite temperature $\frac{1}{L}$ in the mirror theory. This is why the trick is nice: we know how to describe the theory in infinite volume.

Energy $\tilde{E}$ and momentum $\tilde{p}$ in the mirror theory are related to the original theory through $E = \mathrm{i}\tilde{p}$ and $p = \mathrm{i}\tilde{E}$. The dispersion relation in the mirror theory is then an inversion of that in the original theory, e.g. (3.12) turns into

$$\tilde{E} = 2\,\mathrm{arcsinh}\left(\frac{\sqrt{\tilde{p}^2+1}}{4g}\right)\,. \tag{3.24}$$

At large R, the mirror theory partition function is dominated by finite-density states, and we can describe such solutions by a density, $\rho_a(\tilde{p}) \equiv \frac{\Delta N_a}{\Delta \tilde{p}}$, where ΔN_a is the number of particles of type a with momenta between $\tilde{p}$ and $\tilde{p} + \Delta\tilde{p}$. The total energy of a state is then

$$\tilde{E}(\tilde{p}) = \sum_a \int \mathrm{d}\tilde{p}\; \rho_a(\tilde{p})\, \tilde{E}_a(\tilde{p})\,. \tag{3.25}$$

The asymptotic Bethe ansatz equations of the mirror model for a finite number of excitations are schematically of the form

$$1 = e^{\mathbb{i}\tilde{p}_k R} \prod_{j \neq k} \mathcal{S}(\tilde{p}_k, \tilde{p}_j)\,. \tag{3.26}$$

Taking the logarithm of this equation in the thermodynamic limit yields an equation of the kind

$$\tilde{p}_a - \mathbb{i} \sum_b \int \mathrm{d}\tilde{p}'\, \rho_b(\tilde{p}') \log \mathcal{S}_{ab}(\tilde{p}_a, \tilde{p}') = \frac{2\pi n_a}{R}\,, \tag{3.27}$$

where n_a labels the possible modes of the particles of type a. By introducing a *hole density* $\bar{\rho}_a \equiv \frac{\Delta \bar{N}_a}{\Delta \tilde{p}}$ that counts the modes that are not excited, we see that we should have $\frac{\mathrm{d}n_a}{\mathrm{d}\tilde{p}} = \rho_a + \bar{\rho}_a$. The different ways to organise the excitations in the modes of the system leads to an entropy factor in the mirror model partition function (3.23) that we are trying to calculate in order to find the ground state energy of the original model through (3.22). In the thermodynamic limit, the mirror model partition function is an integral that can be estimated by a saddle-point approximation. The result of this procedure is a minimising equation on the ratio $Y_a \equiv \frac{\bar{\rho}_a}{\rho_a}$ that have the schematic form [89]

$$\log Y_a(u) = L\, \tilde{E}_a(u) - \sum_b \int \frac{\mathrm{d}u'}{2\pi} K_{ba}(u', u) \log(1 + Y_b)\,, \tag{3.28}$$

where K is related to the S-matrix through $K_{ab}(u, u') = -\mathbb{i}\partial_u \log \mathcal{S}_{ab}(u, u')$, and we made the usual coordinate change to a spectral parameter $u(\tilde{p})$. This type of equation is what is referred to as *TBA equations*: non-linear integral equations on a set of functions Y depending on a spectral parameter. The solution to these equations gives the information needed to determine the ground state energy in the original theory, but also the excited states through a sophisticated procedure of analytic continuation [88].

The TBA for $\mathbf{AdS_5/CFT_4}$

The applicability of the TBA approach to the $\mathrm{AdS}_5/\mathrm{CFT}_4$ integrable system was first discussed in [79]. The asymptotic Bethe ansatz for the mirror model was described in [91], and a classification of its bound states, the so-called *string hypothesis* in [92]. The TBA procedure outlined above was performed in [93, 94, 95, 96] leading to the $\mathrm{AdS}_5/\mathrm{CFT}_4$ TBA equations.

The $\mathrm{AdS}_5/\mathrm{CFT}_4$ TBA equations relate an infinite zoo of Y-functions corresponding to the different types of excitations in the theory. Unlike the asymptotic Bethe ansatz, their solutions determine the exact spectrum at any value of the coupling. However, they are far less transparent and much harder to solve in practice.

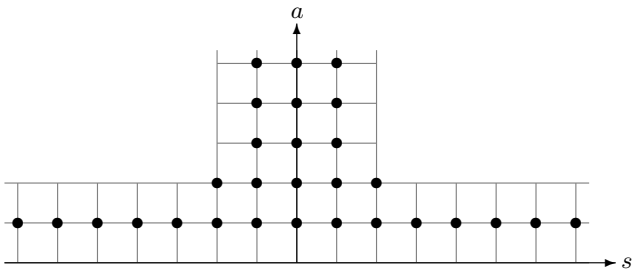

Figure 3.6: The infinite lattice where the Y- and T-functions can be classified. The Y-functions live on the nodes marked by circles, while the T-system lives on the full T-hook.

Explicit results

Precise TBA equations for excitations in the $\mathfrak{sl}(2)$ sector were found in [95, 97] and used for the first numerical studies of the exact anomalous dimension of the Konishi multiplet at finite coupling in [98, 99] and a larger variety of operators in [100]. Exact perturbative results have been obtained up to the fifth loop order for the Konishi operator [101]. The fact that the same result was reached from pure quantum field theoretic calculations questions the usefulness of the integrability-approach as a perturbative tool, but as we will now review, the TBA equations were soon reformulated into much more powerful frameworks yielding results that are unimaginable to ever be reached from perturbative quantum field theory.

3.5 From TBA to QSC

The TBA equations are coupled non-linear integral equations on an infinite set of Y-functions, and they are far from the beauty and transparency of the asymptotic Bethe equations (3.15). We here briefly summarise how the TBA equations were reformulated into a form that is both beautiful and extremely powerful in explicit computations.

Y-system

It was anticipated [93] that the Y-functions can be packaged into a *Y-system* with a single functional relation between the Y-functions, before being derived in [94, 95, 96]. This functional relation has the form

$$Y^{+}_{a,s}Y^{-}_{a,s} = \frac{(1+Y_{a,s+1})(1+Y_{a,s-1})}{(1+\frac{1}{Y_{a-1,s}})(1+\frac{1}{Y_{a+1,s}})}\,, \tag{3.29}$$

and the infinite set of Y-functions can be depicted on a *T-hook*, see figure 3.6. The functional relation (3.29) does not contain the full information of the TBA equations. They have to be supplemented by constraints on the analytic structure of the Y-functions, as investigated in [96, 102, 97, 103].

A nice feature of the Y-system is that it is universal: its structure is determined solely by the $\mathfrak{psu}(2,2|4)$ symmetry of the theory. All multiplets of single-trace operators are

solutions to the same equations. The difference lies in the asymptotical behaviour and analytic structure of the functions.

T-system

It was also clear from the beginning [93] that the set of Y-functions can be reparametrised by an infinite set of T-functions[1] through

$$Y_{a,s} = \frac{T_{a,s+1}T_{a,s-1}}{T_{a+1,s}T_{a-1,s}}\,, \tag{3.30}$$

which then satisfy the Hirota equation [104]

$$T^{+}_{a,s}T^{-}_{a,s} = T_{a+1,s}T_{a-1,s} + T_{a,s+1}T_{a,s-1}\,. \tag{3.31}$$

FiNLIE

The Y-system, and likewise the T-system, contain an infinite set of functions. Inspired by the methods [105], it is possible to reformulate the problem in terms of a *finite* set of nonlinear integral equations, the FiNLIE [106]. See also [107] for a similar development.

The FiNLIE was used first for a 6-loop calculation of the Konishi anomalous dimension [108], and then for an impressive 8-loop calculation [109], the first example of a double-wrapping result.

Quantum Spectral Curve

It was soon pointed out [24, 110] that T-functions have a convenient parametrisation in terms of Q-functions. Indeed, it was observed that the solutions to the T-system can be built from just eight independent Q-functions. It also became clear [106] that these Q-functions should have rather simple analytic properties. Mastering these analytic properties finally led to a beautiful reformulation of the problem: the Quantum Spectral Curve [14, 15].

To briefly summarise the derivation in [15], the T-system is defined up to a certain gauge symmetry, and in a particular choice of gauge, where the T-functions can be denoted $\mathbb{T}_{a,s}$, it is possible to make the parametrisation

$$\mathbb{T}_{0,s} = \begin{cases} \mathbf{P}_1^{[+s]}\mathbf{P}_2^{[-s]} - \mathbf{P}_2^{[+s]}\mathbf{P}_1^{[-s]} & s \geq 1 \\ \mathbf{P}^{4[+s]}\mathbf{P}^{3[-s]} - \mathbf{P}^{3[+s]}\mathbf{P}^{4[-s]} & s \leq -1 \end{cases}\,. \tag{3.32}$$

The functions $\mathbf{P}$ have only a single branch cut on a certain Riemann-sheet. In a different gauge, $\mathbf{T}_{a,s}$, related to the first by $\mathbb{T}_{a,s} = (-1)^{a\cdot s}\mathbf{T}_{a,s}(\mathbf{T}_{0,0}^{[a+s]})^{\frac{a}{2}-1}$, the function $\mathbf{T}_{0,1}^{\frac{1}{2}} \equiv \mu_{12}$

[1] The T-functions are believed to be eigenvalues of transfer matrices, cf. section 2.2, with rectangular representations in the auxiliary space. The precise nature of these transfer matrices, and the R-matrix from which they are constructed, is however not known.

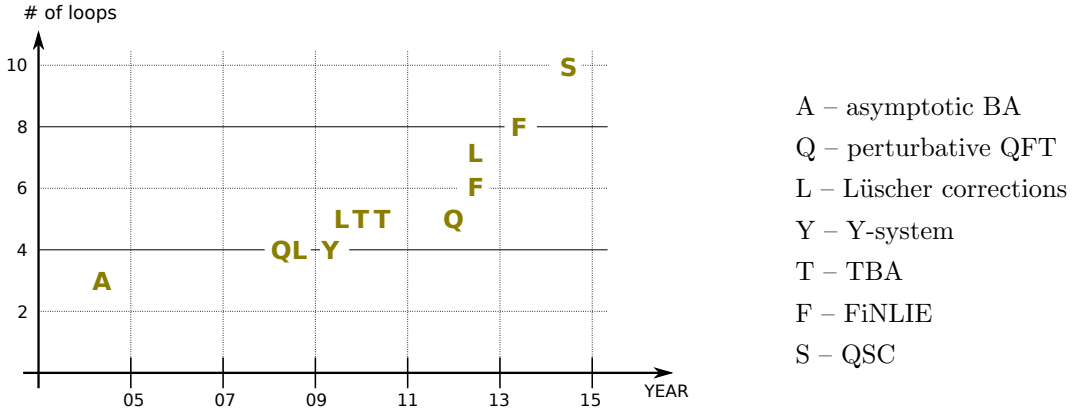

Figure 3.7: Perturbative computations of the Konishi anomalous dimension in planar $\mathcal{N}$=4 SYM.

has the nice property of being $\mathbb{i}$-periodic on a certain Riemann-sheet. Together, the five functions $\mathbf{P}_1$, $\mathbf{P}_2$, $\mathbf{P}^3$, $\mathbf{P}^4$ and μ_{12} contain the information needed to reconstruct the whole T-system via the Hirota equation (3.31). However, control of their analytic continuation is required. By introducing additional functions $\mathbf{P}_3$, $\mathbf{P}_4$, $\mathbf{P}^1$, $\mathbf{P}^2$ and five extra μ_{ab}, a very compact closed system of equations on these functions and their analytic continuations is formed. This $\mathbf{P}\mu$-system is self-contained, but a natural consequence of the system is a similar $\mathbf{Q}\omega$-system and the larger $\mathfrak{psu}(2,2|4)$ Q-system. These systems will be introduced in detail in chapter 4.

Subconclusion

This chapter gave a rough summary of how integrability appears in the planar $\mathrm{AdS}_5/\mathrm{CFT}_4$ spectral problem, and how the assumption of integrability can be used to bootstrap the spectrum. The key object to understand was the S-matrix which, through various adaptions of integrability techniques, captures the spectral information. The end-product is the Quantum Spectral Curve, a relatively comprehensible Riemann-Hilbert problem determining the spectrum, whose explicit solution is the main goal of this thesis. The QSC is of course not guaranteed to be the final and most elegant solution to the problem, but the fact that it has survived more than four years without signs of further simplifications signals that some sort of a fixed point has been reached. With such a formulation at hand, it is time to understand its applications and scope in complete generality. The second part of this thesis is devoted to exploring its power as a perturbative tool. To sum up the developments reviewed in this chapter, and to anticipate the power of the QSC, the chronological development in the computation of the Konishi anomalous dimension is depicted in figure 3.7.

Chapter 4

Quantum Spectral Curve

This chapter presents all technical details about the QSC [14, 15] that will be needed in the second part of the thesis. We first state the fundamental structures of the QSC in an axiomatic form, before using this as a foundation to derive a number of practically useful relations. We then discuss the properties of the QSC at weak coupling, and this discussion will be the foundation of the explicit solution methods described in later chapters. Afterwards, a brief summary of the applications and generalisations of the QSC is given.

The treatment is rather technical, and the bored reader is encouraged to continue to the next chapters, where the usefulness of the various relations should become more clear. The intention is to collect the details here in order to make the later presentation of the applications lighter.

4.1 The Quantum Spectral Curve

The basic structure in the QSC is an algebraic Q-system, which we already encountered in chapter 2 in the context of the algebraic Bethe ansatz. The new feature compared to the spin chain Q-system is that the QSC specifies a more complicated analytic structure of the Q-functions which are multi-valued functions of the spectral parameter u. The spin chain Q-system corresponds to the $g = 0$ limit of the QSC. Again, each solution to the system is characterised by a set of quantum numbers that dictate the asymptotic behaviour of the Q-functions at large values of the spectral parameter.

The analytic continuation of the Q-functions can be described in terms of a set of auxiliary functions, μ and ω, with very particular analytic properties. Together with a small subset of the Q-functions, these auxiliary variables form two closed sets of equations, the $\mathbf{P}\mu$- and $\mathbf{Q}\omega$-systems, which are self-contained formulations of the essential information in the QSC. In this section, which is essentially a summary of the statements presented in the original paper [15], we consider these structures in more detail.

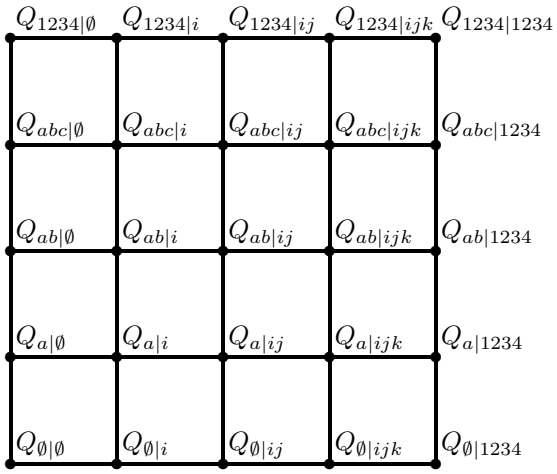

Figure 4.1: The $\mathfrak{gl}(4|4)$ Q-system.

4.1.1 The Q-system

In accordance with the $\mathfrak{psu}(2,2|4)$ symmetry of the theory, the QSC is based on a $\mathfrak{gl}(4|4)$ Q-system, consisting of $2^8 = 256$ functions of the spectral parameter, u. We can label these functions as

$$Q_{A|I} = Q_{a_1a_2\ldots|i_1i_2\ldots} = -Q_{a_2a_1\ldots|i_1i_2\ldots} = -Q_{a_1a_2\ldots|i_2i_1\ldots} \,, \tag{4.1}$$

with A and I denoting between zero and four separately antisymmetric indices that can take the values $a_k, i_k \in \{1,2,3,4\}$. Throughout the thesis we will use the notations

$$Q = Q(u)\,, \qquad Q^{[n]} \equiv Q\Big(u + \tfrac{\mathrm{i}}{2}n\Big)\,, \qquad Q^{\pm} \equiv Q^{[\pm 1]}\,. \tag{4.2}$$

QQ-relations

The Q-functions are related through difference equations of the kind

$$Q_{A|I}Q_{Aab|I} = Q^{+}_{Aa|I}Q^{-}_{Ab|I} - Q^{-}_{Aa|I}Q^{+}_{Ab|I} \tag{4.3a}$$
$$Q_{A|I}Q_{A|Iij} = Q^{+}_{A|Ii}Q^{-}_{A|Ij} - Q^{-}_{A|Ii}Q^{+}_{A|Ij} \tag{4.3b}$$
$$Q_{Aa|I}Q_{A|Ii} = Q^{+}_{Aa|Ii}Q^{-}_{A|I} - Q^{-}_{Aa|Ii}Q^{+}_{A|I}\,. \tag{4.3c}$$

We can depict the Q-system on a 4×4 lattice, where the Q-functions live at the node corresponding to its number of indices of the two kinds, see figure 4.1. On a vertical or horizontal segment of this lattice, the Q-functions then satisfy (4.3a) or (4.3b), which we refer to as *bosonic* QQ-relations. On a square segment, the Q-functions satisfy (4.3c), which we call *fermionic* QQ-relations, as they only appear for superalgebras. See figure 4.2.

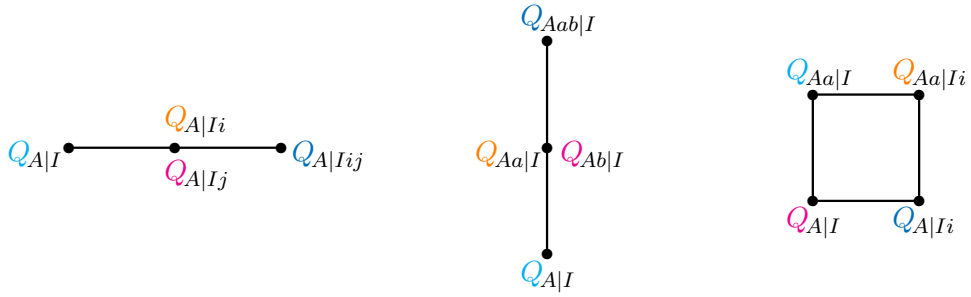

Figure 4.2: The three types of QQ-relations (4.3). According to their colouring, the depicted Q-functions satisfy the QQ-relation $QQ = Q^{+}Q^{-} - Q^{-}Q^{+}$.

Hodge dual

It is convenient to introduce the notion of a Hodge dual Q-system defined through

$$Q^{A|I} \equiv (-1)^{|A'||I|}\epsilon^{A'A}\epsilon^{I'I}Q_{A'|I'}\,, \tag{4.4}$$

where $Q^{A|I}$ satisfy QQ-relations identical to (4.3). $|A|$ denotes the number of indices in the multi-index A and $\epsilon^{1234} = 1$. Note that no sum over the multi-indices A' and I' is implied in (4.4).

4.1.2 Large u asymptotics

As we will see in the discussion of the symmetries of the QSC below in section 4.1.5, it is always possible, and very convenient, to set

$$Q_{\emptyset|\emptyset} = Q_{1234|1234} = 1\,. \tag{4.5}$$

The asymptotic behaviour of the Q-functions at large real u can be stated through the behaviour of the eight single-indexed Q-functions:

$$Q_{a|\emptyset} \simeq \mathsf{A}_a u^{-\hat{\lambda}_a} \tag{4.6a}$$

$$Q_{\emptyset|i} \simeq \mathsf{B}_i u^{-\hat{\nu}_i - 1}\,, \tag{4.6b}$$

where A and B are constant prefactors chosen such that the QQ-relations have the form (4.3). The numbers $\hat{\lambda}_a$ and $\hat{\nu}_i$ can be related to the fundamental $\mathfrak{gl}(4|4)$ weights λ_a and ν_i, cf. sections 1.1.1 and 1.4.2, in a specific grading, $\hat{1}\hat{1}\hat{2}\hat{2}\hat{3}\hat{3}\hat{4}\hat{4}$, see figure 4.3, through

$$\hat{\lambda}_a = \lambda_a^{\hat{1}\hat{1}\hat{2}\hat{2}\hat{3}\hat{3}\hat{4}\hat{4}} + \Lambda \tag{4.7a}$$

$$\hat{\nu}_i = \nu_i^{\hat{1}\hat{1}\hat{2}\hat{2}\hat{3}\hat{3}\hat{4}\hat{4}} - \Lambda\,, \tag{4.7b}$$

where Λ is an arbitrary shift corresponding to the fact that the actual $\mathfrak{psu}(2,2|4)$ quantum numbers are the differences $\lambda_a - \lambda_{a+1}$. We discuss this symmetry in section 4.1.5 below. Notice that the central charge constraint translates to

$$\sum_{a=1}^{4}\hat{\lambda}_a + \sum_{i=1}^{4}\hat{\nu}_i = 0\,, \tag{4.8}$$

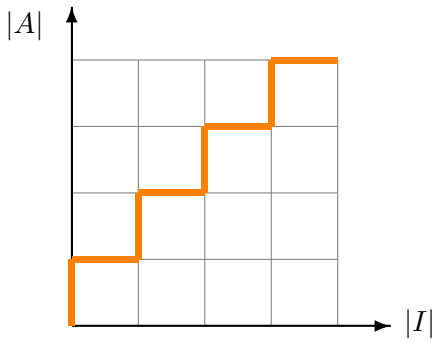

Figure 4.3: Up to an overall shift, $\lambda+\Lambda$ and $\nu-\Lambda$, the fundamental weights in the grading $\hat{1}1\hat{2}2\hat{3}3\hat{4}4$ (or equivalently $\hat{1}1\hat{2}\hat{2}3\hat{3}4\hat{4}$) correspond to $\hat{\lambda}$ and $\hat{\nu}$ that dictate the large u asymptotics of the QSC solutions.

and is unaffected by the value of Λ.

Through the QQ-relations, the asymptotic structure (4.6) along with the general feature (4.5) dictates the asymptotic behaviour of all other Q-functions. We discuss this in more detail in section 4.2.4 below. Note that the asymptotics is where the anomalous dimension γ, through the numbers $\hat{\nu}_i$, enters the QSC.

4.1.3 Analytic structure

The Q-functions are multivalued functions of the spectral parameter u. The fundamental properties of the analytic structure of the Q-system can be captured in the structure of the single-indexed Q-functions, which we denote by

$$\mathbf{P}_a \equiv Q_{a|\emptyset} \qquad \mathbf{P}^a \equiv Q^{a|\emptyset} \qquad \mathbf{Q}_i \equiv Q_{\emptyset|i} \qquad \mathbf{Q}^i \equiv Q^{\emptyset|i}\,. \tag{4.9}$$

For $\mathbf{P}$ there exists a Riemann sheet in u where the functions have only a single branch cut between $u = -2g$ and $u = +2g$. For $\mathbf{Q}$ there exists a Riemann sheet where the functions have only the same two branch points, but instead of being connected by a short branch cut, infinite cuts are placed on the real axis from these points to $u = \pm\infty$. These Riemann sheets are depicted in figure 4.4. The position of branch points is the only explicit appearance of the coupling constant g in the QSC.

From these basic features, we can use the QQ-relations (4.3) to investigate the analytic structure of other Q-functions. To use the QQ-relations, we have to choose the same type of cuts for all Q-functions. For example, $Q_{ab|\emptyset} = \mathbf{P}^+_a\mathbf{P}^-_b - \mathbf{P}^-_a\mathbf{P}^+_b$ should have two short cuts shifted away from the real axis by $\pm\frac{\mathrm{i}}{2}$. To generate Q-functions with both types of indices, i.e. a $Q_{A|J}$ with $J \neq \emptyset, \bar{\emptyset}$, from $\mathbf{P}$, is however not as simple. As we will see below, one can for example derive a relation such as

$$Q^+_{a|i} - Q^-_{a|i} = -\mathbf{P}_a\mathbf{P}^b Q^\pm_{b|i} \tag{4.10}$$

from the basic QQ-relations. A sum over indices that appear in both upper- and lower-case in an expression is always implied unless otherwise stated, e.g. $\mathbf{P}^b Q^\pm_{b|i} \equiv \sum_{b=1}^4 \mathbf{P}^b Q^\pm_{b|i}$. A

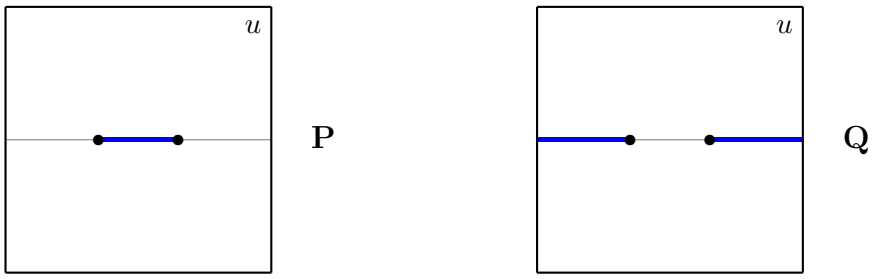

Figure 4.4: The *defining* Riemann sheet for the single-indexed Q-functions. The black dots correspond to branch points at $u = \pm 2g$. The blue lines are branch cuts. The gray line is the real axis, $\mathrm{Im}\,(u) = 0$.

solution to (4.10) can formally be constructed as the infinite product

$$Q_{a|i} = (\delta_a^{a_1} + \mathbf{P}_a^+ \mathbf{P}^{a_1+})(\delta_{a_1}^{a_2} + \mathbf{P}_{a_1}^{[3]} \mathbf{P}^{a_2[3]}) \cdots \tag{4.11}$$

which would generate an infinite ladder of short branch cuts in the lower half-plane between $-\mathbb{i}(\frac{1}{2} + \mathbb{N}_+) \pm 2g$. However, one could equally well construct $Q_{a|i}$ as

$$Q_{a|i} = (\delta_a^{a_1} - \mathbf{P}_a^- \mathbf{P}^{a_1-})(\delta_{a_1}^{a_2} - \mathbf{P}_{a_1}^{[-3]} \mathbf{P}^{a_2[-3]}) \cdots \tag{4.12}$$

resulting in cuts in the upper half-plane. Whether to have analyticity in the upper or lower half-plane is simply a choice. We will always choose analyticity in the upper half-plane. Through the QQ-relations it can be seen that such a semi-infinite ladder of short cuts appear in all $Q_{A|I}$ with $I \neq \emptyset, \bar{\emptyset}$. For the functions $\mathbf{Q}$, this corresponds to choosing to keep the upper half-plane in figure 4.4 on the first Riemann sheet, while replacing the lower half-plane by the analytic continuation through the long cut. See figure 4.5.

In general, for a generic Q-function $Q_{A|I}$ we denote the value on the *first* sheet, where it is analytic in the upper half-plane, by $Q_{A|I}$, and its value on the *second* sheet, arising from analytic continuation through a branch cut on the real axis, by $\tilde{Q}_{A|I}$.

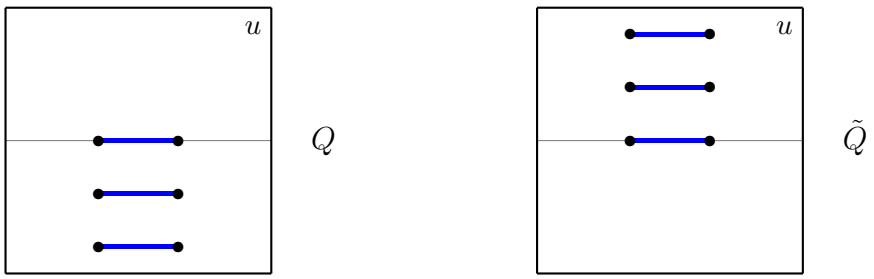

Figure 4.5: The first (left) and second (right) Riemann sheet of $Q_{A|I}$, $I \neq \emptyset, \bar{\emptyset}$, with short cuts (up to a shift of $\frac{\mathbb{i}}{2}$ depending on the total number of indices). The functions $\mathbf{Q}$ have this structure. The upper half-plane on the first sheet and the lower half-plane on the second sheet correspond to the defining sheet for $\mathbf{Q}$ with long cuts in figure 4.4.

We could argue in the same way that $\mathbf{P}$ develops a semi-infinite ladder of long cuts on its first sheet. Translating this to short cuts, we see that on the second sheet, $\mathbf{P}$ has an infinite ladder of cuts in both the upper and lower half-plane, see figure 4.6.

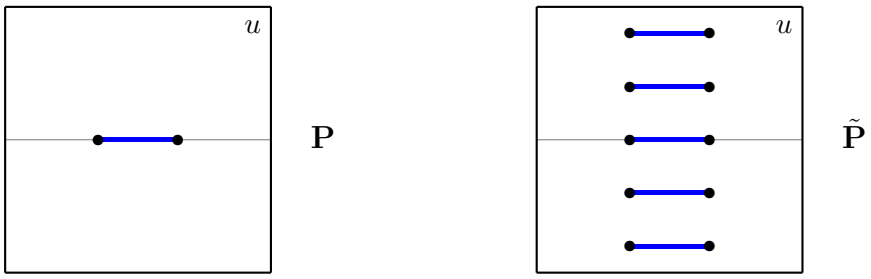

Figure 4.6: The first (left) and second (right) Riemann sheet of **P** with short cuts.

Importantly, from the definition of the QSC, all branch cuts are of squareroot type, i.e. $\tilde{\tilde{f}} = f$, and all functions are required to be regular everywhere, i.e. have no singularities. We will almost always describe the QSC functions in terms of short cuts, and it will always be stated explicitly if long cuts are considered.

4.1.4 The Pμ- and Qω-systems

We now know where the branch points are, but we also need to know how to analytically continue through the cuts. The QSC describes the analytic continuation of **P** and **Q** through their cuts on the real axis in terms of a set of auxiliary functions μ and ω. These functions are in turn closely related to the central Q-functions, $Q_{ab|ij}$.

Construction of μ and ω

Introduce four times six functions, μ_{ab}, μ^{ab}, ω_{ij} and ω^{ij}, all antisymmetric in their indices. All these functions have infinite ladders of branch points at $u = \mathbb{i}\mathbb{Z} \pm 2g$ irrespective of the chosen type of cuts. With **short** cuts, the first sheet of μ_{ab} can be defined as a linear combination of the six functions $Q^-_{ab|ij}$ with $\mathbb{i}$-periodic coefficients, $\omega^{ij} = \omega^{ij[2]}$:

$$\mu_{ab} = \frac{1}{2}\omega^{ij} Q^-_{ab|ij} \,. \tag{4.13a}$$

Similarly, the first sheet of μ^{ab} is given by,

$$\mu^{ab} = \frac{1}{2}\omega_{ij} Q^{ab|ij-} \,. \tag{4.13b}$$

Had we instead chosen to work with **long** cuts, the roles would be reversed: ω would be linear combinations of $Q^-_{ab|ij}$ with $\mathbb{i}$-periodic coefficients μ. The fact that μ are periodic with long cuts translates into the following relation for the analytic continuation of μ with short cuts:

$$\tilde{\mu} = \mu^{[2]} \,. \tag{4.14}$$

A visual argument is given in figure 4.7.

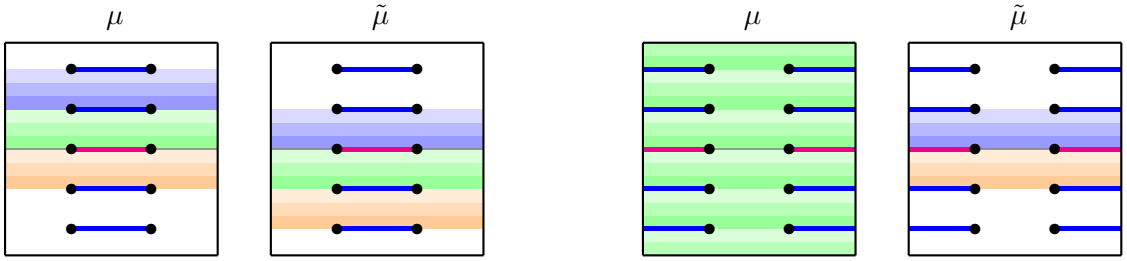

Figure 4.7: The first and second sheet of μ with (left) short and (right) long cuts. The colours correspond to strips with the same value.

Analytic continuation of P and Q

The functions μ dictate the analytic continuation of $\mathbf{P}$ via the relations

$$\tilde{\mathbf{P}}_a = \mu_{ab}\mathbf{P}^b \qquad\qquad \tilde{\mathbf{P}}^a = \mu^{ab}\mathbf{P}_b \,. \tag{4.15}$$

Similarly, ω governs the analytic continuation of $\mathbf{Q}$ via

$$\tilde{\mathbf{Q}}_i = \omega_{ij}\mathbf{Q}^j \qquad\qquad \tilde{\mathbf{Q}}^i = \omega^{ij}\mathbf{Q}_j \,. \tag{4.16}$$

The Pμ-system

The eight functions $\mathbf{P}$ and the 12 functions μ form a self-contained Riemann-Hilbert problem from which the rest of the structure in the QSC, the Q-system and a similar system formed by $\mathbf{Q}$ and ω, can be derived, see [15].

As we saw in (4.13), the functions μ_{ab} are linear combinations of the central Q-functions, $Q_{ab|ij}$, with $\mathbb{i}$-periodic coefficients, and they thus satisfy the same difference equations as these Q-functions. In particular they satisfy a set of six coupled first order difference equations,

$$\mu_{ab} - \mu^{[2]}_{ab} = \mathbf{P}_b\mathbf{P}^c\mu^{[1\pm1]}_{ac} - \mathbf{P}_a\mathbf{P}^c\mu^{[1\pm1]}_{bc} \tag{4.17}$$

to which $Q_{ab|ij}$ are the complete set of solutions. The equation can also be phrased as

$$\mu_{ab} - \mu^{[2]}_{ab} = \tilde{\mathbf{P}}_a\mathbf{P}_b - \mathbf{P}_a\tilde{\mathbf{P}}_b \,, \tag{4.18a}$$

and similarly we get

$$\mu^{ab} - \mu^{ab[2]} = -\tilde{\mathbf{P}}^a\mathbf{P}^b + \mathbf{P}^a\tilde{\mathbf{P}}^b \,. \tag{4.18b}$$

Together with (4.15) and the specified analytic structure, we call this the $\mathbf{P}\mu$*-system*.

We could have derived a similar self-contained $\mathbf{Q}\omega$-system, but as we will not need it in our applications, we leave it out and refer to the original papers for the details.

Asymptotics of μ and ω

For solutions of the QSC that correspond to cyclic single-trace operators, the functions ω can have at most constant asymptotics at large u. We often refer to such solutions as *physical*. This important restriction is the one that singles out the solutions of the QSC that we wish to consider in this thesis.

As it has been discussed in e.g. [111, 112], *unphysical* solutions, by which we mean solutions not corresponding to single-trace operators, require a modification of the asymptotics of ω to include exponential behaviour, e.g. $\omega \sim e^{2\pi u}$ at $u \to \infty$. This is due to the regularity constraint (4.55) discussed below.

4.1.5 Symmetries

The QSC has a large amount of symmetry. We here use the terminology of the original paper [15] and denote the freedom to do spectral parameter dependent rescalings by *gauge* symmetry (note that it has no relation to the $SU(N)$ gauge symmetry of $\mathcal{N} = 4$ SYM), and the possibility to shuffle the basis of Q-functions through linear combinations by *H-symmetry*.

Gauge symmetry

The QQ-relations are invariant under transformations of the kind

$$Q_{A|I} \to \frac{f^{[|A|-|I|+k]}}{f^{[-|A|+|I|-k]}} Q_{A|I}\,, \tag{4.19}$$

where f is formally an arbitrary function of the spectral parameter, and k is an integer. However only two such rescalings are independent, e.g. $k = 0, 1$. For example a $k = 2$ rescaling can be written as

$$\frac{g^{[N+2]}}{g^{[-N-2]}} = \left(\frac{g^{[N+1]}}{g^{[-N-1]}}\right)^{+} \left(\frac{g^{[N+1]}}{g^{[-N-1]}}\right)^{-} \frac{g^{[-N]}}{g^{[N]}} = \frac{(g^{+})^{[N+1]}}{(g^{+})^{[-N-1]}} \frac{(g^{-})^{[N+1]}}{(g^{-})^{[-N-1]}} \frac{(g^{-1})^{[N]}}{(g^{-1})^{[-N]}}\,. \tag{4.20}$$

We choose to demand $Q_{\emptyset|\emptyset} = Q_{1234|1234} = 1$ which removes the freedom to do $k = 1$ transformations and leaves only those of the type $k = 0$. If we want to preserve the branch cut structure of the Q-functions described above, the only remaining gauge symmetry corresponds to the freedom to do rescalings involving the Zhukowsky variable x of the kind

$$Q_{A|I} \to \prod_{k=\frac{|A|-|I|}{2}}^{\frac{|I|-|A|}{2}} (x^{[k]})^{\mathrm{sign}(|A|-|I|)\Lambda} Q_{A|I}\,. \tag{4.21}$$

For the one-indexed Q-functions this means

$$Q_{a|\emptyset} \to x^{\Lambda} Q_{a|\emptyset}, \quad Q_{\emptyset|j} \to x^{-\Lambda} Q_{\emptyset|j}\,. \tag{4.22}$$

and since $x \simeq \frac{u}{g} + \mathcal{O}(\frac{1}{u})$ at large u, this exactly corresponds to the ambiguity in the asymptotic powers $\hat{\lambda}$ and $\hat{\nu}$ in (4.7).

H-symmetry

The QQ-relations are likewise invariant under transformations of the kind

$$Q_{A|I} \to (H^{[|A|-|I|]})_A^B (\hat{H}^{[|A|-|I|]})_I^J Q_{B|J}, \quad |A| = |B|, \quad |I| = |J|, \tag{4.23}$$

where $H_A^B = H_{a_1}^{b_1} H_{a_2}^{b_2} \ldots$ and $\hat{H}_I^J = \hat{H}_{i_1}^{j_1} \hat{H}_{i_2}^{j_2} \ldots$, and where H_a^b and $\hat{H}_i^j$ are 4×4 matrices that i-periodically depend on u and have unit determinants $\det H = \det \hat{H} = 1$ in order to keep $Q_{1234|1234} = 1$.

This symmetry means that we can add and subtract Q-functions with the same types of indices. If we want to maintain analyticity in the upper half-plane and power-like asymptotics then H and $\hat{H}$ must be constant matrices. We can use this symmetry to ensure that Q-functions related by the H-symmetry have distinct asymptotic behaviour at $u \to \infty$, and this fixes a large amount of the symmetry. This choice was in fact already implicit in the asymptotic behaviour described in section 4.1.2. Likewise, we can rescale the constant prefactors A and B (4.6) as long we keep the product $\mathsf{A}_1\mathsf{A}_2\mathsf{A}_3\mathsf{A}_4\mathsf{B}_1\mathsf{B}_2\mathsf{B}_3\mathsf{B}_4$ fixed to maintain $Q_{1234|1234} = 1$.

Relations between solutions

Some solutions of the QSC are related by simple relabelings. Sometimes these relabelings map a solution to itself, which means that the solution has additional symmetries. There are two cases:

- As the QSC equations are invariant under the parity transformation $u \leftrightarrow -u$, then if $\{Q_{A|I}(u)\}$ is a solution to the Q-system, $\{Q_{A|I}(-u)\}$ will be as well. In some cases, the two Q-systems will be identical, and we call such states *parity invariant*. In the spin chain picture, the transformation $u \to -u$ corresponds to a reflection.

- Similarly, the Hodge dual (4.4) of $\{Q_{A|I}\}$, which we denote by $\{Q^{\bigstar}_{A|I}\} \equiv \{Q^{A|I}\}$ will also be a solution, though in general to a Q-system with different asymptotical behaviour. However, for some states the two sets of Q-functions are identical, and we call these *Hodge invariant*. Hodge invariance can occur when the left and right half of the Young diagram corresponding to the quantum numbers at zero coupling are of the same shape, i.e. if in the $\sqcap$ grading

  $$n_{\mathbf{f}_1} = L - n_{\mathbf{f}_4} \qquad n_{\mathbf{f}_2} = L - n_{\mathbf{f}_3} \qquad n_{\mathbf{b}_1} = n_{\mathbf{a}_2} \qquad n_{\mathbf{b}_2} = n_{\mathbf{a}_1}\,. \tag{4.24}$$

  This is also referred to as *left/right symmetry*. When a state is left/right symmetric (4.24), it implies that either $\{Q_{A|I}(u)\} = \{Q^{\bigstar}_{A|I}(u)\}$ or $\{Q_{A|I}(u)\} = \{Q^{\bigstar}_{A|I}(-u)\}$, or both in the case of parity invariance.

$$\begin{array}{ccc} \{Q_{A|I}(u)\} & \leftrightarrow & \{Q_{A|I}(-u)\} \\ \updownarrow & & \updownarrow \\ \{Q^{\bigstar}_{A|I}(u)\} & \leftrightarrow & \{Q^{\bigstar}_{A|I}(-u)\} \end{array}$$

Figure 4.8: All solutions come in sets related by parity and Hodge transformation. In some cases, one or all of these transformations map a solution to itself.

An overview of the related solutions is given in figure 4.8.

4.2 Important relations

In this section we collect a number of convenient formulas that follow from the fundamental relations of the QSC given above.

4.2.1 The full Q-system from $Q_{a|\emptyset}$ and $Q_{\emptyset|i}$

Clearly the knowledge of all 256 Q-functions is not essential. In fact, we just need to know eight of them, for example $Q_{a|\emptyset}$ and $Q_{\emptyset|i}$, to generate the rest.

$Q_{a|j}$ from $Q_{a|\emptyset}$ and $Q_{\emptyset|j}$

To generate $Q_{a|j}$ from $Q_{a|\emptyset}$ and $Q_{\emptyset|j}$ one has to solve the first order difference equations

$$Q^{+}_{a|i} - Q^{-}_{a|i} = \mathbf{P}_a \mathbf{Q}_i \,. \tag{4.25}$$

The solution can formally be written as

$$Q_{a|i} = -\Psi\left(\mathbf{P}^{+}_{a} \mathbf{Q}^{+}_{i}\right) , \tag{4.26}$$

where Ψ is the inverse of the difference operation ∇,

$$\Psi(\nabla(f)) = f + \mathcal{P} \,, \qquad \nabla(f) \equiv f - f^{[2]} \,, \tag{4.27}$$

where $\mathcal{P}$ is an $\mathbb{i}$-periodic function. In (4.26) this $\mathbb{i}$-periodic ambiguity should be a constant to preserve upper half-plane analyticity and power-like asymptotics. The Ψ-operation plays an important role throughout the thesis, and it is discussed in detail in appendix C.1.

The rest

It follows from the QQ-relations that all other Q-functions can be generated from of $Q_{a|\emptyset}$, $Q_{\emptyset|j}$ and $Q_{a|j}$ via determinant formulas of the kind

$$Q_{a_1,\dots,a_m|j_1,\dots,j_n} = \begin{cases} \epsilon^{k_1,\dots,k_n} \prod_{r=1}^{m} Q^{[\bullet]}_{a_r|j_{k_r}} \prod_{s=1}^{n-m} Q^{[n-m+1-2s]}_{\emptyset|j_{k_{m+s}}} & m < n \\ \epsilon^{k_1,\dots,k_m} \prod_{r=1}^{m} Q_{a_{k_r}|j_r} & m = n \\ \epsilon^{k_1,\dots,k_m} \prod_{r=1}^{n} Q^{[\bullet]}_{a_{k_r}|j_r} \prod_{s=1}^{m-n} Q^{[m-n+1-2s]}_{a_{k_{n+s}}|\emptyset} & m > n \end{cases} , \tag{4.28}$$

where $\bullet$ can take any value in $-|m-n|, -|m-n|+2, \dots, |m-n|-2, |m-n|$. The arbitrary constants introduced in (4.26) can be fixed via the demand $Q_{1234|1234} = 1$.

4.2.2 Relations between $Q_{A|I}$ and $Q^{B|J}$

A number of nice relations between the lower- and upper-indexed Q-functions follow directly from the QQ-relations and the property $Q_{\emptyset|\emptyset} = Q_{1234|1234} = 1$.

One can derive the very useful relations

$$\mathbf{P}_a = -\mathbf{Q}^i Q^{\pm}_{a|i} \qquad \mathbf{P}^a = \mathbf{Q}_i Q^{a|i\pm} \qquad \mathbf{Q}_i = -\mathbf{P}^a Q^{\pm}_{a|i} \qquad \mathbf{Q}^i = \mathbf{P}_a Q^{a|i\pm} \,. \tag{4.29}$$

The single-indexed Q-functions satisfy

$$\mathbf{P}_a \mathbf{P}^a = \mathbf{Q}_i \mathbf{Q}^i = 0 \,. \tag{4.30}$$

Furthermore,

$$Q_{a|i} Q^{a|j} = -\delta^j_i \qquad Q_{a|i} Q^{b|i} = -\delta^b_a \,, \tag{4.31}$$

which implies

$$Q_{ab|ij} Q^{ab|kl} = 2(\delta^k_i \delta^l_j - \delta^l_i \delta^k_j) \,. \tag{4.32}$$

4.2.3 Coupled difference equations on $Q_{A|I}$ in terms of $\mathbf{P}$

Using the relations (4.29), one can formulate coupled sets of first order difference equations on Q-functions with a given type of indices, where $\mathbf{P}$ play the role as coefficients. Such equations play a key role in the perturbative algorithms described in chapter 4.

For example, one can combine (4.25) and (4.29) to see that $Q_{a|i}$ are solutions to a set of four coupled first-order difference equations

$$Q^-_{a|i} - Q^+_{a|i} = \mathbf{P}_a \mathbf{P}^b Q^{\pm}_{b|i} \,. \tag{4.33}$$

Each value of i labels a particular solution. Likewise, $Q_{ab|ij}$ are the solutions of the six coupled first-order equations

$$Q^-_{ab|ij} - Q^+_{ab|ij} = -\mathbf{P}_a \mathbf{P}^c Q^{\pm}_{bc|ij} + \mathbf{P}_b \mathbf{P}^c Q^{\pm}_{ac|ij} \,. \tag{4.34}$$

As discussed, μ_{ab} solve these equations as well.

Disentangled higher-order equations

One can start from the coupled first order equations and disentangle them into higher-order difference equations. For example, (4.33) could be turned into a decoupled fourth-order equation on $Q_{a|i}$. For the interested reader, this rather bulky equation is given in appendix A.4.3. We could similarly write a sixth-order equation on $Q_{ab|ij}$. However, as we will see in chapter 6, we will have more use of the simpler coupled first-order equations, and only use the decoupled higher-order equations in special cases where we can lower their degree.

4.2.4 Asymptotic behaviour

We now take a closer look at the implications of the asymptotic behaviour of the single-indexed Q-functions at large u described in section 4.1.2.

The QQ-relations imply that an arbitrary Q-function has the asymptotics [42]

$$Q_{A|I} \simeq \prod_{a\in A} \mathsf{A}_a u^{-\hat{\lambda}_a} \prod_{i\in I} \mathsf{B}_i u^{-\hat{\nu}_i-1} \frac{\prod_{a<b\in A}(\text{-}\mathbb{i})\frac{\hat{\lambda}_a-\hat{\lambda}_b}{u}\prod_{i<j\in I}(\text{-}\mathbb{i})\frac{\hat{\nu}_i-\hat{\nu}_j}{u}}{\prod_{a\in A}\prod_{i\in I}(\text{-}\mathbb{i})\frac{\hat{\lambda}_a+\hat{\nu}_i}{u}} \,. \tag{4.35}$$

Importantly, using (4.8), the behaviour of $Q^{\emptyset|\emptyset} = Q_{1234|1234}$ turns out to be

$$Q_{1234|1234} \simeq \prod_{a=1}^{4} \mathsf{A}_a \prod_{j=1}^{4} \mathsf{B}_j \frac{\prod_{1\le a<b\le 4}(\hat{\lambda}_a-\hat{\lambda}_b)\prod_{1\le i<j\le 4}(\hat{\nu}_i-\hat{\nu}_j)}{\prod_{a=1}^{4}\prod_{i=1}^{4}(\hat{\lambda}_a+\hat{\nu}_i)} \,, \tag{4.36}$$

and thus the constant prefactors A and B should satisfy

$$\prod_{a=1}^{4} \mathsf{A}_a \prod_{j=1}^{4} \mathsf{B}_j = \frac{\prod_{a=1}^{4}\prod_{i=1}^{4}(\hat{\lambda}_a+\hat{\nu}_i)}{\prod_{1\le a<b\le 4}(\hat{\lambda}_a-\hat{\lambda}_b)\prod_{1\le i<j\le 4}(\hat{\nu}_i-\hat{\nu}_j)} \,, \tag{4.37}$$

in order to have $Q_{1234|1234} = 1$.

From (4.35), we also get the asymptotic behaviour of $\mathbf{P}^a$ and $\mathbf{Q}^i$. We will denote their prefactors by A^a and B^i, i.e.

$$\mathbf{P}^a \simeq \mathsf{A}^a u^{\hat{\lambda}_a-1} \qquad\qquad \mathbf{Q}^i \simeq \mathsf{B}^i u^{\hat{\nu}_i} \,, \tag{4.38}$$

which can then be seen to satisfy the relations

$$\mathsf{A}_a\mathsf{A}^a = \mathbb{i}\frac{\prod_j \hat{\lambda}_a+\hat{\nu}_j}{\prod_{b\neq a}\hat{\lambda}_a-\hat{\lambda}_b} \tag{4.39a}$$

$$\mathsf{B}_j\mathsf{B}^j = \mathbb{i}\frac{\prod_a \hat{\nu}_j+\hat{\lambda}_a}{\prod_{k\neq j}\hat{\nu}_j-\hat{\nu}_k} \,, \tag{4.39b}$$

where no sums are implied on the left hand sides.

$\hat{\lambda}$ and $\hat{\nu}$ in terms of $n^{\lceil}$

As we will prefer to label solutions by their oscillator content of their HWS in the $\lceil$ grading at $g = 0$, we here give the relation between these numbers and $\hat{\lambda}$ and $\hat{\nu}$:

$$\hat{\lambda}_a = n^{\lceil}_{\mathbf{f}_a} + \{2, 1, 0, -1\}_a + \Lambda \quad \equiv \quad \lambda^0_a + \Lambda \tag{4.40a}$$

$$\hat{\nu}_i = \{-L^{\lceil} - n^{\lceil}_{\mathbf{b}_{\dot{\alpha}}}, n^{\lceil}_{\mathbf{a}_\alpha}\}_i + \{-1, -2, 1, 0\}_i - \Lambda \quad \equiv \quad \nu^0_i - \Lambda\,. \tag{4.40b}$$

Recall that the weights $\hat{\lambda}$ remain fixed at any g while $\hat{\nu}$ correspond to AdS_5 charges, which include the conformal dimension $\Delta = \Delta_0 + \gamma$, so they will run with the coupling,

$$\hat{\nu}_i = \hat{\nu}_i|_{g=0} + \frac{\gamma}{2}\{-1, -1, 1, 1\}_i\,. \tag{4.41}$$

Note that $\hat{\lambda}_a > \hat{\lambda}_{a+1}$ and $\hat{\nu}_i > \hat{\nu}_{i+1}$, while $\hat{\lambda}_a + \hat{\nu}_i = 0$ can only happen at the unitarity bound.

4.2.5 Analytic continuation in the Pμ-system

Doing analytic continuations of the equations of the $\mathbf{P}\mu$-system leads to useful relations. First note that from a contraction of (4.18) with $\mathbf{P}^b$, it follows that $(\mu_{ab} - \mu^{[2]}_{ab})\mathbf{P}^b = 0$, i.e.

$$\mu_{ab}\mathbf{P}^b = \mu^{[2]}_{ab}\mathbf{P}^b\,. \tag{4.42}$$

By doing an analytic continuation of (4.15) we get

$$\mathbf{P}_a = \mu^{[2]}_{ab}\tilde{\mathbf{P}}^b = \mu_{ab}\tilde{\mathbf{P}}^b\,, \tag{4.43}$$

which is a quite powerful constraint as it relates the value on a sheet with a single branch cut to a bilinear combination of functions with infinite ladders of cuts.

4.2.6 Properties of μ

It is worth investigating the properties of the auxiliary functions μ in more detail. These functions will play a key role in the weak coupling techniques described in chapter 6.

Analytic continuation on the real axis

The fact that all branch cuts are of square-root type means that with short cuts the combinations

$$\mu + \tilde{\mu} = \mu + \mu^{[2]} \qquad \frac{\mu - \tilde{\mu}}{\sqrt{u^2 - 4g^2}} = \frac{\mu - \mu^{[2]}}{\sqrt{u^2 - 4g^2}} \tag{4.44}$$

have a trivial monodromy when crossing the branch cut on the real axis.

Consequences of long cut periodicity

The fact that with long cuts μ is an $\mathbb{i}$-periodic function on its first sheet is a strong constraint. Away from the long cuts we have $\mu(u) = \mu(u+\mathbb{i})$ and also all derivatives must coincide. If we translate this to short cuts, cf. figure 4.7, then only the strip $0 \leq \mathrm{Im}\,(u) \leq 1$ is transferred from the first sheet with long cuts to the first sheet with short cuts. On the first sheet with short cuts the function is subject to a remnant of the $\mathbb{i}$-periodicity: the function should behave similarly when approaching the branch cut between $\pm 2g$ from above and the branch cut between $\mathbb{i} \pm 2g$ from below, i.e.

$$\frac{\mathrm{d}^n}{\mathrm{d}^n u}\mu(u)\Big|_{u\to c+\mathbb{i}0^+} = \frac{\mathrm{d}^n}{\mathrm{d}^n u}\mu(u)\Big|_{u\to c+\mathbb{i}1^-}\,, \qquad -2g < c < 2g\,, \qquad n = 0, 1, 2, \ldots \tag{4.45}$$

As we will see in the next section, this gives us an important constraint on the behaviour of μ at $u = 0$ and $u = \mathbb{i}$ at weak coupling.

The Pfaffian and the relation between μ_{ab} and μ^{ab}

Since $\tilde{\mathbf{P}}_a = \mu_{ab}\mathbf{P}^b = \mu_{ab}\mu^{bc}\tilde{\mathbf{P}}_c$ we can conclude that μ_{ab} and μ^{ab} are mutually inverses, i.e.

$$\mu_{ab}\mu^{bc} = \delta_a^c\,. \tag{4.46}$$

We define the Pfaffian of μ_{ab} through

$$\mathrm{Pf}(\mu_\bullet) \equiv \frac{1}{8}\epsilon^{abcd}\mu_{ab}\mu_{cd} = \mu_{12}\mu_{34} - \mu_{13}\mu_{24} + \mu_{14}\mu_{23}\,. \tag{4.47}$$

One can see, by writing out the explicit possibilities, that

$$\epsilon^{abcd}\mu_{cd}\mu_{be} = -2\delta_e^a\,\mathrm{Pf}(\mu_\bullet)\,. \tag{4.48}$$

We can then combine (4.48) and (4.46) to see that μ^{ab} and μ_{cd} are related through

$$\mu^{ab} = -\frac{1}{2}\epsilon^{abcd}\mu_{cd}\frac{1}{\mathrm{Pf}(\mu_\bullet)}\,. \tag{4.49}$$

By using (4.17) and (4.30) we can infer that $\mathrm{Pf}(\mu_\bullet)$ is $\mathbb{i}$-periodic:

$$\mathrm{Pf}(\mu_\bullet) = (1 + \mathbf{P}_a\mathbf{P}^a)\,\mathrm{Pf}(\mu_\bullet^{[2]}) = \mathrm{Pf}(\mu_\bullet^{[2]})\,, \tag{4.50}$$

and since $\mathrm{Pf}(\mu_\bullet) = \mathrm{Pf}(\mu_\bullet^{[2]}) = \mathrm{Pf}(\tilde{\mu}_\bullet)$, it has no branch points. As it has power-like asymptotics, it must then be a constant, and it can be controlled by the freedom to fix the normalisations A_a.

4.2.7 P and the Zhukowsky map

A key property in the solution methods of the QSC is the simple structure of $\mathbf{P}$. It has integer power-like asymptotics at any value of g, and it has only a single short cut on the first Riemann sheet.

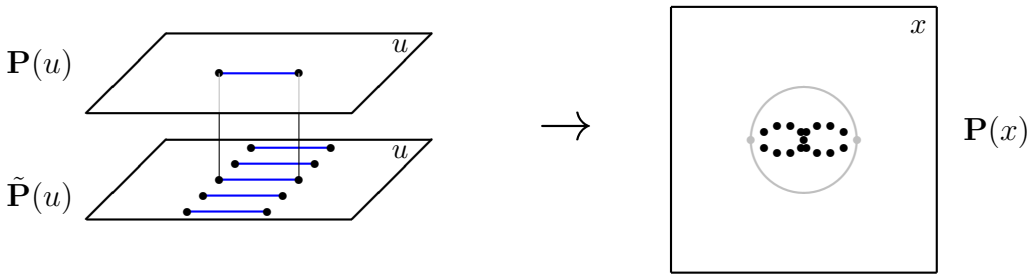

Figure 4.9: For $\mathbf{P}$, the first two Riemann sheets in u (left) gets mapped to a single sheet in x (right). The grey circle on the x-sheet is the unit circle, and the branch points on the real axis in u correspond to the points $x = \pm 1$.

To really exploit these features, one can make a change of variables from the spectral parameter u to the Zhukowsky variable $x(u)$ (3.13). We discuss the properties of the Zhukowsky variable in more detail in appendix A.4.1. The important property is that for $\mathbf{P}$, the first two Riemann sheets in u get mapped to a single Riemann sheet in x. The first sheet, $\mathbf{P}(u)$, is mapped outside the unit circle, $|x| > 1$, while the second sheet, $\tilde{\mathbf{P}}(u)$, is mapped to the inside of the unit circle, $|x| < 1$, see figure 4.9 and 4.10. The branch cut on the real axis is resolved and it is mapped to the unit circle in the x-plane.

We can write $\mathbf{P}(x)$ as a power expansion around $x = \infty$. As x behaves like $x \sim \frac{u}{g}$

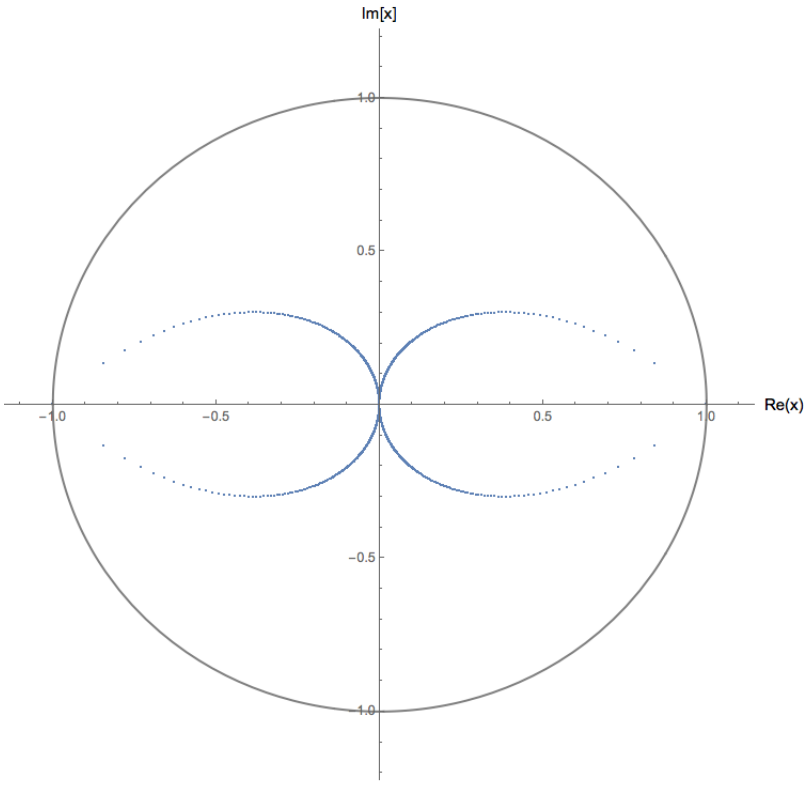

Figure 4.10: Plot showing the position of the points $x(u = \mathrm{i}\mathbb{Z} \pm 2g)$ for $g = 20$. For $g \to 0$ all branch points converge towards $x = 0$.

at large x, $\mathbf{P}(x)$ should have power-like large x asymptotics, $\mathbf{P}_a(x) \sim x^{-\hat{\lambda}_a}$ and $\mathbf{P}^a(x) \sim x^{\hat{\lambda}_a - 1}$. Then the power expansion of $\mathbf{P}$ should have the form

$$\mathbf{P}_a(x) = \sum_{k=\hat{\lambda}_a}^{\infty} \frac{c_{a,k}}{x^k} \qquad\qquad \mathbf{P}^a(x) = \sum_{k=-\hat{\lambda}_a+1}^{\infty} \frac{c^{a,k}}{x^k}\,, \tag{4.51}$$

where c are g-dependent coefficients. The behaviour of c in g is restricted by the values of the prefactors A, cf. section 4.2.4. This expansion should converge until the first branch points are reached in the x-plane, i.e. for $|x| > |x(\mathtt{i}+2g)|$. This means that the expansion is convergent everywhere on the first u-sheet, $\mathbf{P}(u)$, and in a finite region around the branch cut on the real axis on the second u-sheet, $\tilde{\mathbf{P}}(u)$.

Crossing the unit circle in the x-plane corresponds to crossing the short branch cut in $x(u)$. Since we restrict x to be the solution of (3.13) with $|x| > 1$, then this corresponds to the replacement $x \to \frac{1}{x}$ in (4.51).

4.3 The QSC at weak coupling

The main goal of this thesis is the perturbative weak coupling solution of the QSC. We thus need a systematic understanding of the QSC in the limit $g \to 0$.

Considering the analytic structure of the QSC functions, we see that, as depicted in figure 4.11, the branch points at $\mathtt{i}n - 2g$ and $\mathtt{i}n + 2g$ collide at $\mathtt{i}n$. The branch cuts vanish, and the functions develop the possibility of having poles at these points instead.

Our basic assumption is that for solutions corresponding to multiplets of single-trace operators, any function in the QSC can be written as a power expansion in g^2, i.e.

$$f(u,g) = \sum_{j=1}^{\infty} f^{(j)}(u) g^{2(j-1)} = f^{(1)}(u) + f^{(2)}(u) g^2 + f^{(3)}(u) g^4 + \dots\,. \tag{4.52}$$

Note that some functions may come with overall factors of g, and that such prefactors can usually be modified through the symmetry transformations mentioned in section 4.1.5.

For solutions of the QSC corresponding to single-trace operators, the conformal dimension follows the pattern (4.52), and at $g = 0$ it has the classical value (1.31). This means

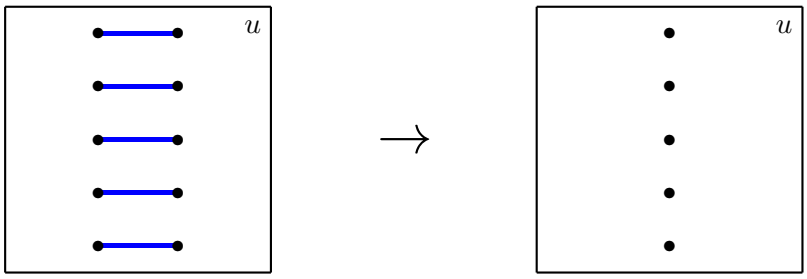

Figure 4.11: As $g \to 0$ the branch points at $\mathtt{i}n \pm g$ collide at $\mathtt{i}n$. The branch cuts disappear, and leave behind possible singularities.

that at the leading order, all functions have integer power-like asymptotics at $u \to \infty$, and the boundary conditions of the QSC coincides with those of a rational spin chain.

4.3.1 Properties of μ

The functions μ have important properties at weak coupling, which play a key role in the applications in the next chapters.

μ at $u = 0$

As discussed, the combinations $\mu + \mu^{[2]}$ and $\frac{\mu - \mu^{[2]}}{\sqrt{u^2-4g}}$ have no branch points on the real axis. As singularities at weak coupling only arise from colliding branch points, these combinations should be regular at $u = 0$ at any order of the weak coupling expansion. This turns out to be a strong constraint.

Polynomiality at the leading order

To satisfy both of the above regularity conditions, we see that μ cannot have poles at neither $u = 0$ or $u = \mathbb{i}$ at the leading order. Furthermore, μ satisfy relations of the type (4.17), which schematically have the form

$$\mu - \mu^{[2]} = (\mu\mathbf{P})\mathbf{P} - \mathbf{P}(\mu\mathbf{P}) = (\mu^{[2]}\mathbf{P})\mathbf{P} - \mathbf{P}(\mu^{[2]}\mathbf{P})\,, \tag{4.53}$$

and we can use these relations to make replacements of the kind

$$\mu^{[n]} = \mu^{[n+2]} + ((\mu\mathbf{P})\mathbf{P} - \mathbf{P}(\mu\mathbf{P}))^{[n]} \tag{4.54a}$$

$$\mu^{[n]} = \mu^{[n-2]} + \Big((\mu\mathbf{P}^{[-2]})\mathbf{P}^{[-2]} - \mathbf{P}^{[-2]}(\mu\mathbf{P}^{[-2]})\Big)^{[n]}\,. \tag{4.54b}$$

Using the first one to replace $\mu^{[2]}$ in the combination $\mu + \mu^{[2]}$, and recalling that $\mathbf{P}$ can only be singular at $u = 0$, we see that $\mu^{[4]}$ has to be regular at $u = 0$, i.e. μ is regular at $u = 2\mathbb{i}$. This argument can be applied recursively to argue that μ has no poles at $\mathbb{i}\mathbb{N}$. Furthermore, the second replacement can be used to argue that μ has no poles at $-\mathbb{i}\mathbb{N}$. In conclusion, μ are completely regular functions at the leading order with integer power-like asymptotics. Thus they are polynomials.

This observation also implies that, at the leading order, $\tilde{\mathbf{P}}$ can only have poles at $u = 0$ and have integer power-like asymptotics.

The zero-momentum condition

As μ are regular everywhere at the leading order, the constraint (4.45) turns into the requirement

$$\lim_{u\to 0} \frac{\mu^{(1)}(u + \mathbb{i})}{\mu^{(1)}(u)} = 1\,. \tag{4.55}$$

Maximal order of poles in perturbative expansion

The perturbative expansion of μ is

$$g^n \mu = \mu^{(1)} + \mu^{(2)} g^2 + \mu^{(3)} g^4 + \dots \,, \tag{4.56}$$

where n is some number. The regularity of $\mu + \mu^{[2]}$ tells us that the poles of μ and $\mu^{[2]}$ at $u = 0$ must be identical. For $\frac{\mu - \mu^{[2]}}{\sqrt{u^2-4g}}$ to also be regular, the maximal order of the poles at $u = 0$ is restricted. Perturbatively, this quantity looks like

$$\begin{aligned} g^n \frac{\mu - \mu^{[2]}}{\sqrt{u^2-4g}} \;\; = \;\; & \frac{\mu^{(1)} - \mu^{(1)[2]}}{u} + g^2 \left(\frac{\mu^{(2)} - \mu^{(2)[2]}}{u} + 2\frac{\mu^{(1)} - \mu^{(1)[2]}}{u^3} \right) \\ & + g^4 \left(\frac{\mu^{(3)} - \mu^{(3)[2]}}{u} + 2\frac{\mu^{(2)} - \mu^{(2)[2]}}{u^3} + 6\frac{\mu^{(1)} - \mu^{(1)[2]}}{u^5} \right) + \mathcal{O}(g^6) \,. \end{aligned} \tag{4.57}$$

As $\mu^{(1)} - \mu^{(1)[2]} \sim u$, the maximal pole in $\mu^{(2)}$ is u^{-1}. Then the maximal pole in $\mu^{(3)}$ is u^{-3}, and recursively we then see that $\mu^{(n)}$ has the maximal pole u^{-2n+3} at $u = 0$. The same holds for $\mu^{(n)[2]}$.

4.3.2 Structure of ω

The functions ω are $\mathbb{i}$-periodic and have at most constant asymptotics at $u \to \infty$ for physical solutions. They are only allowed to have poles at $u = \mathbb{i}\mathbb{Z}$. A general ansatz for such $\mathbb{i}$-periodic functions is given by

$$\omega = \omega^{\{0\}} + \sum_{k=1}^{\infty} \omega^{\{j\}} \mathcal{P}_j \,, \tag{4.58}$$

where $\omega^{\{j\}}$ are g-dependent constants and $\mathcal{P}_j$ are $\mathbb{i}$-periodic functions containing an infinite sum of poles of power j,

$$\mathcal{P}_j(u) = \sum_{k=-\infty}^{\infty} \frac{1}{(u + \mathbb{i}k)^j} \,. \tag{4.59}$$

We discuss these functions and their relation to hyperbolic functions in appendix B.3.1.

Truncation of the ansatz

As $\mu_{ab} = \frac{1}{2}\omega^{ij} Q^-_{ab|ij}$, the restricted pole structure of $\mu^{(n)}$ constrains the allowed terms in the ansatz for $\omega^{(n)}$. The functions $Q_{ab|ij}$ are analytic in the upper half-plane, so $Q^+_{ab|ij}$ cannot have poles at $u = 0$. Using (4.32), we can invert (4.13) to get the relation $\omega_{ij} = \frac{1}{2}\mu^{ab} Q^-_{ab|ij} = \frac{1}{2}\mu^{ab[2]} Q^+_{ab|ij}$. At the perturbative order n, the constraints on the maximal pole order in $\mu^{(n)[2]}$ discussed in section 4.3.1 means that the sum (4.58) is truncated at the term $\omega^{\{2n-3\}}$.

For μ to be polynomial at the leading order, ω must be constant at the leading order, i.e. $\omega^{(1)} = \omega^{(1)}_{\{0\}}$. Note also that, according to (4.35), $Q_{ab|34}$ have negative power-like large u-asymptotics, $u^{-\hat{\lambda}_a-\hat{\lambda}_b-\hat{\nu}_3-\hat{\nu}_4}$, due to the unitarity constraints, so they must be non-polynomial and unable to contribute to $\mu^{(1)}_{ab}$, i.e. $\omega^{34(1)} = 0$. It is then possible to use the $H_i{}^j$ symmetry to rotate the Q-system such that only ω^{12} is nonzero at the leading order. Note that, generically, $Q^{(1)}_{ab|12}$ is the only polynomial subset of $Q^{(1)}_{ab|ij}$ (an argument will be given in chapter 5), and then this follows automatically. Note furthermore that when $\mu^{(1)}_{ab} \propto Q^{(1)-}_{ab|12}$, the requirement (4.55) is the well-known zero-momentum condition

$$\lim_{u\to 0} \frac{Q^{(1)}_{ab|12}(u+\frac{\mathrm{i}}{2})}{Q^{(1)}_{ab|12}(u-\frac{\mathrm{i}}{2})} = 1\,. \tag{4.60}$$

4.3.3 Structure of P

The parametrisation of $\mathbf{P}$ in terms of the Zhukowsky variable and its expansion around $x = \infty$ discussed in section 4.2.7 gives us a lot of information about the structure of $\mathbf{P}(u)$ and $\tilde{\mathbf{P}}(u)$ in the weak coupling limit. This information will be crucial in the perturbative solution methods of chapter 6. We now analyse this structure in more detail.

Explicit ansatz

Let us analyse the g-dependence of the coefficients c in the ansatz (4.51) more carefully. Assuming that the asymptotic behaviour (4.6) is valid at $g = 0$, it follows from the constraints (4.39) that the products $\mathsf{A}_a\mathsf{A}^a$ (no sum over a) are regular in g. These products are generically $\mathcal{O}(g^0)$, except in the case of shortening, where $\mathsf{A}_1\mathsf{A}^1 = \mathcal{O}(g^2)$ if (1.39a) is satisfied, and $\mathsf{A}_4\mathsf{A}^4 = \mathcal{O}(g^2)$ if (1.39b) is satisfied. This means that we can always choose to fix the freedom in A such that all $\mathbf{P}_a(u)$ and $\mathbf{P}^a(u)$ are regular in g with the possibility of some of them being $\mathcal{O}(g^2)$ due to shortening. In the case (1.39a) we set $\mathbf{P}_1 = \mathcal{O}(g^2)$ and in the case (1.39b) we set $\mathbf{P}^4 = \mathcal{O}(g^2)$. We can then write a more precise version of (4.51):

$$\mathbf{P}_a(x) = \frac{1}{(gx)^{\lambda^0_a+\Lambda}} \sum_{k=0}^{\infty} \frac{c_{a,k}}{(gx)^k} \tag{4.61a}$$

$$\mathbf{P}^a(x) = \frac{1}{(gx)^{-\lambda^0_a+1-\Lambda}} \sum_{k=0}^{\infty} \frac{c^{a,k}}{(gx)^k}\,, \tag{4.61b}$$

where λ^0_a is symmetry-independent and was defined in (4.40), and Λ corresponds to the symmetry (4.22). The constants c are here strictly regular in g, and we assume that they can be written as expansions in g^2:

$$c = \sum_{j=0}^{\infty} c^{(j+1)} g^{2j}\,. \tag{4.62}$$

The leading coefficient should match the choice of A, i.e. $c_{a,0} = \mathsf{A}_a$ and $c^{a,0} = \mathsf{A}^a$.

Restricting to $|x| > 1$, the expansion that describes the value on the second sheet $\tilde{\mathbf{P}}(u)$ is obtained through the replacement $x \to \frac{1}{x}$ in (4.61). This gives

$$\tilde{\mathbf{P}}_a(x) = \left(\frac{x}{g}\right)^{\lambda_a^0+\Lambda} \sum_{k=0}^{\infty} c_{a,k} \left(\frac{x}{g}\right)^k \tag{4.63a}$$

$$\tilde{\mathbf{P}}^a(x) = \left(\frac{x}{g}\right)^{-\lambda_a^0+1-\Lambda} \sum_{k=0}^{\infty} c^{a,k} \left(\frac{x}{g}\right)^k . \tag{4.63b}$$

The expansion is convergent in a finite region around $u = 0$. As discussed in section 4.3.1, μ_{ab} are polynomials at the leading order of maximal degree $-\lambda_a^0 - \lambda_b^0 - \nu_1^0 - \nu_2^0$ (the strongest asymptotics among $Q_{ab|ij}$). Since $\tilde{\mathbf{P}}(u)$ are given by (4.15), the ansatz (4.63) must be exact at the leading order, and the leading contributions $\tilde{\mathbf{P}}^{(1)}(u)$ have power-like asymptotics of maximal degree $u^{-\lambda_a^0-\nu_1^0-\nu_2^0-1+\Lambda}$ for $\tilde{\mathbf{P}}_a^{(1)}(u)$ and $u^{\lambda_a^0+\nu_3^0+\nu_4^0-\Lambda}$ for $\tilde{\mathbf{P}}^a_{(1)}(u)$. Due to the behaviour $x \sim \frac{u}{g} + \mathcal{O}(g)$, this puts strong constraints on the scaling in g of the constants c. Denote the last terms contributing to the leading order in the sums (4.63) by $k = M_a$ and $k = M^a$, respectively. Denote the g-scaling of the corresponding c-coefficients by $c_{a,k} \sim g^{2(M_a-N_a)}$ and $c^{a,k} \sim g^{2(M^a-N^a)}$ where $N_a \leq M_a$ and $N^a \leq M^a$. Then we must demand

$$c_{a,k}^{(j)} = 0 \quad \text{if} \quad \begin{cases} j \leq k - N_a & \wedge \quad N_a < k \leq M_a \\ j \leq k - N_a + 1 & \wedge \quad k > M_a \end{cases} , \tag{4.64}$$

and so the leading order of $\tilde{\mathbf{P}}_a(u)$ has the form

$$\tilde{\mathbf{P}}_a^{(1)}(u) = \left(\frac{u}{g^2}\right)^{\lambda_a^0+\Lambda} g^{-2N_a} \sum_{k=N_a}^{M_a} c_{a,k}^{(1+k-N_a)} u^k , \tag{4.65}$$

and similarly for $\tilde{\mathbf{P}}^a$.

Revised ansatz

The above considerations make it appropriate to rephrase the ansatz (4.61) by introducing a new set of constants c and d that are again regular in g:

$$\mathbf{P}_a = (gx)^{-\lambda_a^0-N_a-\Lambda} \left(\sum_{k=0}^{N_a} \mathsf{d}_{a,k} (gx)^k + \sum_{k=1}^{\infty} \mathsf{c}_{a,k} \left(\frac{g}{x}\right)^k \right) , \tag{4.66a}$$

$$\mathbf{P}^a = (gx)^{\lambda_a^0-N^a-1+\Lambda} \left(\sum_{k=0}^{N^a} \mathsf{d}^{a,k} (gx)^k + \sum_{k=1}^{\infty} \mathsf{c}^{a,k} \left(\frac{g}{x}\right)^k \right) . \tag{4.66b}$$

This ansatz makes it more transparent which terms are suppressed by factors of g in $\mathbf{P}(u)$ and $\tilde{\mathbf{P}}(u)$, respectively. The question is what the numbers N_a and N^a are. From the maximal asymptotic power of $\tilde{\mathbf{P}}^{(1)}(u)$, they have an upper bound,

$$N_a \leq -2\lambda_a^0 - \nu_1^0 - \nu_2^0 - 1 \tag{4.67a}$$

$$N^a \leq 2\lambda_a^0 + \nu_3^0 + \nu_4^0 - 1 . \tag{4.67b}$$

The lower bound is $N \geq -1$, where $N = -1$ can only happen in the case of shortening, since it implies that the corresponding $\mathbf{P}(u)$ vanishes at the leading order.

Scaling considerations

From the ansatz (4.66), it is clear that N_a and N^a control the scaling of $\tilde{\mathbf{P}}$ in g, i.e. $\tilde{\mathbf{P}}_a(u) \sim g^{-2(\lambda_a^0+N_a+\Lambda)}$ and $\tilde{\mathbf{P}}^a(u) \sim g^{-2(-\lambda_a^0+1+N^a-\Lambda)}$. From the construction of μ (4.13), it is natural that all μ_{ab} have the same g-scaling. Through the construction of $\tilde{\mathbf{P}}$ (4.15), it is then natural that all $\tilde{\mathbf{P}}_a(u)$ likewise scale with g in the same way. Similarly, $\tilde{\mathbf{P}}^a(u)$ should all have the same g-scaling. This implies that

$$N_a = -\lambda_a^0 + C_\bullet\,, \qquad N^a = \lambda_a^0 - 1 + C^\bullet\,, \tag{4.68}$$

where C are universal constants independent of the index a, that govern the g-scaling: $\tilde{\mathbf{P}}_a(u) \sim g^{-2(C_\bullet+\Lambda)}$ and $\tilde{\mathbf{P}}^a(u) \sim g^{-2(C^\bullet-\Lambda)}$.

Universal choice for C

Assume there is a universal choice for the numbers $C_\bullet$ and $C^\bullet$. We will now try to argue that there is only one such choice. First note that for each solution to the QSC, there should be a Hodge dual solution, which is identical to the original solution up to a relabelling of upper and lower indices. On the level of quantum numbers, the Hodge dual solution corresponds to rotating the Young diagram by an angle of π, which results in the quantum numbers $\lambda_a^{0,\bigstar} = L^{\lrcorner} - \lambda_{5-a}^0 + 1$. Since the solutions should be identical up to relabelling, we should have $N_a^{\bigstar} = N^{5-a}$. The first equation in (4.68) then gives

$$C_\bullet = \lambda_a^{0,\bigstar} + N_a^{\bigstar} = L^{\lrcorner} - \lambda_a^0 + 1 + N^a = L^{\lrcorner} + C^\bullet \quad \Rightarrow \quad L^{\lrcorner} = C_\bullet - C^\bullet\,. \tag{4.69}$$

The next consideration is that the maximal value of λ_a^0 is $\lambda_1^0 = L^{\lrcorner} + \delta$, where $\delta = 1$ only in the case of the shortening (1.39a). The lower bound on N_a then requires that $C_\bullet \geq L^{\lrcorner}$ to accommodate this case. Similarly, the upper bound on N^a (4.67b) turns into $C^\bullet \leq 0$ to accommodate all cases. Combining these two universal bounds with (4.69), we see that

$$C_\bullet = L^{\lrcorner}\,, \qquad C^\bullet = 0\,, \tag{4.70}$$

is a universal choice that is consistent with the bounds on N and the existence of an equivalent Hodge dual solution.

Final ansatz

Under the above assumptions, we arrive at a precise ansatz for the functions $\mathbf{P}$:

$$\boxed{\begin{aligned}\mathbf{P}_a &= (gx)^{-L^{\lrcorner}-\Lambda}\left(\sum_{k=0}^{L^{\lrcorner}-\lambda_a^0}\mathsf{d}_{a,k}\,(gx)^k+\sum_{k=1}^{\infty}\mathsf{c}_{a,k}\left(\frac{g}{x}\right)^k\right)\\ \mathbf{P}^a &= (gx)^{\Lambda}\left(\sum_{k=0}^{\lambda_a^0-1}\mathsf{d}^{a,k}\,(gx)^k+\sum_{k=1}^{\infty}\mathsf{c}^{a,k}\left(\frac{g}{x}\right)^k\right)\end{aligned}} \tag{4.71}$$

where the weights λ_a^0 are defined as

$$\lambda_a^0 = n_{\mathbf{f}_a}^{\lrcorner}+\{2,1,0,-1\}_a\,, \tag{4.72}$$

and where all coefficients c and d have a regular expansion in g^2,

$$\mathsf{c}=\sum_{j=0}^{\infty}\mathsf{c}^{(j+1)}g^{2j},\qquad \mathsf{d}=\sum_{j=0}^{\infty}\mathsf{d}^{(j+1)}g^{2j}. \tag{4.73}$$

The leading coefficient in gx should be identified with the corresponding prefactor A, which is constrained by (4.39).

The ansatz (4.71) is natural from the point of view of gradings of the type 1...4, where the length is always $L^{\lrcorner}$. It inherently sets $\mathbf{P}_1(u)=\mathcal{O}(g^2)$ and $\mathbf{P}^4(u)=\mathcal{O}(g^2)$ in the case of shortenings. In the next chapter we will indeed see that this is natural for the gradings 1...4.

While the the ansatz (4.71) was not derived in complete rigour, it turns out to be consistent with the leading solutions of the QSC that are discussed in chapter 5. Furthermore, it adequately governs the perturbative corrections generated through the algorithms described in chapter 6.

4.4 Applications and generalisations

The practical power of the QSC has been demonstrated in many applications. Furthermore, the QSC has been generalised to accommodate various deformations. A similar construction has likewise been found in the planar limit of the $\mathrm{AdS}_4/\mathrm{CFT}_3$ correspondence. We here summarise these developments.

4.4.1 Near-BPS solution

In [111] a near-BPS solution of the $\mathbf{P}\mu$-system as an expansion in a small $\mathfrak{sl}(2)$ spin S was given. The first two corrections, proportional to S and S^2 were calculated. The result is valid at any coupling, and it allowed to make a new prediction for the third order correction in the strong coupling expansion of the Konishi operator, as well as new predictions about the strong coupling limit of the BFKL regime.

4.4.2 Weak coupling

In [1], an iterative algorithm to solve the $\mathbf{P}\mu$-system as a perturbative expansion in the coupling g for any operator in the $\mathfrak{sl}(2)$ sector was presented. The obtained results include 10-loop results for the anomalous dimension of a variety of $\mathfrak{sl}(2)$ operators. Subsequently, this method has been used to provide enough data points to reconstruct the six- [2] and seven-loop [3] anomalous dimension of twist-2 operators for arbitrary spin, S. Twist-2 operators correspond to highest weight states of the kind $\mathcal{D}_{12}^{S}\mathcal{Z}^2$ in the $1\hat{1}\hat{2}2\hat{3}\hat{3}4\hat{4}$ grading, which corresponds to the quantum numbers

$$n^{\ulcorner} = [0, S-2|1,1,1,1|S-2,0]\,. \tag{4.74}$$

A general Q-system based method to solve the QSC perturbatively was first proposed in [113], while a general method to solve $\mathbf{P}\mu$-system will be presented in [7].

The perturbative solution methods of the QSC are the topic of chapter 6. The reconstruction of the analytic structure of the anomalous dimension of twist-2 operators for arbitrary spin is the topic of chapter 7.

4.4.3 Numerics

A generic algorithm to solve the QSC numerically at any coupling was given in [114]. The method was demonstrated on twist-2 operators in the $\mathfrak{sl}(2)$ sector. The method increases its precision through an iterative procedure that quickly reaches more than 20 digits precision. The method also allows to explore the BFKL regime numerically, and in general to explore the solutions of the QSC at general complex values of the coupling and quantum numbers. The algorithm was implemented in `C++` in [115], allowing an even higher precision which made it possible to make stronger predictions about the strong coupling behaviour of the anomalous dimension of the Konishi operator.

4.4.4 The BFKL limit

The BFKL regime corresponds to an analytic continuation of the QSC for twist-2 operators to spins around $S = -1$. It is a double scaling limit where we set $S \equiv -1 + w$ and make take the limit

$$g \to 0, \qquad w \to 0\,, \qquad \text{with } \Lambda = \frac{g^2}{w} \text{ fixed}\,. \tag{4.75}$$

The main complication compared to the standard weak coupling expansion is that the conformal dimension does not behave as $\Delta = \Delta_0 + \mathcal{O}(g^2)$. In [112] the $\mathbf{P}\mu$-system in this limit was solved to the first two orders in g^2 allowing to reproduce the leading order BFKL Pomeron eigenvalue. In [113] a Q-system based solution method was used to find a range of solutions as expansions around fixed Δ and use this data to reconstruct the first three contributions to the Pomeron eigenvalue.

4.4.5 Deformations

As we saw in chapter 2, integrable models can be deformed by twists while still preserving integrability. A twist can be introduced in the QSC in a similar way, which was done in [42]. Such twists can also be understood on the level of the $\mathcal{N} = 4$ SYM Lagrangian. The twisted QSC was recently studied in an interesting double scaling limit [116]. Very recently, the QSC was also derived for the η-deformed version of $\mathrm{AdS}_5/\mathrm{CFT}_4$ [117].

In [118] it was also understood how to study the cusp anomalous dimension by modifying the asymptotic behaviour and analytic properties of the QSC solutions. This construction was used to investigate the quark-antiquark potential in [119].

As we will return to the twisted QSC in chapter 8, we here briefly summarise its new features compared to the untwisted model.

New features in the twisted QSC

Introducing a general diagonal twist in the QSC leaves all relations and the analytic structure invariant, and the only modification is in the large u asymptotics of the involved functions[1]. In the fully twisted case [42], the asymptotics are

$$\mathbf{P}_a \simeq \mathsf{A}_a\, \mathsf{x}_a^{\mathbb{i}u}\, u^{-\check{\lambda}_a} \qquad \mathbf{P}^a \simeq \mathsf{A}^a\, \mathsf{x}_a^{-\mathbb{i}u}\, u^{\check{\lambda}_a} \qquad \mathbf{Q}_j \simeq \mathsf{B}_j\, \mathsf{y}_j^{-\mathbb{i}u}\, u^{-\check{\nu}_j} \qquad \mathbf{Q}^j \simeq \mathsf{B}^j\, \mathsf{y}_j^{\mathbb{i}u}\, u^{\check{\nu}_j}\ , \tag{4.76}$$

where $\check{\lambda}_a = n_{\mathbf{f}_a} + \Lambda$ and $\check{\nu}_j = \{-L - n_{\mathbf{b}_{\dot{\alpha}}}, n_{\mathbf{a}_\alpha}\} - \Lambda$ and there is no need to specify a grading as all fermionic symmetry is broken. Resultingly, some operators that are supersymmetry descendants in the untwisted theory become highest weight states. Apart from the treatment in [42] of the BMN vacuum, which is no longer protected, no explicit results for physical operators in the twisted theory have been presented yet.

4.4.6 $\mathbf{AdS}_4/\mathbf{CFT}_3$

In analogy to the $\mathrm{AdS}_5/\mathrm{CFT}_4$ case, a QSC [120] has been constructed for the planar limit of the $\mathrm{AdS}_4/\mathrm{CFT}_3$ duality. The $\mathbf{P}\mu$-system is strikingly similar to that of $\mathrm{AdS}_5/\mathrm{CFT}_4$: the equations are the same, but the analytic structure of the functions $\mathbf{P}$ and μ is exchanged. On the level of the Q-system, the systems are less alike.

In [121] the near-BPS solution was studied and a conjecture was made for the exact structure of the interpolating function. A similar conjecture for the ABJ model was given in [122]. The $\mathbf{P}\mu$-system was solved perturbatively in [123] for states in an $\mathfrak{sl}(2)$-like sector. Six non-trivial orders, corresponding to 12 loops in ABJM theory, was reached for a number of operators.

[1] One can alternatively consider power-like Q-functions at the cost of having modified QQ-relations.

Subconclusion

In this chapter, the Quantum Spectral Curve was introduced in an axiomatic form, which we then used to derive a number of properties, first at arbitrary coupling and then in the weak coupling limit. A brief summary of the applications and generalisations of the QSC was given. The scope of its applications demonstrates that the QSC is an incredibly powerful tool.

This chapter concludes the first part of the thesis, which has aimed at introducing the integrable structures that appear in the spectral problem in the AdS_5/CFT_4 correspondence. The second part of the thesis is devoted to exploiting these structures to obtain explicit perturbative results. The analysis of the weak coupling properties of the QSC in section 4.3 lays the foundation for these calculations.

Part II

The explicit spectrum

Chapter 5

The 1-loop Q-system

We first encountered the notion of Q-systems in chapter 2, where they were formed by spin chain Q-operators. The Q-system reappeared in chapter 4 as a clever reformulation of the TBA equations. In both cases, the size and functional relations of the Q-system are dictated solely by the symmetry. The difference lies in the boundary conditions: the asymptotic behaviour and the analytic properties.

The $g \to 0$ limit of the AdS/CFT Q-system is exactly the Q-system of a rational spin chain. The first step in solving the QSC perturbatively is to solve this system, and the goal of this chapter is to do that efficiently. To accomplish this, we will think of Q-systems in an unconventional way. Recall the concept of Young diagrams introduced in chapter 1. They were used to classify irreducible representations of Lie algebras. But the concept of extended Young diagrams allowed us to think of representations as algebra-independent. In this chapter, we will advocate the idea that, at least when dealing with representations of Jordan-Schwinger-type, Q-systems can be constructed on Young diagrams, and that they are not sensitive to the precise Lie algebra rank. The Lie algebra-based Q-systems, see figure 5.1, are in fact just special cases of more general Q-systems living on infinitely extended Young diagrams. This idea will allow us to develop powerful tools to find explicit solutions to the Q-systems, and thus indirectly solve Bethe equations.

Our goal is to explicitly calculate Bethe roots u_j or, equivalently, coefficients in Baxter polynomials $c^{(k)}$,

$$Q \quad \equiv \quad \prod_{j=1}^{M}(u-u_j) \quad = \quad u^M + \sum_{k=0}^{M-1} c^{(k)} u^k \,. \tag{5.1}$$

Since Bethe equations, cf. (2.23) and (2.82), are algebraic equations, and likewise since the Q-functions should arise from diagonalisation of polynomial Q-operators with rational coefficients, it is clear that u_j and $c^{(k)}$ are algebraic numbers, i.e. of the type

$$q_0 + q_1\theta + q_2\theta^2 + \dots q_{K-1}\theta^{K-1}\,, \tag{5.2}$$

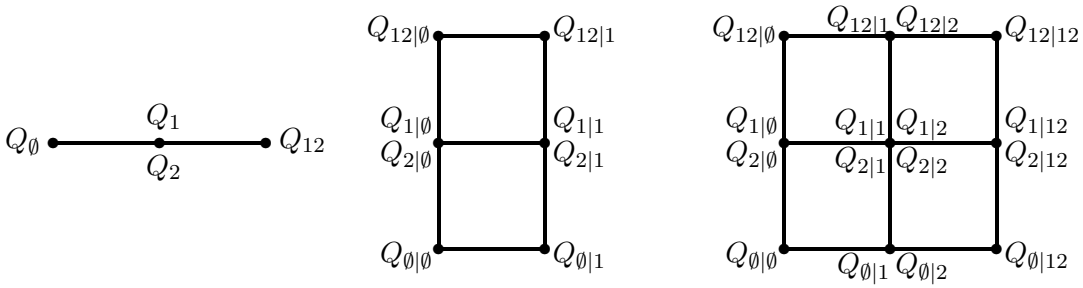

Figure 5.1: Traditionally, see e.g. [124, 17, 125, 26, 42], Q-systems are constructed from the rank of a given Lie algebra, here $\mathfrak{gl}(2)$ (left), $\mathfrak{gl}(2|1)$ (middle), and $\mathfrak{gl}(2|2)$ (right).

where q_i are rational numbers and θ is a root of a degree-K polynomial equation with integer coefficients.

The momentum-carrying Q-function, placed at the central node of the Young diagram, determines the spectrum, i.e. the spin chain energies or the 1-loop anomalous dimensions γ_1, through

$$\gamma_1 = 2E = 2\mathbb{i}\,\partial_u \log \frac{Q^+}{Q^-}\bigg|_{u=0} , \tag{5.3}$$

which is simply a reformulation of the formula (2.24).

5.1 Traditional methods

So why not just solve Bethe equations? Let us take a look at some of the diseases of Bethe equations and related statements of the problem. We will exemplify the discussion on the $\mathfrak{su}(2)$ irreps with weights $\{\lambda_1, \lambda_2\} = \{L-M, M\} = \{3, 2\}$. The 32 possible $L = 5$ spin chain configurations are of the form

$$1 \times \uparrow\uparrow\uparrow\uparrow\uparrow \qquad 5 \times \uparrow\uparrow\uparrow\uparrow\downarrow \qquad 10 \times \uparrow\uparrow\uparrow\downarrow\downarrow \qquad 10 \times \uparrow\uparrow\downarrow\downarrow\downarrow \qquad 5 \times \uparrow\downarrow\downarrow\downarrow\downarrow \qquad 1 \times \downarrow\downarrow\downarrow\downarrow\downarrow$$

and they form one irrep with highest weight $M = 0$, four with $M = 1$, and five with $M = 2$. Thus, we should expect five solutions to the $\mathfrak{su}(2)$ Bethe equations with $L = 5$ and $M = 2$.

Bethe equations

We saw the $\mathfrak{su}(2)$ Bethe equations in (2.23). In our example, there are two equations:

$$\left(\frac{u_1 + \frac{\mathbb{i}}{2}}{u_1 - \frac{\mathbb{i}}{2}}\right)^5 = \frac{u_1 - u_2 + \mathbb{i}}{u_1 - u_2 - \mathbb{i}} , \qquad \left(\frac{u_2 + \frac{\mathbb{i}}{2}}{u_2 - \frac{\mathbb{i}}{2}}\right)^5 = \frac{u_2 - u_1 + \mathbb{i}}{u_2 - u_1 - \mathbb{i}} . \tag{5.4}$$

By eliminating u_2, we are left with polynomial equation in u_1 of degree 29. Only 21 of the 29 solutions are distinct, and we should also remove solutions related by relabelling

$u_1 \leftrightarrow u_2$. This leaves 11 solutions which are most nicely expressed as the polynomials $Q = (u - u_1)(u - u_2)$,

$$u^2\,, \quad u^2 \pm \frac{1}{4}\,, \quad u^2 \pm_1 u\sqrt{5 \pm_2 2\sqrt{5}} + \frac{5}{4} \pm_2 \frac{\sqrt{5}}{2}\,, \quad u^2 \pm_1 u\frac{\sqrt{10 \pm_2 2\sqrt{5}}}{6} + \frac{1}{6} \pm_2 \frac{\sqrt{5}}{12}\,. \quad (5.5)$$

This is six more than we were hoping for. But which correspond to our spin chain states?

Baxter equations

An often preferred alternative to Bethe equations are Baxter equations, which we saw for $\mathfrak{su}(2)$ in (2.64). In our example, the Baxter equation reads

$$TQ = (u + \tfrac{\mathrm{i}}{2})^5 Q^{[-2]} + (u - \tfrac{\mathrm{i}}{2})^5 Q^{[+2]}\,, \qquad T = \sum_{j=0}^{5} d^{(j)} u^j\,, \quad Q = u^2 + c^{(1)}u + c^{(0)}\,, \quad (5.6)$$

and by imposing that each order in u vanishes separately, the coefficients $d^{(j)}$ and $c^{(j)}$ are uniquely fixed. This gives six solutions for Q,

$$u^2 \pm \frac{1}{4}\,, \qquad u^2 \pm_1 u\frac{\sqrt{10 \pm_2 2\sqrt{5}}}{6} + \frac{1}{6} \pm_2 \frac{\sqrt{5}}{12}\,, \quad (5.7)$$

which are a subset of the solutions to the Bethe equations (5.5). It is still one too many.

What is the problem?

Why do we get too many solutions? Let us recall the Q-operator construction for $\mathfrak{su}(2)$. It consisted of two non-trivial Q-operators $\mathcal{Q}_{\{1\}}$ and $\mathcal{Q}_{\{2\}}$, that both, up to an overall exponential prefactor, were polynomials in u. But so far we have only discussed one Q-function. What about the other one? The key to understanding the excess of solutions to Bethe and Baxter equations lies in the polynomiality of this second solution. Neither of these approaches guarantee this. In general, these methods only ensure that a single Q-function at each node of the chosen Dynkin path is polynomial. For example, in the $\mathfrak{gl}(2|2)$ Q-system in figure 5.1 this is only five out of the 16 Q-functions.

In our concrete example, we can take our solutions and plug them into the basic QQ-relation,

$$u^5 = Q_1^+ Q_2^- - Q_1^- Q_2^+ \quad (5.8)$$

and see whether it can be satisfied by a polynomial ansatz for Q_2. For our six solutions to the Baxter equations (5.7) it turns out that $Q_1 = u^2 + \frac{1}{4}$ is the imposter which does not allow a polynomial Q_2.

This solution, $Q = u^2 + \frac{1}{4} = (u + \frac{\mathrm{i}}{2})(u - \frac{\mathrm{i}}{2})$, is an example of what is called *exceptional solutions* which have roots that are separated by i. They are clearly a bit problematic from the point of view of the Bethe and Baxter equations. In general such solutions can

both be good solutions that are part of fully polynomial Q-systems and, as we just saw, bad solutions that are not.

For spin chains in compact representations, we can sum up the mathematical problem we are trying to solve in the conjectured one-to-one correspondence

$$\boxed{\text{spin chain eigenstates} \quad \leftrightarrow \quad \text{polynomial solutions to Q-system}} \tag{5.9}$$

In the non-compact case, the whole Q-system is no longer polynomial, but one can formulate a similar criteria as we will see in section 5.3.

How do we get around it?

We want to have a method that gives us all the right solutions and nothing else. The question is how to ensure the polynomiality of the full Q-system.

- We could of course just solve Bethe or Baxter equations, plug the solutions into QQ-relations, and see which ones allow the other Q's to be polynomial. But neither Bethe equations or the Baxter equations are particularly convenient to solve in practice, in particular not in the nested case. In fact one quickly realises that, using a symbolical programming language such as `Mathematica`, solutions are only found for the most simple quantum numbers.

- Similarly, one could just diagonalise the spin chain Hamiltonian, but again, when the matrices become large, this rarely works in practice. In any case, this only gives us the energy and not the separate Bethe roots.

- We could also take the QQ-relations as our starting point and put in arbitrary polynomial ansätze. In the $\mathfrak{su}(N)$ case, this is in fact rather successful because the Q-functions with all but one index satisfy determinant relations of the kind $Q_\emptyset = \det_{1\leq a,k\leq N}\left(Q_{\bar{a}}^{[-N-1+2k]}\right)$ and the polynomiality of the remaining Q-functions follow from determinant formulas similar to (4.28). The supersymmetric case is less nice, and in the non-compact case not all Q-functions are polynomials, so this strategy is obscured.

- It should be noted that the issues can be overcome by introducing twists, see e.g. [126]. However, the price is that the practical solution of the equations becomes even harder.

- Remarkable results can be obtained from the *homotopy continuation method* presented in [127] for $\mathfrak{su}(2)$ Bethe equations, but this is mainly a numerical tool, and we look for analytic solutions.

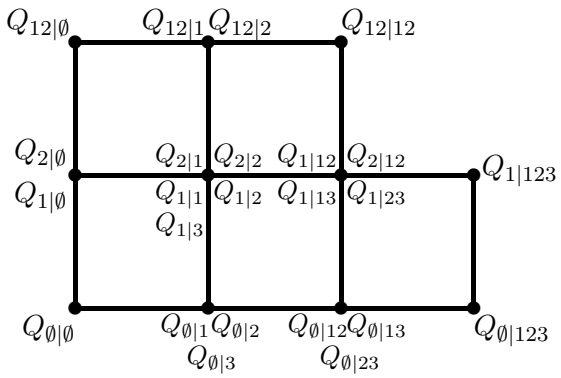

Figure 5.2: Q-system on the Young diagram corresponding to the partition $\lambda = \{3, 2\}$. It contains all Q-functions belonging to the $\mathfrak{gl}(2|2)$ and $\mathfrak{gl}(3|1)$ (and subalgebras thereof) Q-systems.

In conclusion, there are techniques available on the market, but they really only give access to the very simplest results, and they require a case-by-case study. Our ambition is to *explicitly* solve the QSC for a substantial number of states from any sector, and with the outlined techniques this is simply not feasible. The hunt for a more practical way to find the spectrum was the main motivation for the reformulation of the problem that we will now present.

5.2 Q-systems on compact Young diagrams

For clarity, we first discuss our approach for compact $\mathfrak{u}(N|K)$ representations.

Q-systems on Young diagrams

We have already seen a clear connection between Q-systems and representation theory. The $\mathfrak{u}(N|K)$ Q-system can be thought of as living on an $N \times K$ square lattice, see e.g. figure 4.1. This square lattice can be identified with the corner piece of the $N|K$ L-hook, cf. figure 1.4. The Young diagram lives on this L-hook, but it may extend outside the $N\times K$ square into the "wings" of the L-hook. On the other hand, for short representations, the Young diagram does not cover the full $N \times K$ square.

Denote each node in a given compact Young diagram by its position (a, s), where $(0, 0)$ corresponds to the lower left corner. A Q-system can be built on the Young diagram by placing a set of Q-functions $\{Q_{b_1,\dots,b_a|i_1,\dots,i_s}\}$ at the node (a, s). The sets contain Q-functions with indices b_n and i_m that correspond to any possible $\mathfrak{u}(N|K)$ Q-system where the representation is *long*. An example is given in figure 5.2. The Q-functions satisfy the QQ-relations (4.3) as depicted in figure 4.2.

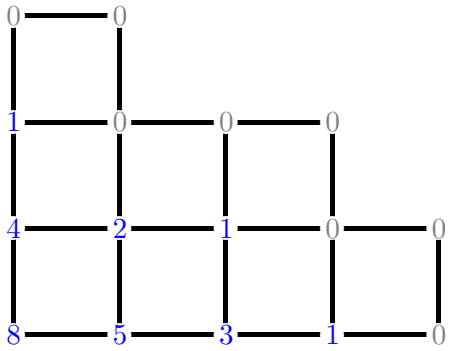

Figure 5.3: The polynomial degree of the distinguished Q-function at a given node equals the number of boxes above and to the right of the node. For a spin chain in the fundamental representation $C = 1$, the eights roots in $\mathbb{Q}_{0,0}$ are trivial, and in the homogeneous case $\mathbb{Q}_{0,0} = u^L = u^8$. For $C = 2$ and homogeneity, we would instead have $L = 4$ and the boundary conditions $\mathbb{Q}_{0,0} = (u + \frac{\mathrm{i}}{2})^4 (u - \frac{\mathrm{i}}{2})^4$ and $\mathbb{Q}_{1,0} = u^4$.

Distinguished Q-functions

The set of Q-functions on the Young diagram is in general quite large, but a small subset of them turns out to be of special interest. These *distinguished* Q-functions $\mathbb{Q}_{a,s}$ are defined as the polynomials $Q_{A|J}$ of the lowest degree among all Q-functions for which the number of indices are $|A| = a$ and $|J| = s$. We can always label the Q-functions such that

$$\mathbb{Q}_{a,s} \equiv Q_{12\ldots(a-1)a|12\ldots(s-1)s}\,. \tag{5.10}$$

There is one distinguished Q-function at each node in the Young diagram, and they are related solely by fermionic QQ-relations (4.3c),

$$\mathbb{Q}_{a+1,s}\mathbb{Q}_{a,s+1} \propto \mathbb{Q}^{+}_{a+1,s+1}\,\mathbb{Q}^{-}_{a,s} - \mathbb{Q}^{-}_{a+1,s+1}\,\mathbb{Q}^{+}_{a,s}\,.$$

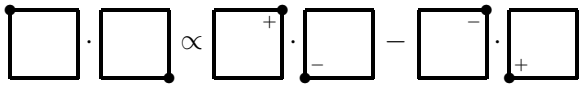

(5.11)

We use $\propto$ to denote equality up to an overall normalisation, and such normalisations are irrelevant to us.

Degree of distinguished Q-functions

The Young diagram provides an intuitive way to find the degree of the distinguished Q-functions: simply count the number of boxes *above and to the right* of the corresponding node, see figure 5.3. More explicitly, the degree $M_{a,s}$ of $\mathbb{Q}_{a,s}$ is

$$M_{a,s} = L - \sum_{b=1}^{a} \lambda_b - \sum_{t=1}^{s} \lambda_t^T + a\,s\,, \tag{5.12}$$

where $\lambda = \{\lambda_1, \lambda_2, \ldots\}$ is the partition defining the diagram and λ^T denotes the transposed diagram.

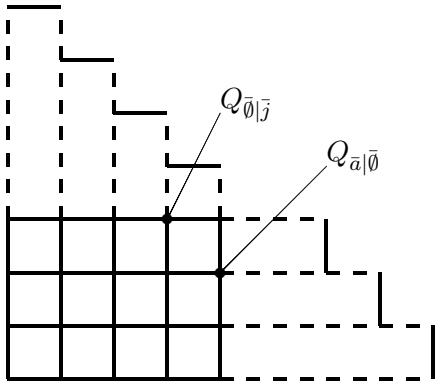

Figure 5.4: Separation of Young diagram into an $N \times M$ rectangle, upper wing and right wing.

Boundary conditions

It is clear that all Q-functions on the upper-right boundary of the diagram are trivial, $\mathbb{Q} \propto 1$. Furthermore, some roots on the left boundary of the diagram are fixed. For central charge C, the functions $\mathbb{Q}_{a,0}$ with $a = 0, \dots C-1$ contain trivial roots. We can in general write the distinguished Q-functions as

$$\mathbb{Q}_{a,s} = f_{a,s}\, q_{a,s}\,, \tag{5.13}$$

where $q_{a,s}$ are polynomials with non-trivial roots, and where, for homogeneous spin chains, the factors $f_{a,s}$ have the form

$$f_{a,s}(u) = \begin{cases} \prod_{k=-C+1+a}^{C-1-a} \left(u - \frac{\mathrm{i}\,k}{2}\right)^L & \text{if} \quad s = 0 \ \wedge \ a < C \\ 1 & \text{otherwise} \end{cases}. \tag{5.14}$$

Note that by power counting $\mathbb{Q}_{0,0}$ is always completely trivial, $q_{0,0} = 1$. Inhomogeneities are easily incorporated by modifying the factors $f_{a,s}$.

5.2.1 Distinguished Q-functions and polynomiality of the full Q-system

We now want to make a bold statement: *if all the distinguished Q-functions on the Young diagram are polynomials, then the full Q-system is guaranteed to be polynomial.* This would allow us to ensure polynomiality much easier. Let us try to prove this statement.

Proof

Consider an arbitrary Young diagram and assume that all distinguished Q-functions are polynomial. The diagram can be decomposed, in several ways, into an $N \times M$ rectangle that touches the boundary of the diagram and two wings above and to the right of the rectangle, see figure 5.4.

On the $N \times M$ rectangle, the Q-function in the upper right corner is $Q_{1\dots N|1\dots M} \equiv Q_{\bar{\emptyset}|\bar{\emptyset}} \equiv \mathbb{Q}_{N,M} = 1$. Let us assume that $Q_{\bar{a}|\bar{\emptyset}}$ and $Q_{\bar{\emptyset}|\bar{j}}$ are polynomials for all a, j. Then

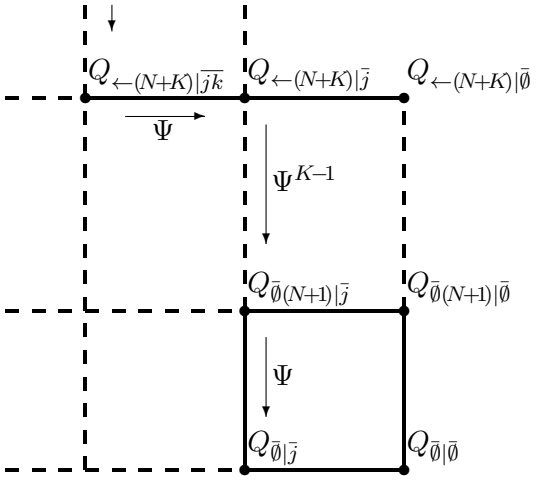

Figure 5.5: Relations between Q-functions in the upper wing.

any $Q_{\bar{a}|\bar{j}}$ is a polynomial as well, since it satisfies the QQ-relation

$$Q_{\bar{a}|\bar{\emptyset}}Q_{\bar{\emptyset}|\bar{j}} \propto Q^{+}_{\bar{a}|\bar{j}} - Q^{-}_{\bar{a}|\bar{j}} \,, \tag{5.15}$$

and thus is given by

$$Q_{\bar{a}|\bar{j}} \propto \Psi^{+}(Q_{\bar{a}|\bar{\emptyset}}Q_{\bar{\emptyset}|\bar{j}}) \,, \tag{5.16}$$

which is a polynomial, cf. the discussion of the Ψ-operation in appendix C.1. In this proof, an overall shift of the spectral parameter u is of no importance, hence in the following we will arbitrarily replace $\Psi^{\pm}$ with Ψ in order to avoid bulky expressions. In analogy to (4.28), all other Q-functions in the $\mathfrak{gl}(N|M)$ Q-system specified by the rectangle are given in terms of determinants of $Q_{\bar{a}|\bar{\emptyset}}$, $Q_{\bar{\emptyset}|\bar{j}}$, and $Q_{\bar{a}|\bar{j}}$. This means that if $Q_{\bar{a}|\bar{\emptyset}}$ and $Q_{\bar{\emptyset}|\bar{j}}$ are polynomial, then all other Q-functions in the $\mathfrak{gl}(N|M)$ Q-system will be.

We will now see how the polynomiality of $Q_{\bar{a}|\bar{\emptyset}}$ and $Q_{\bar{\emptyset}|\bar{j}}$ follows from the polynomiality of the distinguished Q-functions in the wings. As the two wings behave identically, it is sufficient to make the argument in one wing. We here focus on the upper wing to show that $Q_{\bar{\emptyset}|\bar{j}}$ are polynomial. Denote the height of the outermost right column in the wing by K. Noting that $Q_{\bar{\emptyset}|\bar{\emptyset}} \propto Q_{\bar{\emptyset}(N+1)|\bar{\emptyset}} \propto 1$, we can generate $Q_{\bar{\emptyset}|\bar{j}}$ purely in terms of $Q_{\bar{\emptyset}(N+1)|\bar{j}}$ through (5.11):

$$Q_{\bar{\emptyset}(N+1)|\bar{j}} \propto Q^{-}_{\bar{\emptyset}|\bar{j}} - Q^{+}_{\bar{\emptyset}|\bar{j}} \qquad \Rightarrow \qquad Q_{\bar{\emptyset}|\bar{j}} \propto \Psi\Big(Q_{\bar{\emptyset}(N+1)|\bar{j}}\Big) \,, \tag{5.17}$$

which is again a polynomial. We can continue in this way until we reach the end of the column:

$$Q_{\bar{\emptyset}|\bar{j}} \quad \propto \quad \Psi^{K}\Big(Q_{\leftarrow(N+K)|\bar{j}}\Big) \,, \tag{5.18}$$

where the notation $(\leftarrow n) \equiv (12...n)$ is used.

To continue, note that $Q_{\leftarrow(N+K)|\bar{M}} \propto 1$ as it is on the boundary of the diagram. Together with $Q_{\leftarrow(N+K)|\bar{j}}$, $j \neq M$, it forms a bosonic QQ-relation (4.3b) with $Q_{\leftarrow(N+K)|\bar{\emptyset}} \propto 1$ and $Q_{\leftarrow(N+K)|\overline{jM}}$:

$$Q_{\leftarrow(N+K)|\overline{jM}} \propto Q^{-}_{\leftarrow(N+K)|\bar{j}} - Q^{+}_{\leftarrow(N+K)|\bar{j}} \qquad \Rightarrow \qquad Q_{\bar{\emptyset}|\bar{j}} \propto \Psi^{K+1}\Big(Q_{\leftarrow(N+K)|\overline{jM}}\Big)\,. \tag{5.19}$$

For $j = M-1$, the argument of Ψ^{K+1} is a distinguished Q-function, and we have thus proven that $Q_{\bar{\emptyset}|\overline{(M-1)}}$ is polynomial. For $j \leq M-2$, we have rewritten $Q_{\bar{\emptyset}|\bar{j}}$ in terms of a multiple of polynomiality preserving Ψ-operations on $Q_{\leftarrow(N+K)|\overline{jM}}$. See figure 5.5 for an overview. We can now consider what is left of the second column from the right (denote the height by K_2) in exactly the same way as we treated the first. By exactly the same argument as above, we find that $Q_{\bar{\emptyset}|\overline{(M-2)}}$ is polynomial, while the rest are related by Ψ-operations to $Q_{\leftarrow(N+K_2)|\overline{j(M-1)M}}$. By recursion, we then see that all $Q_{\bar{\emptyset}|\bar{j}}$ are related to distinguished Q-functions by multiple Ψ-operations, so if all distinguished Q-functions are polynomial, then it follows that all Q-functions in the $\mathfrak{gl}(N|M)$ Q-system are polynomial as well.

Finally recall that the $N \times M$ rectangle can be chosen arbitrarily as long as it touches the boundary of the Young diagram, so we can prove the polynomiality of any Q-function in this way. In conclusion,

$$\boxed{\text{all } \mathbb{Q} \text{ on Young diagram polynomial } \Rightarrow \text{ full Q-system polynomial}} \tag{5.20}$$

5.2.2 Finding distinguished Q-functions

We have reduced the task of finding polynomial Q-systems to that of finding polynomial distinguished Q-functions. The question is how to do this efficiently in practice. We here propose an algorithm that exactly imposes this polynomiality requirement and finds the distinguished Q-functions analytically. It is based on polynomial division.

Step 1: Make ansatz on a path

The starting point is the Young diagram of the representation in question, see figure 5.3 for an example. Choose a path form the point $(0,0)$ to any point on the upper-right boundary. On this path, make a generic ansatz for the non-trivial polynomial parts of the distinguished Q-functions (5.13),

$$q_{a,s} = u^{M_{a,s}} + \sum_{k=0}^{M_{a,s}-1} c_{a,s}^{(k)}\, u^k\,, \tag{5.21}$$

where $M_{a,s}$ is the degree of $q_{a,s}$. As discussed below, it is often preferable to choose a path that minimises the total number of roots.

Step 2: Generate all $\mathbb{Q}$

Starting from the $\mathbb{Q}$ on the chosen path, now generate the remaining $\mathbb{Q}$ from the QQ-relation (5.11):

$$q_{a,s} \propto \frac{1}{f_{a,s}} \frac{\mathbb{Q}^+_{a\pm1,s}\mathbb{Q}^-_{a,s\mp1} - \mathbb{Q}^-_{a\pm1,s}\mathbb{Q}^+_{a,s\mp1}}{\mathbb{Q}_{a\pm1,s\mp1}} \,. \tag{5.22}$$

The unknown Q-function is a ratio of two polynomials, but it is required to be a polynomial itself, and thus it should be the quotient of the polynomial division of the numerator by the denominator,

$$q_{a,s} \propto \text{Quotient}[\ \mathbb{Q}^+_{a\pm1,s}\mathbb{Q}^-_{a,s\mp1} - \mathbb{Q}^-_{a\pm1,s}\mathbb{Q}^+_{a,s\mp1}\,,\ f_{a,s}\mathbb{Q}_{a\pm1,s\mp1}\ ] \tag{5.23}$$

The remainder of this polynomial division[1] should vanish, but it is not necessary to impose this yet.

In this way all distinguished Q-functions are generated in terms of the $c^{(k)}_{a,s}$ that were introduced on the path. All the remainders of the polynomial divisions are collected.

Step 3: Solve constraints

After all $\mathbb{Q}$'s are generated, we have gathered a set of constraints of the kind

$$0 = \text{Remainder}[\ \mathbb{Q}^+_{a\pm1,s}\mathbb{Q}^-_{a,s\mp1} - \mathbb{Q}^-_{a\pm1,s}\mathbb{Q}^+_{a,s\mp1}\,,\ f_{a,s}\mathbb{Q}_{a\pm1,s\mp1}\ ]\,. \tag{5.24}$$

Simultaneously imposing these constraints[2] is equivalent to demanding polynomiality of all distinguished Q-functions. These algebraic equations completely fix the original ansatz $\{c^{(k)}_{a,s}\}$, and have a finite set of solutions.

As we discuss below, the number of solutions to these equations turn out to be in exact one-to-one correspondence to the multiplicity of the irreps of the type specified by the Young diagram in the tensor product specified by the central charge. Furthermore, the method is significantly faster than any of the traditional methods.

Example

Let us demonstrate the method on the same example as in our discussion of Bethe and Baxter equations: the partition $\lambda = \{3,2\}$ and central charge $C = 1$, see figure 5.6.

We can, for example, choose the path $\hat{1}1\hat{2}$, on which the ansatz for the $\mathbb{Q}$ is

$$\mathbb{Q}_{0,0} \propto u^5\,, \qquad \mathbb{Q}_{1,0} \propto u^2 + c^{(1)}_{1,0}\,u + c^{(0)}_{1,0}\,, \qquad \mathbb{Q}_{1,1} \propto u + c^{(0)}_{1,1}\,, \qquad \mathbb{Q}_{2,1} \propto 1\,. \tag{5.25}$$

[1] The `Mathematica`-functions `PolynomialQuotient` and `PolynomialRemainder` nicely implement these operations.

[2] This can be done by standard routines in most symbolical programming languages, e.g. the `Mathematica`-function `Solve`.

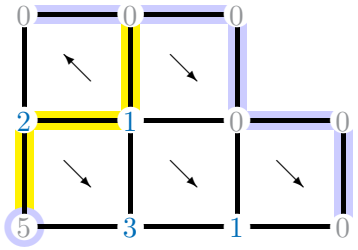

Figure 5.6: The solution method for the Young diagram $\lambda = \{3, 2\}$. The yellow path shows a possible choice of path where a generic ansatz is made, and the upper-right boundary is marked in blue. The arrows point towards Q-functions that are generated recursively through (5.11).

To generate $\mathbb{Q}_{2,0}$ we use (5.11):

$$\begin{aligned}\mathbb{Q}_{2,0} \propto \frac{\mathbb{Q}^+_{2,1}\mathbb{Q}^-_{1,0} - \mathbb{Q}^-_{2,1}\mathbb{Q}^+_{1,0}}{\mathbb{Q}_{1,1}} &\propto \frac{\left(u^2 + c^{(1)}_{1,0}u + c^{(0)}_{1,0}\right)^- - \left(u^2 + c^{(1)}_{1,0}u + c^{(0)}_{1,0}\right)^+}{u+d} \\ &\propto -2\mathbb{i} + \mathbb{i}\frac{2c^{(0)}_{1,1} - c^{(1)}_{1,0}}{u + c^{(0)}_{1,1}}\end{aligned} \tag{5.26}$$

Since $\mathbb{Q}_{2,0}$ should be polynomial, the second term must vanish. Store this constraint, $2c^{(0)}_{1,1} - c^{(1)}_{1,0} = 0$, and set $\mathbb{Q}_{2,0} \propto -2\mathbb{i} \propto 1$.

We can continue in this way to generate $\mathbb{Q}_{0,1}$, $\mathbb{Q}_{1,2}$, $\mathbb{Q}_{0,2}$ and $\mathbb{Q}_{0,3}$. Solving the combined sets of constraints gives the solutions

$$\left\{c^{(0)}_{1,0} = -\frac{1}{4}\,,\, c^{(1)}_{1,0} = c^{(0)}_{1,1} = 0\right\}\,, \quad \left\{c^{(0)}_{1,0} = \frac{1}{6} \pm_2 \frac{\sqrt{5}}{12}\,,\, c^{(1)}_{1,0} = 2c^{(0)}_{1,1} = \pm_1 \frac{\sqrt{10 \pm_2 2\sqrt{5}}}{6}\right\}\,, \tag{5.27}$$

and we see that $\mathbb{Q}_{1,0}$ (5.25) then matches the five good solutions to the $\mathfrak{su}(2)$ Bethe equations (5.5).

5.2.3 Comments on the method

A few comments about the performance of the algorithm and possible improvements of the method are in place.

Performance

The practical advantage of the method compared to the conventional analytical methods is clearly demonstrated in our very simple `Mathematica`-implementation[3] which is available in the ancillary files of [4] at arxiv.org. In this file, we also discuss how the computation time is correlated with the number of Bethe roots on the chosen path and the total number of solutions to the system. As an example of the power of the algorithm, see table 5.1

[3]The implementation is for fundamental spin chains, but the generalisation is straightforward.

which lists the computation times for finding any $L = 12$ solution for the fundamental $\mathfrak{su}(2)$ spin chain.

M	0	1	2	3	4	5	6
Solutions	1	11	54	154	275	297	132
Time (s)	0.01	0.10	0.96	4.65	39	24	18

Table 5.1: Computation time on a single core of a 3.2 GHz desktop for all $L = 12$ solutions for the fundamental $\mathfrak{su}(2)$ case.

We stress that in the vast amount of examples that we have investigated, the method always finds *exactly* the number of solutions expected from representation theory.

An even stronger statement?

One can wonder whether there is a more minimal version of (5.20) that ensures polynomiality of the full Q-system. Indeed, in all explicit examples we have investigated, it seems to be enough to require polynomiality of all $\mathbb{Q}_{a,s}$ on the maximal quadratic square that fits inside the Young diagram. In other words, the $\mathbb{Q}_{a,s}$ with $0 \leq a, s \leq N_{\text{min}}$, where $\mathfrak{u}(N_{\text{min}}|N_{\text{min}})$ corresponds to the smallest possible symmetric L-hook that accommodates the Young diagram. However, we have not been able to prove this conjecture, as we did not find a way to rule out the possibility of exceptional solutions that could lead to non-polynomiality.

Even if this conjecture holds, imposing polynomiality of the full Young diagram Q-system often leads to a significantly faster solution in practice, compared to only imposing polynomiality on the $N_{\text{min}} \times N_{\text{min}}$ square. It seems as if the Young diagram disentangles the equations and makes the solution easier for symbolical programming languages.

5.3 Q-systems on non-compact Young diagrams

Let us now turn towards the non-compact case, which is our real goal. Q-systems can just as well be built on non-compact Young diagrams, and it is natural to include the infinite extension in the discussion. In fact, all compact Young diagrams have a non-compact extension, so we can simply see this as a generalisation of the above method. Let us discuss the additional features in the non-compact case.

5.3.1 Structure of the Q-functions

We can build a Q-system on an extended Young diagram in analogy to the compact case. The set of Q-functions are those that belong to any $\mathfrak{u}(N, M|K)$ χ-hook where the diagram

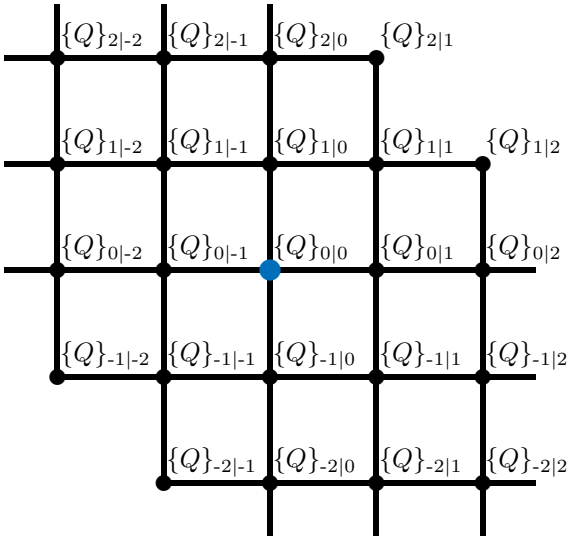

Figure 5.7: The Q-system on the central part of a non-compact diagram in terms of the sets (5.29). The central node is marked in blue.

corresponds to a long representation. This set is of course infinite, but we can often focus on the set living on the non-trivial extension of the diagram, cf. figure 1.9.

Notation

To label the Q-functions in a convenient way, we introduce a new notation:

$$Q_{A,B|I,J} \tag{5.28}$$

where A, B, I and J are antisymmetric multi-indices containing positive integer numbers. We will classify the Q-functions in sets

$$\{Q\}_{m|n} = \left\{ \, Q_{A,B|I,J} \mid m = |B| - |A| \, , \; n = |J| - |I| \, \right\} . \tag{5.29}$$

Denote the central node in the Young diagram by $(0,0)$. The Q-functions $\{Q\}_{m|n}$ then live at the point (n,m) in the diagram, see figure 5.7. The Q-functions on the diagram are again related through QQ-relations following the pictorial rule described in figure 4.2. For example,

$$Q_{a,\emptyset|\emptyset,\emptyset} Q_{\emptyset,b|\emptyset,\emptyset} \propto Q^{+}_{\emptyset,\emptyset|\emptyset,\emptyset} Q^{-}_{a,b|\emptyset,\emptyset} - Q^{-}_{\emptyset,\emptyset|\emptyset,\emptyset} Q^{+}_{a,b|\emptyset,\emptyset} \, , \tag{5.30}$$

where $Q_{a,\emptyset|\emptyset,\emptyset} \in \{Q\}_{-1|0}$, $Q_{\emptyset,b|\emptyset,\emptyset} \in \{Q\}_{1|0}$ and $Q_{\emptyset,\emptyset|\emptyset,\emptyset}, Q_{a,b|\emptyset,\emptyset} \in \{Q\}_{0|0}$.

Rational and non-rational Q-functions

As discussed in section 1.2.2, a non-compact Young diagram can be split into a left and a right half that are both equivalent to compact Young diagrams. We can define two

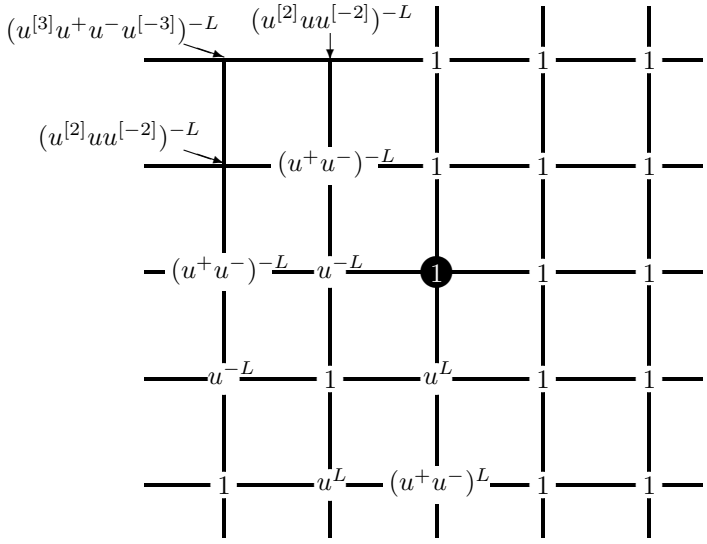

Figure 5.8: The value of $f_{a,s}$ in the central part of a diagram. The central node is marked with a black circle.

separate Q-systems that live on these two parts: $Q_{A,B|I,\emptyset}$ on the left half and $Q_{A,B|\emptyset,J}$ on the right half. These two subsets are both rational. In fact, one can use symmetry transformations of the kind (4.21) to make them polynomial, but not simultaneously.

The Q-functions for which both $I \neq \emptyset$ and $J \neq \emptyset$ are in general non-rational. These Q-functions are allowed to have poles at $u = \mathbb{i}\mathbb{Z}$, and they can be written in terms of rational functions in u and Hurwitz η-functions,

$$\eta_k(u) \equiv \sum_{n=0}^{\infty} \frac{1}{(u+\mathbb{i}n)^k}\,. \tag{5.31}$$

We will see below, in section 5.4.3, how these functions appear when the non-rational Q-functions are generated from the rational ones by solving finite-difference QQ-relations.

Distinguished Q-functions

There is a single distinguished Q-function at each node in the Young diagram,

$$\mathbb{Q}_{a,s} \equiv \begin{cases} Q_{\emptyset,12\ldots a|\emptyset,12\ldots s} & a \geq 0, s \geq 0 \\ Q_{12\ldots(-a),\emptyset|\emptyset,12\ldots s} & a < 0, s \geq 0 \\ Q_{\emptyset,12\ldots a|12\ldots(-s),\emptyset} & a \geq 0, s < 0 \\ Q_{12\ldots(-a),\emptyset|12\ldots(-s),\emptyset} & a < 0, s < 0 \end{cases}, \tag{5.32}$$

and they relate via fermionic QQ-relations (5.11). Importantly, all $\mathbb{Q}$ are rational, and have the following structure:

- **Asymptotic power**

  To find the asymptotic power at large u of a given $\mathbb{Q}_{a,s}$, one should start from a point on the left boundary of the diagram that is below the point (s,a). Denote this point (s_0,a_0). Then choose a path from (s_0,a_0) to the point (s,a) and add all the weights, λ and ν, that are encountered on the way. The asymptotics of $\mathbb{Q}_{a,s}$ is given by

$$\mathbb{Q}_{a,s} \simeq u^{(s_0-a_0)L-\sum_{b=a_0}^{a}\lambda_b-\sum_{j=s_0}^{s}\nu_j}\,. \tag{5.33}$$

- **Full structure**

  The full structure of $\mathbb{Q}_{a,s}$ is

$$\mathbb{Q}_{a.s} = f_{a,s}\; q_{a,s}\,, \tag{5.34}$$

  where $q_{a,s}$ is a polynomial, and where for homogeneous $\mathfrak{u}(N,M|K)$ chains with central charge C, the factors $f_{a,s}$ have the form

$$f_{a,s} = \phi_{a,s}^{L}\,, \tag{5.35}$$

  with

$$\phi_{a,s}(u) = \begin{cases} \prod_{k=-|s-a|}^{|s-a|}\left(u-\frac{\mathrm{i}\,k}{2}\right)^{\mathrm{sign}(s-a)} & \text{if} \quad s<0\vee(s=0\wedge a<0) \\ 1 & \text{otherwise} \end{cases}\,. \tag{5.36}$$

  On the central part of the diagram, the factors $f_{a,s}$ are distributed as shown in figure 5.8. Note that this corresponds to a particular choice of the gauge symmetry of the Q-system as discussed in section 4.1.5. The factors $f_{a,s}$ can be modified by using symmetry transformations of the kind (4.21).

- **Bethe roots**

  The degree of the polynomial $q_{a,s}$ can be found as the difference of the asymptotic power (5.33) and the power coming from $f_{a,s}$ (5.35). Young diagrams provide an intuitive way of counting Bethe roots, see figure 5.9. In the right half of the diagram, the Bethe roots in each $\mathbb{Q}$ equals the number of boxes to the right and above its position. In the left half of the diagram, the number of Bethe roots equals the number of boxes below and to the left. On the central vertical line ($\mathbb{Q}_{a,0}$), the counting towards the right should be used above the central point ($\mathbb{Q}_{0,0}$), while the counting towards the left should be used below the central point.

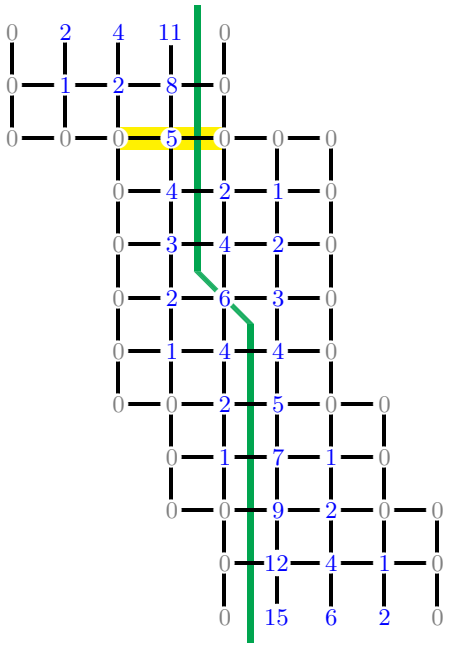

Figure 5.9: Number of Bethe roots in the distinguished Q-functions. To the right of the green line, the number of roots equals the boxes to the right and above the location. To the left of the green line, the number of roots equals the boxes below and to the left of the location. The path from the left to the right boundary with the minimal number of roots is highlighted.

Requirements on "good" solutions

For compact representations, a good solution corresponded to a fully polynomial Q-system. We clearly have to adjust this criterion for non-compact representations. On the other hand, we know that we can map non-compact representations to compact ones via the extended Young diagram. We know that solving the Q-system on a compact Young diagram gives exactly the right number of solutions, and the number of solutions does not depend on the algebra, but simply on the Young diagram. So polynomiality in one of the two halves of the diagram must be enough to pick out exactly the right solutions, and they must all be good, since otherwise we would have too few.

In conclusion, polynomiality of $q_{a,s}$ in (5.34) for all distinguished Q-functions should be a necessary and sufficient condition for a solution of the Q-system to correspond to a physical spin chain multiplet.

5.3.2 Generalised solution algorithm

Polynomiality of the distinguished Q-functions on a non-compact diagram can be imposed similarly to the compact case. It is enough to consider the non-trivial part of the diagram, i.e. to forget about the infinite vertical wings that are aligned completely with the central vertical line. As discussed above, it is even enough to only consider either the left or the right half of the diagram. However, considering both halves of the diagram gives us more

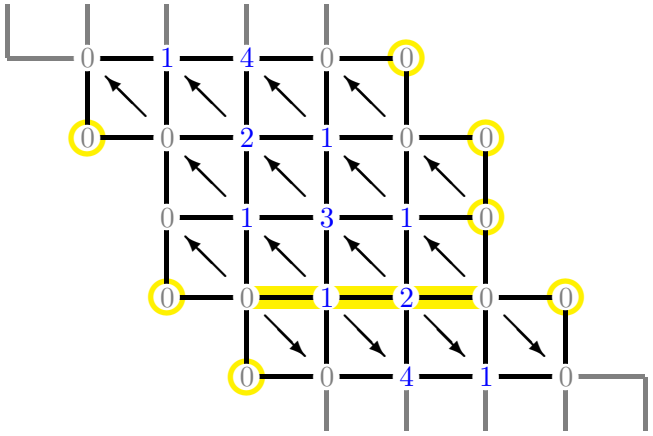

Figure 5.10: Example: generating all $\mathbb{Q}$ within the non-trivial part of a Young diagram from a generic ansatz on a path that minimises the total number of Bethe roots. The $\mathbb{Q}$'s at the nodes encircled in yellow are set to 1 by default.

freedom. See figure 5.10 for a pictorial example.

We can choose any path from the left boundary to the right boundary of the diagram and make a generic ansatz there. This freedom gives new possibilities to minimise the total number of roots compared to the compact case. Note that the numbers of roots grow monotonically in the trivial extensions, so the optimal path is always within the non-trivial part of the diagram. Note also that in some cases there are paths without any Bethe roots, and the Q-system is completely fixed without solving any equations. We return to such solutions in chapter 7.

The method turns out to be very powerful compared to the traditional approaches, and we discuss the obtained results for the $\mathfrak{pu}(2,2|4)$ case in the next section.

5.4 Leading solution to the Quantum Spectral Curve

We are now ready to face the problem that was the motivation behind the development of the above method: the leading solution of the QSC, or, equivalently, the Q-system of cyclic $\mathfrak{pu}(2,2|4)$ spin chain states.

There is one subtlety that has been lurking in the background, which we must now deal with: the joining of short multiplets. These short multiplets correspond to solutions on different Young diagrams, and thus with different structure. At finite coupling, there should be just a single solution describing the long multiplet. How can this be? It turns out that there is a delicate interplay between the symmetries of the Q-system and cyclicity, in the form of the zero-momentum condition, that allows joining to be consistent on the level of the $\mathfrak{psu}(2,2|4)$ Q-system.

Notation

The notation (5.28) was convenient for general Young diagram Q-systems. However, we would like to use a notation consistent with the $\mathfrak{gl}(4|4)$ Q-system that appears in the QSC, cf. figure 4.1. We thus redefine the central point to be $(2,2)$ and use the notation $Q_{A|J}$ for a general Q-function, such that e.g. $\mathbb{Q}_{2,2} = Q_{12|12} = Q_{\emptyset,\emptyset|\emptyset,\emptyset}$. Note also that we similarly redefine the factor $\phi_{a,s} \to \phi_{a-2,s-2}$ in (5.36).

5.4.1 Shortening and cyclicity

Shortening happens when the Young diagram does not touch the points $(0,0)$ or $(4,4)$. Consequently, the points $(1,1)$ or $(3,3)$, respectively, are on the boundary of the diagram, which in turn means that $\mathbb{Q}_{1,1} = Q_{1|1} \propto 1$ or $\mathbb{Q}_{3,3} = Q_{123|123} \propto 1$. Let us consider the first case. Then the fermionic QQ-relation that relates $\mathbb{Q}_{1,1}$ and $\mathbb{Q}_{2,2}$ reads

$$\mathbb{Q}^{+}_{2,2} - \mathbb{Q}^{-}_{2,2} = \mathbb{Q}_{1,2}\,\mathbb{Q}_{2,1} = q_{1,2}\,q_{2,1}\,. \tag{5.37}$$

The zero-momentum condition and trivial roots

Solutions corresponding to cyclic states satisfy the zero-momentum condition,

$$\lim_{u\to 0} \frac{\mathbb{Q}_{2,2}\left(u+\frac{i}{2}\right)}{\mathbb{Q}_{2,2}\left(u-\frac{i}{2}\right)} = 1\,. \tag{5.38}$$

This means that the left-hand side in (5.37) should vanish at $u = 0$, and consequently either $q_{1,2}$ or $q_{2,1}$ has a root at $u = 0$. Likewise, if $\mathbb{Q}_{3,3} \propto 1$ then either $q_{2,3}$ or $q_{3,2}$ contains a factor of u.

5.4.2 Back to the $\mathfrak{psu}(2,2|4)$ Q-system

To really understand the interplay between cyclicity and joining, we need to discuss the transition from the Young diagram Q-system back to the $\mathfrak{psu}(2,2|4)$ Q-system, which is the basic structure in the QSC. The $\mathfrak{psu}(2,2|4)$ Q-system will be the starting point for the calculation of perturbative corrections in chapter 6.

In most cases, the Young diagram Q-system contains Q-functions not present in the $\mathfrak{psu}(2,2|4)$ Q-system. For short representations, the opposite is also true. Importantly, the $\mathfrak{psu}(2,2|4)$ Q-system contains the functions

$$Q_{\emptyset|\emptyset} = Q_{1234|1234} = 1\,. \tag{5.39}$$

Let us first try to understand how the distinguished Q-functions are transferred between the two pictures. For long multiplets, there is no ambiguity. The $\mathfrak{psu}(2,2|4)$ Q-system simply picks out the 25 functions $\mathbb{Q}_{a,s}$ with $0 \le a,s \le 4$. An example of such a long diagram is given in figure 5.11.

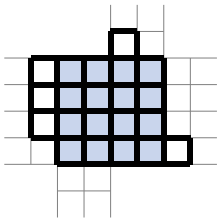

Figure 5.11: The Young diagram for the $\mathfrak{pu}(2,2|4)$ multiplets $n^{\ulcorner} = [0,0|3,2,2,2|1,0]$. The diagram covers the whole 4×4 square and thus the $\mathfrak{psu}(2,2|4)$ $\mathbb{Q}$'s are identical to those on the Young diagram.

Shortening and vanishing Q-functions

The transition is not as smooth for short representations. In the case where $\mathbb{Q}_{1,1}$ is on the boundary of the diagram, corresponding to the shortening $\lambda_1 + \nu_1 = 0$, the function $\mathbb{Q}_{0,0}$ does not belong to the Young diagram Q-system. From the point of view of the $\mathfrak{psu}(2,2|4)$ Q-system, this case corresponds to $\mathbb{Q}_{0,0} \propto \mathbb{Q}_{1,1} \propto 1$, and the fermionic QQ-relation between these two Q-functions is then

$$\mathbb{Q}_{1,0}\mathbb{Q}_{0,1} = 0\,, \tag{5.40}$$

which means that either $\mathbb{Q}_{1,0}$ or $\mathbb{Q}_{0,1}$ vanishes. If $\mathbb{Q}_{1,0}$ vanishes, then it follows from the QQ-relations that also $\mathbb{Q}_{2,0} = \mathbb{Q}_{3,0} = \mathbb{Q}_{4,0} = 0$. Likewise, if $\mathbb{Q}_{0,1} = 0$ then $\mathbb{Q}_{0,s} = 0$ for $s = 1,2,3,4$.

To understand which of $\mathbb{Q}_{1,0}$ and $\mathbb{Q}_{0,1}$ is zero, recall the concept of nested Bethe equations. They are effectively equations on the zeros of seven non-vanishing distinguished Q-functions along a Dynkin path. Importantly, they depend on the length L. The Dynkin path is that of the chosen grading, which defines the HWS. The HWS in a short multiplet only remains a HWS in the long multiplet at finite coupling in a particular grading. We should then choose to set the one of $\mathbb{Q}_{1,0}$ and $\mathbb{Q}_{0,1}$ that is not on the Dynkin path of this grading to zero. A grading of the type $1\ldots$ corresponds to $\mathbb{Q}_{1,0} = 0$, and $\hat{1}\ldots$ corresponds to $\mathbb{Q}_{0,1} = 0$.

An analogous treatment of the shortening $\lambda_4 + \nu_4 = 0$ shows that $\mathbb{Q}_{3,4} = 0$ in the $\ldots 4$ grading, and $\mathbb{Q}_{4,3} = 0$ in the $\ldots \hat{4}$ grading.

Agreement between short multiplets

Consider a representation with only the shortening $\lambda_1 + \nu_1 = 0$. We then have to make the choice of either transferring the 20 $\mathbb{Q}_{a,s}$ with $a \geq 1$ from the Young diagram Q-system corresponding to the highest weight states in the $\hat{1}\ldots$ gradings within the long multiplet, or the 20 $\mathbb{Q}_{a,s}$ with $s \geq 1$ from the Young diagram corresponding to the $1\ldots$ highest weight states. The situation is depicted in figure 5.12.

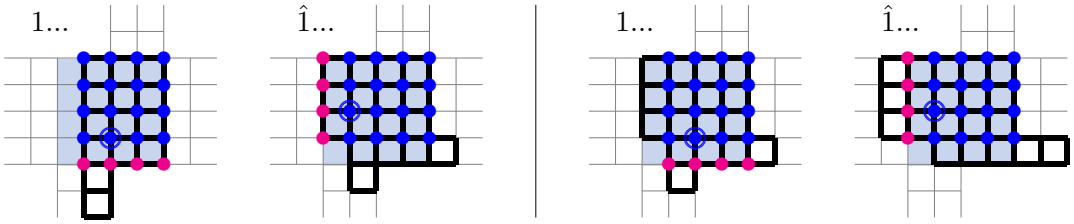

Figure 5.12: Defining the $\mathfrak{psu}(2,2|4)$ Q-system for the case of a short representation. The two diagrams on the left are a pair of short multiplets that join at finite coupling. The two diagrams on the right are another such pair. On each diagram, the marked nodes are the 20 distinguished Q-functions which are transferred from the Young diagram to the $\mathfrak{psu}(2,2|4)$ Q-system. The $\mathbb{Q}$'s that must coincide (up to symmetry rescalings) on both Young diagrams are marked in blue. The $\mathbb{Q}$'s that can be transferred to the $\mathfrak{psu}(2,2|4)$ Q-system from only one of the diagrams are marked in red. The node that has a trivial Bethe root is encircled; the position of this node determines the grading in which the multiplet is going to join (note that the second and the third Young diagrams are identical but the gradings are different).

In the perturbative solution of the QSC, setting $\mathbb{Q}_{a,0}$ or $\mathbb{Q}_{0,s}$ to zero is simply a question of a subset of the $\mathbb{Q}$'s being suppressed by a factor of g^2. This factor can be shuffled around by the symmetries of the Q-system. This means that, up to symmetry transformations, the 16 $\mathbb{Q}_{a,s}$ with $a,s \geq 1$ on the two Young diagrams have to agree. From the counting of Bethe roots, cf. figure 5.9 this seems problematic: the degrees of the polynomials do not agree. The only way for the Q-systems to be compatible is if some of $q_{a,s}$ on each of the diagrams have trivial roots that can be absorbed into the factors $f_{a,s}$, on which the diagrams do not agree either, since L is different. Indeed, it follows from (1.40), that if a multiplet in the grading 1... has length L, a compatible multiplet for joining should be of length $L+1$ in the grading $\hat{1}$....

Concretely, the compatibility requirement is that

$$q^{1\dots}_{a,s} = \phi_{a,s}\, q^{\hat{1}\dots}_{a,s}\,, \quad a\,,s>0\,, \tag{5.41a}$$

where $\phi_{a,s}$ is given in (5.36) up to the change of conventions $\phi_{a,s} \to \phi_{a-2,s-2}$. This clarifies the question of where to place the trivial roots that are a consequence of the zero-momentum condition. We have $q^{1\dots}_{1,\dot{2}} = u\, q^{\hat{1}\dots}_{1,\dot{2}}$, which implies that $q^{1\dots}_{1,\dot{2}}$ has a trivial zero (i.e. $u=0$). Also, from $q^{1\dots}_{2,\dot{1}} = u^{-1}\, q^{\hat{1}\dots}_{2,\dot{1}}$, we see that $q^{\hat{1}\dots}_{2,\dot{1}}$ has a trivial zero.

The analysis of the $\lambda_4+\nu_4=0$ shortening can be done in complete analogy. In that case $\mathbb{Q}_{a,s}$ with $a,s<4$, and they should satisfy the compatibility constraint

$$q^{\dots 4}_{a,s} = \phi_{4-a,4-s}\, q^{\dots\hat{4}}_{a,s}\,, \quad a\,,s<4\,. \tag{5.41b}$$

Note that, while the Young diagram Q-systems corresponding to the gradings $\hat{1}\dots$ and $\dots\hat{4}$ must contain several trivial roots, the Young diagram Q-systems corresponding to the gradings $1\dots$ and $\dots 4$ only have possible trivial roots in $q_{1,2}$ or $q_{3,2}$. Thus the compatibility constraint is easy to impose in the $\lrcorner$ grading.

Recipe

To summarise, the transition between the Young diagram Q-system and the $\mathfrak{psu}(2,2|4)$ Q-system follows the rules:

- Given a Q-system on a Young diagram, decide the grading according to:

$$\begin{aligned}
&\lambda_1+\nu_1=0\,, \quad q_{1,2} \text{ has root at } u=0 \quad \Rightarrow \quad 1...\,,\\
&\lambda_1+\nu_1=0\,, \quad q_{2,1} \text{ has root at } u=0 \quad \Rightarrow \quad \hat{1}...\,,\\
&\lambda_4+\nu_4=0\,, \quad q_{3,2} \text{ has root at } u=0 \quad \Rightarrow \quad ...4\,,\\
&\lambda_4+\nu_4=0\,, \quad q_{2,3} \text{ has root at } u=0 \quad \Rightarrow \quad ...\hat{4}\,.
\end{aligned} \tag{5.42}$$

- Given the grading, choose which $\mathbb{Q}_{a,s}$ should vanish in the $\mathfrak{psu}(2,2|4)$ Q-system:

$$\begin{aligned}
1... \quad &\Rightarrow \quad \mathbb{Q}_{a>0,0}=0\,,\\
\hat{1}... \quad &\Rightarrow \quad \mathbb{Q}_{0,s>0}=0\,,\\
...4 \quad &\Rightarrow \quad \mathbb{Q}_{a<4,4}=0\,,\\
...\hat{4} \quad &\Rightarrow \quad \mathbb{Q}_{4,s<4}=0\,.
\end{aligned} \tag{5.43}$$

- Set $\mathbb{Q}_{0,0}=\mathbb{Q}_{4,4}=1$.

- All other $\mathbb{Q}_{a,s}$ should be the same as $\mathbb{Q}_{a,s}$ on the Young diagram.

5.4.3 Generating the full Q-system

To obtain the full $\mathfrak{psu}(2,2|4)$ Q-system from the 25 $\mathbb{Q}_{a,s}$ one needs to solve 12 first-order difference equations. We will here focus on determining $Q_{a|\emptyset}$ and $Q_{\emptyset|j}$ as the remaining Q-functions are easily reconstructed from these using the relations in section 4.2.1.

$Q_{a|\emptyset}$ from $\mathbb{Q}$

All four $Q_{a|\emptyset}$ belong to the left compact Young diagram and should thus be rational. Their structure is

$$Q_{a|\emptyset}=\frac{q_{a|\emptyset}}{u^L}\,, \quad q_{a|\emptyset}=\sum_{k=0}^{p_{a|\emptyset}} c_k u^k\,. \tag{5.44}$$

The asymptotic powers $p_{a|\emptyset}$ can be found from power counting in the QQ-relations and are

$$p_{2|\emptyset}=L-n_{\mathbf{f}_2}^{\lceil}-1\,, \quad p_{3|\emptyset}=L-n_{\mathbf{f}_3}^{\lceil}\,, \quad p_{4|\emptyset}=L-n_{\mathbf{f}_4}^{\lceil}+1\,. \tag{5.45}$$

An easy way to find $Q_{a|\emptyset}$ is to simply fit polynomials in the determinant relations

$$Q_{A|\emptyset}=\det_{1\leq a,j\leq|A|}\left(Q_{a|\emptyset}^{[|A|+1-2j]}\right)\,. \tag{5.46}$$

In practice, one can first fix $Q_{2|\emptyset}$ from $Q_{12|\emptyset}=\mathbb{Q}_{2,0}$, then fix $Q_{3|\emptyset}$ from $Q_{123|\emptyset}=\mathbb{Q}_{3,0}$, and finally $Q_{4|\emptyset}$ from $Q_{1234|\emptyset}=\mathbb{Q}_{4,0}$.

$Q_{\emptyset|j}$ from $\mathbb{Q}$

$Q_{\emptyset|2}$ belongs to the left compact diagram and should be rational. Its structure is

$$Q_{\emptyset|2} = u^L q_{\emptyset|2} \quad q_{\emptyset|2} = \sum_{k=0}^{p_{\emptyset|2}} c_k u^k \,, \quad p_{\emptyset|2} = n_{\mathbf{b}_2}^{\lceil} + 1 \,, \tag{5.47}$$

and it can be found by fitting a polynomial to

$$Q_{\emptyset|12} = Q^+_{\emptyset|1} Q^-_{\emptyset|2} - Q^-_{\emptyset|1} Q^+_{\emptyset|2} \,. \tag{5.48}$$

$Q_{\emptyset|3}$ and $Q_{\emptyset|4}$ do not belong to the left or right compact diagram and are thus not expected to be rational. The basic QQ-relation $Q_{\emptyset|3}Q_{\emptyset|312} = ...$ can be rewritten as

$$Q_{\emptyset|3} = Q_{\emptyset|2}\Psi\left(\frac{Q_{\emptyset|1}Q_{\emptyset|123}}{Q^-_{\emptyset|12}Q^+_{\emptyset|12}}\right) - Q_{\emptyset|1}\Psi\left(\frac{Q_{\emptyset|2}Q_{\emptyset|123}}{Q^-_{\emptyset|12}Q^+_{\emptyset|12}}\right) . \tag{5.49}$$

As we explain in appendix A.4.2, evaluating these Ψ-operations leads to poles only at $i\mathbb{Z}$. Also, the way we choose to define Ψ leads to poles only in the lower half-plane, $\mathrm{Im}\,(u) < 0$, and the results can be written in terms of η-functions (6.4).

Similarly the QQ-relation $Q_{\emptyset|4}Q_{\emptyset|412} = ...$ can be rewritten as

$$Q_{\emptyset|4} = Q_{\emptyset|2}\Psi\left(\frac{Q_{\emptyset|1}Q_{\emptyset|124}}{Q^-_{\emptyset|12}Q^+_{\emptyset|12}}\right) - Q_{\emptyset|1}\Psi\left(\frac{Q_{\emptyset|2}Q_{\emptyset|124}}{Q^-_{\emptyset|12}Q^+_{\emptyset|12}}\right) . \tag{5.50}$$

$Q_{\emptyset|124}$ belongs to the right compact Young diagram, i.e. it is rational, and it can be found by fitting a polynomial to

$$Q_{\emptyset|12}Q_{\emptyset|1234} = Q^+_{\emptyset|123}Q^-_{\emptyset|124} - Q^-_{\emptyset|123}Q^+_{\emptyset|124} \,. \tag{5.51}$$

The rest

As described in section 4.2.1, all other Q-functions follow from the eight functions $Q_{a|\emptyset}$ and $Q_{\emptyset|i}$. Note that, superficially, one introduces 16 constants by solving the first order difference equations on $Q_{a|i}$ (4.25), but these can in practice be fixed by comparing the re-generated values of the distinguished Q-functions with the known values.

5.4.4 Results

In table 5.2 and in appendix A.3 we mark the multiplets with $\Delta_0^{\lceil} \leq 8$ for which we were able to generate the Q-system in less than 15 minutes on a standard laptop with our `Mathematica`-implementation of the algorithm described in this chapter. This `Mathematica`-file is available in the ancillary files of [5] at arxiv.org. The algorithm also imposes the joining criteria (5.41) and the zero-momentum condition (5.38), which ensure that only cyclic states appear and that each long multiplet only appears once. The obtained results include all 495 $\mathfrak{psu}(2,2|4)$ multiplets with $\Delta_0^{\lceil} \leq \frac{13}{2}$. Even more results can be generated by allowing longer runtimes and tailoring the algorithm to explicit examples.

Δ_0	# diagrams solved	total # solutions found
2	1 / 1	1 / 1
3	1 / 1	1 / 1
4	7 / 7	10 / 10
5	13 / 13	27 / 27
5.5	12 / 12	36 / 36
6	39 / 39	144 / 144
6.5	36 / 36	276 / 276
7	68 / 77	600 / 918
7.5	54 / 84	694 / 2204
8	107 / 180	1395 / 6918

Table 5.2: Leading solutions to the QSC found with the generic `Mathematica`-implementation of the algorithm published with [5]. 15 minutes of computation time was allowed per diagram. The explicit multiplet content is given in appendix A.3.

Subconclusion

In this chapter we provided a new way of thinking about Q-systems for rational spin chains. The main idea is that the Q-system can be built on the Young diagram of the investigated irrep. The conventional methods to determine the spectrum, through Bethe and Baxter equations, do not guarantee the right structure of the full Q-system, and therefore these methods are marred by unwanted solutions. We proved that a sufficient criteria for the full Q-system to have the correct structure is that the distinguished Q-functions, of which there is one at each node in the Young diagram, are polynomial, up to factors of $(u+\frac{\mathrm{i}n}{2})^{\pm L}$. We provided an efficient way to impose this criterion based on polynomial division, which makes it possible to obtain a far larger range of explicit analytic solutions than previously.

We now have access to the explicit analytic solutions to the Quantum Spectral Curve for the first thousands of multiplets. The QSC is formulated in terms of a $\mathfrak{psu}(2,2|4)$ Q-system, and the weights of the representations become non-integer at finite coupling due to the anomalous dimension, which obscures the Young diagram philosophy presented here. Thus we had to make the transition back to the $\mathfrak{psu}(2,2|4)$ Q-system to be able to use our results as the seed for perturbative calculations in the QSC, which is the topic of the next chapter. This transition taught us that the joining compatibility of Q-systems on Young diagrams corresponding to short multiplets is provided by the presence of trivial Bethe roots. These trivial roots are in turn guaranteed by the zero-momentum condition that singles out the cyclic states.

Chapter 6

Perturbative algorithms

Most of what we have done so far has been building up to this point: using the Quantum Spectral Curve to generate the explicit perturbative spectrum. Having understood how to classify and find the leading solutions, we are ready to turn on the coupling g. This chapter is devoted to the design of algorithms that efficiently generate perturbative corrections by imposing the analytic constraints from the QSC.

We start with a subset of the spectrum: the $\mathfrak{sl}(2)$ sector, where certain simplifications make it possible to work with a very small set of functions. Afterwards, we discuss how to design algorithms that are completely general. We will leave out some of the technical details that can be found in [1, 7] and focus on the general idea behind the algorithms.

6.1 Generalities

Let us start by discussing the general features that the different perturbative solution strategies have in common.

6.1.1 The key: all-loop ansatz for P

The cornerstone in the perturbative algorithms is the rational all-loop ansatz (4.71) for the eight functions $\mathbf{P}$ that was analysed in sections 4.2.7 and 4.3.3. It allows us to write an ansatz for $\mathbf{P}(u)$ in terms of a finite number of constants, c and d, at each perturbative order. For example, if we expand the ansatz (4.71) for $\mathbf{P}_4$ for the Konishi multiplet, $n^{\lrcorner} = [0,0|1,1,1,1|0,0]$, around $g=0$, we get

$$(gx)^{2+\Lambda}\mathbf{P}_4(u) \;=\; \mathsf{d}^{(1)}_{4,0}+u\,\mathsf{d}^{(1)}_{4,1}+u^2\,\mathsf{d}^{(1)}_{4,2}+g^2\left(\frac{\mathsf{c}^{(1)}_{4,1}-\mathsf{d}^{(1)}_{4,1}}{u}+\mathsf{d}^{(2)}_{4,0}-2\mathsf{d}^{(1)}_{4,2}+u\,\mathsf{d}^{(2)}_{4,1}+u^2\,\mathsf{d}^{(2)}_{4,2}\right)+\mathcal{O}(g^4)\,. \tag{6.1}$$

Note that the coefficients of the leading power, $u^2\cdot\sum_{j=0}^{\infty}\mathsf{d}^{(j+1)}_{4,2}g^{2j}$, should match the choice of A_4, which is given in terms of the quantum numbers, including the anomalous

dimension. The product of the prefactors A_4 and A^4 is fixed by (4.39), which for the Konishi multiplet gives

$$\mathsf{A}_4\mathsf{A}^4 = -\mathbb{i}\gamma_1 g^2 - \mathbb{i}\left(\gamma_2 + \frac{19}{24}\gamma_1^2\right) g^4 - \mathbb{i}\left(\gamma_3 + \frac{19}{12}\gamma_1\gamma_2 + \frac{1}{6}\gamma_1^3\right) g^6 + \mathcal{O}(g^8)\,, \tag{6.2}$$

and this shows how the perturbative anomalous dimension sneaks in through the ansatz. We can use some of the leftover H-symmetry (4.23) to remove some terms in the ansatz. For example, we can use the freedom to add $\mathbf{P}_3$ to $\mathbf{P}_4$ to set the coefficients $\mathsf{d}_{4,1}^{(j)}$ to zero in (6.1). In the end, we have a rather simple ansatz for $\mathbf{P}(u)$ at all orders in perturbation theory.

The value on the second sheet, $\tilde{\mathbf{P}}(u)$, also plays a crucial role in the perturbative algorithms. By making the replacement $x \to \frac{1}{x}$ in the ansatz for $\mathbf{P}$ (4.71), and replacing x by the value $|x(u)| > 1$, we get an expansion that converges in a finite region around $u = 0$ on the sheet $\tilde{\mathbf{P}}(u)$. This time, the ansatz contains infinitely many unknown constants at each perturbative order. For example, the ansatz for $\tilde{\mathbf{P}}_4(u)$ for the Konishi multiplet is

$$\left(\frac{g}{x}\right)^{2+\Lambda} \tilde{\mathbf{P}}_4(u) \;=\; \mathsf{d}_{4,0}^{(1)} + \sum_{k=1}^{\infty} \mathsf{c}_{4,k}^{(1)}\, u^k + g^2\left(\mathsf{d}_{4,0}^{(2)} + \sum_{k=1}^{\infty} \mathsf{c}_{4,k}^{(2)}\, u^k - \sum_{k=0}^{\infty} k\, \mathsf{c}_{4,k}^{(1)}\, u^{k-2} + \frac{\mathsf{d}_{4,1}^{(1)}}{u}\right) + \mathcal{O}(g^4)\,. \tag{6.3}$$

The perturbative algorithms will generate exact expressions for the functions $\tilde{\mathbf{P}}^{(n)}(u)$. By expanding the obtained expressions at $u = 0$ and comparing with the ansatz, e.g. (6.3), all the coefficients $\{\mathsf{d}_{a,k}^{(n)}, \mathsf{c}_{a,k}^{(n)}\}$ will be fixed. Notice that this gives us knowledge about higher-order terms in $\mathbf{P}(u)$. For example, the coefficient $\mathsf{c}_{4,1}^{(1)}$ which first appears at the order g^2 in (6.1) can be determined from the order g^0 in (6.3).

To summarise, the finite ansatz for $\mathbf{P}^{(n)}(u)$ is our starting point for generating the functions of the QSC at a given perturbative order n. From this ansatz, we can generate all other functions in terms of a finite number of unknown constants. Finally, these constants are fixed by requiring that the obtained values for $\tilde{\mathbf{P}}^{(n)}$ are consistent with the all-loop ansatz. The last step is an example of what we refer to as *gluing*: enforcing the analytic requirements of the QSC by comparing the value of particular functions on two different Riemann sheets at the point where the branch cut between them has collapsed.

6.1.2 The encountered basis of functions

Only a restricted class of functions appears in the perturbative solution of the QSC, and all applied operations are closed with respect to these functions. This means that the perturbative algorithms can be automatised and, in principle, run recursively to any loop order. The main operation is the Ψ-operation that is applied in the solution of finite-difference equations. This operation is discussed in detail in appendix C.1.

We have already seen that the 1-loop Q-system can be expressed in terms of rational functions in u and multiple Hurwitz η-functions,

$$\eta_{k_1,k_2,\ldots,k_n}(u) \equiv \sum_{0\leq j_1<\ldots<j_n<\infty} \frac{1}{(u+\mathbb{i}j_1)^{k_1}\cdots(u+\mathbb{i}j_n)^{k_n}}. \tag{6.4}$$

The functions ω, μ and $\tilde{\mathbf{P}}$ furthermore contain $\mathbb{i}$-periodic functions of the kind

$$\mathcal{P}_k \equiv \sum_{j=-\infty}^{\infty} \frac{1}{(u+\mathbb{i}j)^k}\,. \tag{6.5}$$

The properties of these functions are described in more detail in appendix B.3. The crucial property is that the Ψ-operation is closed with respect to this set of functions. First, note that applying Ψ to the $\mathbb{i}$-periodic functions is completely trivial: $\Psi(\mathcal{P}_k\cdot f) = \mathcal{P}_k\Psi(f)$. Applying the Ψ-operation to a polynomial simply returns another polynomial of one degree higher, e.g.

$$\Psi(1+2u+6u^2) = u+(3+\mathbb{i})u^2+2\mathbb{i}u^3\,,$$

while the application to negative powers results in η-functions:

$$\Psi\left(\frac{1}{u^k}\right) = \sum_{n=0}^{\infty}\frac{1}{(u+\mathbb{i}n)^k} \equiv \eta_k\,.$$

The nice thing about η-functions is that applying Ψ to them simply produces more η-functions, e.g.

$$\Psi\left(\frac{u^2+3}{u}\eta_5\right) = -\frac{\mathbb{i}}{2}\eta_3+\frac{1}{2}\eta_4+\frac{\mathbb{i}u^2+u}{2}\eta_5+3\eta_6+3\eta_{1,5}\,.$$

Note that since the η-functions satisfy stuffle-relations, one can always linearise a given expression in these functions.

As explained above, we also need to power-expand the functions around $u=0$. The power expansion of η-functions introduces *multiple zeta values* (MZVs),

$$\zeta_{k_1,\ldots,k_n} = \sum_{1\leq j_1<\ldots<j_n}^{\infty}\frac{1}{j_1^{k_1}\cdots j_n{}^{k_n}}\,,$$

which we describe in more detail in appendix B.1. For example,

$$\eta_{3,2} = -\frac{\zeta_2}{u^3}-\frac{2\mathbb{i}\zeta_3}{u^2}+\frac{3\zeta_4}{u}+\mathbb{i}(4\zeta_5-\zeta_{3,2})+u\,(-5\zeta_6+2\zeta_{3,3}+3\zeta_{4,2})+\mathcal{O}(u^2)\,. \tag{6.6}$$

These numbers are interrelated by a high number of algebraic relations which means that they can be expressed in terms of a very small basis. We define the *transcendentality* of the ζ-values by the sum of their indices, and all MZVs with transcendentality less or equal to 10 can, for example, be expressed in terms of

$$\zeta_1\,,\quad \zeta_2\,,\quad \zeta_3\,,\quad \zeta_5\,,\quad \zeta_7\,,\quad \zeta_{2,6}\,,\quad \zeta_9\,,\quad \zeta_{2,8}\,. \tag{6.7}$$

As will be clear from the algorithms described in this chapter, the function types described here are everything that is encountered at *any* order of perturbation theory.

6.1.3 Overview of algorithms

In the following three sections, we will present three strategies to solve the QSC perturbatively.

- The algorithm presented in section 6.2 solves the $\mathbf{P}\mu$-system for solutions corresponding to multiplets containing operators in the $\mathfrak{sl}(2)$ sector. This algorithm has the big advantage that it is automatically linear in η-functions, so there is no need to linearise the intermediate results, which in practice is a rather time-consuming process.
- In section 6.3, we present a general algorithm that determines all quantities of the QSC, including the full Q-system. This method involves a large number of functions, requires a significant amount of linearisation in η-functions, and it involves the full H-symmetry of the QSC.
- There are tricks to overcome some of these issues, but the general strategy to solve the $\mathbf{P}\mu$-system presented in section 6.4 directly circumvents the issues by doing a significant short-cut.

6.2 Pμ-system for the $\mathfrak{sl}(2)$ sector

This section reviews the algorithm to solve the $\mathbf{P}\mu$-system for the $\mathfrak{sl}(2)$ sector, which was presented in [1]. The $\mathfrak{sl}(2)$ sector is specified by the quantum numbers

$$n^{\lrcorner} = [0, S-2|L-1, L-1, 1, 1|S-2, 0]\,, \tag{6.8}$$

which corresponds to a HWS of the kind $\mathcal{D}_{12}^{S}\mathcal{Z}^{L}$ in the grading $1\hat{1}\hat{2}23\hat{3}\hat{4}4$.

6.2.1 Left/right symmetry

The $\mathfrak{sl}(2)$ quantum numbers have the left/right symmetry (4.24), which means that all quantities in the QSC with lower indices are equivalent to the Hodge dual quantities with upper indices. For the $\mathbf{P}\mu$-system, this concretely means that it is possible to fix parts of the symmetry such that $\mathbf{P}_a$ and μ_{ab} are directly related to $\mathbf{P}^a$ and μ^{ab} through

$$\mathbf{P}^a = \chi^{ab}\mathbf{P}_b\,, \qquad\qquad \mu^{ab} = \chi^{ac}\chi^{bd}\mu_{cd}\,, \tag{6.9}$$

where

$$\chi^{ab} = \begin{pmatrix} 0 & 0 & 0 & -1 \\ 0 & 0 & +1 & 0 \\ 0 & -1 & 0 & 0 \\ +1 & 0 & 0 & 0 \end{pmatrix}. \tag{6.10}$$

Furthermore, $\mu_{14} = \mu_{23}$ due to (6.9) and (4.49) with $\mathrm{Pf}(\mu_\bullet) = 1$, which leaves us with nine functions in total: four $\mathbf{P}_a$ and five linearly independent μ_{ab}. The following algorithm explains how to determine these nine functions in a recursive procedure.

6.2.2 The structure of $\mathbf{P}_a$

Due to the left/right symmetry, the relations between the constant prefactors of the **P**-functions (4.39) turn into the relations

$$\mathsf{A}_1\mathsf{A}_4 = \frac{\big((L-S+2)^2-\Delta^2\big)\big((L+S)^2-\Delta^2\big)}{16iL(L+1)}\,, \tag{6.11a}$$

$$\mathsf{A}_2\mathsf{A}_3 = \frac{\big((L+S-2)^2-\Delta^2\big)\big((L-S)^2-\Delta^2\big)}{16iL(L-1)}\,. \tag{6.11b}$$

When we plug the perturbative structure of the conformal dimension,

$$\Delta = L + S + \sum_{j=1}^{\infty} \gamma_j g^{2j}\,, \tag{6.12}$$

into (6.11), we get

$$\mathsf{A}_1\mathsf{A}_4 = -\mathbb{i}\frac{(S-1)(L+S)}{2L}\gamma_1\, g^2 + \mathcal{O}(g^4)\,, \tag{6.13a}$$

$$\mathsf{A}_2\mathsf{A}_3 = -\mathbb{i}S\frac{(L+S-1)}{L-1} + \mathcal{O}(g^2)\,. \tag{6.13b}$$

We see that $\mathsf{A}_1\mathsf{A}_4 = \mathcal{O}(g^2)$ and consequently either $\mathbf{P}_1$ or $\mathbf{P}_4$ should vanish at the leading order. From the discussion of shortening in chapter 5 it is indeed natural that $\mathbf{P}_1 \propto \mathbb{Q}_{1,0}$ vanishes, and we choose to fix the symmetry such that this is the case. Notice that the anomalous dimension enters in the ansatz for $\mathbf{P}$ through the prefactors (6.13).

The ansatz for $\mathbf{P}_a$ (4.71), where we have set $\Lambda = -\frac{L}{2}$ to have (6.9), also reveals that $\mathbf{P}_2$ has a quite simple structure as the expansion in positive powers of x is absent. The vanishing of $\mathbf{P}_1$ and the fact that $\mathbf{P}_2$ is a pure power at the leading order,

$$\mathbf{P}_1 = \mathcal{O}(g^2)\,, \qquad \mathbf{P}_2 = u^{-\frac{L}{2}} + \mathcal{O}(g^2)\,, \tag{6.14}$$

are the two key properties that we exploit in the algorithm. The absence of these properties for states outside the $\mathfrak{sl}(2)$ sector explains why the method is not applicable there.

6.2.3 The $\mathbf{P}\mu$ equations

In the left/right symmetric case, the relations of the $\mathbf{P}\mu$-system can be summarised in three simple equations,

$$\mu_{ab} - \tilde{\mu}_{ab} = \tilde{\mathbf{P}}_a\mathbf{P}_b - \tilde{\mathbf{P}}_b\mathbf{P}_a\,, \tag{6.15a}$$

$$\tilde{\mathbf{P}}_a = (\mu\chi)_a{}^b\,\mathbf{P}_b\,, \tag{6.15b}$$

$$\tilde{\mu}_{ab} = \mu^{[2]}_{ab}\,, \tag{6.15c}$$

where $(\mu\chi)_a{}^b = \mu_{ac}\chi^{cb}$. We will also make use of the property (4.42) which now reads

$$(\mu\chi - \mu^{[2]}\chi)_a{}^b\,\mathbf{P}_b = 0\,. \tag{6.16}$$

6.2.4 Baxter equation on μ_{12}

By combining the equations (6.15) and using the property (6.16) one can derive a second order difference equation on μ_{12} on the form

$$\begin{aligned}\frac{1}{\mathbf{P}_2^2}\,\mu_{12} - \left(\frac{\mathbf{P}_3}{\mathbf{P}_2} - \frac{\mathbf{P}_3^{[2]}}{\mathbf{P}_2^{[2]}} + \frac{1}{\mathbf{P}_2^2} + \frac{1}{\left(\mathbf{P}_2^{[2]}\right)^2}\right)\mu_{12}^{[2]} + \frac{1}{\left(\mathbf{P}_2^{[2]}\right)^2}\,\mu_{12}^{[4]} \\ = \frac{\mathbf{P}_1^{[2]}\tilde{\mathbf{P}}_2^{[2]}}{\left(\mathbf{P}_2^{[2]}\right)^2} - \frac{\mathbf{P}_1\tilde{\mathbf{P}}_2}{\mathbf{P}_2^2} + \left(\frac{\mathbf{P}_1}{\mathbf{P}_2} - \frac{\mathbf{P}_1^{[2]}}{\mathbf{P}_2^{[2]}}\right)\mu_{14}^{[2]}\,.\end{aligned} \tag{6.17}$$

The important point here is that the right-hand side is proportional to $\mathbf{P}_1$, which means that the n'th order contributions to $\tilde{\mathbf{P}}_2$ and μ_{14} are suppressed by a factor of g^2 compared to those of μ_{12}. We have an all-loop ansatz for $\mathbf{P}_a$, so at a given order the right hand side is known up to a finite number of unknown constants. Likewise, all terms on the left-hand side not containing the n'th contribution to μ_{12} are known. At order n, we can then write the equation as

$$u^L\mu_{12}^{(n)} - \left(\mathbf{p}_3 - \mathbf{p}_3^{[2]} + u^L + (u+\mathbb{i})^L\right)\mu_{12}^{(n)[2]} + (u+\mathbb{i})^L\mu_{12}^{(n)[4]} \;=\; U_{12}^{(n)}\,, \tag{6.18}$$

where $U_{12}^{(n)}$ is a source term known up to a finite number of constants. We used that $\mathbf{P}_2^{(1)} = u^{-\frac{L}{2}}$ and defined $\mathbf{p}_3 = u^{\frac{L}{2}}\mathbf{P}_3^{(1)}$ which is a polynomial of degree $L-1$.

The leading order

At the leading order, the source terms vanishes, $U_{12}^{(1)} = 0$. Setting $\mu_{12}^{(1)} \propto Q^-$, the equation is then simply the $\mathfrak{sl}(2)$ Baxter equation,

$$T\,Q \;=\; \left(u+\tfrac{\mathbb{i}}{2}\right)^L Q^{[2]} + \left(u-\tfrac{\mathbb{i}}{2}\right)^L Q^{[-2]}\,, \tag{6.19}$$

where $T(u)$ is a polynomial of degree L. This second-order difference equation has two solutions, one of which is polynomial and one which is non-rational [128]. We will denote the polynomial solution by Q_1. Since the second solution is non-rational, and since the roots of Q_1 are known to be real which rules out the possibility of exceptional solutions, there is no ambiguity in the solutions to the $\mathfrak{sl}(2)$ Baxter equation. In fact, the Baxter equation can be solved very efficiently in this particular example. There are in general several solutions to the Baxter equation, and at this stage we choose a specific solution, corresponding to choosing a specific eigenstate.

With the polynomial solution Q_1 at hand, we can construct the second solution Q_2 by making the ansatz $Q_2 = Q_1\, f(u)$. Using (6.19) to write T in terms of Q_1, this gives a difference equation on f,

$$(u+\tfrac{\mathbb{i}}{2})^L Q_1^{[2]}\left(f - f^{[2]}\right) \;=\; (u-\tfrac{\mathbb{i}}{2})^L Q_1^{[-2]}\left(f^{[-2]} - f\right). \tag{6.20}$$

Upon multiplying by Q_1, we can rewrite this equation using the difference operator ∇ (4.27),

$$\nabla\left((u+\tfrac{\mathbb{i}}{2})^L Q_1 Q_1^{[2]} \nabla(f)\right) = 0\,. \tag{6.21}$$

The solution can be written as

$$Q_2 = Q_1 f = Q_1 \Psi\left(\frac{1}{(u+\frac{\mathbb{i}}{2})^L Q_1 Q_1^{[2]}}\right). \tag{6.22}$$

Appendix A.4.2 explains how to evaluate such expressions, and the result has the form [1]

$$Q_2 = q_2 + Q_1 \sum_{k=1}^{L} r_k\, \eta_k^+\,, \tag{6.23}$$

where r_k are constants, q_2 is a polynomial of degree at most $S-1$, and η_k is the Hurwitz η-function (6.4). Notice that only poles at $\mathbb{i}\mathbb{Z}$ are generated.

As discussed in section 4.3.1, μ is not allowed to contain poles at the leading order, and we must then have $\mu_{12}^{(1)} \propto Q_1^-$.

Higher orders

At sub-leading orders, the source term U_{12} does not vanish. We then have to solve the inhomogeneous version of the Baxter equation (6.18). As above, we can make the ansatz $\mu_{12}^{(n)} = Q_1^- f^-$ and rewrite the equation as

$$\nabla\left((u+\tfrac{\mathbb{i}}{2})^L Q_1 Q_1^{[2]} \nabla(f)\right) = Q^{[2]} U_{12}^{(n)+}\,. \tag{6.24}$$

with solution [1]

$$\mu_{12}^{(n)} = Q_1^- \Psi\left(\frac{\Psi\left(Q_1^+\, U_{12}^{(n)}\right)}{u^L\, Q_1^- Q_1^+}\right) = q_2^- \Psi\left(Q_1^+ U_{12}^{(n)}\right) + Q_1^- \Psi\left(\sum_{k=1}^{L} \frac{r_k}{u^k} \Psi\left(Q_1^+ U_{12}^{(n)}\right) - q_2^+ U_{12}^{(n)}\right). \tag{6.25}$$

The ambiguity in Ψ exactly corresponds to the freedom to add the two homogeneous solutions $\Phi_1 Q_1^-$ and $\Phi_2 Q_2^-$, with Φ_i being $\mathbb{i}$-periodic coefficients, to the solution.

Regularity at $u = 0$

The coefficients Φ_i should be consistent with the fact that μ have power-like asymptotics and poles only at $\mathbb{i}\mathbb{Z}$. They can thus be written on the form

$$\Phi_i = \phi_{i,0} + \sum_{k=1}^{\infty} \phi_{i,k} \mathcal{P}_k \,, \tag{6.26}$$

where $\phi_{i,k}$ are constants and $\mathcal{P}_k$ are the $\mathbb{i}$-periodic functions (4.59). The sum in general truncates quickly.

Now recall that, as discussed in section 4.3.1, the combinations $\mu + \mu^{[2]}$ and $\frac{\mu+\mu^{[2]}}{\sqrt{u^2-4g^2}}$ should be regular at $u = 0$. Writing these quantities as power expansions around $u = 0$ and demanding that all singular terms vanish fixes the coefficients $\phi_{i,k}$. We discuss the power expansion of the relevant functions in appendix B.3.

Status

We have now generated a solution for $\mu_{12}^{(n)}$ that still contains a finite number of constants stemming from the ansatz for $\mathbf{P}_a$. At this point we can also determine the value of $\tilde{\mathbf{P}}_1^{(n)}$ directly from (note that $\tilde{\mathbf{P}}_2^{(n)}$ is suppressed)

$$\mu_{12} - \mu_{12}^{[2]} = \tilde{\mathbf{P}}_1 \mathbf{P}_2 - \tilde{\mathbf{P}}_2 \mathbf{P}_1 \,. \tag{6.27}$$

This expression for $\tilde{\mathbf{P}}_1$ is valid everywhere on the Riemann sheet, but it should be consistent with the ansatz close to $u = 0$. We can thus expand it at this point and match it to the ansatz for $\tilde{\mathbf{P}}_1$. This fixes some of the free parameters in the functions.

Finally, μ_{13} can be found directly from (note again that μ_{14} is suppressed)

$$\tilde{\mathbf{P}}_1 = \mathbf{P}_3 \mu_{12} - \mathbf{P}_2 \mu_{13} + \mathbf{P}_1 \mu_{14} \,. \tag{6.28}$$

6.2.5 First-order difference equation on $\tilde{\mathbf{P}}_2$

The next step in the algorithm is to consider a first order difference equation satisfied by $\tilde{\mathbf{P}}_2$,

$$\frac{\tilde{\mathbf{P}}_2}{\mathbf{P}_2} - \frac{\tilde{\mathbf{P}}_2^{[2]}}{\mathbf{P}_2^{[2]}} = \left(\frac{\mathbf{P}_4}{\mathbf{P}_2} - \frac{\mathbf{P}_4^{[2]}}{\mathbf{P}_2^{[2]}} \right) \mu_{12}^{[2]} + \left(\frac{\mathbf{P}_1}{\mathbf{P}_2} - \frac{\mathbf{P}_1^{[2]}}{\mathbf{P}_2^{[2]}} \right) \mu_{24}^{[2]} \,, \tag{6.29}$$

which can be derived from (6.15). The equation is solved by applying the Ψ-operation, which again introduces an $\mathbb{i}$-periodic function. By expanding the result at $u = 0$ and matching it to the ansatz for $\tilde{\mathbf{P}}_2$, this ambiguity is fixed. This additionally fixes some of the remaining free constants in our functions, including the anomalous dimension at the given order, γ_n.

Afterwards, $\mu_{14} = \mu_{23}$ follows directly from e.g.

$$\tilde{\mathbf{P}}_2 = \mathbf{P}_4\mu_{12} - \mathbf{P}_2\mu_{23} + \mathbf{P}_1\mu_{24}\,, \tag{6.30}$$

while $\tilde{\mathbf{P}}_3$ follows directly from

$$\tilde{\mathbf{P}}_3 = \mathbf{P}_4\mu_{13} - \mathbf{P}_3\mu_{23} + \mathbf{P}_1\mu_{34}\,. \tag{6.31}$$

6.2.6 Baxter equation on μ_{24}

The third, and final, difference equation to be solved is a second order equation on μ_{24}:

$$\begin{aligned}\frac{1}{\mathbf{P}_2^2}\mu_{24} - \left(\frac{\mathbf{P}_3}{\mathbf{P}_2} - \frac{\mathbf{P}_3^{[2]}}{\mathbf{P}_2^{[2]}} + \frac{1}{\mathbf{P}_2^2} + \frac{1}{\left(\mathbf{P}_2^{[2]}\right)^2}\right)\mu_{24}^{[2]} + \frac{1}{\left(\mathbf{P}_2^{[2]}\right)^2}\mu_{24}^{[4]} \\ = \frac{\tilde{\mathbf{P}}_2\mathbf{P}_4}{\mathbf{P}_2^2} - \frac{\tilde{\mathbf{P}}_2^{[2]}\mathbf{P}_4^{[2]}}{\left(\mathbf{P}_2^{[2]}\right)^2} + \left(\frac{\mathbf{P}_4^{[2]}}{\mathbf{P}_2^{[2]}} - \frac{\mathbf{P}_4}{\mathbf{P}_2}\right)\mu_{14}^{[2]}\,.\end{aligned} \tag{6.32}$$

The left hand side is exactly that of the Baxter equation on μ_{12} (6.17) and in fact the right-hand side is the same up to the replacement $\mathbf{P}_1 \to -\mathbf{P}_4$. In conclusion, this is simply the inhomogeneous Baxter equation (6.18) with a different source term. The solution can thus be constructed in exactly the same way as (6.25). Again, we impose regularity of $\mu + \mu^{[2]}$ and $\frac{\mu+\mu^{[2]}}{\sqrt{u^2-4g^2}}$ at $u = 0$ to fix the periodic functions introduced.

What remains is to get $\tilde{\mathbf{P}}_4$ directly from

$$\mu_{24} - \mu_{24}^{[2]} = \tilde{\mathbf{P}}_2\mathbf{P}_4 - \tilde{\mathbf{P}}_4\mathbf{P}_2\,, \tag{6.33}$$

and μ_{34} from

$$\tilde{\mathbf{P}}_4 = \mathbf{P}_4\,\mu_{14} - \mathbf{P}_3\,\mu_{24} + \mathbf{P}_2\,\mu_{34}\,. \tag{6.34}$$

Any left-over constant freedoms can be fixed by matching the expressions for $\tilde{\mathbf{P}}_3$ and $\tilde{\mathbf{P}}_4$ with their ansatz at $u = 0$.

6.2.7 Iterations

The above procedure can be applied recursively to fix the ansätze for $\mathbf{P}_a$ and generate the perturbative corrections to $\tilde{\mathbf{P}}_a$ and μ_{ab}. The crucial feature behind the algorithm is the all-loop ansatz for $\mathbf{P}_a$. At each order, the three main steps are the solution of three finite difference equations:

- Second-order equation on μ_{12}
- First-order equation on $\tilde{\mathbf{P}}_2$
- Second-order equation on μ_{24}

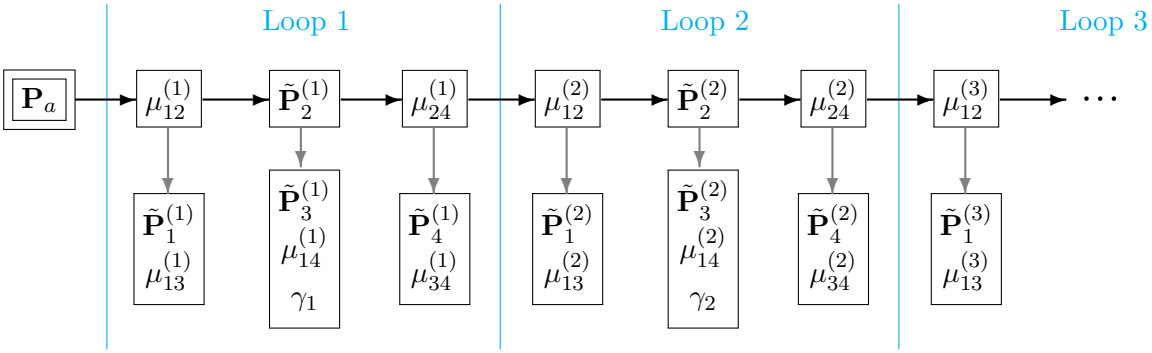

Figure 6.1: Flow of the algorithm to solve the $\mathbf{P}\mu$-system for operators in the $\mathfrak{sl}(2)$ sector.

Each time a new value of $\tilde{\mathbf{P}}_a$ is generated, its expansion at $u = 0$ is compared to the all-loop ansatz. This fixes the unknown coefficients in the ansatz uniquely. The algorithm is summarised in figure 6.1.

It is clear that the algorithm only introduces functions of the type described at the beginning of the chapter. A nice feature of the algorithm is that since all the used relations are linear in μ and $\tilde{\mathbf{P}}$, the expressions are always linear in η-functions, i.e. it is not necessary to linearise using stuffle relations. Furthermore, it is clear that the only place where non-rational algebraic numbers can be introduced is in the solution of the Baxter equation (6.19).

6.3 Solving the Q-system in general

In this section we describe a general method to solve the QSC in its full glory: the Q-system and the functions μ and ω. Such a method was first described in [113]. The key step in this algorithm is to solve 16 coupled first-order difference equations on $Q_{a|i}$.

The starting point is again the ansatz for $\mathbf{P}$, but as we wish to consider general states, there is no way to identify $\mathbf{P}_a$ and $\mathbf{P}^a$. Let us consider the n'th perturbative order and assume that we know all functions at lower loop orders completely. The ansatz (4.71) then gives us a rational ansatz for $\mathbf{P}^{(n)}_a$ and $\mathbf{P}^a_{(n)}$ with a finite number of unknown coefficients.

6.3.1 Difference equations on $Q_{a|i}$

In chapter 4, we saw that the 16 functions $Q_{a|i}$ satisfy the coupled first-order difference equations,

$$Q^-_{a|i} - Q^+_{a|i} = \mathbf{P}_a \mathbf{P}^b Q^+_{b|i} \,. \tag{6.35}$$

As in the previous section, we can think of the equation at subleading orders as an inhomogeneous version of the equation at the leading order,

$$Q^{(n)-}_{a|i} - Q^{(n)+}_{a|i} = \mathbf{P}^{(1)}_a \mathbf{P}^b_{(1)} Q^{(n)+}_{b|i} + U^{(n)}_{a|i} \,, \tag{6.36}$$

where we again refer to $U^{(n)}_{a|i}$ as a source term. The solution has the simple form

$$\boxed{Q^{(n)}_{a|i} = -Q^{(1)}_{a|j}\Psi\left(Q^{b|j}_{(1)}U^{(n)+}_{b|i}\right)} \tag{6.37}$$

which can easily be checked by plugging this expression into (6.36), but let us also provide a direct derivation similar to the one given in [113].

Proof

We start by making the ansatz

$$Q_{a|j} = (\delta^k_j + f^k_j)Q^{(1)}_{a|k}\,, \tag{6.38}$$

where $f^k_j(u) = \mathcal{O}(g^2)$ captures the contribution at subleading orders,

$$f^k_j = \sum_{n=1}^{\infty} g^{2n} f^{k\,(n+1)}_j\,. \tag{6.39}$$

At $\mathcal{O}(g^{2n})$ the equation (6.36) looks like

$$f^{j\,(n)-}_i Q^{(1)-}_{a|j} - f^{j\,(n)+}_i Q^{(1)+}_{a|j} = \mathbf{P}^{(1)}_a \mathbf{P}^b_{(1)} f^{j\,(n)+}_i Q^{(1)+}_{b|j} + U^{(n)}_{a|i}\,. \tag{6.40}$$

Now use (6.35) to make the replacement $Q^{(1)+}_{a|j} = Q^{(1)-}_{a|j} - \mathbf{P}^{(1)}_a \mathbf{P}^b_{(1)} Q^{(1)+}_{b|j}$ on the left-hand side to get

$$\left(f^{j\,(n)-}_i - f^{j\,(n)+}_i\right) Q^{(1)-}_{a|j} = U^{(n)}_{i|a}\,. \tag{6.41}$$

Finally, contract this equation with $Q^{a|k\,-}_{(1)}$ and use that $Q_{a|i}Q^{a|j} = -\delta^j_i$ to obtain

$$f^{j\,(n)+}_i - f^{j\,(n)-}_i = U^{(n)}_{a|i} Q^{a|j\,-}_{(1)}\,, \tag{6.42}$$

which has the solution

$$f^{j\,(n)}_i = -\Psi\left(U^{(n)+}_{a|i} Q^{a|j}_{(1)}\right)\,, \tag{6.43}$$

and this is exactly the statement (6.37).

6.3.2 Generating the Q-system

We now have the eight $\mathbf{P}$ and the 16 $Q_{a|i}$ at hand. We still have a bunch of unknown coefficients from the $\mathbf{P}$-ansatz, and the Ψ-operation in (6.37) introduces another 16 constants to be fixed. Note that, in order to preserve the upper half-plane analyticity and power-like asymptotics of $Q_{a|i}$, more general $\mathbb{i}$-periodic functions are not allowed.

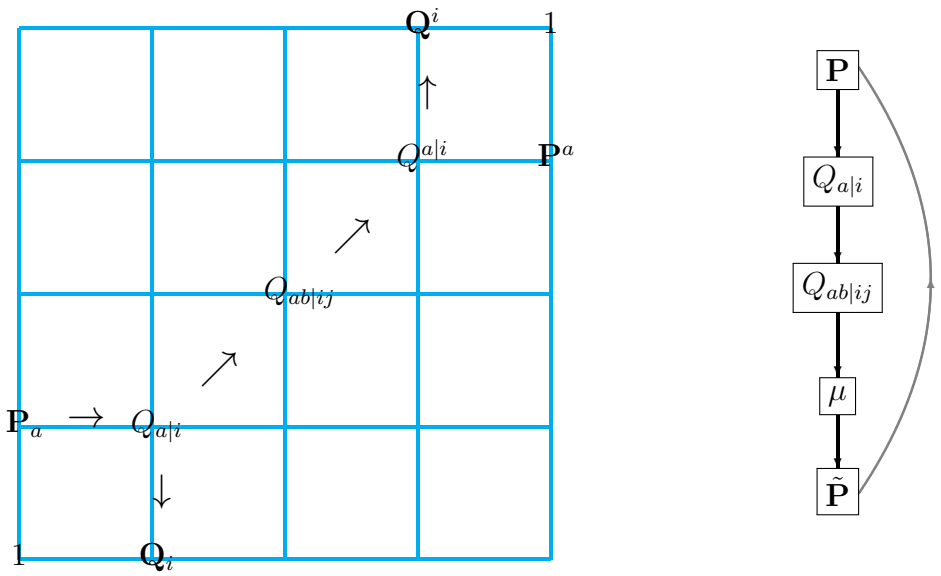

Figure 6.2: Overview of the algorithm to solve the Q-system.

This knowledge is sufficient to generate the remaining Q-system without solving any more difference equations, cf. section 4.2. Everything else can be found from the determinant formulas in section 4.2.1. The Q-functions of interest are

$$\mathbf{Q}_i = Q_{\emptyset|i} = -\mathbf{P}^a Q^{\pm}_{a|i} \tag{6.44a}$$

$$Q_{ab|ij} = \begin{vmatrix} Q_{a|i} & Q_{a|j} \\ Q_{b|i} & Q_{b|j} \end{vmatrix} \tag{6.44b}$$

$$Q_{abc|ijk} = \begin{vmatrix} Q_{a|i} & Q_{a|j} & Q_{a|k} \\ Q_{b|i} & Q_{b|j} & Q_{b|k} \\ Q_{c|i} & Q_{c|j} & Q_{c|k} \end{vmatrix} \tag{6.44c}$$

$$\mathbf{Q}^i = Q^{\emptyset|i} = \mathbf{P}_a Q^{a|i\pm} \,. \tag{6.44d}$$

We are thus able to generate the full Q-system, still containing a set of unknown coefficients. The 16 constants arising in the solution (6.37) can be controlled by fixing the H-symmetry, which can for example be done by eliminating certain asymptotic powers in the functions $\mathbf{P}$ and $\mathbf{Q}$. However, to control the symmetry on the indices i, j etc. in practice, this involves power expanding non-rational Q-functions at $u = \infty$, which is possible, see e.g. [109], but computationally demanding.

6.3.3 Gluing

To fix the unknown constants in the Q-system, we need a way to enforce the analytic requirements prescribed by the QSC. In particular, we need to consider the value of some of the Q-functions on their second Riemann sheet and require that they are consistent with the value on the first sheet at the point where the branch cut between them collapsed, $u = 0$. This is illustrated in figure 6.3.

Figure 6.3: At the point where the branch cuts between the first and second sheet collapsed, $u = 0$, the functions still satisfy gluing conditions.

As discussed, a way to do this is by constructing $\tilde{\mathbf{P}}^{(n)}$ through

$$\tilde{\mathbf{P}}_a = \mu_{ab}\mathbf{P}^b \qquad \tilde{\mathbf{P}}^a = \mu^{ab}\mathbf{P}_b\,, \tag{6.45}$$

and then impose that the expansion of $\tilde{\mathbf{P}}^{(n)}$ around $u{=}0$ is consistent with the $\mathbf{P}$-ansatz. To do this, we first need to build the functions μ. We recall that these functions are linear combination of the central Q-functions $Q_{ab|ij}$ with ω as coefficients:

$$\mu_{ab} = \tfrac{1}{2}\omega^{ij}Q^{-}_{ab|ij} \qquad \mu^{ab} = -\tfrac{1}{2}\epsilon^{abcd}\frac{\mu_{cd}}{\mathrm{Pf}(\mu_\bullet)}\,, \tag{6.46}$$

and that the $\mathbb{i}$-periodic functions ω^{ij} are of the form

$$\omega^{ij} = \omega^{ij}_{\{0\}} + \sum_{k=1}^{\infty}\omega^{ij}_{\{k\}}\mathcal{P}_k\,, \tag{6.47}$$

where $\mathcal{P}_k$ are the $\mathbb{i}$-periodic functions (4.59) and where the sum truncates at each order in perturbation theory. One can use the regularity at $u = 0$ of $\mu + \mu^{[2]}$ and $\frac{\mu-\mu^{[2]}}{\sqrt{u^2-4g^2}}$ to fix most of the constants $\omega^{ij}_{\{k\}}$.

Imposing the complete agreement between the obtained values of $\tilde{\mathbf{P}}^{(n)}$ and the ansatz (4.71) at $u = 0$ fixes all left-over degrees of freedom. We summarise the algorithm in figure 6.2.

6.3.4 Comments

The beauty of the outlined solution strategy is that it encompasses all parts of the QSC. However, it is rather painful to implement in practice, for the following reasons:

- It includes a large number of functions: 8 $\mathbf{P}$'s, 16 $Q_{a|i}$, 36 $Q_{ab|ij}$, etc.
- The generation of e.g. $Q_{ab|ij}$ as determinants of $Q_{a|i}$ results in large expressions containing products of η-functions that needs to be linearised using stuffle relations.
- One has to control the full H-symmetry of the QSC, i.e. the parts acting on both types of indices (a, b,.. and i, j,...). Controlling the symmetry on the indices i, j

etc. is harder in practice because there are no rational functions on which to fix it in a simple way. To do it by constraining asymptotic behaviour involves power expansion at $u = \infty$.

There are ways to get around some of these issues, at least in special cases. As proposed in [113], one can instead perform the gluing by using relations between $\tilde{\mathbf{Q}}_j$ and the complex conjugation of $\mathbf{Q}^k$ described in [15]. In fact, one can avoid the construction of ω and μ completely in this way[1]. For left/right symmetric states, one can then get away with treating only the lower left corner of the square in figure 6.2, i.e. the 24 functions $\mathbf{P}_a$, $\mathbf{Q}_i$ and $Q_{a|i}$. However, for generic states one also needs to treat the upper right corner, which is another 24 functions. This is a large number of functions, and the practical nuisance of the $H_i{}^j$-symmetry is still present.

6.4 Solving the Pμ-system in general

In this section we present a conceptually very simple algorithm to solve the $\mathbf{P}\mu$-system for generic states. It is in some sense a hybrid of the two algorithms above.

Using only the $\mathbf{P}\mu$-system has clear advantages: it includes only 14 functions: eight $\mathbf{P}$'s and six μ's. The indices i, j, etc. are absent, which means that this part of the H-symmetry is absent as well. Finally, the presented method is only mildly non-linear in η-functions.

6.4.1 First-order equations on μ_{ab}

The key equations in this approach are the coupled first-order difference equations on μ_{ab},

$$\mu_{ab} - \mu_{ab}^{[2]} = -\mathbf{P}_a\mathbf{P}^c\mu_{bc}^{[1\pm1]} + \mathbf{P}_b\mathbf{P}^c\mu_{ac}^{[1\pm1]} \,. \tag{6.48}$$

The exact same equation is satisfied by $Q^-_{ab|ij}$. In fact, $Q^-_{ab|ij}$ parametrise the six linearly independent set of solutions to the equation, and μ_{ab} is just a particular linear combination of these with certain boundary conditions (that $\mu+\mu^{[2]}$ and $\frac{\mu-\mu^{[2]}}{\sqrt{u^2-4g^2}}$ are regular at $u=0$).

At the n'th perturbative order, we can again think of (6.48) as an inhomogeneous version of the leading order equation,

$$\mu_{ab}^{(n)} - \mu_{ab}^{(n)[2]} = -\mathbf{P}_a^{(1)}\mathbf{P}^c_{(1)}\mu_{bc}^{(n)[2]} + \mathbf{P}_b^{(1)}\mathbf{P}^c_{(1)}\mu_{ac}^{(n)[2]} + U_{ab}^{(n)} \,. \tag{6.49}$$

Let us label the six sets of solutions to the homogeneous equation by

$$\hat{\mu}_{ab|k} = Q^{(1)-}_{ab|\{12,13,14,23,24,34\}_k} \qquad k = 1,\ldots,6 \,. \tag{6.50}$$

[1]For unphysical solutions, this is a particularly nice property, because ω has a more complicated structure in this case. For physical solutions ω is easy to control, so this property is not a major advantage here.

The solution to (6.49) is then

$$\boxed{\mu_{ab}^{(n)} = \hat{\mu}_{ab|k}\Psi\left(\hat{\mu}^{cd|k}U_{cd}^{(n)}\right)} \tag{6.51}$$

Proof

$Q_{ab|ij}$ satisfy the equation

$$Q_{ab|ij}^{-} - Q_{ab|ij}^{+} = \left(\delta_a^c \mathbf{P}_b \mathbf{P}^d - \delta_b^c \mathbf{P}_a \mathbf{P}^d\right) Q_{cd|ij}^{\pm}\,, \tag{6.52}$$

which at the n'th order can be formulated as

$$Q_{ab|ij}^{(n)-} - Q_{ab|ij}^{(n)+} = \left(\delta_a^c \mathbf{P}_b^{(1)} \mathbf{P}_{(1)}^d - \delta_b^c \mathbf{P}_a^{(1)} \mathbf{P}_{(1)}^d\right) Q_{cd|ij}^{(n)+} + U_{ab|ij}^{(n)}\,. \tag{6.53}$$

As in section 6.3.1, we make the ansatz $Q_{ab|ij}^{-} = \left(\delta_i^k\delta_j^l + f_{ij}^{kl}\right) Q_{ab|kl}^{(1)-}$ with $f_{ij}^{kl}(u) \sim \mathcal{O}(g^2)$. We plug this into (6.53) and replace $Q_{ab|ij}^{(1)+}$ on the left hand side by using the homogeneous equation. We then contract the equation with $Q_{(1)}^{ab|ij-}$ using (4.32), and apply the Ψ-operation. The result is

$$Q_{ab|ij}^{(n)-} = \tfrac{1}{4} Q_{ab|kl}^{(1)-} \Psi\left(Q_{(1)}^{cd|kl-} U_{cd|ij}^{(n)}\right)\,. \tag{6.54}$$

We can contract this expression with $\frac{1}{2}\omega^{ij}$, which turns the left hand side into $\mu_{ab}^{(n)}$, while on the right hand side, since ω is an $\mathbb{i}$-periodic function insensitive to the Ψ-operation, this means that the source is replaced by that of (6.49). Summing over the single index $k = 1, \ldots 6$ instead of two antisymmetric indices removes the remaining factor of $\frac{1}{2}$, and we have (6.51).

Periodic functions and regularity

As μ can have poles in both the upper and lower half-plane, the periodic functions arising from the Ψ-operation in (6.51) are of the form

$$\Phi_i = \phi_{i,0} + \sum_{k=1}^{\infty} \phi_{i,k} \mathcal{P}_k\,, \tag{6.55}$$

where $\mathcal{P}_k$ are again the $\mathbb{i}$-periodic functions (4.59). The sum truncates at each perturbative order and most of the coefficients $\phi_{i,k}$ can be fixed directly by imposing that $\mu + \mu^{[2]}$ and $\frac{\mu - \mu^{[2]}}{\sqrt{u^2 - 4g^2}}$ are regular at $u = 0$.

6.4.2 Gluing

The gluing is exactly as in the other algorithms: construct $\tilde{\mathbf{P}}^{(n)}$ through (6.45), power expand around $u = 0$ and match each order in u with the ansatz (4.71).

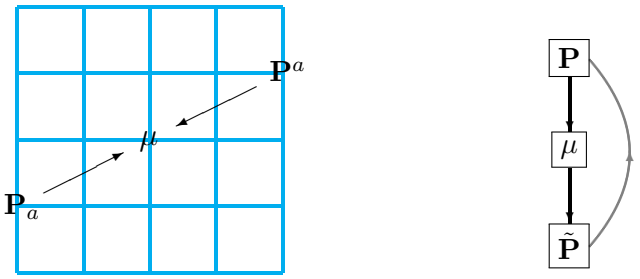

Figure 6.4: Overview of the algorithm to solve the $\mathbf{P}\mu$-system for generic states.

In practice, power expansion is one of the most time-consuming steps in the algorithm. The matching of powers can be truncated at some maximal power in u, which means that the coefficients $\mathsf{c}_{a,k}^{(n)}$ present in the ansatz for $\tilde{\mathbf{P}}^{(n)}(u)$ are only determined up to a certain k. These coefficients are suppressed by a factor of g^{2k} in $\mathbf{P}$ anyway. In general, the non-trivial constraints in the gluing come from the singular parts of $\tilde{\mathbf{P}}$. Due to the expansion of the Zhukowsky variable x, the coefficients $\mathsf{c}_{a,k}^{(n)}$ start appearing in the singular terms at subsequent orders. One should therefore be careful to fix all $\mathsf{c}_{a,k}^{(n)}$ that appear in singular terms at the maximal perturbative order that one wants to reach. We refer to [1, 7] and the related `Mathematica`-notebooks for the details on how to do this in a minimal way.

6.4.3 Comments on the method

The presented method only requires the determination of six functions μ_{ab} by solving difference equations. The knowledge of the $6 \times 6 = 36$ general solutions to these equations, $Q^{-}_{ab|ij}$, is not necessary. The functions μ^{ab} are identical to μ_{ab} up to a factor of the Pfaffian, see (4.49),

$$\mu^{ab} = -\frac{1}{2}\epsilon^{abcd}\mu_{cd}\frac{1}{\mathrm{Pf}(\mu_\bullet)}\,. \tag{6.56}$$

One has the freedom to set $\mathrm{Pf}(\mu_\bullet) = 1$, which is related to the choice of normalisations A, but this is rather tricky to implement in practice. Instead the constant $\mathrm{Pf}(\mu_\bullet)$ can simply be included as a free parameter that is eventually fixed by the gluing.

The $\mathbf{P}\mu$-based method described here is significantly simpler than the method described in section 6.3. Only 14 functions are calculated: eight $\mathbf{P}$ (on both the first, $\mathbf{P}(u)$, and second sheet, $\tilde{\mathbf{P}}(u)$) and six μ_{ab}. The only non-linearity in η-functions arises in the expression (6.51), but it is only a mild non-linearity, because two of the three factors are leading-order Q-functions with only simple η-functions. Finally, the H-symmetry only needs to be controlled on the indices a, b, etc.

In conclusion, we have arrived at a method that fits our ambition: a simple algorithm to solve the QSC perturbatively for general states.

6.5 Results

In this section we take a look at the results that can be produced by the perturbative algorithms. We present a sample of results obtained with `Mathematica`-implementations of the algorithms in section 6.2 and 6.4. These results are representatives of calculations that can be completed on a standard laptop. A much larger database of $\mathfrak{sl}(2)$ results is available in the ancillary files of [1] at arxiv.org, and a database for the general spectrum will appear in [7].

Working with algebraic numbers

Before looking at specific results, let us make a comment about the practical solution. In general, the leading solutions to the Q-system, cf. chapter 5, contain algebraic numbers, which in some cases are rather complicated. In practice, such numbers are hard to work with analytically in a symbolical programming language such as `Mathematica`. The algorithms rely on delicate cancellations between terms, and such cancellations are often hidden when complicated algebraic numbers are present, at least without applying time-consuming simplification procedures. In practice, we have not managed to handle such numbers in a completely analytic way. Instead, the algorithm treats such solutions by evaluating the coefficients in the leading solution numerically with a high precision. The ζ-values generated from power expansions are kept symbolically, and we refer to this procedure as *semi-numerics*.

In fact, another simple observation means that the semi-numerical results can be used to reconstruct the analytic results. Consider a solution for which the anomalous dimension can be written in terms of some algebraic number, θ, which is a root of some polynomial with integer coefficients of degree k. Then there exists k multiplets with the same quantum numbers for which the anomalous dimension is given in terms of the other roots of this algebraic equation. For example, there are three multiplets of the kind $n^{\ulcorner} = [0,0|5,3,3,1|0,0]$, and their one-loop anomalous dimension, which follows directly from the found $\mathbb{Q}_{2,2}$, are

$$\gamma_{1,j} = \frac{40}{3} + \theta_j \,, \qquad \theta_j = \texttt{Root}[27x^3 - 1872x - 4160, j] \,, \qquad j = 1,2,3 \,, \tag{6.57}$$

where $\sum_{j=1}^{k} \theta_j = 0$. At a higher loop, the anomalous dimension should be of the form

$$\gamma_{n,j} = c_0 + c_1\theta_j + c_2\theta_j^2 \,, \tag{6.58}$$

where c_i are rational numbers. Calculating $\gamma_{n,j}$ numerically for $j = 1,2,3$, we have three equations (6.58) on three unknowns, c_i. If the numerical precision is sufficient, the rational numbers can easily be reconstructed e.g. with the `Mathematica`-function `Rationalize`.

6.5.1 The $\mathfrak{sl}(2)$ sector

The algorithm to solve the $\mathbf{P}\mu$-system in the $\mathfrak{sl}(2)$ sector described in section 6.2 allows the calculation of a wide range of new results. The obtained results include analytic 10-loop results for a variety of multiplets for which the Q-system contains only rational coefficients. As an example, we here show the 10-loop result for the Konishi multiplet, $n^{\lceil} = [0,0|1,1,1,1|0,0]$:

$$
\begin{aligned}
\gamma \;=\;& 12g^2 - 48g^4 + 336g^6 + g^8\big(-2496 + 576\,\zeta_3 - 1440\,\zeta_5\big) \\
&+g^{10}\big(15168 + 6912\,\zeta_3 - 5184\,\zeta_3^2 - 8640\,\zeta_5 + 30240\,\zeta_7\big) \\
&+g^{12}\big(-7680 - 262656\,\zeta_3 - 20736\,\zeta_3^2 + 112320\,\zeta_5 + 155520\,\zeta_3\,\zeta_5 + 75600\,\zeta_7 - 489888\,\zeta_9\big) \\
&+g^{14}\big(-2135040 + 5230080\,\zeta_3 - 421632\,\zeta_3^2 + 124416\,\zeta_3^3 - 229248\,\zeta_5 + 411264\,\zeta_3\,\zeta_5 \\
&\quad - 993600\,\zeta_5^2 - 1254960\,\zeta_7 - 1935360\,\zeta_3\,\zeta_7 - 835488\,\zeta_9 + 7318080\,\zeta_{11}\big) \\
&+g^{16}\Big(54408192 - 83496960\,\zeta_3 + 7934976\,\zeta_3^2 + 1990656\,\zeta_3^3 - 19678464\,\zeta_5 - 4354560\,\zeta_3\,\zeta_5 \\
&\quad - 3255552\,\zeta_3^2\,\zeta_5 + 2384640\,\zeta_5^2 + 21868704\,\zeta_7 - 6229440\,\zeta_3\,\zeta_7 + 22256640\,\zeta_5\,\zeta_7 \\
&\quad + 9327744\,\zeta_9 + 23224320\,\zeta_3\,\zeta_9 + \tfrac{65929248}{5}\,\zeta_{11} - 106007616\,\zeta_{13} - \tfrac{684288}{5}\,Z_{11}^{(2)}\Big) \\
&+g^{18}\Big(-1014549504 + 1140922368\,\zeta_3 - 51259392\,\zeta_3^2 - 20155392\,\zeta_3^3 + 575354880\,\zeta_5 \\
&\quad - 14294016\,\zeta_3\,\zeta_5 - 26044416\,\zeta_3^2\,\zeta_5 + 55296000\,\zeta_5^2 + 15759360\,\zeta_3\,\zeta_5^2 - 223122816\,\zeta_7 \\
&\quad + 34020864\,\zeta_3\,\zeta_7 + 22063104\,\zeta_3^2\,\zeta_7 - 92539584\,\zeta_5\,\zeta_7 - 113690304\,\zeta_7^2 - 247093632\,\zeta_9 \\
&\quad + 119470464\,\zeta_3\,\zeta_9 - 245099520\,\zeta_5\,\zeta_9 - \tfrac{186204096}{5}\,\zeta_{11} - 278505216\,\zeta_3\,\zeta_{11} - 253865664\,\zeta_{13} \\
&\quad + 1517836320\,\zeta_{15} + \tfrac{15676416}{5}\,Z_{11}^{(2)} - 1306368\,Z_{13}^{(2)} + 1306368\,Z_{13}^{(3)}\Big) \\
&+g^{20}\Big(16445313024 - 13069615104\,\zeta_3 - 1509027840\,\zeta_3^2 + 578949120\,\zeta_3^3 - 14929920\,\zeta_3^4 \\
&\quad - 11247547392\,\zeta_5 + 1213581312\,\zeta_3\,\zeta_5 + 1234206720\,\zeta_3^2\,\zeta_5 - 70170624\,\zeta_3^3\,\zeta_5 - 1390279680\,\zeta_5^2 \\
&\quad - 654842880\,\zeta_3\,\zeta_5^2 + \tfrac{6966252288}{175}\,\zeta_5^3 + 377212032\,\zeta_7 - 1610841600\,\zeta_3\,\zeta_7 + 154680192\,\zeta_3^2\,\zeta_7 \\
&\quad + 222341760\,\zeta_5\,\zeta_7 + 133788672\,\zeta_3\,\zeta_5\,\zeta_7 + 868662144\,\zeta_7^2 + 4915257984\,\zeta_9 - 332646912\,\zeta_3\,\zeta_9 \\
&\quad - 91072512\,\zeta_3^2\,\zeta_9 + 1099699200\,\zeta_5\,\zeta_9 + 2275620480\,\zeta_7\,\zeta_9 + \tfrac{9793211904}{5}\,\zeta_{11} \\
&\quad - 2334572928\,\zeta_3\,\zeta_{11} + 2713772160\,\zeta_5\,\zeta_{11} - \tfrac{787483944}{175}\,\zeta_{13} + 3372969600\,\zeta_3\,\zeta_{13} \\
&\quad - \tfrac{4308536566944}{875}\,\zeta_{15} - 21661960320\,\zeta_{17} + \tfrac{752219136}{5}\,Z_{11}^{(2)} - \tfrac{5070791808}{175}\,Z_{13}^{(2)} \\
&\quad - \tfrac{7159104}{7}\,Z_{13}^{(3)} + \tfrac{2716063488}{175}\,Z_{15}^{(2)} - \tfrac{17895168}{25}\,Z_{15}^{(3)} + 11943936\,\zeta_3\,Z_{11}^{(2)}\Big) \\
&+\mathcal{O}(g^{22})\,,
\end{aligned}
\tag{6.59}
$$

where $Z_a^{(n)}$ denote so-called *single-valued multiple zeta-values* [129] given in (B.9). These numbers are special combinations of ζ-values, e.g. $Z_{13}^{(2)} = -\zeta_{5,3,5} + 11\,\zeta_5\,\zeta_{3,5} + 5\,\zeta_5\,\zeta_8$, and we discuss them further below.

# of loops	runtime		memory usage
	$\mathfrak{sl}(2)$	general	general
5	4 s	40 s	20 MB
6	15 s	2 m	35 MB
7	1 m	4 m	70 MB
8	5 m	13 m	120 MB
9	27 m	52 m	340 MB
10	3.1 h	4.5 h	1.6 GB

Table 6.1: Runtime on a single 3.2 GHz core of a standard desktop for the calculation of the anomalous dimension of the Konishi multiplet using the `Mathematica`-implementation of the $\mathfrak{sl}(2)$ algorithm described in section 6.2, which was published with [1], and with a `Mathematica`-implementation of the general algorithm described in section 6.4, which will be published with [7]. Note that the $\mathfrak{sl}(2)$ code terminates after finding $\tilde{\mathbf{P}}_2$ at the given loop, while the general code determines *all* functions in the $\mathbf{P}\mu$-system at the given loop and does not assume left/right symmetry. The general code is furthermore more suitable for parallelisation. The memory usage was measured by the `Mathematica`-function `MaxMemoryUsed`.

A `Mathematica`-implementation of the algorithm, as well as an extensive database of results, is available in the ancillary files of [1] at arxiv.org. It includes results for all 91 multiplets with $L + S = \Delta_0^{\ulcorner} + 2 \leq 10$ up to at least eight loop orders. The code is in general efficient for states with $L + S \leq 15$. The `Mathematica`-code reaches 10 loops for the Konishi solution in about three hours on a standard desktop, using about 2 GB of memory. See table 6.1 for more details on the performance and a comparison with the performance of a `Mathematica`-implementation of the general algorithm described in section 6.4. Higher quantum numbers L and S naturally lead to longer runtimes and higher memory consumption.

6.5.2 The $\mathfrak{su}(2)$ sector

The compact $\mathfrak{su}(2)$ sector is characterised by the quantum numbers

$$n^{\ulcorner} = [0, 0|L-3, L-M-1, M-1, 1|0, 0]\,, \tag{6.60}$$

corresponding to a $\hat{1}12\hat{2}\hat{3}34\hat{4}$ HWS of the kind $\mathcal{Z}^{L-M}\mathcal{X}^{M}$. It contains a finite number of multiplets with a given length L, and since the results up to the L'th loop are obtainable from the asymptotic Bethe equations, there is in practice only a limited amount of additional data to gain by using the QSC.

One multiplet is however of particular interest: the so-called *exceptional* solution that appears for the single multiplet of the kind $n^{\ulcorner} = [0, 0|3, 2, 2, 1|0, 0]$, for which the central

Q-function is

$$\mathbb{Q}_{2,2} = u^3 + \frac{u}{4} = \left(u - \tfrac{\mathrm{i}}{2}\right) u \left(u + \tfrac{\mathrm{i}}{2}\right) . \tag{6.61}$$

Due the position of its Bethe roots, it requires extra care when solving the asymptotic Bethe equations, and similarly when solving the TBA equations, which was done up to six loops in [130]. However, from the point of view of the QSC this state requires no special care, and the algorithm of section 6.4 handles it completely unproblematically. We here present the 10-loop result:

$$\begin{aligned}
\gamma \;=\; & 12g^2 - 36g^4 + 252g^6 - 2484g^8 + g^{10}\left(28188 - 288\zeta_3\right) \\
& + g^{12}\left(-339012 + 7776\zeta_3 + 12096\zeta_5 - 18144\zeta_9\right) \\
& + g^{14}\big(4214268 - 39744\zeta_3 - 181440\zeta_5 + 57024\zeta_3^2 - 260064\zeta_7 \\
& \quad -34560\zeta_3\zeta_5 - 60480\zeta_9 - 8640\zeta_5^2 - 96768\zeta_3\zeta_7 + 665280\zeta_{11}\big) \\
& + g^{16}\Big(- 53785620 - 820800\zeta_3 - 699840\zeta_3^2 - 82944\zeta_3^3 + 1664064\zeta_5 - 1510272\zeta_3\zeta_5 \\
& \quad -290304\zeta_3^2\zeta_5 + 250560\zeta_5^2 + 4257792\zeta_7 + 628992\zeta_3\zeta_7 + 1451520\zeta_5\zeta_7 + 4711968\zeta_9 \\
& \quad +2903040\zeta_3\zeta_9 + \tfrac{11144736}{5}\zeta_{11} - 16061760\zeta_{13} - \tfrac{124416}{5}Z_{11}^{(2)}\Big) \\
& + g^{18}\Big(702413532 + 25507872\zeta_3 - 2282688\zeta_3^2 - 1119744\zeta_3^3 - 248832\zeta_3^4 - 502848\zeta_5 \\
& \quad +25653888\zeta_3\zeta_5 + 3836160\zeta_3^2\zeta_5 + 5987520\zeta_5^2 + 6635520\zeta_3\zeta_5^2 - 45170784\zeta_7 \\
& \quad +22037184\zeta_3\zeta_7 + 6676992\zeta_3^2\zeta_7 - 5766336\zeta_5\zeta_7 - 16027200\zeta_7^2 - 75035808\zeta_9 \\
& \quad +10018944\zeta_3\zeta_9 - 38361600\zeta_5\zeta_9 - 79511328\zeta_{11} - 58848768\zeta_3\zeta_{11} - \tfrac{273255552}{5}\zeta_{13} \\
& \quad +324324000\zeta_{15} + 311040Z_{11}^{(2)} - \tfrac{601344}{5}Z_{13}^{(2)} + 145152Z_{13}^{(3)}\Big) \\
& + g^{20}\Big(-9354033252 - 461062368\zeta_3 + 198500544\zeta_3^2 - 2778624\zeta_3^3 + 2239488\zeta_3^4 - 348634368\zeta_5 \\
& \quad -201128832\zeta_3\zeta_5 + 50865408\zeta_3^2\zeta_5 + 14681088\zeta_3^3\zeta_5 - 187012800\zeta_5^2 - 51010560\zeta_3\zeta_5^2 \\
& \quad -\tfrac{1310563584}{35}\zeta_5^3 + 343359648\zeta_7 - 351993600\zeta_3\zeta_7 - 56909952\zeta_3^2\zeta_7 - 147334464\zeta_5\zeta_7 \\
& \quad -221543424\zeta_3\zeta_5\zeta_7 + 29465856\zeta_7^2 + 911464704\zeta_9 - 312035328\zeta_3\zeta_9 - 107619840\zeta_3^2\zeta_9 \\
& \quad +75755520\zeta_5\zeta_9 + 633225600\zeta_7\zeta_9 + \tfrac{5846706576}{5}\zeta_{11} + \tfrac{740306304}{5}\zeta_3\zeta_{11} + 745303680\zeta_5\zeta_{11} \\
& \quad +\tfrac{226451356776}{175}\zeta_{13} + 1017080064\zeta_3\zeta_{13} + \tfrac{96109333632}{175}\zeta_{15} - 5951088000\zeta_{17} + \tfrac{41036544}{5}Z_{11}^{(2)} \\
& \quad +\tfrac{746496}{5}Z_{11}^{(2)}\zeta_3 + \tfrac{406415232}{175}Z_{13}^{(2)} - \tfrac{18719424}{7}Z_{13}^{(3)} + \tfrac{30710016}{35}Z_{15}^{(2)} - \tfrac{850176}{5}Z_{15}^{(3)}\Big) \\
& + \mathcal{O}(g^{22}) .
\end{aligned} \tag{6.62}$$

This result is special in the sense that the ζ-values stemming from the dressing factor are delayed compared to other results. However, in the QSC, it is not immediately transparent why this delay occurs.

In fact, this is just the first result in an infinite series of exceptional solutions. The same solution (6.61) reappears for $M = 3$ and $L = 6 + 2n$ with $n \in \mathbb{N}$. Though also obtainable

$L^{\mathfrak{su}(2)}$	γ_1	γ_2	γ_3	γ_4	γ_5	γ_6
6	12	-36	252	-2484	$28188-288\zeta_3$	$-339012+7776\zeta_3+12096\zeta_5-18144\zeta_9$
8	12	-36	264	-2592	28848	$345024-288\zeta_3$
10	12	-36	264	-2580	28716	-344088
12	12	-36	264	-2580	28728	-344244
14	12	-36	264	-2580	28728	-344232

Table 6.2: Anomalous dimensions of the first states in the series of exceptional solutions.

from the asymptotic Bethe equations, we list the quite peculiar anomalous dimensions of the operators in the series at the first perturbative orders in table 6.2. The delay in the appearance of ζ-values is rather unique. All other investigated solutions follow a strict pattern: ζ-values start appearing at $\mathcal{O}(g^8)$, i.e. in γ_4, and the appearing transcendentality then steadily increases order by order.

6.5.3 Semi-short multiplets

After revisiting the two usual suspects, it is time to look at something more exotic. Let us look at an example that only satisfies one of the two shortening conditions (1.39). This is the case for the two multiplets with quantum numbers $n^{\lceil} = [0,0|2,2,1,1|2,0]$ belonging to the $\mathfrak{su}(2,1|2)$ sector, which are only subject to the shortening (1.39b). See figure 6.5 for the corresponding Young diagram. Note that there are two conjugate solutions with quantum numbers $n^{\lceil} = [0,2|3,3,2,2|0,0]$ in the $\mathfrak{su}(1,2|2)$ sector subject to the other shortening (1.39a).

The two solutions have leading-order central Q-functions

$$\mathbb{Q}_{2,2\,\pm} = u^4 + u^2(-\tfrac{13}{14} \mp \tfrac{4\sqrt{2}}{21}) + \tfrac{29}{336} \pm \tfrac{\sqrt{2}}{21}\,. \tag{6.63}$$

Though not impossible to treat solutions with only simple squareroots completely analyt-

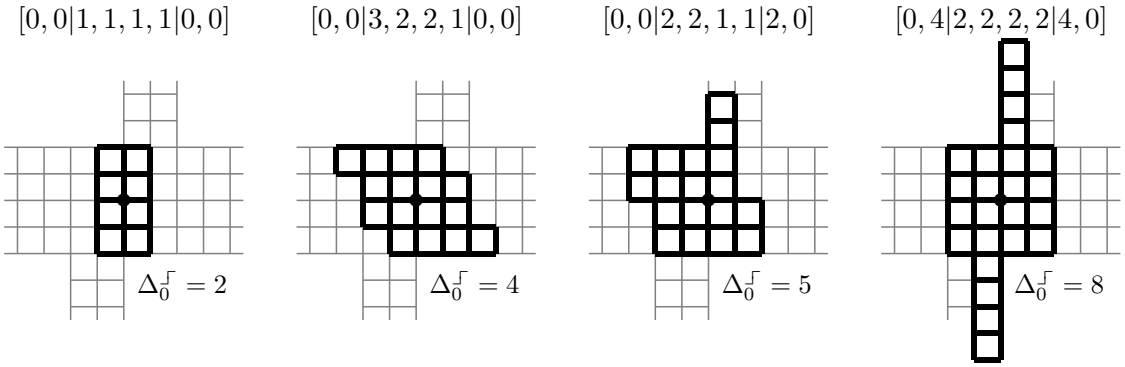

Figure 6.5: Young diagrams for the four considered examples of solutions (6.59), (6.62), (6.65) and (6.67).

ically, it is simpler to treat them semi-numerically. The semi-numerical results for the two solutions have the form

$$\gamma_+ = 18.82843g^2 - 69.75305g^4 + 479.03195g^6 + g^8(-4096.90889 - 280.14214\zeta_3) + \mathcal{O}(g^{10}) \quad (6.64)$$
$$\gamma_- = 13.17157g^2 - 49.24695g^4 + 340.21805g^6 + g^8(-2821.02861 - 251.85786\zeta_3) + \mathcal{O}(g^{10})\,.$$

As a simpler example of the discussion above, the analytic result can be reconstructed by studying the sum and difference of these solutions. The 9-loop result is

$$\begin{aligned}
\gamma_\pm = {} & g^2(16 \pm 2\sqrt{2}) + g^4\big(-\tfrac{119}{2} \mp \tfrac{29}{4}\sqrt{2}\big) + g^6\big(\tfrac{3277}{8} \pm \tfrac{3141}{64}\sqrt{2}\big) \\
& + g^8\big(\tfrac{110687}{32} \mp \tfrac{230959}{512}\sqrt{2} - (266 \pm 10\sqrt{2})\zeta_3\big) \\
& + g^{10}\big(\tfrac{4208765}{128} \pm \tfrac{95147579}{16384}\sqrt{2} + (3670 \pm 2726\sqrt{2})\zeta_3 + (8540 \mp 6140\sqrt{2})\zeta_5 + (-5880 \pm 2520\sqrt{2})\zeta_7\big) \\
& + g^{12}\big(-\tfrac{173168415}{512} \mp \tfrac{11585963899}{131072}\sqrt{2} + (-\tfrac{259641}{8} \pm \tfrac{2288325}{64}\sqrt{2})\zeta_3 + (-8553 \mp 39669\sqrt{2})\zeta_5 \\
& \quad + (20736 \mp 26424\sqrt{2})\zeta_3^2 + (-218890 \pm 131740\sqrt{2})\zeta_7 + (-36000 \pm 12240\sqrt{2})\zeta_3\zeta_5 \\
& \quad + (157248 \mp 89712\sqrt{2})\zeta_9\big) \\
& + g^{14}\Big(\tfrac{22048999927}{6144} \pm \tfrac{8421552810475}{6291456}\sqrt{2} + (\tfrac{1782313}{24} \mp \tfrac{307985969}{256}\sqrt{2})\zeta_3 + (\tfrac{7171273}{12} \pm \tfrac{78905645}{96}\sqrt{2})\zeta_5 \\
& \quad + (145290 \mp \tfrac{76843}{2}\sqrt{2})\zeta_3^2 + (\tfrac{445949}{2} \pm \tfrac{10782779}{48}\sqrt{2})\zeta_7 + (-1039360 \pm 646010\sqrt{2})\zeta_3\zeta_5 \\
& \quad + (-70272 \pm 16512\sqrt{2})\zeta_3^3 + (421600 \mp 158720\sqrt{2})\zeta_5^2 + (689920 \mp 406784\sqrt{2})\zeta_3\zeta_7 \\
& \quad + (4000472 \mp \tfrac{6841184}{3}\sqrt{2})\zeta_9 + (-2971584 \pm 2091936\sqrt{2})\zeta_{11}\Big) \\
& + g^{16}\Big(-\tfrac{300286892351}{8192} \mp \tfrac{310312617444303}{16777216}\sqrt{2} + (-\tfrac{1815233191}{384} \pm \tfrac{818789643655}{49152}\sqrt{2})\zeta_3 \\
& \quad + (-\tfrac{129268663}{48} \mp \tfrac{178955539}{192}\sqrt{2})\zeta_5 + (-\tfrac{8035131}{2} \mp 2954707\sqrt{2})\zeta_3^2 + (-\tfrac{29726453}{8} \mp \tfrac{1480367983}{192}\sqrt{2})\zeta_7 \\
& \quad + (-1016480 \pm \tfrac{7081753}{8}\sqrt{2})\zeta_3\zeta_5 + (-1271264 \pm 205280\sqrt{2})\zeta_3^3 + (-\tfrac{46245709}{9} \mp \tfrac{62018965}{72}\sqrt{2})\zeta_9 \\
& \quad + (14512736 \mp 7343308\sqrt{2})\zeta_3\zeta_7 + (10129460 \mp 3934300\sqrt{2})\zeta_5^2 + (-\tfrac{965226764}{15} \pm \tfrac{185149308}{5}\sqrt{2})\zeta_{11} \\
& \quad + (2475872 \mp 1311072\sqrt{2})\zeta_3^2\zeta_5 + (-9609600 \pm 8433600\sqrt{2})\zeta_3\zeta_9 + (-12633600 \pm 6878592\sqrt{2})\zeta_5\zeta_7 \\
& \quad + (49256064 \mp 40868256\sqrt{2})\zeta_{13} + (-\tfrac{520032}{5} \mp \tfrac{190368}{5}\sqrt{2})Z_{11}^{(2)}\Big) \\
& + g^{18}\Big(\tfrac{10426829965853}{32768} \pm \tfrac{235830866890042803}{1073741824}\sqrt{2} + (\tfrac{103506743759}{384} \mp \tfrac{2744026791787}{32768}\sqrt{2})\zeta_3 \\
& \quad + (-\tfrac{276665471}{6} \mp \tfrac{32420391253}{768}\sqrt{2})\zeta_3^2 + (\tfrac{8840920}{3} \pm 22175487\sqrt{2})\zeta_3^3 + (735232 \mp 943744\sqrt{2})\zeta_3^4 \\
& \quad + (-\tfrac{6273900189}{64} \mp \tfrac{4291223737195}{24576}\sqrt{2})\zeta_5 + (\tfrac{381113863}{6} \mp \tfrac{55154251}{192}\sqrt{2})\zeta_3\zeta_5 + (46556932 \mp 457124\sqrt{2})\zeta_3^2\zeta_5 \\
& \quad + (-\tfrac{107227490}{3} \pm \tfrac{31550065}{3}\sqrt{2})\zeta_5^2 + (-25320320 \pm 22619520\sqrt{2})\zeta_3\zeta_5^2 + (\tfrac{14437075583}{96} \pm \tfrac{2626144329215}{12288}\sqrt{2})\zeta_7 \\
& \quad + (\tfrac{46990300}{3} \mp \tfrac{108785719}{6}\sqrt{2})\zeta_3\zeta_7 + (-22634752 \pm 22092672\sqrt{2})\zeta_3^2\zeta_7 + (-256729984 \pm 94803408\sqrt{2})\zeta_5\zeta_7 \\
& \quad + (89017600 \mp 58788464\sqrt{2})\zeta_7^2 + (\tfrac{1089393967}{54} \pm \tfrac{2982598613}{96}\sqrt{2})\zeta_9 + (-\tfrac{1737826384}{9} \pm \tfrac{770357488}{9}\sqrt{2})\zeta_3\zeta_9 \\
& \quad + (163920000 \mp 124002240\sqrt{2})\zeta_5\zeta_9 + (\tfrac{470423502}{5} \mp \tfrac{320613021}{20}\sqrt{2})\zeta_{11} + (119243520 \mp 145271808\sqrt{2})\zeta_3\zeta_{11} \\
& \quad + (\tfrac{72811803608}{75} \mp \tfrac{14575123306}{25}\sqrt{2})\zeta_{13} + (-767566800 \pm 727927200\sqrt{2})\zeta_{15} + (-\tfrac{29532132}{5} \pm \tfrac{5078244}{5}\sqrt{2})Z_{11}^{(2)} \\
& \quad + (-\tfrac{15966848}{25} \mp \tfrac{3801792}{25}\sqrt{2})Z_{13}^{(2)} + (791168 \pm 178752\sqrt{2})Z_{13}^{(3)}\Big) \\
& + \mathcal{O}(g^{20})\,.
\end{aligned} \quad (6.65)$$

6.5.4 Long multiplets

Finally, let us take a look at an example of a multiplet that remains long at $g = 0$. For obvious combinatorial reasons, the spectrum of $\mathcal{N} = 4$ SYM is dominated by such solutions, except at the lowest values of $\Delta_0^{\ulcorner}$. For example, of the 6918 multiplets with $\Delta_0^{\ulcorner} = 8$ only 348 multiplets have both shortenings at zero coupling, 1624 have a single shortening, while 4946 of them are long.

Solutions for long multiplets containing only rational coefficients are very rare, but they do appear after browsing through the solutions for a while. A neat example is one of the 18 multiplets with $n^{\ulcorner} = [0, 4|2, 2, 2, 2|4, 0]$, see again figure 6.5 for the Young diagram, with central Q-function

$$\mathbb{Q}_{2,2} = u^8 - \frac{13}{3}u^6 + \frac{41}{24}u^4 + \frac{19}{48}u^2 + \frac{841}{2304}\,. \tag{6.66}$$

The 8-loop result, corresponding to the first double-wrapping order, for this solution is

$$\begin{aligned}
\gamma = {} & 12g^2 - \tfrac{114}{5}g^4 + \tfrac{81375909}{702250}g^6 + g^8\big(-\tfrac{76584649592643}{98631012500} - \tfrac{144}{5}\zeta_3 - \tfrac{288}{5}\zeta_5\big) \\
& + g^{10}\big(\tfrac{7557157119579028047}{1385272570562500} + \tfrac{5077548}{6625}\zeta_3 - \tfrac{71568}{53}\zeta_5 - \tfrac{5184}{25}\zeta_3^2 + \tfrac{18144}{5}\zeta_7\big) \\
& + g^{12}\big(-\tfrac{154229918575800932044660827}{3891230650710062500000} - \tfrac{5509872145602}{465240625}\zeta_3 - \tfrac{281495043162}{18609625}\zeta_5 \\
& \quad - \tfrac{36464256}{6625}\zeta_3^2 + \tfrac{97515936}{1325}\zeta_7 + \tfrac{93312}{5}\zeta_3\zeta_5 - \tfrac{2884896}{25}\zeta_9\big) \\
& + g^{14}\big(\tfrac{411159115509736510653261072871 89}{13663083622305706953125 0000} + \tfrac{147723346547996562}{1306860915625}\zeta_3 - \tfrac{8136755919612}{465240625}\zeta_3^2 \\
& \quad + \tfrac{124416}{5}\zeta_3^3 + \tfrac{227800256165730936}{1306860915625}\zeta_5 + \tfrac{487864512}{1325}\zeta_3\zeta_5 - \tfrac{1007424}{5}\zeta_5^2 \\
& \quad + \tfrac{21191283987174}{93048125}\zeta_7 - \tfrac{12386304}{25}\zeta_3\zeta_7 - \tfrac{2551539744}{1325}\zeta_9 + \tfrac{66394944}{25}\zeta_{11}\big) \\
& + g^{16}\big(-\tfrac{22730186914498905243446426320435681497}{95949004737641827078320312 50000} - \tfrac{3569464600430241216297321}{3670972311990625000}\zeta_3 \\
& \quad + \tfrac{8659804551029605422}{32671522890625}\zeta_3^2 + \tfrac{3265526016}{6625}\zeta_3^3 - \tfrac{53787653656926843535083}{36709723119906250}\zeta_5 + \tfrac{36588395264904}{93048125}\zeta_3\zeta_5 \\
& \quad - \tfrac{178391808}{125}\zeta_3^2\zeta_5 - \tfrac{24948434592}{6625}\zeta_5^2 - \tfrac{18579338632506856491}{6534304578125}\zeta_7 - \tfrac{47046267072}{6625}\zeta_3\zeta_7 + \tfrac{200212992}{25}\zeta_5\zeta_7 \\
& \quad - \tfrac{301302404501904}{93048125}\zeta_9 + \tfrac{48190464}{5}\zeta_3\zeta_9 + \tfrac{1295628042816}{33125}\zeta_{11} - \tfrac{260200512}{5}\zeta_{13} - \tfrac{10513152}{625}Z_{11}^{(2)}\big) \\
& + \mathcal{O}(g^{18})\,.
\end{aligned} \tag{6.67}$$

Note that for long solutions the prefactor products $\mathsf{A}_a\mathsf{A}^a$ and $\mathsf{B}_i\mathsf{B}^i$ (4.39) are all $\mathcal{O}(g^0)$, which means that n-loop correction to the anomalous dimension γ_n only appears naturally in these factors, and thus in the **P**-ansatz, at $\mathcal{O}(g^{2n})$ compared to $\mathcal{O}(g^{2(n-1)})$ in the case of a shortening. This means that in the algorithm described in section 6.4, γ_n is not fixed until the $(n+1)$'th iteration. More precisely, γ_n is fixed when imposing the regularity constraints on μ at the $(n+1)$'th loop. As discussed in [14], it also possible to extract γ_n from $\mu_{12}^{(n)}$ by a careful analysis of its poles.

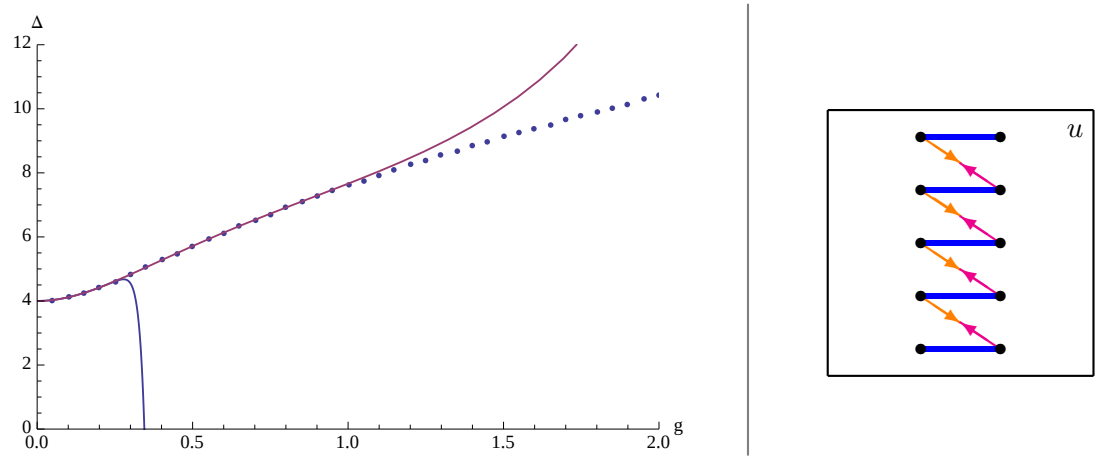

Figure 6.6: (Left) conformal dimension for $\mathfrak{sl}(2)$ Konishi operator: 10-loop perturbative power expansion (blue line), Padé approximant (red line) and numerical results [99] (dotted line). (Right) the branch points at $u = \pm 2g$ collide in the u-plane as $g \to \frac{\mathrm{i}}{4}$.

6.5.5 Comments on the number fields

The described algorithms are completely recursive, and as discussed in section 6.1.2 only a simple class of functions appear, under which the applied operations are closed. This means that the only transcendental numbers that can appear in the anomalous dimensions at *any* order in perturbation theory are multiple zeta-values. The only other irrational numbers introduced by the algorithm are the algebraic numbers that arise when solving the algebraic equations that fix the 1-loop Q-system.

By inspecting the data, we observe that only a subclass of multiple zeta-values appear: zeta-values with a single odd index, and the *single-valued multiple zeta-values* [129]. It has been argued [131] that only these special combinations of multiple zeta-values should appear for a large class of Feynman diagrams. Our results can indeed be written in terms of these values in all investigated examples. See appendix B.1 for the explicit structure of the combinations $Z_a^{(n)}$.

6.5.6 Convergence and Padé approximants

By comparison with numerical results, see e.g. [99, 100, 114], it can be observed that the found perturbative expansions converge up to $g = \frac{1}{4}$. This is not so surprising, since the branch points at e.g. $2g$ and $-2g + \mathrm{i}$ collide at the value $g = \frac{\mathrm{i}}{4}$, see figure 6.6.

The convergence of the expansion can be improved by the construction of a Padé approximant. In this procedure one introduces a new parameter $w = (1 + 16g^2)^\alpha$ and turns the power expansion in w, $\gamma(w) = \sum_{j=0}^{m+n} a_j w^j$, into a Padé approximant of the form

$$R(w) = \frac{\sum_{j=0}^{m} c_j w^j}{1 + \sum_{j=1}^{n} d_j w^j} \tag{6.68}$$

by ensuring that the first $n+m$ derivatives match: $R(0) = \gamma(0)$, $R'(0) = \gamma'(0)$, ..., $R^{(n+m)}(0) = \gamma^{(n+m)}(0)$. For the states that are known to 10 loops, we find that the Padé approximant with $m = n = 5$ converges up to $g \approx 0.7$. With $\alpha = \frac{1}{4}$ we get the best match with the numerical data with roughly a five-digit precision at $g \approx 0.4$ and a three-digit precision at $g \approx 0.7$. Around $g \approx 1.0$ the Padé approximant starts to diverge significantly from the numerical results.

See figure 6.6 for a comparison of the Taylor expansion, Padé approximation and numerical result for the Konishi multiplet.

Subconclusion

In this chapter we have seen how to solve the Quantum Spectral Curve perturbatively at weak coupling. The starting point was the leading solutions found through the methods of chapter 5, and the perturbative algorithms used the analytic structure of the QSC, discussed in chapter 4, to recursively generate corrections. Our conclusion is that considering just the $\mathbf{P}\mu$-system is the simplest way to do such calculations. In this way, the calculations involve only a small set of functions that are relatively easy to control.

Together with the algorithm to solve the leading Q-system given in chapter 5, the algorithm described in section 6.4 fulfils the main goal pursued in this thesis, which is to automatise the weak coupling solution of the QSC for the general spectrum of single-trace operators. The combined algorithm will appear as part of the publication [7]. In practice, this opens the window to a dataset of results far beyond what has been studied before. Certainly, explicit analytical results can automatically be generated for the more than 1000 multiplets with $\Delta_0^{\lceil} \leq 7$ up to *at least* eight loops. Going further is simply a matter of optimisation and computer power[2].

The new data availability opens the possibility to look for patterns in the results. In the next chapter, we take a look at a particular pattern satisfied by an infinite family of multiplets that can be united by analytic continuation in a single quantum number.

[2]Note that to go beyond 10 loops using our publicly available `Mathematica`-notebooks, it is necessary to update the files containing relations between ζ-values, which are used to write intermediate results in a linearly independent basis. The currently used files, which are available with [1], contain all such relations up to transcendentality 15, which is sufficient to go to 10 loops. Algorithms to produce such relations are available in the `Mathematica`-files connected to [109], and going further is again simply a matter of computer power. See also [132].

Chapter 7

Twist-2 operators

With the perturbative data at hand, it is natural to look for patterns in the result. In this chapter we discuss infinite series of solutions for which it is possible to obtain a general result that describes all multiplets within the series by analytic continuation in a single quantum number. Due to particular number theoretical properties, it is possible to obtain such results by extrapolation from results at fixed quantum numbers. The general result can then be analytically continued to regimes such as the BFKL limit.

The discussion in this chapter gives a basic introduction to the analytic properties of series of anomalous dimensions, before summarising the tricks and techniques that went into the reconstruction of the analytic structure of the anomalous dimension of twist-2 operators at six [2] and seven loops [3]. Many details about these rather technical calculations are left out, and the interested reader is encouraged to consult the papers for the complete story.

7.1 Series of solutions and patterns in the data

In this section, we discuss how series of related solutions appear in the QSC. We also discuss some of the mathematical properties that these series of solutions possess. This understanding will pave the way for reconstructions in the following sections.

7.1.1 Solution series

The spectrum contains solutions that are connected. This can be seen already at the level of the 1-loop Q-system where the solutions for certain types of multiplets follow various patterns. The Young diagram Q-system provides a new way to understand how some of these families of solutions arise.

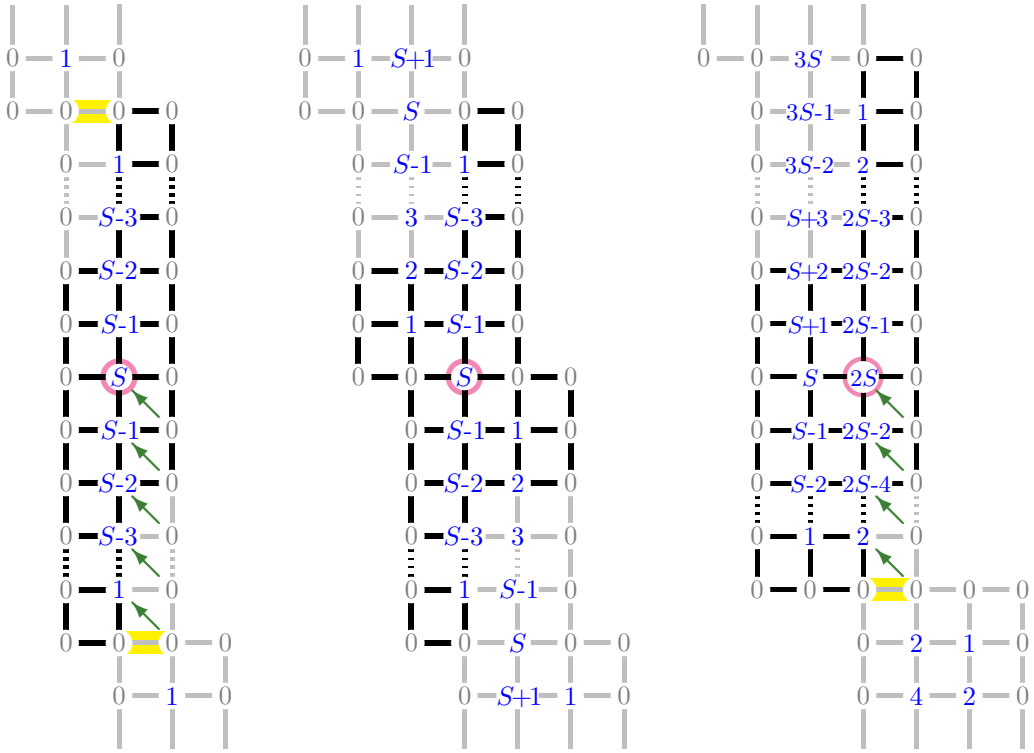

Figure 7.1: Young diagram (for the short multiplet that remains HWS in the 1...4 grading) and number of roots in the distinguished Q-functions for twist-2 operators (left), twist-3 operators (middle), and another series of length-3 operators (right). The central nodes are encircled. Paths with no Bethe roots are marked in yellow. The green arrows show how to generate the central Q-functions via trivial QQ-relations.

Twist-2 operators

The classical example is the twist-2 operators. They are usually referred to by their $1\hat{1}\hat{2}2\hat{3}\hat{4}4$ HWS which has the form $\mathcal{D}_{12}^{S}\mathcal{Z}^{2}$ and belongs to the $\mathfrak{sl}(2)$ sector. In fact, these multiplets contain all unprotected operators of length two in the $\mathcal{N}=4$ SYM spectrum. They are described by the quantum numbers,

$$n^{\lceil} = [0, S-2|1,1,1,1|S-2,0]\,. \tag{7.1}$$

The corresponding Young diagram is shown in figure 7.1, which is the only allowed type of Young diagram with length two. The Young diagram reveals a special property: there exists a path from the left to the right boundary where no roots are encountered. In fact, this means that the central Q-function is simply

$$\mathbb{Q}_{2,2}(S) \propto \nabla^{S} \prod_{k=1}^{S} \left(u + \tfrac{\mathrm{i}}{2} - \mathrm{i}k\right)^{2}\,, \tag{7.2}$$

where ∇ is the difference operator (4.27).

This result coincides with the well-known result [52, 133] that the $\mathfrak{sl}(2)$ Baxter equation

for $L = 2$,

$$\left(u + \tfrac{\mathbb{i}}{2}\right)^2 Q^{[2]} + \left(u - \tfrac{\mathbb{i}}{2}\right)^2 Q^{[-2]} + \left(-2u^2 + S(S+1) + \tfrac{1}{2}\right) Q = 0\,, \tag{7.3}$$

is solved by the hypergeometric function

$$Q(u) \propto {}_3F_2\left(\begin{matrix}-S, S+1, \frac{1}{2} - \mathbb{i}u \\ 1, 1\end{matrix}; 1\right)\,, \tag{7.4}$$

which for integer S are Hahn polynomials. These solutions only satisfy the zero-momentum condition (5.38) for even S.

Twist-3 operators

Another series of operators that has been studied in the literature are the twist-3 operators. They are likewise named after their $\mathfrak{sl}(2)$ HWS of the form $\mathcal{D}_{12}^S\mathcal{Z}^3$. Note that, unlike the twist-2 operators, there is in general more than one HWS of this kind for a given S. The typically studied series of twist-3 operators picks out only a single of these states.

For $L = 3$, the $\mathfrak{sl}(2)$ Baxter equation is

$$\left(u + \tfrac{\mathbb{i}}{2}\right)^3 Q^{[2]} + \left(u - \tfrac{\mathbb{i}}{2}\right)^3 Q^{[-2]} + \left(-2u^3 + \left(S^2 + 2S + \tfrac{3}{2}\right) u + t_0\right) Q = 0\,. \tag{7.5}$$

and the typical series of twist-3 operators is singled out by assuming parity invariance $u \leftrightarrow -u$, which removes the arbitrary constant t_0. In this case, the solution can again be written as a hypergeometric function [134, 135]

$$Q(u) = {}_4F_3\left(\begin{matrix}-\frac{S}{2}, \frac{S}{2}+1, \frac{1}{2} + \mathbb{i}u, \frac{1}{2} - \mathbb{i}u \\ 1, 1, 1\end{matrix}; 1\right)\,, \tag{7.6}$$

which for even S is a polynomial that satisfies the zero-momentum condition. Note that on the level of the Young diagram, it is not obvious how the twist-3 solution emerges, see figure 7.1.

Another series

The extended Young diagrams provide a new intuition that can be used to search for other series of operators. For example, we can ask whether there exists other families of diagrams where there is a path without any roots.

The rightmost diagram in figure 7.1 is one such example. They correspond to

$$n^{\lrcorner} = [S-2, S-2|1, 1, 1, 1|2S-2, 0] \tag{7.7}$$

for $S > 1$. These multiplets have components in the $su(2,1|2)$ sector, and in the grading $\hat{1}\hat{2}123\hat{3}\hat{4}4$ the HWS is of the kind $\mathcal{D}_{11}^S\mathcal{D}_{12}^S\mathcal{Z}^3$. The $S = 1$ state also exists, but it has an extra shortening that changes the $\lrcorner$ HWS to $n^{\lrcorner} = [0, 0|1, 1, 1, 1|0, 0]$, which is the Konishi

S	Q	γ_1	γ_2	γ_3	γ_4
0	1	0	0	0	0
2	$u^2 - \frac{1}{12}$	12	-48	336	$-2496 + 576\zeta_3 - 1440\zeta_5$
4	$u^4 - \frac{13}{14}u^2 + \frac{27}{560}$	$\frac{50}{3}$	$-\frac{1850}{27}$	$\frac{241325}{486}$	$-\frac{8045275}{2187} + \frac{114500}{81}\zeta_3 - \frac{25000}{9}\zeta_5$
6	$u^6 - \frac{155}{44}u^4$ $+\frac{329}{176}u^2 - \frac{375}{4928}$	$\frac{98}{5}$	$-\frac{91238}{1125}$	$\frac{300642097}{506250}$	$-\frac{393946504469}{91125000} + \frac{11736088}{5625}\zeta_3 - \frac{19208}{5}\zeta_5$
8	$u^8 - \frac{133}{15}u^6 + \frac{5341}{312}u^4$ $-\frac{17807}{2640}u^2 + \frac{8575}{36608}$	$\frac{761}{35}$	$-\frac{138989861}{1543500}$	$\frac{180298033531853}{272273400000}$	$-\frac{5685358151649447407}{1200725694000000}$ $+\frac{142906863577}{54022500}\zeta_3 - \frac{1158242}{245}\zeta_5$

Table 7.1: Central Q-functions, $Q = \mathbb{Q}_{2,2} = Q^{(1)}_{12|12}$, and perturbative corrections to the anomalous dimension, $\gamma = \sum_{j=1}^{\infty} \gamma_j g^{2j}$, for the first states in the series of twist-2 operators.

multiplet. The case $S = 0$ corresponds to the protected length-three BMN vacuum. In general, the states are not left/right symmetric. Note that there is an equivalent family with $n^{\lceil} = [0, 2S-2|2,2,2,2|S-2, S-2]$ corresponding to a rotation of the diagram by π.

Starting from the lower right corner of the non-trivial extension of the diagram, one can trivially generate the central Q-function

$$\mathbb{Q}_{2,2}(S) \propto \nabla^S \prod_{k=1}^{S} \left(u + \tfrac{\mathbb{i}}{2} - \mathbb{i}k\right)^3 , \tag{7.8}$$

as depicted in figure 7.1.

7.1.2 Properties of the perturbative anomalous dimension

For certain series of multiplets, there is evidence that the anomalous dimension can be described as an analytic function of a continuous variable. This has led to conjectures of certain number theoretical properties which we now review. Table 7.1 shows a sample of explicit results for the first multiplets in the twist-2 series.

The anomalous dimension as a function of S

As we saw above, the series of solutions have central Q-functions that can be united in a general solution with a free parameter S. Inserting the expression (7.4) for the central Q-function of twist-2 operators in the energy formula (5.3), one obtains the one-loop anomalous dimension

$$\gamma_1 = 8\,\mathbf{S}_1(S)\,. \tag{7.9}$$

where $\mathbf{S}$ denotes the harmonic sum,

$$\mathbf{S}_a(S) = \sum_{j=1}^{S} \frac{\mathrm{sign}(a)^j}{j^{|a|}}\,, \qquad \mathbf{S}_{a_1,\ldots,a_n}(S) = \sum_{j=1}^{S} \frac{\mathrm{sign}(a_1)^j}{j^{|a_1|}}\,\mathbf{S}_{a_2,\ldots,a_n}(j)\,, \tag{7.10}$$

which is described in more detail in appendix B.2. Thus it is possible to describe the one-loop anomalous dimension of any twist-2 operator by a very compact expression.

This feature is not limited to the leading order. In [136], a general two-loop result was obtained from direct field-theory calculations, and, based on the *maximal transcendentality principle*, the result was extended to three-loops in [137]. As the integrability techniques developed, it also became feasible to reconstruct the four- [82] and five-loop [83] results, again assuming maximal transcendentality. In [138, 139], the solution to the asymptotic Bethe ansatz equations for twist-2 operators was found as an analytic expression in S up to the fourth loop-order, providing a direct derivation not relying on maximal transcendentality. Similar results have been obtained for twist-3 operators up to six loops [135, 134, 140].

The explicit results depend on S only through harmonic sums. The 2-loop result for twist-2 operators can be written as

$$\gamma_2(S) = -16\left(\mathbf{S}_3 + \mathbf{S}_{-3} - 2\mathbf{S}_{-2,1} + 2\mathbf{S}_1\big(\mathbf{S}_2 + \mathbf{S}_{-2}\big)\right) , \tag{7.11}$$

where all harmonic sums have argument S, i.e. $\mathbf{S} \equiv \mathbf{S}(S)$. The three-loop result is already quite involved, and the four loop result takes up about a full page of space. As is also apparent from table 7.1, the four loop result contains ζ-values, and we can split it in three parts,

$$\gamma_4(S) = \gamma_4^{\text{rat}}(S) + \gamma_4^{\zeta_3}(S)\,\zeta_3 + \gamma_4^{\zeta_5}(S)\,\zeta_5 , \tag{7.12}$$

where the parts $\gamma_4^{\zeta_i}(S)$ turn out to be quite simple:

$$\gamma_4^{\zeta_3}(S) = -256\,\mathbf{S}_1\,(\mathbf{S}_3 - \mathbf{S}_{-3} + 2\mathbf{S}_1\mathbf{S}_{-2} + 2\mathbf{S}_{-2,1}) \tag{7.13a}$$

$$\gamma_4^{\zeta_5}(S) = -640\,\mathbf{S}_1^2 . \tag{7.13b}$$

The principle of maximal transcendentality

Apart from the direct derivations mentioned above, which provides full results up to three loops [138], the above results were based on the *maximal transcendentality principle* [141]. This principle states that all terms in the analytically continued anomalous dimension have transcendentality $2k-1$ where k is the loop order. The anomalous dimension is given in terms of products of ζ-values and harmonic sums. The transcendentality of harmonic sums $\mathbf{S}_{a_1,\ldots,a_n}$ and ζ-values $\zeta_{a_1,\ldots,a_n}$ is defined as $\sum_{j=1}^{n}|a_j|$ and it is additive in products of these numbers, e.g. $\mathbf{S}_{2,3}\zeta_5$ has transcendentality 10.

The alert reader may already have noticed this property in the above results. It explains e.g. why the expression $\gamma_4^{\zeta_5}$ is so simple: as it multiplies ζ_5 with transcendentality 5 and the four-loop anomalous dimension has transcendentality 7, it must be of transcendentality 2, and the basis of such harmonic sums is very limited.

The basis of harmonic sums with given transcendentality

So exactly how big is the basis of combinations of harmonic sums with a given transcendentality? Naively, the bases of transcendentality 1 and 2 look like

$$\mathcal{B}_1 = \{\mathbf{S}_1, \mathbf{S}_{-1}\} \tag{7.14}$$

$$\mathcal{B}_2 = \{\mathbf{S}_1^2, \mathbf{S}_1\mathbf{S}_{-1}, \mathbf{S}_{-1}^2, \mathbf{S}_2, \mathbf{S}_{-2}, \mathbf{S}_{1,1}, \mathbf{S}_{1,-1}, \mathbf{S}_{-1,1}, \mathbf{S}_{-1,-1}\}\,. \tag{7.15}$$

As discussed in appendix B.2, all these terms are not linearly independent. The basis of harmonic sums of a given transcendentality k has the size $2 \times 3^{k-1}$, and it is natural to choose a linearised basis formed by all multi-indexed harmonic sums [142]. For example, this reduces the basis of transcendentality 2 terms to

$$\mathcal{B}_2 = \{\mathbf{S}_2, \mathbf{S}_{-2}, \mathbf{S}_{1,1}, \mathbf{S}_{1,-1}, \mathbf{S}_{-1,1}, \mathbf{S}_{-1,-1}\}\,. \tag{7.16}$$

However, as we will now see, there is a way to work with an even smaller basis by considering a different quantity than the anomalous dimension and by using another type of sums.

Reciprocity

Consider the *reciprocity function*, $\mathcal{P}$, related to the anomalous dimension through [143]

$$\gamma(S) = \mathcal{P}\big(S + \tfrac{1}{2}\gamma(S)\big)\,. \tag{7.17}$$

A modified version of the maximal transcendentality principle states that the reciprocity function satisfies a similar criterion where harmonic sums are replaced by *binomial sums*,

$$\mathbb{S}_{a_1,\ldots,a_n}(N) = (-1)^N \sum_{j=1}^{N} (-1)^j \binom{N}{j} \binom{N+j}{j} \mathbf{S}_{a_1,\ldots,a_n}(j)\,. \tag{7.18}$$

Importantly, only binomial sums with positive indices should appear [83]. All expressions of binomial sums with a given transcendentality can similarly to the harmonic sums be written in a linearised basis [142], and thus the number of possible terms of transcendentality k is 2^{k-1}, which is a significant reduction compared to the basis of harmonic sums. For example, the basis of terms with transcendentality 2 is simply $\{\mathbb{S}_2, \mathbb{S}_{1,1}\}$.

Conversion between γ and $\mathcal{P}$

It should clearly be easier to reconstruct $\mathcal{P}$ than γ. However, we first need to understand how to convert our results for γ to $\mathcal{P}$. The reciprocity function has a perturbative structure similar to that of the anomalous dimension,

$$\mathcal{P}(S) = \sum_{j=1}^{\infty} g^{2j} \mathcal{P}_j(S)\,. \tag{7.19}$$

Expanding (7.17) in g^2 gives

$$g^2\gamma_1 + g^4\gamma_2 + \mathcal{O}(g^6) \;=\; g^2\mathcal{P}_1 + g^4\left(\tfrac{1}{2}\mathcal{P}_1'\gamma_1 + \mathcal{P}_2\right) + \mathcal{O}(g^6)\,, \tag{7.20}$$

where all γ and $\mathcal{P}$ have the same argument S. We see that $\mathcal{P}_1 = \gamma_1$, but for higher orders we need to know how to take derivatives $\mathcal{P}_j' = \frac{\mathrm{d}}{\mathrm{d}S}\mathcal{P}_j$. Analytic continuation and power expansion of harmonic sums is discussed in appendix B.2.

7.1.3 Reconstruction from data points

The methods of chapter 6 gave us tools to generate results for arbitrary states, but with fixed quantum numbers. We will now discuss how to use such results to reconstruct the general result for series of solutions, assuming the principle of maximal transcendentality and a basis of only harmonic sums. We will use the twist-2 operators (7.1) as an example.

Direct matching

We should be able to uniquely determine the result for general S if we have as many values for fixed S as the size of the basis. For the twist-2 series, the data in table 7.1 should be enough to get a few results. First of all, γ_1 should be given in terms of $\mathcal{B}_1$:

$$\gamma_1(S) = c_1\mathbf{S}_1(S) + c_{\text{-}1}\mathbf{S}_{\text{-}1}(S)\,. \tag{7.21}$$

We thus need two[1] values for fixed spin to fix c_i. For $S = 2, 4$ we get

$$\left\{12 = \tfrac{3}{2}c_1 - \tfrac{1}{2}c_{\text{-}1}\,,\; \tfrac{50}{3} = \tfrac{25}{12}c_1 - \tfrac{7}{12}c_{\text{-}1}\right\} \quad\Rightarrow\quad c_1 = 8\,,\; c_{\text{-}1} = 0\,, \tag{7.22}$$

so we should have $\gamma_1(S) = 8\mathbf{S}_1(S)$, and this indeed reproduces the values for $S = 6, 8$ in table 7.1. We would need six points to reconstruct $\gamma_4^{\zeta_5}$ of transcendentality 2, which is two more point than in table 7.1 (note that the point $S = 0$ is no good). To reconstruct γ_2 directly we would need 18 points to match with $\mathcal{B}_3$. This is already a lot, so let us try to reconstruct the reciprocity function instead.

Converting to the reciprocity

To reconstruct $\mathcal{P}_2$, which has transcendentality 3, we need only four data points. However, we first need to convert our results at fixed values, $\gamma_2(S_0)$ to $\mathcal{P}_2(S_0)$. From (7.20) we have

$$\mathcal{P}_2(S) \;=\; \gamma_2(S) - \tfrac{1}{2}\mathcal{P}_1'(S)\gamma_1(S) \;=\; \gamma_2(S) - 32\mathbf{S}_1(S)\big(\zeta_2 - \mathbf{S}_2(S)\big)\,, \tag{7.23}$$

which gives

[1] In fact, since $\gamma_1 = \mathcal{P}_1$, we know that it should be expressed only in terms of $\mathbf{S}_1 = \frac{1}{2}\mathbb{S}_1$. Note that the constraints on the basis of $\mathcal{P}$ also puts constraints on the basis of γ.

S	2	4	6	8	10
$\mathcal{P}_2$	$12-48\zeta_2$	$\frac{475}{18}-\frac{200}{3}\zeta_2$	$\frac{16121}{450}-\frac{392}{5}\zeta_2$	$\frac{7548787}{176400}-\frac{3044}{35}\zeta_2$	$\frac{383492923}{7938000}-\frac{29524}{315}\zeta_2$

Note that $\mathcal{P}_2 = \mathcal{P}_2^{\text{rat}} + \mathcal{P}_2^{\zeta_2}\,\zeta_2$, with $\mathcal{P}_2^{\zeta_2} = -32\mathbf{S}_1$. We should be able to fix $\mathcal{P}_2^{\text{rat}}$ by matching the four values for $S = 2,\ldots,8$ with the ansatz

$$\mathcal{P}_2^{\text{rat}}(S) = d_3\mathbb{S}_3(S) + d_{2,1}\mathbb{S}_{2,1}(S) + d_{1,2}\mathbb{S}_{1,2}(S) + d_{1,1,1}\mathbb{S}_{1,1,1}(S)\,, \tag{7.24}$$

which results in

$$d_3 = 0\,, \quad d_{2,1} = -8\,, \quad d_{1,2} = 8\,, \quad d_{1,1,1} = 0\,. \tag{7.25}$$

As a check, the result correctly reproduces the $S = 10$ value.

Converting back to γ_2, we get

$$\gamma_2 = \mathcal{P}_2 + \tfrac{1}{2}\mathcal{P}_1'\gamma_1 = \mathcal{P}_2^{\text{rat}} - 32\mathbf{S}_1\mathbf{S}_2 = 16\left(\mathbf{S}_3 + \mathbf{S}_{\text{-}3} - 2\mathbf{S}_{2,1} - 2\mathbf{S}_{1,2} - 2\mathbf{S}_{1,\text{-}2}\right)\,, \tag{7.26}$$

which is simply another way to write the well-known result (7.11). See appendix B.2 for conversions between harmonic and binomial sums at fixed arguments.

Using less points than the basis size

In the reconstructions below, we will sometimes need to reconstruct results out of fewer constraints than unknowns. The extra condition that makes this possible is the observation that the variables we are trying to determine are *integers*, and in fact rather simple integers. For example, we see that this is the case in e.g. (7.11) and (7.13). This means that we are dealing with a case of the so-called *integer linear programming* problem, and the equation satisfied by the coefficients d is a linear Diophantine equation. The Lenstra-Lenstra-Lovász (LLL) algorithm [144] provides a method to look for solutions to such problems. We briefly describe this method in appendix A.5 where we as an example reconstruct $\mathcal{P}_2^{\text{rat}}$ for the twist-2 operators out of just three data points. We refer to [145] and references therein for a more detailed explanation.

7.1.4 Checks from analytic continuation in S

The general results can be analytically continued to non-integer and negative S, see appendix B.2. Harmonic sums have poles at negative integers, and the anomalous dimension has a very particular behaviour around such points.

For twist-2 operators, the behaviour of the anomalous dimension is known to behave in certain ways around negative integer spin. The most well-known example is the BFKL regime [146], $S = -1$, but also the behaviour in the *double-logarithmic limit* [147, 141], $S = -2$, and the *generalised double logarithmic limit* $S = -2n$ with $n = 2, 3, \ldots$ have been studied [148].

For example, in the double-logarithmic limit $S = -2 + w$, the anomalous dimension should satisfy

$$\gamma \cdot (2\omega + \gamma) = -16g^2 + \mathcal{O}(g^4) \,, \tag{7.27}$$

and the right hand side is conjectured to be regular in w to all orders in g^2 [135, 148]. This puts strong constraints on the left hand side as all poles in w must cancel.

Together with similar constraints coming from the BFKL and generalised double-logarithmic limits, this provides a range of non-trivial checks of the results obtain through reconstructions using data points at fixed positive S. The results described in the next sections pass all these checks.

7.2 Twist-2 at six loops

The following is a summary of the strategy behind the reconstruction of the six-loop anomalous dimension for twist-2 operators done in [2].

7.2.1 The structure of γ_6

The six-loop correction to the anomalous dimension of twist-2 operators, i.e. the coefficient of g^{12} in the perturbative expansion, takes the form

$$\gamma_6 = \gamma_6^{\text{rat}} + \gamma_6^{\zeta_3}\,\zeta_3 + \gamma_6^{\zeta_5}\,\zeta_5 + \gamma_6^{\zeta_3^2}\,\zeta_3^2 + \gamma_6^{\zeta_7}\,\zeta_7 + \gamma_6^{\zeta_3\zeta_5}\,\zeta_3\zeta_5 + \gamma_6^{\zeta_3^3}\,\zeta_3^3 + \gamma_6^{\zeta_9}\,\zeta_9 \,. \tag{7.28}$$

The corresponding non-trivial terms in $\mathcal{P}_6$ and the size of the basis of binomial sums in the ansatz for these terms are summarised in table 7.2. One can split each of the terms in two contributions: one coming from the asymptotic Bethe ansatz, $\mathcal{P}_{6,\text{ABA}}$, and one coming from wrapping corrections, $\mathcal{P}_{6,\text{wrap}}$. Importantly, from an analysis of Lüscher corrections [83], it is known that the wrapping contribution has a much simpler structure than the contribution from the asymptotic Bethe ansatz. This observation reduces the dimension of the basis for the wrapping contributions significantly [2].

Contribution	$\mathcal{P}_6^{\text{rat}}$	$\mathcal{P}_6^{\zeta_3}$	$\mathcal{P}_6^{\zeta_5}$	$\mathcal{P}_6^{\zeta_3^2}$	$\mathcal{P}_6^{\zeta_7}$	$\mathcal{P}_6^{\zeta_3\zeta_5}$	$\mathcal{P}_6^{\zeta_3^3}$	$\mathcal{P}_6^{\zeta_9}$
Transcendentality	11	8	6	5	4	3	2	2
Size of basis	1024	128	32	16	8	4	2	2

Table 7.2: The (non-trivial) contributions to $\mathcal{P}_6$, their transcendentality, and the size of the basis of binomial sums in terms of which the general result should be expressed.

7.2.2 Data collection

To reconstruct the result, the contributions from the asymptotic Bethe ansatz and the wrapping contribution were treated separately.

Asymptotic Bethe ansatz

To fix the ansatz, we need 1024 values of γ_6 at fixed S. The asymptotic Bethe ansatz equations for the $\mathfrak{sl}(2)$ sector (3.20) can be solved perturbatively very efficiently. However, the analytical solution for $S \sim 1000$ is out of reach in practice. Because the full range of results is only needed for the reconstruction of $\gamma^{\text{rat}}_{6,\text{ABA}}$, one can ignore the dressing factor as it does not contribute to the rational part. These equations can be solved numerically with extremely high precision, which, as we explain below, is sufficient for our purposes. We thus calculated $\gamma^{\text{rat}}_{6,\text{ABA}}(S)$ numerically for $S = 1, 2, \ldots, 1024$ with a 1000-digit precision. We performed analytic calculations including the dressing factor for the first 40 values, i.e. for $S = 1, 2, \ldots 40$.

QSC

The solution of the QSC is more involved, and with the current methods available the generation of six-loop results for $S \sim 1000$ is far beyond reach. Using the method to solve the $\mathbf{P}\mu$-system in the $\mathfrak{sl}(2)$ sector described in section 6.2, we calculated $\gamma_6(S)$ for the first 40 even integer values of S, i.e. $S = 2, 4, \ldots, 80$, which can be done automatically by the `Mathematica`-notebook that was published with [1] without any modifications. As we explain below, this is enough to reconstruct the wrapping contribution.

7.2.3 Reconstruction

For the contributions from the asymptotic Bethe ansatz we directly matched the ansätze for the different contributions to the obtained results for $\mathcal{P}_{6,\text{ABA}}$, except for $\mathcal{P}^{\zeta_3}_{6,\text{ABA}}$. For $\mathcal{P}^{\text{rat}}_{6,\text{ABA}}$, this determines the coefficients of the different binomial sums numerically. It turns that these numbers are always extremely close to integers, so we can safely round these numbers and thus obtain an exact result. For all other terms except $\mathcal{P}^{\zeta_3}_{6,\text{ABA}}$ we did the matching analytically, which for example yields

$$\mathcal{P}^{\zeta_7}_{6,\text{ABA}} = 3360(-2\mathbb{S}_4 - \mathbb{S}_{1,3} + \mathbb{S}_{2,2} + \mathbb{S}_{1,2,1} + \mathbb{S}_{2,1,1})\,. \tag{7.29}$$

To reconstruct $\mathcal{P}^{\zeta_3}_{6,\text{ABA}}$, with a 128-dimensional basis, the LLL-algorithm was applied to the first 39 values, which yields a result consistent with the $M = 40$ value.

For the wrapping corrections, all contributions except for $\mathcal{P}^{\text{rat}}_{6,\text{wrap}}$ and $\mathcal{P}^{\zeta_3}_{6,\text{wrap}}$ were found by direct matching. For example, the wrapping contribution to $\mathcal{P}^{\zeta_7}_6$ is

$$\mathcal{P}^{\zeta_7}_{6,\text{wrap}} = 224\mathbb{S}_1\left(12\mathbb{S}_1^3 + 151\mathbb{S}_1\mathbb{S}_2 - 72\mathbb{S}_3 - 52\mathbb{S}_{2,1}\right)\,. \tag{7.30}$$

The basis for the last two terms $\mathcal{P}^{\text{rat}}_{6,\text{wrap}}$ and $\mathcal{P}^{\zeta_3}_{6,\text{wrap}}$ can, based on the constraints from Lüscher formulae [83], be reduced to 323 and 51 terms, respectively. Remarkably, using

only the first 35 data points, the LLL-algorithm[2] is able to obtain a result by that is consistent with the last five, $M = 72, \ldots, 80$. We refer the interested reader to [2] for the full result, which is rather bulky. The result passes all constraints from the BFKL and double-logarithmic limits, which is a strong check of its validity.

7.3 Twist-2 at seven loops

This section summarises the strategy behind the reconstruction of the seven-loop anomalous dimension of twist-2 operators carried out in [3].

7.3.1 The structure of γ_7

The structure of γ_7 is

$$\begin{aligned}\gamma_7 \;=\; & \gamma_7^{\text{rat}} + \gamma_7^{\zeta_3}\,\zeta_3 + \gamma_7^{\zeta_5}\,\zeta_5 + \gamma_7^{\zeta_3^2}\,\zeta_3^2 + \gamma_7^{\zeta_7}\,\zeta_7 + \gamma_7^{\zeta_3\zeta_5}\,\zeta_3\zeta_5 \\ & + \gamma_7^{\zeta_3^3}\,\zeta_3^3 + \gamma_7^{\zeta_9}\,\zeta_9 + \gamma_7^{\zeta_3\zeta_7}\,\zeta_3\zeta_7 + \gamma_7^{\zeta_5^2}\,\zeta_5^2 + \gamma_7^{\zeta_{11}}\,\zeta_{11}\,. \end{aligned} \tag{7.31}$$

The corresponding non-trivial parts of $\mathcal{P}_7$ and the size of the basis of binomial sums in the ansatz for these terms are summarised in table 7.3.

Contribution	$\mathcal{P}_7^{\text{rat}}$	$\mathcal{P}_7^{\zeta_3}$	$\mathcal{P}_7^{\zeta_5}$	$\mathcal{P}_7^{\zeta_3^2}$	$\mathcal{P}_7^{\zeta_7}$	$\mathcal{P}_7^{\zeta_3\zeta_5}$	$\mathcal{P}_7^{\zeta_3^3}$	$\mathcal{P}_7^{\zeta_9}$	$\mathcal{P}_7^{\zeta_3\zeta_7}$	$\mathcal{P}_7^{\zeta_5^2}$	$\mathcal{P}_7^{\zeta_{11}}$
Transcendentality	13	10	8	7	6	5	4	4	3	3	2
Size of basis	4096	512	128	64	32	16	8	8	4	4	2

Table 7.3: The contributions to $\mathcal{P}_7$ and the size of the basis of binomial sums.

7.3.2 Data collection

Contrary to the six-loop reconstruction, we chose to not make a subdivision in parts coming from the asymptotic Bethe ansatz and wrapping corrections for all contributions, except for the rational part.

Asymptotic Bethe ansatz

We calculated[3] $\gamma_{7,\text{ABA}}^{\text{rat}}$ numerically for the first 2700 integer values of S. Again, the dressing factor was ignored in these computations as it does not contribute to the rational part.

[2] For the rational case, we made use of a `C++` implementation of the *fplll-4.0* version of the LLL-algorithm [149].

[3] We gratefully acknowledge the North-German Supercomputing Alliance (HLRN) and Cluster of UNIX Machines at Humboldt Universität zu Berlin (CLOU) for providing the resources to make these calculations possible.

S	2	4	6	8	10	20	30	40	50	60	70
full	1	2.1	3.3	4.8	7.0	27	113				
rational and ζ_3	0.55	1.3	1.8	2.7	3.7	11	26	51	87	132	201
rational	0.33	0.65	1.0	1.5	2.0	6.4	14	26	45	74	108

Table 7.4: Computation time normalised by the $S = 2$ computation time for the full result (120 seconds on a single 1.8GHz core of a standard laptop). To go beyond $S \sim 30$ for the full result, one needs to use high-performance clusters due to the memory usage. Note that the reduced codes use significantly less memory than the full code which makes it possible to go to much higher S before lack of memory becomes an issue.

Partial results from the QSC

To generate results for the complete γ_7, we again used the $\mathbf{P}\mu$-system algorithm specific to the $\mathfrak{sl}(2)$ sector, see section 6.2. However, this time it was necessary to optimise and tailor the implementation to twist-2 operators to produce the needed results.

The computation time and memory usage grows with S, and this limits the results that are within reach, even on high-performance computer clusters. To be able to generate enough data, we exploited the fact that it is possible to work with only partial results. Just as γ and $\mathcal{P}$, we can split the functions of the $\mathbf{P}\mu$-system into parts proportional to different ζ-values, e.g.

$$\mathbf{P}_a = \mathbf{P}_a^{\text{rational}} + \zeta_3 \mathbf{P}_a^{\zeta_3} + \zeta_5 \mathbf{P}_a^{\zeta_5} + \zeta_3^2 \mathbf{P}_a^{\zeta_3^2} + \dots \tag{7.32}$$

All operations in the algorithm simply multiply these terms, so a term proportional to ζ_3 will never contribute to the part without ζ-value dependence, a term proportional to ζ_5 will never influence the ζ_3 part, and so on. This means that it is possible to run the algorithm with only parts of the results, and the obtained partial functions still satisfy the analytical requirements imposed in the algorithm.

Exploiting this property, we used two modifications of the algorithm: one keeping only the rational part of the results, and another keeping also the part proportional to ζ_3. Sample computation times for the different versions of the `Mathematica`-implementation are given in Table 7.4. We computed the full γ_7 for the 32 lowest even integer spins, $M = 2, 4, \dots, 64$. For the next 25 values, $M = 66, 68, \dots, 114$, we computed $\gamma_7^{\text{rat}} + \gamma_7^{\zeta_3}\,\zeta_3$. Finally, we computed γ_7^{rat} for another 88 values, $M = 116, 118, \dots, 290$.

7.3.3 Reconstruction

To reconstruct $\mathcal{P}_{7,\text{ABA}}^{\text{rat}}$, we had 2700 values at hand, but a 4096-dimensional basis. By studying the lower-order results, it became clear that binomial sums of similar type, e.g. $\mathbb{S}_{b,a,a,a,a,c}$, $\mathbb{S}_{a,b,a,a,a,c}$, ..., $\mathbb{S}_{a,a,a,a,b,c}$, appear with identical coefficients. We used this assumption to simplify the ansatz to less than 2700 terms, and indeed it was possible to find

a result that fits the data and predicts the values not used in the construction. Note that the LLL-algorithm is not applicable to this case simply because the dimension of the basis is too large to handle in practice.

All results of transcendentality 6 or lower was reconstructed directly from the QSC results, leaving only $\mathcal{P}_7^{\zeta_3^2}$, $\mathcal{P}_7^{\zeta_5}$, $\mathcal{P}_7^{\zeta_3}$ and $\mathcal{P}_{7,\text{wrap}}^{\text{rat}}$. The 32 values were sufficient to construct the first two using the LLL-algorithm, while 57 values were used for $\mathcal{P}_7^{\zeta_3}$.

The final challenge is $\mathcal{P}_{7,\text{wrap}}^{\text{rat}}$ for which a reduced ansatz of about 1400 binomial sums can be made, while we have 145 available data points. Directly applying the LLL-algorithm turned out not be fruitful in this case. Instead, we found a way to divide the reconstruction even further. Using the relations discussed in appendix B.2, it is always possible to rewrite $\mathbb{S}_{1,I}$ where I is a multi-index as $\mathbb{S}_{I_1}+\mathbb{S}_1\mathbb{S}_{I_2}+\mathbb{S}_1^2\mathbb{S}_{I_3}+\ldots$, where the first index in I_j, which we will call i_1, is not equal to 1. We can then write $\mathcal{P}_{7,\text{wrap}}^{\text{rat}}$ as

$$\mathcal{P}_{7,\text{wrap}}^{\text{rat}} = \sum_{j=0}^{13} \mathbb{S}_1^j \sum_{\substack{|I|=13-j \\ i_1\neq 1}} c_I^{(j)} \mathbb{S}_I \,, \tag{7.33}$$

where $|I|$ is the sum of the indices in I. Assuming that $c_I^{(j)}$ are integers, the combination

$$\mathcal{P}_{7,\text{wrap}}^{\text{rat}} - \sum_{\substack{|I|=13-j \\ i_1\neq 1}} c_I^{(0)} \mathbb{S}_I \tag{7.34}$$

should be divisible by $\mathbb{S}_1$. In fact, the numerator of (7.34) should be divisible by the numerator of $\mathbb{S}_1$. Denoting the numerator of (7.34) by

$$\{\mathcal{P}_{7,\text{wrap}}^{\text{rat}}\} - \sum_{\substack{|I|=13-j \\ i_1\neq 1}} c_I^{(0)} \{\mathbb{S}_I\} \,, \tag{7.35}$$

where $\{\}$ simply denotes multiplication by the common denominator, we can formulate this as the equation

$$\left(\{\mathcal{P}_{7,\text{wrap}}^{\text{rat}}\} \bmod \texttt{Num}[\mathbb{S}_1]\right) - \sum_{\substack{|I|=13-j \\ i_1\neq 1}} c_I^{(0)} \left(\{\mathbb{S}_I\} \bmod \texttt{Num}[\mathbb{S}_1]\right) = d_S^{(0)} \texttt{Num}[\mathbb{S}_1] \,, \tag{7.36}$$

where we consider the terms up their modulus with respect to the numerator of $\mathbb{S}_1$ to get simpler numbers. We here introduced a new set of integers $d_S^{(0)}$. The basis is in this case reduced to 62 binomial sums, i.e. 62 different $c_I^{(0)}$. If we consider our 145 data points, we introduce 145 unknown integers $d_S^{(0)}$. This leaves us with 145 linear equations on 207 unknown integers, and the LLL-algorithm successfully finds a solution to this problem, fixing $\{c_I^{(0)}\}$ in the ansatz (7.33). The next step is to determine $\{c_I^{(1)}\}$ by requiring that

$$\mathcal{P}_{7,\text{wrap}}^{\text{rat}} - \sum_{\substack{|I|=13-j \\ i_1\neq 1}} c_I^{(0)} \mathbb{S}_I - \mathbb{S}_1 \sum_{\substack{|I|=12-j \\ i_1\neq 1}} c_I^{(1)} \mathbb{S}_I \tag{7.37}$$

is divisible by $\mathbb{S}_1^2$, and we successfully continue in this way until all $c_I^{(j)}$ are fixed.

The full result obtained in this way again passes the very non-trivial checks from the BFKL and double-logarithmic limits. The interested reader is referred to [3] and the ancillary data files at arxiv.org for the, very bulky, explicit results.

Subconclusion

In this chapter we have demonstrated the power of the perturbative algorithms of chapter 6 by exploiting them to generate enough data to reconstruct the analytic structure of the six- and seven-loop anomalous dimension of twist-2 operators. This required both optimisation and high-performance computing, and it tested the performance of the methods.

The seven-loop result seems to be the end-station with the currently available techniques. The data collection necessary for the seven-loop reconstruction already pushed the methods to their limits and required a good amount of optimisation and tricks. In addition to the huge basis for the eight-loop result, it also corresponds to double-wrapping, where the intuition from Lüscher corrections used to reduce the basis is no longer available, at least not immediately.

It poses an interesting question to study the analytic structure of other series than the twist-operators in more detail. For example, it would be interesting to study the analytic structure of the new series of length-3 operators described in section 7.1.1 and also that of *all* length-3 operators in the $\mathfrak{sl}(2)$ sector and not just the single series that has previously been studied.

The solutions to the asymptotic Bethe equations for the twist-series are expressible in terms of hypergeometric functions, not just at the leading order, see [138, 139][4]. It would be interesting to understand the connection in more detail, and whether it is possible to solve the QSC perturbatively in terms of such functions, thus not relying on the principle of maximal transcendentality and the other assumptions used in this chapter.

[4]The PhD thesis of Stefan Zieme contains even further attempts in this direction.

Chapter 8

QSC with Q-operators?

In addition to its elegance, the QSC has proven its worth as a practically useful formulation of the AdS/CFT spectral problem. But can we get more information out of it? Let us repeat the dilatation operator eigenproblem:

$$D\,\mathcal{O} = \Delta\,\mathcal{O}\,. \tag{8.1}$$

So far, the QSC has told us something about the eigenvalues Δ, but it is natural to wonder if it also tells us something about the eigenstates and the dilatation operator itself. The question is how the QSC lifts from the eigenvalue level to the operatorial level.

Where do we start? There is no known R-matrix for the AdS/CFT integrable system. However, at the leading order the the R-matrix should be equivalent to that of the XXX spin chain. In chapter 2, we discussed the operatorial formulation of the Q-system for this model. Can we take this as an input and use the QSC to generate perturbative corrections to the Q-operators, just as we did for the Q-functions?

First, we need to master the leading order. In chapter 2, we saw that in the non-compact case the evaluation of explicit Q-operator matrix elements is not directly manageable due to inner products in the infinite-dimensional physical spaces. This chapter summarises the findings of [6], where this technicality was overcome by providing a general prescription for the explicit evaluation of Q-operators for non-compact super spin chains. We will then discuss the possibility of using this as an input for calculations of perturbative corrections to Q-operators of the $\mathrm{AdS}_5/\mathrm{CFT}_4$ integrable system via the QSC.

8.1 Evaluating Q-operators for non-compact super spin chains

Let us recall the construction of Q-operators introduced in chapter 2. For $\mathfrak{u}(N,M|K)$, the Q-operators are labelled by a set $J \subset \{1,2,\ldots,N+M+K\}$ and given by

$$\mathcal{Q}_J(z) = \left(\prod_{j\in J} \mathsf{x}_j^{(-1)^{p_j+1}z}\right) \widehat{\mathrm{str}}_{\mathcal{A}}\left(\mathcal{L}_J^{(1)}\cdots\mathcal{L}_J^{(L)}\right), \tag{8.2}$$

where the Lax operators are given by

$$\mathcal{L}_J(z) \;=\; e^{\sum(\text{-}1)^{p_j+p_j p_{\bar{j}}}\bar{\boldsymbol{\xi}}_{j\bar{j}}\bar{\boldsymbol{\chi}}_{\bar{j}}\boldsymbol{\chi}_j}\left[z+1-\frac{C}{2}-\frac{\sum(\text{-}1)^{p_j}}{2}\right]_{\sum\bar{\boldsymbol{\chi}}_{\bar{j}}\boldsymbol{\chi}_{\bar{j}}} e^{-\sum(\text{-}1)^{p_j+p_{\bar{j}}+p_j p_{\bar{j}}}\boldsymbol{\xi}_{j\bar{j}}\bar{\boldsymbol{\chi}}_j\boldsymbol{\chi}_{\bar{j}}}\,. \tag{8.3}$$

The auxiliary space oscillators satisfy the algebra

$$\boldsymbol{\xi}_{a\bar{a}}\bar{\boldsymbol{\xi}}_{b\bar{b}}-(\text{-}1)^{(p_a+p_{\bar{a}})(p_b+p_{\bar{b}})}\bar{\boldsymbol{\xi}}_{b\bar{b}}\boldsymbol{\xi}_{a\bar{a}}=\delta_{ab}\delta_{\bar{a}\bar{b}}\,, \tag{8.4}$$

while $E_{mn}=\bar{\boldsymbol{\chi}}_m\boldsymbol{\chi}_n$ is the Jordan-Schwinger oscillator realisation of $\mathfrak{u}(N,M|K)$, cf. (1.16).

It is clear from the construction that Q-operators act block-diagonally and only mixes states with the same quantum numbers. Our goal is to evaluate Q-operators as explicit matrices acting on these subspaces, which we refer to as magnon blocks.

Strategy

Our strategy to evaluate Q-operators can be split into four steps:

1 Understand which single-site vectors are present in the chosen magnon block.

2 Evaluate matrix elements of single-indexed Lax operators on this basis.

3 Evaluate single-indexed Q-operators by tracing over the infinite-dimensional auxiliary space.

4 Use QQ-relations to generate the full Q-system.

Step 1 is a simple combinatorial exercise. Step 2 turns out to be the hard part, and it involves a significant amount of gymnastics with special functions. Step 3 is a somewhat simpler exercise in evaluating infinite sums over a restricted set of functions. Step 4 is a similar challenge, but one that we have already mastered: the Ψ-operation, only this time on a slightly more general basis due to the twisting.

Magnon blocks

Let us say that we want to consider $\mathcal{N}=4$ SYM states with quantum numbers $n=[0,1|2,1,1,0|1,0]$, which through $C=0$ fixes the length to $L=2$. Note that there is no need to specify the grading as the symmetry is broken by the twists. There are six possible ways to distribute the oscillators on a length-two tensor product:

$$(\mathcal{D}_{12}\mathcal{Z})\mathcal{X}\qquad\mathcal{X}(\mathcal{D}_{12}\mathcal{Z})\qquad(\mathcal{D}_{12}\mathcal{X})\mathcal{Z}\qquad\mathcal{Z}(\mathcal{D}_{12}\mathcal{X})\qquad\Psi_{11}\bar{\Psi}_{42}\qquad\bar{\Psi}_{42}\Psi_{11} \tag{8.5}$$

where e.g. $(\mathcal{D}_{12}\mathcal{Z})\mathcal{X}=\mathbf{a}_1^\dagger\mathbf{b}_2^\dagger\mathbf{f}_1^\dagger\mathbf{f}_2^\dagger|0\rangle\otimes\mathbf{f}_1^\dagger\mathbf{f}_3^\dagger|0\rangle$ and $\Psi_{11}\bar{\Psi}_{42}=\mathbf{a}_1^\dagger\mathbf{f}_1^\dagger|0\rangle\otimes\mathbf{b}_2^\dagger\mathbf{f}_1^\dagger\mathbf{f}_2^\dagger\mathbf{f}_3^\dagger|0\rangle$. Note that at this stage we are discussing spin chain configurations and not single-trace operators, so

we do not impose cyclicity. We discuss cyclicity in section 8.2.1. The possible length-two operators (8.5) contain six different single-field configurations:

$$\mathcal{Z} \qquad \mathcal{D}_{12}\mathcal{Z} \qquad \mathcal{X} \qquad \mathcal{D}_{12}\mathcal{X} \qquad \Psi_{11} \qquad \bar{\Psi}_{42} \tag{8.6}$$

Whereas (8.5) is the basis on which we want to evaluate the Q-operators, (8.6) is the space on which we want to evaluate our Lax operators.

In general, it is a simple combinatorial exercise to decompose a set of oscillator numbers into all possible states in the magnon block.

8.1.1 Matrix elements of $\mathfrak{sl}(2)$ Lax operators

As discussed in chapter 2, we are facing the problem that the matrix elements of Lax operators seem to involve infinite sums caused by the non-truncating exponentials. Let us see how this can be overcome in the simplest example, $\mathfrak{sl}(2)$. We consider the representation with $C = -1$, which is often referred to as spin $-\frac{1}{2}$, though this restriction is not important below. Again using the redefined spectral parameter $z = \mathbb{i}u - \frac{1}{2}$, the four $\mathfrak{sl}(2)$ Lax operators are

$$\mathcal{L}_{\emptyset} = \left[z+\tfrac{3}{2}\right]_{-1} = -\frac{1}{z+\frac{1}{2}} \tag{8.7a}$$

$$\mathcal{L}_{\{1\}} = e^{\bar{\boldsymbol{\xi}}_{12}\mathbf{a}^\dagger\mathbf{b}^\dagger}\,[z+1]_{n_\mathbf{a}}\,e^{\boldsymbol{\xi}_{12}\mathbf{ab}} \tag{8.7b}$$

$$\mathcal{L}_{\{2\}} = e^{-\bar{\boldsymbol{\xi}}_{21}\mathbf{ab}}\,[z+1]_{-1-n_\mathbf{b}}\,e^{-\boldsymbol{\xi}_{21}\mathbf{a}^\dagger\mathbf{b}^\dagger} \tag{8.7c}$$

$$\mathcal{L}_{\{1,2\}} = \left[z+\tfrac{1}{2}\right]_0 = 1\,. \tag{8.7d}$$

The $\mathfrak{sl}(2)$ Hilbert space has an orthonormal basis, $\langle n|m\rangle = \delta_{nm}$, of states $|m\rangle \equiv \frac{1}{m!}(\mathbf{a}^\dagger\mathbf{b}^\dagger)^m|0\rangle$. Let us try to evaluate an arbitrary matrix element, $\langle n|\mathcal{L}_J|m\rangle$, for the two non-trivial cases, $\mathcal{L}_{\{1\}}$ and $\mathcal{L}_{\{2\}}$.

The truncating Lax

Let us start with $\mathcal{L}_{\{1\}}$, for which the exponentials clearly truncate. In the following, we use a number of identities for Pochhammer symbols which are summarised in appendix B.4.1. Denoting $\boldsymbol{\xi} = \boldsymbol{\xi}_{12}$, the inner product of $\mathcal{L}_{\{1\}}$ with two arbitrary states is

$$\begin{aligned}\langle n|\mathcal{L}_{\{1\}}|m\rangle &= \langle n|\sum_{k_1=0}^{\infty}\frac{(\bar{\boldsymbol{\xi}}\mathbf{a}^\dagger\mathbf{b}^\dagger)^{k_1}}{k_1!}[z+1]_{n_\mathbf{a}}\sum_{k_2=0}^{\infty}\frac{(\boldsymbol{\xi}\mathbf{ab})^{k_2}}{k_2!}|m\rangle \\ &= \sum_{k_1=0}^{n}\sum_{k_2=0}^{m}\binom{n}{k_1}\binom{m}{k_2}\bar{\boldsymbol{\xi}}^{k_1}\boldsymbol{\xi}^{k_2}[z+1]_{m-k_2}\delta_{n-k_1,m-k_2}\,. \end{aligned}\tag{8.8}$$

At this stage we choose to write the auxiliary space oscillators according to

$$\begin{aligned}\bar{\boldsymbol{\xi}}^a\boldsymbol{\xi}^b &= \bar{\boldsymbol{\xi}}^{\Theta(a-b)}[\mathbf{N}-\min_{a,b}+1]_{\min_{a,b}}\boldsymbol{\xi}^{\Theta(b-a)} \\ &= \bar{\boldsymbol{\xi}}^{\Theta(a-b)}(\text{-}1)^{\min_{a,b}}[\text{-}\mathbf{N}]_{\min_{a,b}}\boldsymbol{\xi}^{\Theta(b-a)}\,, \end{aligned}\tag{8.9}$$

where $\Theta(a-b) \equiv \max_{a-b,0}$. We then get

$$\langle n|\mathcal{L}_{\{1\}}|m\rangle = \bar{\boldsymbol{\xi}}^{\Theta(n-m)} \sum_{k=0}^{\min_{n,m}} (\text{-}1)^k \binom{n}{\min_{n,m}-k} \binom{m}{\min_{n,m}-k} [\text{-}\mathbf{N}]_k [z+1]_{\min_{n,m}-k} \boldsymbol{\xi}^{\Theta(m-n)} . \tag{8.10}$$

This is a nice expression for a general matrix element that is very easy to evaluate in practice. However, let us note that we can also write it in terms of a hypergeometric function:

$$\begin{aligned}\langle n|\mathcal{L}_{\{1\}}|m\rangle &= \bar{\boldsymbol{\xi}}^{\Theta(n-m)} [z+1]_{\min_{n,m}} \binom{\max_{n,m}}{\min_{n,m}} \sum_{k=0}^{\min_{n,m}} \frac{[-\mathbf{N}]_k [-\min_{m,n}]_k [-\min_{m,n}]_k}{[|m-n|+1]_k [-z-\min_{n,m}]_k} \frac{1^k}{k!} \boldsymbol{\xi}^{\Theta(m-n)} \\ &= \bar{\boldsymbol{\xi}}^{\Theta(n-m)} [z+1]_{\min_{n,m}} \binom{\max_{n,m}}{\min_{n,m}} {}_3F_2\left(\begin{matrix}-\mathbf{N}, -\min_{m,n}, -\min_{m,n} \\ |m-n|+1, -z-\min_{n,m}\end{matrix}; 1\right) \boldsymbol{\xi}^{\Theta(m-n)} .\end{aligned} \tag{8.11}$$

Definitions and identities for hypergeometric functions are collected in appendix B.4.

The non-truncating Lax

We can proceed in the same way to rewrite a generic matrix element of $\mathcal{L}_{\{2\}}$. Denoting $\boldsymbol{\xi} = \boldsymbol{\xi}_{21}$, we get

$$\langle n|\mathcal{L}_{\{2\}}|m\rangle = \langle n| \sum_{k_1=0}^{\infty} \frac{(\text{-}\bar{\boldsymbol{\xi}}\mathbf{ab})^{k_1}}{k_1!} [z+1]_{-1-n_{\mathbf{b}}} \sum_{k_2=0}^{\infty} \frac{(\text{-}\boldsymbol{\xi}\mathbf{a}^\dagger\mathbf{b}^\dagger)^{k_2}}{k_2!} |m\rangle \tag{8.12}$$

$$\begin{aligned}&= \bar{\boldsymbol{\xi}}^{\Theta(m\text{-}n)} \sum_{k=0}^{\infty} (\text{-}1)^{n+m+k} \binom{\max_{n,m}+k}{n} \binom{\max_{n,m}+k}{m} [\text{-}\mathbf{N}]_k [z+1]_{\text{-}1\text{-}\max_{n,m}\text{-}k} \boldsymbol{\xi}^{\Theta(n\text{-}m)} \\ &= \bar{\boldsymbol{\xi}}^{\Theta(m\text{-}n)} \frac{(\text{-}1)^{\min_{n,m}+1}}{[z+1]_{\max_{n,m}+1}} \binom{\max_{n,m}}{\min_{n,m}} \sum_{k=0}^{\min_{n,m}} \frac{[\text{-}\mathbf{N}]_k [\max_{m,n}+1]_k [\max_{m,n}+1]_k}{[|m-n|+1]_k [-z+\max_{n,m}+1]_k} \frac{1^k}{k!} \boldsymbol{\xi}^{\Theta(n\text{-}m)} \\ &= \bar{\boldsymbol{\xi}}^{\Theta(m\text{-}n)} \frac{(\text{-}1)^{\min_{n,m}+1}}{[z+1]_{\max_{n,m}+1}} \binom{\max_{n,m}}{\min_{n,m}} {}_3F_2\left(\begin{matrix}\text{-}\mathbf{N}, \max_{m,n}+1, \max_{m,n}+1 \\ |m-n|+1, -z+\max_{n,m}+1\end{matrix}; 1\right) \boldsymbol{\xi}^{\Theta(n\text{-}m)} .\end{aligned}$$

We seem to have reached a dead end: an infinite sum that appears not to truncate. However, after searching the textbooks on hypergeometric functions, one finds the relation (B.48), which allows to replace the encountered hypergeometric function by one where the sums do in fact truncate:

$$\begin{aligned}\langle n|\mathcal{L}_{\{2\}}|m\rangle &= \text{-}\bar{\boldsymbol{\xi}}^{\Theta(n\text{-}m)} \binom{\max_{n,m}}{\min_{n,m}} \frac{[z+1]_{\min_{n,m}}}{[-z+\mathbf{N}-\min_{n,m}]_{m+n+1}} {}_3F_2\left(\begin{matrix}\text{-}\mathbf{N}, -\min_{m,n}, -\min_{m,n} \\ |m-n|+1, -z-\min_{n,m}\end{matrix}; 1\right) \boldsymbol{\xi}^{\Theta(m\text{-}n)} \\ &= -\frac{\langle m|\mathcal{L}_{\{1\}}|n\rangle}{[-z+\mathbf{N}-\min_{n,m}]_{m+n+1}} .\end{aligned} \tag{8.13}$$

We have not only succeeded in writing the matrix element of $\mathcal{L}_{\{2\}}$ as a finite sum of rational terms in z and $\mathbf{N}$, we also see that it has a very simple relation to the matrix element of $\mathcal{L}_{\{1\}}$.

A more general approach

We reached our goal for $\mathfrak{sl}(2)$, but we could have proceeded in a different way. Let us consider the single-indexed $\mathfrak{gl}(2)$ Lax operator more generally. We can in general rewrite it as ($n_{\boldsymbol{\chi}} \equiv \bar{\boldsymbol{\chi}}\boldsymbol{\chi}$)

$$\begin{aligned}\mathcal{L}_{\{a\}} &= e^{\bar{\boldsymbol{\xi}}\bar{\boldsymbol{\chi}}_{\bar{a}}\boldsymbol{\chi}_a}\,[z+1]_{n_{\boldsymbol{\chi}_{\bar{a}}}}\,e^{-\boldsymbol{\xi}\bar{\boldsymbol{\chi}}_a\boldsymbol{\chi}_{\bar{a}}} \\ &= \sum_{m=-\infty}^{\infty}\frac{1}{|m|!}\left(\bar{\boldsymbol{\xi}}\bar{\boldsymbol{\chi}}_{\bar{a}}\boldsymbol{\chi}_a\right)^{\Theta(m)}[z+1]_{n_{\boldsymbol{\chi}_{\bar{a}}}}\,{}_3F_2\left(\begin{matrix}-\mathbf{N},-n_{\boldsymbol{\chi}_{\bar{a}}},n_{\boldsymbol{\chi}_a}+1\\ |m|+1,-z-n_{\boldsymbol{\chi}_{\bar{a}}}\end{matrix};1\right)\left(\text{-}\boldsymbol{\xi}\bar{\boldsymbol{\chi}}_a\boldsymbol{\chi}_{\bar{a}}\right)^{\Theta(-m)}.\end{aligned} \tag{8.14}$$

For a specific matrix element, only one term in the outer sum over m is nonzero. The question is how to evaluate the hypergeometric function in general.

The only case where the hypergeometric function does not truncate immediately is when the c-gradings are $c_a = 0$ and $c_{\bar{a}} = 1$, i.e. $n_{\boldsymbol{\chi}_a} \geq 0$ and $n_{\boldsymbol{\chi}_{\bar{a}}} \leq -1$. In this case we can use the Euler integral transform (B.47) to rewrite the hypergeometric function:

$${}_3F_2\left(\begin{matrix}\text{-}\mathbf{N},\text{-}n_{\boldsymbol{\chi}_{\bar{a}}},n_{\boldsymbol{\chi}_a}+1\\ |m|+1,-z-n_{\boldsymbol{\chi}_{\bar{a}}}\end{matrix};1\right) = \frac{\Gamma(-z-n_{\boldsymbol{\chi}_{\bar{a}}})}{\Gamma(-n_{\boldsymbol{\chi}_{\bar{a}}})\Gamma(-z)}\int_0^1 \mathrm{d}t\; t^{-n_{\boldsymbol{\chi}_{\bar{a}}}}(1-t)^{-z-1}\;{}_2F_1\left(\begin{matrix}\text{-}\mathbf{N},n_{\boldsymbol{\chi}_a}+1\\ |m|+1\end{matrix};t\right). \tag{8.15}$$

Next, we can do an Euler transform (B.46) on the ${}_2F_1$:

$${}_2F_1\left(\begin{matrix}-\mathbf{N},n_{\boldsymbol{\chi}_a}+1\\ |m|+1\end{matrix};t\right) = (1-t)^{|m|+\mathbf{N}-n_{\boldsymbol{\chi}_a}}\;{}_2F_1\left(\begin{matrix}|m|+1-\mathbf{N},|m|-n_{\boldsymbol{\chi}_a}\\ |m|+1\end{matrix};t\right). \tag{8.16}$$

Due to the structure (8.14), we will always have $|m| - n_{\boldsymbol{\chi}_a} \leq 0$, so the hypergeometric function on the right hand side is a truncating sum:

$${}_2F_1\left(\begin{matrix}|m|+1-\mathbf{N},|m|-n_{\boldsymbol{\chi}_a}\\ |m|+1\end{matrix};t\right) = \sum_{k=0}^{n_{\boldsymbol{\chi}_a}-|m|}\frac{[|m|+1+\mathbf{N}]_k[|m|-n_{\boldsymbol{\chi}_a}]_k}{[|m|+1]_k}\frac{t^k}{k!}. \tag{8.17}$$

The integration over t is now more transparent, and by realising that it is simply a Beta-function, cf. (B.44), we can see that it yields

$$\int_0^1 \mathrm{d}t\; t^{k-n_{\boldsymbol{\chi}_{\bar{a}}}-1}(1-t)^{-z-1+|m|+\mathbf{N}-n_{\boldsymbol{\chi}_a}} = \frac{\Gamma(k-n_{\boldsymbol{\chi}_{\bar{a}}})\Gamma(-z+|m|+\mathbf{N}-n_{\boldsymbol{\chi}_a})}{\Gamma(-z+k+|m|+\mathbf{N}-n_{\boldsymbol{\chi}_a}-n_{\boldsymbol{\chi}_{\bar{a}}})}. \tag{8.18}$$

Putting all this together, we have achieved to rewrite (8.14) in terms of a finite sum over Pochhammer symbols. This method might seem cumbersome, but it turns out to be applicable more generally than the more direct strategy given for $\mathfrak{sl}(2)$ above.

8.1.2 Matrix elements of single-indexed Lax operators for $\mathfrak{u}(N,M|K)$

When we increase the rank of the algebra, we may encounter more than one non-truncating sum in the Lax operators. Furthermore, the exponential factors in the Lax operators (8.3)

can contain a sum of oscillator combinations where the different terms can combine to one overall term in several ways. For example, a two-indexed $\mathfrak{u}(2,2)$ Lax operator would be

$$\mathcal{L}_{\{1,3\}} = e^{-\boldsymbol{\xi}_{12}\mathbf{b}_2\mathbf{b}_1^\dagger+\boldsymbol{\xi}_{14}\mathbf{a}_2^\dagger\mathbf{b}_1^\dagger-\boldsymbol{\xi}_{32}\mathbf{b}_2\mathbf{a}_1+\boldsymbol{\xi}_{34}\mathbf{a}_2^\dagger\mathbf{a}_1} \ \dots \ , \tag{8.19}$$

and we see that the power expansion of the exponential will produce e.g. the term $\mathbf{b}_1^\dagger\mathbf{b}_2\mathbf{a}_1\mathbf{a}_2^\dagger$ in multiple ways. This extra complication is however absent in the single-indexed Lax operators, and we will focus on these. Note that the Lax operators with all but one index have the same property.

To avoid overloading the reader with technical details, we will leave out the explicit treatment of the general $\mathfrak{u}(N,M|K)$ case and refer the interested reader to [6], where it is discussed in detail. Let us simply sketch the strategy. One can rewrite a general Lax operator similarly to (8.14), but this time there will be more than one summation in the middle part. One of these sums can be expressed as a hypergeometric function, ${}_3F_2$. The arguments of this function will however contain the other summation variables, and though we could apply the formula (B.48), it would not be very beneficial in this case. Instead, an integral transform as in (8.15) can be used to disentangle the summation variables and express the middle part as a generalised version of (8.15) where the integral is over a product of ${}_2F_1$'s. This integration can be carried out along the same lines as above to yield a finite sum expression for the single-indexed Lax operators that is explicitly rational in both the spectral parameter and the auxiliary space number operators.

In conclusion, we have a recipe to compute matrix elements of the single-indexed Lax operators for arbitrary $\mathfrak{u}(N,M|K)$.

8.1.3 Tracing over the auxiliary space

So far, so good: we have managed to write the matrix elements of Lax operators as rational functions in z and the auxiliary space number operators $\mathbf{N}_{jk}$. To get the Q-operators we need to evaluate supertraces over the auxiliary space,

$$\widehat{\mathrm{str}}_{\mathcal{A}}\,(f) = \frac{\mathrm{str}_{\mathcal{A}}\left(\prod_{j,k=1,j\neq k}^{N+M+K}\left(\frac{\mathsf{x}_j}{\mathsf{x}_k}\right)^{\mathbf{N}_{jk}} f\right)}{\mathrm{str}_{\mathcal{A}}\left(\prod_{j,k=1,j\neq k}^{N+M+K}\left(\frac{\mathsf{x}_j}{\mathsf{x}_k}\right)^{\mathbf{N}_{jk}}\right)}\,. \tag{8.20}$$

Recall the discussion of the structure of the representation in the auxiliary space in section 2.3.2. For $\mathfrak{u}(N,M|K)$ the space is a tensor product of $(N{+}M{+}K)(N{+}M{+}K{-}1)$ individual oscillator spaces $|0\rangle_{ab}$ with $a \neq b$. The trace over each of these spaces corresponds to an infinite sum $\sum_{\mathbf{N}_{ab}=0}^{\infty}$. We have to evaluate $(N+M+K)(N+M+K-1)$ sums, though many of them are trivial since the corresponding oscillator is absent in the Lax operator in question.

We start from a rational expression in the number operators, i.e. in principle two types of terms:

$$\mathbf{N}^k\,, \qquad \frac{1}{(\mathbf{N}+r)^k}\,. \tag{8.21}$$

We already discussed how to trace over a monomial expression in section 2.3.3, and the supertrace is similar. The supertrace over negative powers will introduce a new type of function, the Lerch transcendents, which are related to a twisted version of η-functions,

$$\Phi^{\mathsf{x}}_k(r) \equiv \sum_{j=0}^{\infty} \frac{\mathsf{x}^j}{(r+j)^k} = \mathbb{i}^k\, \eta^{\mathsf{x}}_k(\mathbb{i}r)\,. \tag{8.22}$$

Subsequent sums will then, in addition to (8.21), be over terms of the kind

$$\mathbf{N}^k \Phi^{\mathsf{x}}_l(\mathbf{N}+r)\,. \tag{8.23}$$

As we explain in appendix C.2, where we summarise all explicit formulas needed to evaluate normalised supertraces (8.20), the result of such a sum is simply a linear combination of terms of the three types (8.21) and (8.23). This is in perfect agreement with what we have seen in subsequent chapters: the Q-functions are all expressed in terms of rational functions and η-functions in the spectral parameter.

8.1.4 The full Q-system from the lowest level

Having the single-indexed Q-operators at hand, we have reached the final step in our strategy: using QQ-relations to get the rest.

To get $\mathcal{Q}_{\{a,b\}}$ with $p_a \neq p_b$ we need to solve the first order difference equation

$$\mathcal{Q}_{\{a\}}(z)\mathcal{Q}_{\{b\}}(z) \;\propto\; \mathcal{Q}_{\{a,b\}}(z+\tfrac{1}{2})\mathcal{Q}_{\emptyset}(z-\tfrac{1}{2}) - \mathcal{Q}_{\{a,b\}}(z-\tfrac{1}{2})\mathcal{Q}_{\emptyset}(z+\tfrac{1}{2})\,. \tag{8.24}$$

In our current conventions (8.3), the structure of $\mathcal{Q}_{\emptyset}$ is

$$\mathcal{Q}_{\emptyset} \propto \mathbb{I} \prod_{j=1}^{|C|} \left(z - \frac{|C|}{2} + j\right)^{\mathrm{sign}(C)\,L}\,, \tag{8.25}$$

but we can always use the symmetries of the Q-system, in particular the rescalings (4.21), to set $\mathcal{Q}_{\emptyset} = \mathbb{I}$. Then, as discussed in section 4.2.1, $\mathcal{Q}_{\{a,b\}}$ with $p_a \neq p_b$ takes the simple form

$$\mathcal{Q}_{\{a,b\}}(z) \propto \Psi\left(\mathcal{Q}_{\{a\}}(z+\tfrac{1}{2})\mathcal{Q}_{\{b\}}(z+\tfrac{1}{2})\right)\,, \tag{8.26}$$

where $\Psi\left(f(z) - f(z+1)\right) = f(z)$. The action of Ψ on the twisted basis of functions is discussed in appendix C.1.2, and it is a direct generalisation of the untwisted case.

We can generate the remaining Q-system via determinant formulas similar to those those described in section 4.2.1. In fact, we can use exactly the same formulas (4.28) if we are careful with the normalisation of the Q-operators. Generating the expected value of $\mathcal{Q}_{\bar{\emptyset}}$ in this way is a very non-trivial check that a given set of single-indexed Q-operators are indeed solutions of the Q-system.

8.2 Q-operators in the Quantum Spectral Curve

The conclusion of the above section is that we are able to explicitly evaluate Q-operators for the $\mathfrak{u}(2,2|4)$ spin chain, which should be related to the $g \to 0$ limit of the QSC. As an example, the explicit 1-indexed Q-operators for the quantum numbers $n = [0,0|L,L,0,0|0,0]$, corresponding to the BMN vacuum $\mathrm{Tr}(\mathcal{Z}^L)$, are given in [6]. The next step is to try to apply the methods of chapter 6 to generate perturbative corrections to the obtained Q-operators. The attempt to do this is work in progress, and this section simply lists a few comments on the potential procedure. Below, we return to the QSC-language, labelling the Q-operators/functions by $\mathcal{Q}_{A|J}/Q_{A|J}$ and using the spectral parameter $u = -\mathbb{i}z - \frac{\mathbb{i}}{2}$.

8.2.1 The $\mathcal{N} = 4$ SYM Hilbert space

The Q-operator construction described above is for spin-chain states. It does not equate states that are related by cyclic permutations, i.e. $\mathcal{Z}\mathcal{X}$ is a different state than $\mathcal{X}\mathcal{Z}$. In $\mathcal{N} = 4$ SYM, also in the twisted case [150], these states are identical, as they appear within a trace, $\mathrm{Tr}[\mathcal{X}\mathcal{Z}] = \mathrm{Tr}[\mathcal{Z}\mathcal{X}]$. Consequently, the spin chain Hilbert space is larger than that of $\mathcal{N} = 4$ SYM. The question is whether it is natural to work with Q-operators for the full spin chain magnon blocks, or if one should project out the subspace corresponding to cyclic states.

Physical operators in the twisted QSC

Recall that in the QSC all eigenvalues must satisfy the constraint

$$\lim_{u\to 0} \frac{\mu^{(1)}_{ab}(u+\mathbb{i})}{\mu^{(1)}_{ab}(u)} = 1\,. \tag{8.27}$$

The physical solutions are singled out by requiring that $\mu^{(1)}_{ab} \propto Q^{(1)-}_{ab|12}$ such that $Q^{(1)}_{ab|12}$ satisfy the zero-momentum condition

$$\lim_{u\to 0} \frac{Q^{(1)}_{ab|12}(u+\frac{\mathbb{i}}{2})}{Q^{(1)}_{ab|12}(u-\frac{\mathbb{i}}{2})} = 1\,. \tag{8.28}$$

However, for the fully twisted QSC [42], all states generically have nonzero momentum. The fully twisted case includes eight twists that are usually denoted x_1, x_2, x_3, x_4, y_1, y_2, y_3, y_4 subject to the constraints $\prod_{a=1}^4 \mathsf{x}_a = \prod_{i=1}^4 \mathsf{y}_i = 1$, so six independent twists in total. The asymptotics of the single-indexed Q-functions $\mathbf{P}_a \equiv Q_{a|\emptyset}$ and $\mathbf{Q}_i \equiv Q_{\emptyset|i}$ are

$$\mathbf{P}_a \simeq \mathsf{A}_a\, \mathsf{x}_a^{\mathbb{i}u}\, u^{-\check{\lambda}_a} \qquad \mathbf{P}^a \simeq \mathsf{A}^a\, \mathsf{x}_a^{-\mathbb{i}u}\, u^{\check{\lambda}_a} \qquad \mathbf{Q}_j \simeq \mathsf{B}_j\, \mathsf{y}_j^{-\mathbb{i}u}\, u^{-\check{\nu}_j} \qquad \mathbf{Q}^j \simeq \mathsf{B}^j\, \mathsf{y}_j^{\mathbb{i}u}\, u^{\check{\nu}_j}\,, \tag{8.29}$$

with $\check{\lambda}_a = n_{\mathbf{f}_a} + \Lambda$ and $\check{\nu}_j = \{-L - n_{\mathbf{b}_{\dot{\alpha}}}, n_{\mathbf{a}_\alpha}\} - \Lambda$.

The simplest example of a solution is the BMN vacuum, $\mathrm{Tr}(\mathcal{Z}^L)$, for which the central Q-operator (or Q-function, it is a 1×1 matrix) is simply a constant times an exponential factor: $\mathcal{Q}_{12|12} \propto \left(\frac{\mathsf{x}_1\mathsf{x}_2}{\mathsf{y}_1\mathsf{y}_2}\right)^{\mathbb{i}u}$. It is clear that it only satisfies (8.28) in the special case $\frac{\mathsf{x}_1\mathsf{x}_2}{\mathsf{y}_1\mathsf{y}_2}=1$. More generally, the eigenvalues of $\mathcal{Q}^{(1)}_{ab|12}$ behave as

$$Q^{(1)}_{ab|12}\left(-\tfrac{\mathbb{i}}{2}\right) \;=\; e^{\frac{2\mathbb{i}\pi\, m}{L}}\left(\frac{\mathsf{x}_1^{n_{\mathbf{f}_1}}\mathsf{x}_2^{n_{\mathbf{f}_2}}\mathsf{x}_3^{n_{\mathbf{f}_3}}\mathsf{x}_4^{n_{\mathbf{f}_4}}\mathsf{y}_3^{n_{\mathbf{a}_1}}\mathsf{y}_4^{n_{\mathbf{a}_2}}}{\mathsf{y}_1^{L+n_{\mathbf{b}_1}}\mathsf{y}_2^{L+n_{\mathbf{b}_2}}}\right)^{\frac{1}{L}} Q^{(1)}_{ab|12}\left(\tfrac{\mathbb{i}}{2}\right)\,. \tag{8.30}$$

The root of unity $e^{\frac{2\mathbb{i}\pi\, m}{L}}$ where $m\in\{1,2,...,L\}$ is independent of the twist, and corresponds to the shift eigenvalue of the state in the untwisted case. Again, (8.28) can only be satisfied at special values of the twists.

The above discussion shows that it only makes sense to talk about physical solutions to the QSC if the twists have very particular properties. For generic twists, none of the eigenstates have nonzero total momentum, and they thus have no interpretation as cyclic trace operators. There are two ways to proceed. We can keep the full spin chain Hilbert space and try to apply the QSC. One immediate consequence is that the asymptotics of the quantities ω, and thus μ, have to be modified to include exponential terms in order to satisfy (8.27). As discussed in chapter 4, it is not completely understood how to constrain such solutions. The alternative is to put extra constraints on the twists that ensure the existence of physical states. We now discuss this possibility.

Special twists

To satisfy (8.28), the product of the two factors on the right hand side of (8.30) must be 1. If we furthermore want to preserve the same Hilbert space of operators as in the untwisted theory, they should separately be 1. Then the twists must have the additional property

$$\frac{\mathsf{x}_1^{n_{\mathbf{f}_1}}\mathsf{x}_2^{n_{\mathbf{f}_2}}\mathsf{x}_3^{n_{\mathbf{f}_3}}\mathsf{x}_4^{n_{\mathbf{f}_4}}\mathsf{y}_3^{n_{\mathbf{a}_1}}\mathsf{y}_4^{n_{\mathbf{a}_2}}}{\mathsf{y}_1^{L+n_{\mathbf{b}_1}}\mathsf{y}_2^{n_{\mathbf{b}_2}}}=1\,. \tag{8.31}$$

The well-studied γ-deformation of $\mathcal{N}=4$ SYM [150] is exactly of this type. It corresponds to $\mathsf{y}_i=1$ and

$$\mathsf{x}_1 \;=\; \Gamma_1^{n_{\mathbf{f}_4}-n_{\mathbf{f}_3}}\Gamma_2^{n_{\mathbf{f}_2}-n_{\mathbf{f}_4}}\Gamma_3^{n_{\mathbf{f}_2}-n_{\mathbf{f}_3}} \tag{8.32a}$$

$$\mathsf{x}_2 \;=\; \Gamma_1^{n_{\mathbf{f}_3}-n_{\mathbf{f}_4}}\Gamma_2^{n_{\mathbf{f}_3}-n_{\mathbf{f}_1}}\Gamma_3^{n_{\mathbf{f}_4}-n_{\mathbf{f}_1}} \tag{8.32b}$$

$$\mathsf{x}_3 \;=\; \Gamma_1^{n_{\mathbf{f}_1}-n_{\mathbf{f}_2}}\Gamma_2^{n_{\mathbf{f}_4}-n_{\mathbf{f}_2}}\Gamma_3^{n_{\mathbf{f}_1}-n_{\mathbf{f}_4}} \tag{8.32c}$$

$$\mathsf{x}_4 \;=\; \Gamma_1^{n_{\mathbf{f}_2}-n_{\mathbf{f}_1}}\Gamma_2^{n_{\mathbf{f}_1}-n_{\mathbf{f}_3}}\Gamma_3^{n_{\mathbf{f}_3}-n_{\mathbf{f}_2}}\,, \tag{8.32d}$$

where Γ_i are phases. The twists (8.32) have the property $\mathsf{x}_1^{n_{\mathbf{f}_1}}\mathsf{x}_2^{n_{\mathbf{f}_2}}\mathsf{x}_3^{n_{\mathbf{f}_3}}\mathsf{x}_4^{n_{\mathbf{f}_4}}=1$, which ensures that (8.31) is always fulfilled.

The regularity of Q-operators demands that in general all eight twists must differ. To construct such a twist, one idea would be to twist the $\mathfrak{su}(2,2)$ part of the symmetry in analogy to the γ-twist,

$$\mathsf{y}_1 = \Omega_1^{\nu_3-\nu_4}\Omega_2^{\nu_2-\nu_4}\Omega_3^{\nu_2-\nu_3} \tag{8.33a}$$

$$\mathsf{y}_2 = \Omega_1^{\nu_4-\nu_3}\Omega_2^{\nu_3-\nu_1}\Omega_3^{\nu_4-\nu_1} \tag{8.33b}$$

$$\mathsf{y}_3 = \Omega_1^{\nu_2-\nu_1}\Omega_2^{\nu_4-\nu_2}\Omega_3^{\nu_1-\nu_4} \tag{8.33c}$$

$$\mathsf{y}_4 = \Omega_1^{\nu_1-\nu_2}\Omega_2^{\nu_1-\nu_3}\Omega_3^{\nu_3-\nu_2}\,, \tag{8.33d}$$

with the property

$$\mathsf{y}_1^{\nu_1}\mathsf{y}_2^{\nu_2}\mathsf{y}_3^{\nu_3}\mathsf{y}_4^{\nu_4} = \frac{\mathsf{y}_3^{n_{\mathbf{a}_1}+\frac{\gamma}{2}}\mathsf{y}_4^{n_{\mathbf{a}_2}+\frac{\gamma}{2}}}{\mathsf{y}_1^{L+n_{\mathbf{b}_1}+\frac{\gamma}{2}}\mathsf{y}_2^{L+n_{\mathbf{b}_2}+\frac{\gamma}{2}}} = 1\,. \tag{8.34}$$

Note that the dependence on the weights ν_i introduces a coupling constant dependence in the twists y_i through the anomalous dimension γ.

In some sectors, including $\mathfrak{sl}(2)$, the "double γ-twist" obtained by combining (8.32) and (8.33) seems to work fine: all twists are different and (8.31) is guaranteed. However, for some quantum numbers in other sectors, e.g. $n = [0,0|1,1,1,1|0,0]$, coinciding twists do occur, so in the generic case a more general twist satisfying (8.31) should be constructed.

Projecting out the cyclic states

The reduced Hilbert space that we wish to consider is spanned by the states with eigenvalue 1 of the shift operator. Back in section 2.1.1, more precisely in (2.8), we saw how the shift operator acted on the three-dimensional space of $\mathfrak{su}(2)$ states with $L = 3$ and $M = 1$. Only one of these states, $\mathcal{Z}\mathcal{Z}\mathcal{X} + \mathcal{Z}\mathcal{X}\mathcal{Z} + \mathcal{X}\mathcal{Z}\mathcal{Z}$, has eigenvalue 1, so in this case we would keep only this state and throw away the other two. This reduces the corresponding Q-operator from a 3×3 to a 1×1 matrix.

It is plausible that the space spanned by the cyclic states is invariant under the action of the higher-loop Q-operators as well. Indeed, a generalisation of the shift operator belongs to the infinite family of commuting operators that can be generated from the Q-operators.

The point made in this section is that it might be favourable to consider special twists which ensure that a subspace of the eigenstates of the Q-operators are cyclicly invariant, and thus have an interpretation as single-trace operators. The strategy is then to to block-diagonalise the leading Q-operator and pick out the zero-momentum block. This reduced Q-operator should have a preferred role in the Quantum Spectral Curve with simpler analytic properties. In particular, the quantities ω should have constant asymptotics which makes them easier to control in practice.

8.2.2 Perturbation theory with twists and matrices

There is no immediate reason why the general perturbative strategies to solve the QSC presented in sections 6.3 and 6.4 should not be applicable to Q-operators as well. The twists of course pose a new challenge, but this is a technical challenge rather than a conceptual one. In particular, the Ψ-operation is easily generalised to the twisted algebra of functions, see appendix C.1.2.

Ansatz for P

The key input that makes the perturbative algorithms possible is the control of the all-loop structure of $\mathcal{Q}_{a|\emptyset} \equiv \mathbf{P}_a$ and $\mathcal{Q}^{a|\emptyset} \equiv \mathbf{P}^a$. The natural generalisation of the ansatz for $\mathbf{P}$ derived in section 4.3.3 to the fully twisted case is

$$\mathbf{P}_a = \mathsf{x}_a^{+iu}(gx)^{-L-\Lambda}\left(\sum_{k=1}^{\infty}\mathsf{c}_{a,k}\left(\frac{g}{x}\right)^k + \sum_{k=0}^{L-n_{\mathbf{f}_a}}\mathsf{d}_{a,k}\,(gx)^k\right), \tag{8.35a}$$

$$\mathbf{P}^a = \mathsf{x}_a^{-iu}(gx)^{\Lambda}\left(\sum_{k=1}^{\infty}\mathsf{c}^{a,k}\left(\frac{g}{x}\right)^k + \sum_{k=0}^{n_{\mathbf{f}_a}}\mathsf{d}^{a,k}\,(gx)^k\right), \tag{8.35b}$$

with

$$\mathsf{c} = \sum_{j=0}^{\infty}\mathsf{c}^{(j)}g^{2j}, \qquad \mathsf{d} = \sum_{j=0}^{\infty}\mathsf{d}^{(j)}g^{2j}, \tag{8.36}$$

being matrix-valued constants. Again, by expressing (8.35) in u and expanding in g, we get a finite ansatz at any given loop order.

Applying the machinery

The next step is to generate the remaining Q-system by solving a set of coupled first-order difference equations. Section 6.3 and 6.4 explained how to do this for either $\mathcal{Q}_{a|i}$ or μ_{ab}, and the same formulas apply directly here. Once this is done, an expression for $\tilde{\mathbf{P}}$ can be obtained via the relations of the QSC. The crucial requirement is then that the expansions of the obtained values for $\tilde{\mathbf{P}}$ at $u = 0$ are consistent with the ansatz (8.35).

The application of this strategy is left for future work. The only conclusion of the preliminary attempts is that the presence of six twist variables, some of them coupling-dependent, quickly makes the expressions extremely bulky.

Subconclusion

In this final chapter, we initiated the quest to lift the Quantum Spectral Curve to the operatorial level. We managed to get started: we have developed the technology to explicitly generate the full 1-loop operatorial Q-system.

The next step is to make the perturbative calculations work in practice. As this thesis is being written, this is an ongoing endeavour, and a verdict on the success of the approach would be premature. The technical complications of having six twist variables probably means that the scope of the method is limited. Certainly, it seems unlikely that 10-loop corrections to Q-operators can be generated in this way, but the generation of 2- and 3-loop corrections to Q-operators for a variety of simple magnon blocks should be realistic first goals.

If the attempts turn out to be fruitful, it could shed light on the still quite mysterious nature of AdS/CFT integrability. In particular, it would give hints on the structure of Q-operators and transfer matrices at higher loops. It would also provide information about perturbative corrections to the dilatation operator and its eigenstates.

Conclusion

This thesis has been devoted to the spectral problem in planar $\mathcal{N} = 4$ super Yang-Mills theory, and thus in the planar limit of the $\mathrm{AdS}_5/\mathrm{CFT}_4$ correspondence. The ambition was to exploit a recently discovered framework, the Quantum Spectral Curve, to generate explicit perturbative data of previously unseen precision and generality.

We started by classifying the objects in question: symmetry multiplets of single-trace operators. We saw how to characterise these multiplets by Young diagrams, and how to count them using characters.

The anomalous part of the dilatation operator appears to act on the basis of single-trace operators like the Hamiltonian of an integrable model. To handle such objects, we went on a journey into the mathematical structure underlying integrable models: the Bethe ansätze. This framework encodes the information about the model in a Q-system, to which each multiplet corresponds to a solution with particular boundary conditions.

The precise integrable model underlying the AdS/CFT spectrum is not known, but assuming that integrability is an exact property, it is possible to use the large amount of symmetry of the theory to capture the spectrum in a relatively simple mathematical problem via the asymptotic and thermodynamic Bethe ansatz. This information can be further condensed into the Quantum Spectral Curve.

The main result of this thesis are the algorithms to solve the QSC perturbatively outlined in chapter 5 and 6. The algorithms demonstrate that the QSC is an extremely powerful perturbative tool, both in depth and broadness. 10-loop results were reached, and going further is in principle only a question of computer power. A by-product of this effort is a new general way to solve Bethe equations for rational spin chains that is both faster and cleaner than the traditional approaches. The generality of the algorithms allows to explicitly study the full spectrum, in practice at least the first thousands of multiplets in the infinite spectrum. The end-product of the main direction pursued in this thesis is a database of results that will appear with the publication [7].

The obtained results open the possibility of spectral data mining. One well-known pattern in the data is the maximal transcendentality structure of the analytically continued anomalous dimension for twist-2 operators, and we managed to add two new loop orders to this result. A quick inspection of the spectral data gives clear hints that there are many

other similar structures waiting to be analysed.

The perturbative spectrum has so far been a central object in the study of AdS/CFT integrability. This thesis stands on the shoulders of many great achievements to capture the spectrum, and it is an attempt to conclude this long-standing effort by putting the discoveries to work and demonstrating their practical power in full generality. With an automatised solution algorithm that applies to all corners of the spectrum, we can finally call the problem solved with more confidence.

The potential of the QSC is not only perturbative. Its non-perturbative abilities are perhaps even more remarkable. It would be interesting to implement the numerical algorithm [114] in complete generality and study the behaviour at quantum numbers where multiple solutions to the equations exist. A systematic algorithm to solve the QSC analytically in the strong coupling limit is also still missing. Even perturbatively, it is still not completely clear how to treat unphysical solutions to the equations. It is known that exponentially growing asymptotic behaviour should be allowed, see e.g. [111], but a systematic understanding of how to completely constrain the solutions is still lacking. Such an understanding would for example allow a study of the double-logarithmic limit. Hopefully, the explicit solutions in different regimes can provide the intuition needed to obtain exact analytic results valid at any coupling, which would provide the ultimate solution to the spectral problem.

The impressive control of the spectrum of anomalous dimensions is not the final destination of AdS/CFT integrability. It is only the beginning. We need to fully understand how to apply integrability to other quantities than the spectrum, such as structure constants. We also need to understand the deeper nature of AdS/CFT integrability. We have to prove that integrability is in fact an exact property of planar AdS/CFT, and we also need to understand more deeply what the integrable model is itself.

Using the QSC to study perturbative corrections to Q-operators is one direction that could give us new hints about the integrable model and how it fits into the algebraic Bethe ansatz. This thesis outlined the initiation of this effort by providing an explicit strategy to generate the leading Q-operators. It remains to be seen how much the QSC is willing to reveal about higher orders, but surely there are lessons to be learned by attempting to use it on the operatorial level.

For all these efforts to be worthwhile, we should of course attempt to generalise the methods to more realistic theories. We should understand which properties are special to $\mathcal{N} = 4$ SYM and which are simpler versions of features common to more general theories. If we get a better understanding of the nature of AdS/CFT integrability, we might be able to answer these questions more precisely.

Many ambitious attempts are already being made to attack the open problems outlined here. The study of three- [151] and four-point functions [152] is currently undergoing a

revolution similar to the developments for two-point functions. An interesting attempt to investigate what happens to the integrability structures in more general settings is being made in the study of conformal defects in the AdS/CFT set-up [153]. Here, one-point functions seem to display higher-loop integrability [154]. The study of a simple integrable quantum field theory that appears in a double-scaling limit of γ-deformed $\mathcal{N} = 4$ SYM [155] could be the key to understanding how integrability can appear in four-dimensional theories. Finally, the study of other integrable systems, in particular the $\mathrm{AdS}_3/\mathrm{CFT}_2$ correspondence where the integrability program is steadily progressing [156], can give us a more general understanding of the phenomenon of AdS/CFT integrability.

One thing is for sure: AdS/CFT integrability has given rise to a hope for more powerful tools to analyse quantum field theories. The explicit tools on which this thesis is based hopefully encourage the search for similar structures in the physics of the real world. Even if such a connection is never made, the author has thoroughly enjoyed exploring the fascinating Riemann sheets of the Quantum Spectral Curve.

Acknowledgements

Many people deserve to be thanked for their help and support which made my three and a half years as a PhD student a rather enjoyable and positive experience.

First of all, I thank Dmytro Volin, under whose supervision I have always felt very fortunate. It has been a privilege to be taught by and collaborate with someone with such a deep intuition that only comes from a true passion for physics. I thank Dima both for guiding me, but also for letting me take responsibility and allowing me to go my own ways. I also thank him for countless invaluable comments on this thesis. I am certain Dima will supervise far greater students in the future, and I feel lucky to be the first in that line.

I thank Vitaly Velizhanin, Rouven Frassek, David Meidinger and Leonard Zippelius for collaboration on various projects, many discussions, and for their patience with me. I am also grateful to David for comments on this manuscript.

I warmly thank everyone in the School of Mathematics at Trinity College Dublin, not least Emma, Helen and Karen in the administrative office, for making my time here great. I thank my fellow students/postdocs Argia, Ben, Cian, 3×David, Francesco, George, Hanna, Kiko, Lorenzo, Mark, Martijn, Nicolas, Philipp, 2×Robert, Tim, Vanessa and Yushen/Jeff for many good moments, pints, burritos, glorious 5-a-side defeats, and discussions about black holes. A special thank you goes to Philipp Hähnel to whom I am deeply indebted for always promptly helping me out, whether I needed a sharp eye to read through drafts or test run `Mathematica`-codes.

The second year of my PhD was spent in Adlershof, at Humboldt Universität zu Berlin. I am grateful to Matthias Staudacher for this opportunity and for guidance and discussions throughout that year. I thank the entire group, in particular my fellow students Brenda, David, Dennis, Edoardo, Gregor, Hagen, Israel Ramírez (who I also thank for useful comments on the manuscript), Josua, Laura, Leo, Lorenzo, Matthias, Nils, Pavel, Sourav and Wadim for being exceptional officemates, for always exciting trips to the Mensa, and for countless table tennis matches.

I thank the theoretical high energy physics group at the Niels Bohr Institute, in particular Charlotte Kristjansen and her research group, for warm hospitality on several occasions. I also thank Didina Serban and Ivan Kostov for the kind invitations to visit IPhT in Saclay in May and October-November 2016, and for their warm hospitality during

these visits.

I am perhaps the single person who has benefitted the most from the training network *Gauge Theory as an Integrable System*[1]. My PhD would have been a much less enriching experience without GATIS, who not only funded my stay in Berlin, but also made it possible for me to take part in conferences, schools and workshops all over Europe. The month I spent in the french alps during the *Les Houches school on integrability* in June 2016 was the absolute highlight.

Apart from the people mentioned above, I wish to thank Misha Alfimov, Andrea Cavaglià, Frank Coronado, Burkhard Eden, Sergey Frolov, Kolya Gromov, Volodya Kazakov, Rob Klabbers, Fedor Levkovich-Maslyuk, Pedro Liendo, Tristan McLoughlin, Alessandro Sfondrini, Christoph Sieg, Grisha Sizov, Ryu Suzuki, Stijn van Tongeren, Pedro Vieira and Stefan Zieme for enlightening discussions that helped shape my scientific understanding.

I thank my friends, not least my housemates in Bridgewater Quay, for putting up with me over the years. I am grateful and indebted to Carmen, Argia and Daniele for their continuous support, especially during the last year where I was quite poor company.

Finally, I wish to thank my family for their unlimited support throughout all stages of this process. Had the quality of this thesis been high enough, it would have been dedicated to you.

[1]People Programme (Marie Curie Actions) of the European Union's Seventh Framework Programme FP7/2007-2013/ under REA Grant Agreement No 317089 (GATIS).

Appendix A

Miscellanea

In this appendix we collect various technical details that supplement the main text.

A.1 Quantum number dictionary

We here provide a dictionary between the oscillator numbers n and often encountered parametrisations of the quantum numbers in the literature.

S^5 and AdS_5 spins: J, S and Δ_0

A typical notation for the quantum numbers, often used in the QSC context, are the $SO(6)\times SO(2,4)$ charges $\{J_1, J_2, J_3|\Delta, S_1, S_2\}$. These are related to the oscillator numbers through

$$\begin{aligned} J_1 &= \frac{n_{\mathbf{f}_1} + n_{\mathbf{f}_2} - n_{\mathbf{f}_3} - n_{\mathbf{f}_4}}{2} \\ J_2 &= \frac{n_{\mathbf{f}_1} - n_{\mathbf{f}_2} + n_{\mathbf{f}_3} - n_{\mathbf{f}_4}}{2} \\ J_3 &= \frac{-n_{\mathbf{f}_1} + n_{\mathbf{f}_2} + n_{\mathbf{f}_3} - n_{\mathbf{f}_4}}{2} \\ \Delta_0 &= L + \frac{n_{\mathbf{b}} + n_{\mathbf{a}}}{2} = \frac{n_{\mathbf{f}}}{2} + n_{\mathbf{a}} \\ S_1 &= \frac{-n_{\mathbf{b}_1} + n_{\mathbf{b}_2} + n_{\mathbf{a}_1} - n_{\mathbf{a}_2}}{2} \\ S_2 &= \frac{-n_{\mathbf{b}_1} + n_{\mathbf{b}_2} - n_{\mathbf{a}_1} + n_{\mathbf{a}_2}}{2}\,. \end{aligned} \tag{A.1}$$

At finite coupling these six numbers are enough to specify the representation, but they do not give us a complete description of the multiplet at $g = 0$ (unless both shortenings (1.39) happen).

Dynkin labels

Another convention encountered in the literature, e.g. [34], is to use the $\mathfrak{so}(4)$ Dynkin labels $[s_1, s_2]$ and $\mathfrak{so}(6)$ labels $[q_1, p, q_2]$, which are related to the oscillator numbers by

$$s_1 = n_{\mathbf{b}_2} - n_{\mathbf{b}_1}, \quad s_2 = n_{\mathbf{a}_1} - n_{\mathbf{a}_2}; \quad q_1 = n_{\mathbf{f}_1} - n_{\mathbf{f}_2}, \quad p = n_{\mathbf{f}_2} - n_{\mathbf{f}_3}, \quad q_2 = n_{\mathbf{f}_3} - n_{\mathbf{f}_4}\,. \tag{A.2}$$

Additionally Δ_0, L, and the hypercharge

$$B = \frac{n_{\mathbf{b}} - n_{\mathbf{a}}}{2} \tag{A.3}$$

are usually specified. The multiplet is completely described by the data $[\Delta_0; s_1, s_2; q_1, p, q_2]_L^B$. Sometimes, a parity label is also given to a state related to its eigenvalue under the parity transformation $\Pi|\Phi_1\Phi_2\cdots\Phi_N\rangle = (-1)^N|\Phi_N\Phi_{N-1}\cdots\Phi_1\rangle$. This does not influence the weights, but it is related to parity properties of the Q-system related to the multiplet.

A.2 Characters in practice

In this appendix, we demonstrate the usage of characters to decompose tensor product representations into irreps, and how to account for equivalence relations in the vector space. We start by a simple $\mathfrak{su}(2)$ example before treating the lowest spectrum of $\mathcal{N} = 4$ SYM. Finally we discuss how to practically treat cases of high rank.

A.2.1 Example: $\mathfrak{su}(2)$, length 4

In $\mathcal{N} = 4$ SYM, states containing only two types of scalars, e.g. $\mathrm{Tr}[\mathcal{Z}\mathcal{X}\mathcal{Z}\mathcal{Z}\mathcal{X}...]$ form a closed subsector, i.e. the (all-loop) dilatation operator will have eigenstates that are linear combinations of only such states. The states form multiplets (irreps) under the su(2) symmetry (in $\mathcal{N} = 4$ SYM an R-symmetry), which simply acts by flipping $\mathcal{Z} \leftrightarrow \mathcal{X}$.

For $L = 4$ we get two multiplets of trace-operators (a singlet and a five-dimensional one):

$$\mathrm{Tr}[\mathcal{Z}\mathcal{Z}\mathcal{Z}\mathcal{Z}] \rightleftharpoons \mathrm{Tr}[\mathcal{Z}\mathcal{Z}\mathcal{Z}\mathcal{X}] \rightleftharpoons 2\,\mathrm{Tr}[\mathcal{Z}\mathcal{Z}\mathcal{X}\mathcal{X}]+\mathrm{Tr}[\mathcal{Z}\mathcal{X}\mathcal{Z}\mathcal{X}] \rightleftharpoons \mathrm{Tr}[\mathcal{Z}\mathcal{X}\mathcal{X}\mathcal{X}] \rightleftharpoons \mathrm{Tr}[\mathcal{X}\mathcal{X}\mathcal{X}\mathcal{X}]$$
$$\mathrm{Tr}[\mathcal{Z}\mathcal{Z}\mathcal{X}\mathcal{X}]-\mathrm{Tr}[\mathcal{Z}\mathcal{X}\mathcal{Z}\mathcal{X}] \tag{A.4}$$

Denote the number of $\mathcal{Z}$'s and $\mathcal{X}$'s by $L-M$ and M. Each multiplet can be characterised by its highest weight state, which we can define as the one with the maximal numbers of $\mathcal{Z}$'s within the multiplet, i.e. $M = 0$ and $M = 2$ for the $L = 4$ multiplets above. These multiplets thus correspond to the Young diagrams

The character of an $\mathfrak{su}(2)$ representation is the polynomial

$$\chi_{\{L-M,M\}} = \frac{\begin{vmatrix} x_1^{L-M+1} & x_1^M \\ x_2^{L-M+1} & x_2^M \end{vmatrix}}{\begin{vmatrix} x_1 & 1 \\ x_2 & 1 \end{vmatrix}}, \tag{A.5}$$

so for our examples we get

$$\chi_{\{4,0\}} = x_1^4 + x_1^3 x_2 + x_1^2 x_2^2 + x_1 x_2^3 + x_2^4 \tag{A.6}$$

$$\chi_{\{2,2\}} = x_1^2 x_2^2 \,. \tag{A.7}$$

The $\mathfrak{su}(2)$ irreps are sub-representations of the tensor product of L fundamental representations. The fundamental representation is the single-field vector space

$$\mathcal{Z} \rightleftharpoons \mathcal{X} \quad \leftrightarrow \quad \square \quad \leftrightarrow \quad \chi_{\{1,0\}} = x_1 + x_2 \,.$$

The character of the tensor product representation is simply $\chi_{\{1,0\}}^L$ and can be decomposed into irreps by looking at the character, e.g. for $L = 4$ we have

$$\chi_{\{1,0\}}^4 = (x_1 + x_2)^4 = x_1^4 + 4x_1^3 x_2 + 6x_1^2 x_2^2 + 4x_1 x_2^3 + x_2^4 = \chi_{\{4,0\}} + 3\chi_{\{3,1\}} + 2\chi_{\{2,2\}} \,, \tag{A.8}$$

which on the level of Young diagrams is the statement

In (A.4) we listed the multiplets of trace-operators with $L = 4$. There were only two multiplets (a five- and a one-dimensional irrep), which does not fit with (A.8). Using Polya theory, we instead get

$$\begin{aligned} Z_4 &= \frac{\phi(1)}{4}\chi_{\{1,0\}}(x_1, x_2)^4 + \frac{\phi(2)}{4}\chi_{\{1,0\}}(x_1^2, x_2^2)^2 + \frac{\phi(4)}{4}\chi_{\{1,0\}}(x_1^4, x_2^4) \\ &= \frac{1}{4}(x_1 + x_2)^4 + \frac{1}{4}(x_1^2 + x_2^2)^2 + \frac{1}{2}(x_1^4 + x_2^4) \\ &= x_1^4 + x_1^3 x_2 + 2x_1^2 x_2^2 + x_1 x_2^3 + x_2^4 \\ &= \chi_{\{4,0\}} + \chi_{\{2,2\}} \,. \end{aligned} \tag{A.9}$$

A.2.2 Example: all $\mathcal{N} = 4$ SYM multiplets with $\Delta_0^{\ulcorner} \leq 4$

To describe the spectrum up to $\Delta_0^{\ulcorner} \leq 4$, we should consider $\mathfrak{u}(8)$ representations with central charge $C = 4$. The single-site representation has a character of the form

$$\chi_1(x_1, ..., x_8) = x_1 x_2 x_3 x_4 + x_1 x_2 x_3 x_5 + ... \tag{A.10}$$

and the Vandermonde determinant looks like

$$\Delta_V = x_1^3 x_2^2 x_3 - x_1^2 x_2^3 x_3 \pm \dots \tag{A.11}$$

The truncated sum of states is

$$\begin{aligned} Z \;=\; & \frac{\phi(1)}{2}\chi_1(x_i)^2 + \frac{\phi(2)}{2}\chi_1(x_i^2) + \frac{\phi(1)}{3}\chi_1(x_i)^3 + \frac{\phi(3)}{3}\chi_1(x_i^3) \\ & + \frac{\phi(1)}{4}\chi_1(x_i)^4 + \frac{\phi(2)}{4}\chi_1(x_i^2)^2 + \frac{\phi(4)}{4}\chi_1(x_i^4)\,. \end{aligned} \tag{A.12}$$

It is straightforward, though already computationally demanding, to expand the product $\Delta_V Z$. The dominant terms in the expression corresponding to $\Delta_0 \leq 4$ are

$$\begin{aligned} \frac{\Delta_V Z|_{\text{dominant},\Delta_0\leq 4}}{x_1^7 x_2^6 x_3^5 x_4^4 x_5^3 x_6^2 x_7} \;=\; & x_1^2x_2^2x_3^2x_4^2 + x_1^2x_2^2x_3^1x_4^1x_5^1x_6^1 \\ & + x_1^3x_2^3x_3^3x_4^3 + x_1^3x_2^3x_3^2x_4^2x_5^2 + x_1^3x_2^3x_3^3x_4^1x_5^1x_6^1 + x_1^3x_2^3x_3^2x_4^2x_5^1x_6^1 \\ & + x_1^4x_2^4x_3^4x_4^4 + x_1^4x_2^4x_3^4x_4^2x_5^2 + x_1^4x_2^4x_3^3x_4^3x_5^2 + x_1^4x_2^4x_3^4x_4^2x_5^1x_6^1 \\ & + x_1^4x_2^4x_3^3x_4^2x_5^2x_6^1 + 2x_1^3x_2^2x_3^2x_4^2x_5^1x_6^1x_7^1 + 2x_1^4x_2^4x_3^2x_4^2x_5^2x_6^2 \\ & + 2x_1^4x_2^4x_3^3x_4^3x_5^1x_6^1 + x_1^1x_2^1x_3^1x_4^1x_5^1x_6^1x_7^1x_8^1 \\ & + x_1^2x_2^2x_3^2x_4^2x_5^2x_6^2 + x_1^3x_2^3x_3^1x_4^1x_5^1x_6^1x_7^1x_8^1\,. \end{aligned} \tag{A.13}$$

The dominant terms corresponding to protected chiral primaries are marked in grey, while the short representations that make up the Konishi multiplet are marked in blue, and those that make up the $n^{\lceil} = [0,0|2,2,1,1|0,0]$ multiplet (containing the first twist-3 operator) is marked in purple (one term with $\Delta_0 = 5$ is missing due to the truncation).

Combining short multiplets into long ones, shifting to oscillator number notation $n^{\lceil}$, and leaving out chiral primaries, the spectrum of unprotected multiplets with $\Delta_0^{\lceil} \leq 4$ is

$$\begin{aligned} & [0,0|1,1,1,1|0,0] + [0,0|2,2,1,1|0,0] + [0,0|1,1,1,1|2,0] \\ & + [0,0|3,2,2,1|0,0] + [0,2|1,1,1,1|2,0] + [0,2|2,2,2,2|0,0] \\ & + 2\cdot[0,0|2,2,2,2|0,0] + 2\cdot[0,0|3,3,1,1|0,0] + 2\cdot[0,1|2,2,1,1|1,0]\,. \end{aligned} \tag{A.14}$$

Note that for higher $\Delta_{\max}$ the $\mathfrak{su}(2\Delta_{\max})$ sum of states (1.30) will contain representations that lie outside the spectrum of $\mathfrak{psu}(2,2|4)$, i.e. where the Young diagram does not fit inside the $\mathfrak{psu}(2,2|4)$ χ-hook. These can simply be dropped from the sum.

A.2.3 Efficient computation of the sum of states for high rank

In this appendix we explain how the relevant terms in the sum of states

$$\Delta_{\mathrm{V}}\, Z = \sum_{\lambda} c_\lambda W_\lambda \tag{A.15}$$

can be generated for high rank of the considered group.

Step 1 List all possible dominant terms. These correspond to all strictly decreasing partitions of $\Delta_{\max} \cdot L + \Delta_{\max}(2\Delta_{\max} - 1)$ into $2\Delta_{\max}$ numbers, with the restriction that the first number does not exceed $L + 2\Delta_{\max} - 1$ (for $\Delta_{\max} > 2$ the last $\Delta_{\max} - 2$ numbers satisfy a stronger upper bound).

Example: For $\Delta_{\max} = 2$ and $L = 2$, the possible dominant terms (all allowed length-4 partitions of 10) are $x_1^4\, x_2^3\, x_3^2\, x_4$, $x_1^5\, x_2^4\, x_3$, and $x_1^5\, x_2^3\, x_3^2$.

Step 2 For each dominant term, list all possible contributions from Δ_V and the corresponding contribution from Z. No row in the contribution from Z can exceed L.

Example: The term $x_1^5\, x_2^3\, x_3^2$ can arise from $x_1^3\, x_2^2\, x_3 \cdot x_1^2\, x_2\, x_3$ and from $x_1^3\, x_2\, x_3^2 \cdot x_1^2\, x_2^2$.

Step 3 The terms from Δ_V come with a factor of ± 1. Each term in Z come with a coefficient that can be found by counting the number of ways that the term can be constructed from building blocks of the kind $x_{i_1}^d x_{i_2}^d \cdots x_{i_{\Delta_{\max}}}^d$.

Example: $x_1^2 x_2 x_3$ must stem from $\chi_1(x^1)^2$ and can come from $x_1 x_2 \cdot x_1 x_3$ and $x_1 x_3 \cdot x_1 x_2$. Thus its coefficient in Z is 2. $x_1^2 x_2^2$ can stem from $\chi_1(x^1)^2$, and can only arise as $x_1 x_2 \cdot x_1 x_2$, but it can also stem from $\chi_1(x^2)^1$, again with coefficient 1. So its coefficient in Z is also 2.

Step 4 For each dominant term add up all contributions to $\Delta_V Z$.

Example: The term $x_1^5\, x_2^3\, x_3^2$ comes with a coefficient $2 \cdot (-1) + 2 \cdot 1 = 0$ in $\Delta_V Z$.

An implementation of this algorithm can be found in the ancillary `Mathematica`-notebook connected to [5].

A.3 Multiplet content of $\mathcal{N} = 4$ SYM

We here list all multiplets with $\Delta_0^{\lceil} \leq 8$. Multiplets for which the corresponding $\mathbb{Q}$-system is not found by our `Mathematica`-implementation of the solution algorithm described in section 5.3.2 within 15 minutes on a standard laptop are marked in grey.

$\Delta_0^{\lceil}$	Multiplets			
2	$1 \cdot [0,0\|1,1,1,1\|0,0]$			
3	$1 \cdot [0,0\|2,2,1,1\|0,0]$			
4	$1 \cdot [0,0\|1,1,1,1\|2,0]$	$1 \cdot [0,0\|3,2,2,1\|0,0]$	$1 \cdot [0,2\|1,1,1,1\|2,0]$	$1 \cdot [0,2\|2,2,2,2\|0,0]$
	$2 \cdot [0,0\|2,2,2,2\|0,0]$	$2 \cdot [0,0\|3,3,1,1\|0,0]$	$2 \cdot [0,1\|2,2,1,1\|1,0]$	
5	$1 \cdot [0,0\|3,1,1,1\|2,0]$	$1 \cdot [0,2\|2,2,1,1\|2,0]$	$1 \cdot [0,2\|3,3,3,1\|0,0]$	$2 \cdot [0,0\|2,2,1,1\|2,0]$
	$2 \cdot [0,0\|3,3,3,1\|0,0]$	$2 \cdot [0,0\|4,2,2,2\|0,0]$	$2 \cdot [0,0\|4,3,2,1\|0,0]$	$2 \cdot [0,0\|4,4,1,1\|0,0]$
	$2 \cdot [0,1\|2,2,2,2\|1,0]$	$2 \cdot [0,1\|3,3,1,1\|1,0]$	$2 \cdot [0,2\|3,3,2,2\|0,0]$	$4 \cdot [0,0\|3,3,2,2\|0,0]$
	$4 \cdot [0,1\|3,2,2,1\|1,0]$			
$\frac{11}{2}$	$2 \cdot [0,0\|4,3,1,1\|1,0]$	$2 \cdot [0,1\|3,2,1,1\|2,0]$	$2 \cdot [0,1\|4,4,2,1\|0,0]$	$2 \cdot [0,2\|2,1,1,1\|3,0]$
	$2 \cdot [0,2\|3,3,2,1\|1,0]$	$2 \cdot [0,3\|2,2,2,1\|2,0]$	$4 \cdot [0,0\|3,2,2,2\|1,0]$	$4 \cdot [0,0\|3,3,2,1\|1,0]$
	$4 \cdot [0,1\|2,2,2,1\|2,0]$	$4 \cdot [0,1\|3,3,3,2\|0,0]$	$4 \cdot [0,1\|4,3,2,2\|0,0]$	$4 \cdot [0,2\|3,2,2,2\|1,0]$
6	$1 \cdot [0,0\|1,1,1,1\|4,0]$	$1 \cdot [0,0\|4,2,1,1\|2,0]$	$1 \cdot [0,2\|1,1,1,1\|4,0]$	$1 \cdot [0,2\|4,4,3,1\|0,0]$
	$1 \cdot [0,4\|1,1,1,1\|4,0]$	$1 \cdot [0,4\|2,2,2,2\|1,1]$	$1 \cdot [0,4\|2,2,2,2\|2,0]$	$1 \cdot [0,4\|3,3,3,3\|0,0]$
	$1 \cdot [1,1\|1,1,1,1\|4,0]$	$2 \cdot [0,0\|2,2,2,2\|1,1]$	$2 \cdot [0,2\|2,2,2,2\|1,1]$	$2 \cdot [0,2\|3,2,2,1\|2,0]$
	$2 \cdot [0,3\|2,2,1,1\|3,0]$	$2 \cdot [1,1\|2,2,2,2\|1,1]$	$2 \cdot [1,1\|2,2,2,2\|2,0]$	$2 \cdot [1,1\|3,3,3,3\|0,0]$
	$3 \cdot [0,0\|2,2,2,2\|2,0]$	$3 \cdot [0,0\|4,4,3,1\|0,0]$	$3 \cdot [0,0\|5,3,2,2\|0,0]$	$3 \cdot [0,0\|5,3,3,1\|0,0]$
	$3 \cdot [0,0\|5,4,2,1\|0,0]$	$3 \cdot [0,0\|5,5,1,1\|0,0]$	$3 \cdot [0,2\|3,3,3,3\|0,0]$	$4 \cdot [0,0\|3,3,1,1\|2,0]$
	$4 \cdot [0,1\|2,2,1,1\|3,0]$	$4 \cdot [0,1\|3,3,3,1\|1,0]$	$4 \cdot [0,1\|4,2,2,2\|1,0]$	$4 \cdot [0,1\|4,4,1,1\|1,0]$
	$4 \cdot [0,2\|4,4,2,2\|0,0]$	$4 \cdot [0,3\|3,3,2,2\|1,0]$	$5 \cdot [0,0\|3,3,3,3\|0,0]$	$5 \cdot [0,2\|3,3,1,1\|2,0]$
	$6 \cdot [0,0\|3,2,2,1\|2,0]$	$6 \cdot [0,2\|4,3,3,2\|0,0]$	$7 \cdot [0,2\|2,2,2,2\|2,0]$	$8 \cdot [0,1\|4,3,2,1\|1,0]$
	$9 \cdot [0,0\|4,3,3,2\|0,0]$	$10 \cdot [0,0\|4,4,2,2\|0,0]$	$16 \cdot [0,1\|3,3,2,2\|1,0]$	
$\frac{13}{2}$	$2 \cdot [0,0\|2,2,2,1\|3,0]$	$2 \cdot [0,0\|5,2,2,2\|1,0]$	$2 \cdot [0,0\|5,4,1,1\|1,0]$	$2 \cdot [0,1\|2,1,1,1\|4,0]$
	$2 \cdot [0,1\|4,4,4,1\|0,0]$	$2 \cdot [0,1\|5,5,2,1\|0,0]$	$2 \cdot [0,3\|3,2,2,2\|1,1]$	$2 \cdot [0,3\|4,3,3,3\|0,0]$
	$2 \cdot [0,4\|3,3,3,2\|1,0]$	$2 \cdot [1,1\|2,2,2,1\|3,0]$	$4 \cdot [0,0\|3,2,1,1\|3,0]$	$4 \cdot [0,0\|5,3,2,1\|1,0]$
	$4 \cdot [0,1\|4,3,1,1\|2,0]$	$4 \cdot [0,1\|5,4,3,1\|0,0]$	$4 \cdot [0,2\|3,2,1,1\|3,0]$	$4 \cdot [0,2\|4,4,2,1\|1,0]$
	$4 \cdot [0,3\|3,3,2,1\|2,0]$	$4 \cdot [0,3\|4,4,3,2\|0,0]$	$6 \cdot [0,1\|4,2,2,1\|2,0]$	$6 \cdot [0,2\|2,2,2,1\|3,0]$
	$6 \cdot [0,2\|4,3,3,1\|1,0]$	$6 \cdot [0,3\|3,2,2,2\|2,0]$	$8 \cdot [0,1\|3,2,2,2\|1,1]$	$8 \cdot [1,1\|3,3,3,2\|1,0]$
	$10 \cdot [0,0\|4,3,3,1\|1,0]$	$10 \cdot [0,0\|4,4,2,1\|1,0]$	$10 \cdot [0,1\|5,3,3,2\|0,0]$	$10 \cdot [0,1\|5,4,2,2\|0,0]$
	$12 \cdot [0,0\|3,3,3,2\|1,0]$	$12 \cdot [0,1\|4,3,3,3\|0,0]$	$16 \cdot [0,1\|3,3,2,1\|2,0]$	$16 \cdot [0,2\|4,3,2,2\|1,0]$
	$20 \cdot [0,1\|3,2,2,2\|2,0]$	$20 \cdot [0,2\|3,3,3,2\|1,0]$	$24 \cdot [0,0\|4,3,2,2\|1,0]$	$24 \cdot [0,1\|4,4,3,2\|0,0]$

Table A.1: Spectrum of unprotected multiplets $[n_{\mathbf{b}}|n_{\mathbf{f}}|n_{\mathbf{a}}]^{\lceil}$ with $\Delta_0^{\lceil} \leq \frac{13}{2}$. We find complete agreement with the results in [34]. Our algorithm finds the $\mathbb{Q}$-system for all these multiplets in a matter of minutes.

$\Delta_0^{\ulcorner}$	Multiplets			
7	$2\cdot[0,0\|2,2,1,1\|4,0]$	$2\cdot[0,0\|3,1,1,1\|4,0]$	$2\cdot[0,0\|5,2,2,1\|2,0]$	$2\cdot[0,2\|3,1,1,1\|4,0]$
	$2\cdot[0,2\|5,4,4,1\|0,0]$	$2\cdot[0,3\|1,1,1,1\|5,0]$	$2\cdot[0,4\|3,3,2,2\|1,1]$	$2\cdot[0,4\|3,3,3,1\|2,0]$
	$2\cdot[0,4\|4,4,3,3\|0,0]$	$2\cdot[0,4\|4,4,4,2\|0,0]$	$2\cdot[0,5\|2,2,2,2\|3,0]$	$2\cdot[1,1\|2,2,1,1\|4,0]$
	$3\cdot[0,0\|5,3,1,1\|2,0]$	$3\cdot[0,0\|6,6,1,1\|0,0]$	$3\cdot[0,2\|5,5,3,1\|0,0]$	$3\cdot[0,4\|2,2,1,1\|4,0]$
	$3\cdot[1,2\|2,2,2,2\|2,1]$	$4\cdot[0,0\|6,4,3,1\|0,0]$	$4\cdot[0,1\|4,2,1,1\|3,0]$	$4\cdot[0,3\|3,3,1,1\|3,0]$
	$4\cdot[0,3\|4,4,3,1\|1,0]$	$5\cdot[0,0\|5,4,4,1\|0,0]$	$5\cdot[0,0\|6,3,3,2\|0,0]$	$6\cdot[0,0\|6,5,2,1\|0,0]$
	$6\cdot[0,1\|5,5,1,1\|1,0]$	$6\cdot[0,2\|4,2,2,2\|1,1]$	$6\cdot[0,3\|2,2,2,2\|2,1]$	$6\cdot[1,1\|3,3,3,1\|2,0]$
	$6\cdot[1,2\|2,2,2,2\|3,0]$	$7\cdot[0,1\|2,2,2,2\|2,1]$	$7\cdot[0,2\|2,2,1,1\|4,0]$	$7\cdot[0,2\|4,4,1,1\|2,0]$
	$7\cdot[0,4\|3,3,2,2\|2,0]$	$7\cdot[1,2\|3,3,3,3\|1,0]$	$8\cdot[0,0\|5,5,3,1\|0,0]$	$8\cdot[0,0\|6,4,2,2\|0,0]$
	$8\cdot[0,1\|5,3,3,1\|1,0]$	$8\cdot[1,1\|3,3,2,2\|1,1]$	$9\cdot[0,0\|4,2,2,2\|1,1]$	$9\cdot[1,1\|4,4,4,2\|0,0]$
	$10\cdot[0,0\|3,3,2,2\|1,1]$	$10\cdot[0,0\|3,3,3,1\|2,0]$	$10\cdot[0,0\|4,4,1,1\|2,0]$	$10\cdot[0,2\|5,3,3,3\|0,0]$
	$10\cdot[0,2\|5,5,2,2\|0,0]$	$10\cdot[0,3\|2,2,2,2\|3,0]$	$10\cdot[0,3\|3,2,2,1\|3,0]$	$10\cdot[1,1\|4,4,3,3\|0,0]$
	$12\cdot[0,1\|2,2,2,2\|3,0]$	$12\cdot[0,1\|3,3,1,1\|3,0]$	$12\cdot[0,3\|3,3,3,3\|1,0]$	$12\cdot[0,3\|4,4,2,2\|1,0]$
	$14\cdot[0,2\|3,3,3,1\|2,0]$	$14\cdot[0,2\|4,2,2,2\|2,0]$	$15\cdot[0,0\|4,4,4,2\|0,0]$	$15\cdot[0,0\|5,3,3,3\|0,0]$
	$16\cdot[0,0\|4,2,2,2\|2,0]$	$16\cdot[0,2\|4,4,4,2\|0,0]$	$18\cdot[0,0\|4,4,3,3\|0,0]$	$18\cdot[0,0\|5,5,2,2\|0,0]$
	$18\cdot[0,1\|3,2,2,1\|3,0]$	$18\cdot[0,1\|5,4,2,1\|1,0]$	$18\cdot[0,2\|3,3,2,2\|1,1]$	$18\cdot[0,2\|4,3,2,1\|2,0]$
	$18\cdot[0,3\|4,3,3,2\|1,0]$	$18\cdot[1,1\|3,3,2,2\|2,0]$	$22\cdot[0,0\|4,3,2,1\|2,0]$	$22\cdot[0,1\|4,4,3,1\|1,0]$
	$22\cdot[0,1\|5,3,2,2\|1,0]$	$22\cdot[0,2\|5,4,3,2\|0,0]$	$23\cdot[0,1\|3,3,3,3\|1,0]$	$24\cdot[0,0\|3,3,2,2\|2,0]$
	$24\cdot[0,2\|4,4,3,3\|0,0]$	$42\cdot[0,0\|5,4,3,2\|0,0]$	$43\cdot[0,2\|3,3,2,2\|2,0]$	$52\cdot[0,1\|4,4,2,2\|1,0]$
	$74\cdot[0,1\|4,3,3,2\|1,0]$			
$\frac{15}{2}$	$2\cdot[0,4\|2,1,1,1\|5,0]$	$2\cdot[0,5\|2,2,2,1\|4,0]$	$2\cdot[0,5\|3,3,3,2\|1,1]$	$2\cdot[1,1\|2,1,1,1\|5,0]$
	$4\cdot[0,0\|6,5,1,1\|1,0]$	$4\cdot[0,1\|5,2,2,2\|1,1]$	$4\cdot[0,1\|6,6,2,1\|0,0]$	$4\cdot[0,2\|2,1,1,1\|5,0]$
	$4\cdot[0,5\|3,3,3,2\|2,0]$	$4\cdot[1,1\|4,4,4,1\|1,0]$	$6\cdot[0,0\|6,3,3,1\|1,0]$	$6\cdot[0,1\|6,4,4,1\|0,0]$
	$6\cdot[0,3\|3,2,1,1\|4,0]$	$6\cdot[0,4\|3,3,2,1\|3,0]$	$7\cdot[0,4\|3,2,2,2\|2,1]$	$7\cdot[1,2\|2,2,2,1\|4,0]$
	$8\cdot[0,0\|6,3,2,2\|1,0]$	$8\cdot[0,0\|6,4,2,1\|1,0]$	$8\cdot[0,1\|5,5,4,1\|0,0]$	$8\cdot[0,1\|6,5,3,1\|0,0]$
	$10\cdot[0,0\|4,4,4,1\|1,0]$	$10\cdot[0,1\|5,4,1,1\|2,0]$	$10\cdot[0,1\|6,3,3,3\|0,0]$	$10\cdot[0,2\|4,2,2,1\|3,0]$
	$10\cdot[0,2\|5,5,2,1\|1,0]$	$10\cdot[0,3\|2,2,2,1\|4,0]$	$10\cdot[0,3\|4,3,3,1\|2,0]$	$10\cdot[0,4\|3,2,2,2\|3,0]$
	$11\cdot[0,0\|3,2,2,2\|2,1]$	$11\cdot[0,1\|2,2,2,1\|4,0]$	$11\cdot[0,4\|4,3,3,3\|1,0]$	$11\cdot[1,2\|4,4,4,3\|0,0]$
	$12\cdot[0,0\|4,3,1,1\|3,0]$	$12\cdot[0,1\|3,2,1,1\|4,0]$	$12\cdot[0,1\|5,2,2,2\|2,0]$	$12\cdot[0,2\|4,3,1,1\|3,0]$
	$12\cdot[0,2\|4,4,4,1\|1,0]$	$12\cdot[0,3\|4,4,2,1\|2,0]$	$12\cdot[0,3\|5,5,3,2\|0,0]$	$12\cdot[0,4\|4,4,3,2\|1,0]$
	$14\cdot[0,0\|4,2,2,1\|3,0]$	$14\cdot[0,3\|5,4,4,2\|0,0]$	$14\cdot[1,1\|3,2,2,2\|2,1]$	$14\cdot[1,2\|3,3,3,2\|1,1]$
	$16\cdot[0,0\|3,3,2,1\|3,0]$	$16\cdot[0,3\|4,3,2,2\|1,1]$	$16\cdot[0,3\|5,4,3,3\|0,0]$	$16\cdot[1,1\|3,3,2,1\|3,0]$
	$18\cdot[0,0\|3,2,2,2\|3,0]$	$18\cdot[0,1\|5,3,2,1\|2,0]$	$18\cdot[0,2\|5,4,3,1\|1,0]$	$18\cdot[0,3\|4,4,4,3\|0,0]$
	$20\cdot[0,0\|5,5,2,1\|1,0]$	$20\cdot[0,1\|6,5,2,2\|0,0]$	$20\cdot[0,3\|3,3,3,2\|1,1]$	$20\cdot[1,1\|3,2,2,2\|3,0]$
	$31\cdot[0,2\|3,2,2,2\|2,1]$	$31\cdot[1,2\|3,3,3,2\|2,0]$	$38\cdot[0,0\|5,4,3,1\|1,0]$	$38\cdot[0,1\|3,3,3,2\|1,1]$
	$38\cdot[0,1\|6,4,3,2\|0,0]$	$38\cdot[0,2\|3,3,2,1\|3,0]$	$38\cdot[0,3\|4,3,2,2\|2,0]$	$38\cdot[1,1\|4,3,3,3\|1,0]$
	$43\cdot[0,0\|4,3,3,3\|1,0]$	$43\cdot[0,1\|4,4,4,3\|0,0]$	$48\cdot[0,1\|4,3,3,1\|2,0]$	$48\cdot[0,1\|4,4,2,1\|2,0]$
	$48\cdot[0,2\|3,2,2,2\|3,0]$	$48\cdot[0,2\|5,3,3,2\|1,0]$	$48\cdot[0,2\|5,4,2,2\|1,0]$	$48\cdot[0,3\|3,3,3,2\|2,0]$
	$52\cdot[0,1\|4,3,2,2\|1,1]$	$52\cdot[1,1\|4,4,3,2\|1,0]$	$72\cdot[0,0\|5,3,3,2\|1,0]$	$72\cdot[0,0\|5,4,2,2\|1,0]$
	$72\cdot[0,1\|5,4,4,2\|0,0]$	$72\cdot[0,1\|5,5,3,2\|0,0]$	$77\cdot[0,1\|3,3,3,2\|2,0]$	$77\cdot[0,2\|4,3,3,3\|1,0]$
	$80\cdot[0,0\|4,4,3,2\|1,0]$	$80\cdot[0,1\|5,4,3,3\|0,0]$	$120\cdot[0,1\|4,3,2,2\|2,0]$	$120\cdot[0,2\|4,4,3,2\|1,0]$

Table A.2: Spectrum of unprotected multiplets $[n_{\mathbf{b}}|n_{\mathbf{f}}|n_{\mathbf{a}}]^{\ulcorner}$ with $\Delta_0^{\ulcorner}=7$ and $\Delta_0^{\ulcorner}=\frac{15}{2}$.

$\Delta_0^{\lceil}$	Multiplets			
8	$1\cdot[0,0\|1,1,1,1\|6,0]$	$1\cdot[0,0\|5,1,1,1\|4,0]$	$1\cdot[0,4\|1,1,1,1\|6,0]$	$1\cdot[0,4\|5,5,5,1\|0,0]$
	$1\cdot[0,6\|1,1,1,1\|6,0]$	$1\cdot[0,6\|2,2,2,2\|2,2]$	$1\cdot[0,6\|2,2,2,2\|3,1]$	$1\cdot[0,6\|2,2,2,2\|4,0]$
	$1\cdot[0,6\|3,3,3,3\|1,1]$	$1\cdot[0,6\|4,4,4,4\|0,0]$	$1\cdot[1,1\|1,1,1,1\|6,0]$	$1\cdot[1,3\|1,1,1,1\|6,0]$
	$1\cdot[2,2\|1,1,1,1\|6,0]$	$2\cdot[0,2\|1,1,1,1\|6,0]$	$2\cdot[0,3\|3,1,1,1\|5,0]$	$2\cdot[0,5\|2,2,1,1\|5,0]$
	$2\cdot[0,5\|3,3,3,1\|3,0]$	$2\cdot[0,6\|3,3,3,3\|2,0]$	$2\cdot[1,3\|2,2,2,2\|2,2]$	$2\cdot[2,2\|2,2,2,2\|3,1]$
	$3\cdot[0,0\|6,2,2,2\|1,1]$	$3\cdot[0,0\|6,2,2,2\|2,0]$	$3\cdot[0,2\|5,5,5,1\|0,0]$	$3\cdot[1,1\|5,5,5,1\|0,0]$
	$3\cdot[2,2\|2,2,2,2\|2,2]$	$4\cdot[0,0\|7,4,4,1\|0,0]$	$4\cdot[0,0\|7,7,1,1\|0,0]$	$4\cdot[0,1\|3,1,1,1\|5,0]$
	$4\cdot[0,5\|4,4,4,2\|1,0]$	$5\cdot[0,0\|2,2,2,2\|2,2]$	$5\cdot[0,0\|2,2,2,2\|3,1]$	$5\cdot[0,0\|6,4,1,1\|2,0]$
	$5\cdot[0,2\|6,6,3,1\|0,0]$	$5\cdot[0,4\|2,2,2,2\|2,2]$	$5\cdot[1,1\|2,2,2,2\|2,2]$	$5\cdot[1,3\|4,4,4,4\|0,0]$
	$5\cdot[2,2\|2,2,2,2\|4,0]$	$5\cdot[2,2\|3,3,3,3\|1,1]$	$5\cdot[2,2\|4,4,4,4\|0,0]$	$6\cdot[0,0\|5,5,5,1\|0,0]$
	$6\cdot[0,0\|7,3,3,3\|0,0]$	$6\cdot[0,5\|3,3,2,2\|2,1]$	$6\cdot[1,2\|2,2,1,1\|5,0]$	$7\cdot[0,0\|2,2,2,2\|4,0]$
	$7\cdot[0,0\|4,2,1,1\|4,0]$	$7\cdot[0,0\|7,6,2,1\|0,0]$	$7\cdot[0,4\|4,4,4,4\|0,0]$	$7\cdot[0,4\|5,5,4,2\|0,0]$
	$8\cdot[0,0\|6,3,2,1\|2,0]$	$8\cdot[0,1\|2,2,1,1\|5,0]$	$8\cdot[0,1\|6,6,1,1\|1,0]$	$8\cdot[0,2\|4,2,1,1\|4,0]$
	$8\cdot[0,2\|6,5,4,1\|0,0]$	$8\cdot[0,4\|3,3,1,1\|4,0]$	$8\cdot[0,4\|4,4,3,1\|2,0]$	$8\cdot[0,5\|4,4,3,3\|1,0]$
	$9\cdot[0,4\|3,2,2,1\|4,0]$	$10\cdot[0,0\|3,3,1,1\|4,0]$	$10\cdot[0,0\|7,5,3,1\|0,0]$	$10\cdot[0,1\|5,2,2,1\|3,0]$
	$10\cdot[0,1\|5,3,1,1\|3,0]$	$10\cdot[0,2\|2,2,2,2\|2,2]$	$10\cdot[0,3\|2,2,1,1\|5,0]$	$10\cdot[0,3\|5,4,4,1\|1,0]$
	$10\cdot[0,3\|5,5,3,1\|1,0]$	$10\cdot[0,4\|2,2,2,2\|3,1]$	$10\cdot[0,4\|4,4,2,2\|1,1]$	$10\cdot[0,4\|5,5,3,3\|0,0]$
	$10\cdot[0,5\|3,3,2,2\|3,0]$	$10\cdot[1,1\|3,3,1,1\|4,0]$	$10\cdot[1,3\|2,2,2,2\|3,1]$	$10\cdot[1,3\|2,2,2,2\|4,0]$
	$10\cdot[2,2\|3,3,3,3\|2,0]$	$12\cdot[0,2\|5,5,1,1\|2,0]$	$12\cdot[0,3\|4,4,1,1\|3,0]$	$13\cdot[0,0\|3,2,2,1\|4,0]$
	$13\cdot[0,4\|5,4,4,3\|0,0]$	$14\cdot[0,0\|6,6,3,1\|0,0]$	$14\cdot[0,0\|7,5,2,2\|0,0]$	$14\cdot[1,1\|2,2,2,2\|3,1]$
	$14\cdot[1,3\|3,3,3,3\|1,1]$	$15\cdot[0,0\|5,5,1,1\|2,0]$	$15\cdot[0,2\|6,6,2,2\|0,0]$	$16\cdot[0,4\|3,3,3,3\|1,1]$
	$16\cdot[1,1\|2,2,2,2\|4,0]$	$18\cdot[0,0\|6,5,4,1\|0,0]$	$18\cdot[0,0\|7,4,3,2\|0,0]$	$18\cdot[0,3\|4,2,2,2\|2,1]$
	$18\cdot[0,4\|2,2,2,2\|4,0]$	$18\cdot[0,4\|4,3,3,2\|1,1]$	$18\cdot[1,1\|3,2,2,1\|4,0]$	$18\cdot[1,2\|3,3,3,1\|3,0]$
	$20\cdot[0,0\|3,3,3,3\|1,1]$	$20\cdot[0,0\|4,4,4,4\|0,0]$	$20\cdot[1,1\|4,4,4,4\|0,0]$	$24\cdot[0,2\|2,2,2,2\|3,1]$
	$24\cdot[1,3\|3,3,3,3\|2,0]$	$26\cdot[0,2\|3,3,1,1\|4,0]$	$26\cdot[0,4\|4,4,2,2\|2,0]$	$28\cdot[0,1\|4,4,1,1\|3,0]$
	$28\cdot[0,3\|5,5,2,2\|1,0]$	$30\cdot[0,1\|6,5,2,1\|1,0]$	$30\cdot[0,2\|2,2,2,2\|4,0]$	$30\cdot[0,3\|3,3,3,1\|3,0]$
	$30\cdot[0,3\|4,2,2,2\|3,0]$	$30\cdot[0,4\|3,3,3,3\|2,0]$	$33\cdot[0,0\|3,3,3,3\|2,0]$	$33\cdot[0,2\|4,4,4,4\|0,0]$
	$34\cdot[0,0\|6,6,2,2\|0,0]$	$34\cdot[0,2\|5,3,2,2\|1,1]$	$34\cdot[0,3\|4,3,2,1\|3,0]$	$34\cdot[1,1\|4,4,3,1\|2,0]$
	$35\cdot[1,1\|3,3,3,3\|1,1]$	$36\cdot[0,1\|6,4,3,1\|1,0]$	$38\cdot[0,2\|5,3,3,1\|2,0]$	$39\cdot[1,1\|4,4,2,2\|1,1]$
	$40\cdot[1,2\|3,3,2,2\|2,1]$	$41\cdot[0,2\|3,2,2,1\|4,0]$	$41\cdot[0,4\|4,3,3,2\|2,0]$	$43\cdot[0,0\|4,4,2,2\|1,1]$
	$43\cdot[1,1\|5,5,3,3\|0,0]$	$44\cdot[0,1\|3,3,3,1\|3,0]$	$44\cdot[0,3\|5,3,3,3\|1,0]$	$45\cdot[0,0\|5,3,2,2\|1,1]$
	$45\cdot[0,2\|5,4,2,1\|2,0]$	$45\cdot[1,1\|5,5,4,2\|0,0]$	$46\cdot[0,0\|5,3,3,1\|2,0]$	$46\cdot[0,2\|6,4,4,2\|0,0]$
	$49\cdot[0,0\|4,4,3,1\|2,0]$	$49\cdot[0,2\|6,4,3,3\|0,0]$	$52\cdot[0,1\|5,4,4,1\|1,0]$	$52\cdot[0,1\|6,3,3,2\|1,0]$
	$54\cdot[0,1\|4,2,2,2\|2,1]$	$54\cdot[0,2\|3,3,3,3\|1,1]$	$54\cdot[1,1\|3,3,3,3\|2,0]$	$54\cdot[1,1\|4,3,3,2\|1,1]$
	$54\cdot[1,2\|4,4,4,2\|1,0]$	$60\cdot[0,0\|4,3,3,2\|1,1]$	$60\cdot[0,1\|5,5,3,1\|1,0]$	$60\cdot[0,1\|6,4,2,2\|1,0]$
	$60\cdot[0,3\|3,3,2,2\|2,1]$	$60\cdot[1,1\|5,4,4,3\|0,0]$	$60\cdot[1,2\|3,3,2,2\|3,0]$	$63\cdot[0,0\|5,4,2,1\|2,0]$
	$63\cdot[0,2\|6,5,3,2\|0,0]$	$71\cdot[0,0\|5,5,3,3\|0,0]$	$72\cdot[0,2\|4,4,2,2\|1,1]$	$72\cdot[1,1\|4,4,2,2\|2,0]$
	$73\cdot[0,2\|4,4,3,1\|2,0]$	$73\cdot[0,2\|5,3,2,2\|2,0]$	$74\cdot[0,1\|4,2,2,2\|3,0]$	$74\cdot[0,3\|4,4,4,2\|1,0]$
	$77\cdot[0,0\|5,4,4,3\|0,0]$	$77\cdot[0,0\|5,5,4,2\|0,0]$	$77\cdot[0,0\|6,4,3,3\|0,0]$	$80\cdot[0,1\|3,3,2,2\|2,1]$
	$80\cdot[1,2\|4,4,3,3\|1,0]$	$84\cdot[0,0\|6,4,4,2\|0,0]$	$90\cdot[0,0\|4,4,2,2\|2,0]$	$90\cdot[0,2\|5,5,3,3\|0,0]$
	$92\cdot[0,3\|3,3,2,2\|3,0]$	$96\cdot[0,0\|5,3,2,2\|2,0]$	$96\cdot[0,1\|4,3,2,1\|3,0]$	$96\cdot[0,2\|5,5,4,2\|0,0]$
	$96\cdot[0,3\|5,4,3,2\|1,0]$	$101\cdot[0,2\|3,3,3,3\|2,0]$	$110\cdot[0,1\|3,3,2,2\|3,0]$	$110\cdot[0,3\|4,4,3,3\|1,0]$
	$112\cdot[0,0\|6,5,3,2\|0,0]$	$120\cdot[0,0\|4,3,3,2\|2,0]$	$120\cdot[0,2\|5,4,4,3\|0,0]$	$122\cdot[0,2\|4,3,3,2\|1,1]$
	$122\cdot[1,1\|4,3,3,2\|2,0]$	$130\cdot[0,1\|5,5,2,2\|1,0]$	$160\cdot[0,1\|4,4,4,2\|1,0]$	$160\cdot[0,1\|5,3,3,3\|1,0]$
	$176\cdot[0,2\|4,4,2,2\|2,0]$	$210\cdot[0,1\|4,4,3,3\|1,0]$	$256\cdot[0,2\|4,3,3,2\|2,0]$	$378\cdot[0,1\|5,4,3,2\|1,0]$

Table A.3: Spectrum of unprotected multiplets $[n_{\mathbf{b}}|n_{\mathbf{f}}|n_{\mathbf{a}}]^{\lceil}$ with $\Delta_0^{\lceil}=8$.

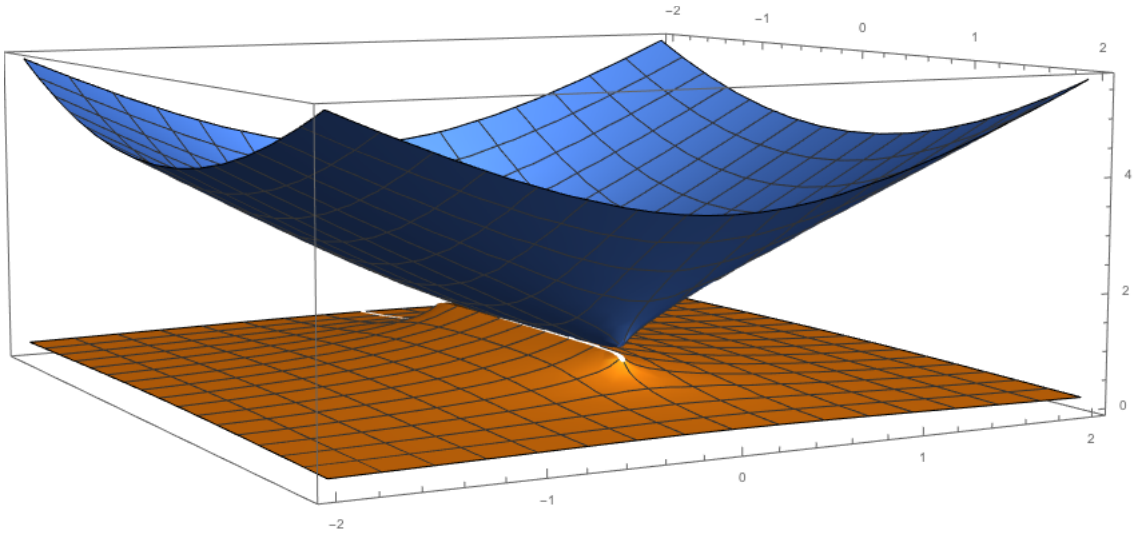

Figure A.1: Plot of $|x(u)|$. The axes are the real and imaginary values of $\frac{u}{2g}$, placing the branch points on the real axis at $\frac{u}{2g} = \pm 1$.

A.4 QSC-related technicalities

A.4.1 The Zhukowsky variable

The Zhukowsky variable, x, is defined in terms of the spectral parameter u through

$$\frac{u}{g} = x + \frac{1}{x}. \tag{A.16}$$

This quadratic equation on x has the solutions

$$x = \frac{u}{2g} \pm \sqrt{\frac{u^2}{4g^2} - 1}. \tag{A.17}$$

The variable $x(u)$ is multivalued with branch points at $u = \pm 2g$ and lives on a two-sheeted Riemann surface, see figure A.1. The two solutions (A.17) are related through $x_+ = \frac{1}{x_-}$. We will make the choice to describe the function by a short branch cut between $u = \pm 2g$ and define the first sheet by the value of $x(u)$ for which $|x(u)| > 1$. We will refer to this value as $x(u)$ and denote the value on the second sheet by $\tilde{x}(u) = \frac{1}{x(u)}$ such that $|\tilde{x}(u)| < 1$. At large u, the values on the two sheets behave as $x \sim \frac{u}{g}$ and $\tilde{x} \sim \frac{g}{u}$.

A.4.2 Solving QQ-relations

Consider the standard QQ-relation

$$Q_{ab}Q_{\emptyset} = Q_a^+ Q_b^- - Q_a^- Q_b^+ \quad \Rightarrow \quad Q_b = Q_a \Psi \left(\frac{Q_{ab}^+ Q_{\emptyset}^+}{Q_a Q_a^{[2]}} \right) \tag{A.18}$$

and use that all Q-functions are allowed to have poles only at $i\mathbb{Z}$ (or $i(\frac{1}{2} + \mathbb{Z})$ for an even number of indices). Then it should be that apparent poles coming from non-trivial zeros of

Q_a in the argument of Ψ cancel out. We are going to derive an expression which explicitly accounts for this cancellation.

We consider only the case when all Q-functions on the right-hand side of (A.18) are rational. If Q_{ab} involves Ψ-functions, an equivalent nested argument can be generated. Rewrite the Q-functions as

$$Q_A = \frac{q_A p_A}{r_A}\,, \tag{A.19}$$

where p_A and r_A are fused factors of u of the type $\prod(u+in)^k$ (or $\prod(u+in+\frac{i}{2})^k$ for $|A|$ even), where $n \in \mathbb{Z}$, and q_A contains no such factors. Then it is possible to uniquely split the argument of the Ψ-summation in (A.18) as

$$\frac{Q^+_{ab}Q^+_\emptyset}{Q_a Q^{[2]}_a} = \frac{q^+_{ab}q^+_\emptyset}{q_a q^{++}_a}\underbrace{\frac{p^+_{ab}p^+_\emptyset r_a r^{++}_a}{p_a p^{++}_a r^+_{ab} r^+_\emptyset}}_{P/R} = \frac{A}{q_a} + \frac{B}{q^{++}_a} + \frac{C}{R} + D\,, \tag{A.20}$$

where R and P are polynomials, and where A and B are polynomials of lower degree than q_a, C is a polynomial of lower degree than R, and D is a polynomial of at most the total asymptotic degree of the left-hand side. The polynomials A, B, C and D can be fixed by simply matching coefficients of individual powers in

$$q^+_{ab}q^+_\emptyset P = Aq^{++}_a R + Bq_a R + Cq_a q^{++}_a + Dq_a q^{++}_a R\,. \tag{A.21}$$

Now,

$$\begin{aligned} Q_b &= Q_a\Psi\left(\frac{Q^+_{ab}Q^+_\emptyset}{Q_a Q^{[2]}_a}\right) = Q_a\left(\frac{A}{q_a} + \Psi\left(\frac{A^{++}+B}{q^{++}_a}\right) + \Psi\left(\frac{C}{R}+D\right)\right) \\ &= \frac{p_a A}{r_a} + Q_a\Psi\left(\frac{A^{++}+B}{q^{++}_a}\right) + Q_a\Psi\left(\frac{C}{R}+D\right)\,. \end{aligned} \tag{A.22}$$

In this expression, the only potential poles away from $i\mathbb{Z}$ arise from the second term. Then it should be that $A^{++}+B=0$, since $A^{++}+B$ is of lower degree than q_a and thus unable to cancel the poles otherwise. Conclusion:

$$Q_b = \frac{p_a A}{r_a} + Q_a\Psi\left(\frac{C}{R}+D\right)\,. \tag{A.23}$$

A.4.3 Fourth-order difference equation on $Q_{a|i}$

We here give an example of a decoupled higher-order difference equation that follows from the QQ-relations. A fourth-order difference equation on $\mathbf{Q}$ was given in [112]. Likewise,

one could write a fourth order equation on $Q_{a|i}$ for fixed a. For example, for $Q_{1|i}$ we get

$$\begin{aligned} 0 \;=\; & -\frac{D_{-3}}{\mathbf{P}_1^{[-3]}}Q_{1|i}^{[-4]} + Q_{1|i}^{[-2]}\left(\frac{D_{-1}}{\mathbf{P}_1^{[-1]}} + \frac{D_{-3}}{\mathbf{P}_1^{[-3]}} + \frac{\mathbf{P}_a^{[-1]}\mathbf{P}^{a[-3]}D_{-3}}{\mathbf{P}_1^{[-1]}}\right) \\ & + Q_{1|i}^{[0]}\left(-\frac{D_{-1}}{\mathbf{P}_1^{[-1]}} - \frac{D_1}{\mathbf{P}_1^{[1]}} - \frac{\mathbf{P}_a^{[-1]}\mathbf{P}^{a[-3]}D_{-3}}{\mathbf{P}_1^{[-1]}} + \frac{\mathbf{P}_a^{[1]}\mathbf{P}^{a[3]}D_3}{\mathbf{P}_1^{[1]}} + D\right) \\ & + Q_{1|i}^{[2]}\left(\frac{D_1}{\mathbf{P}_1^{[1]}} + \frac{D_3}{\mathbf{P}_1^{[3]}} - \frac{\mathbf{P}_a^{[1]}\mathbf{P}^{a[3]}D_3}{\mathbf{P}_1^{[1]}}\right) - \frac{D_3}{\mathbf{P}_1^{[3]}}Q_{1|i}^{[4]}\,, \end{aligned} \tag{A.24}$$

where

$$\begin{aligned} D_{-3} &\equiv \begin{vmatrix} \mathbf{P}^{2[-1]} & \mathbf{P}^{3[-1]} & \mathbf{P}^{4[-1]} \\ \mathbf{P}^{2[1]} & \mathbf{P}^{3[1]} & \mathbf{P}^{4[1]} \\ \mathbf{P}^{2[3]} & \mathbf{P}^{3[3]} & \mathbf{P}^{4[3]} \end{vmatrix}, \quad D_{-1} \equiv \begin{vmatrix} \mathbf{P}^{2[-3]} & \mathbf{P}^{3[-3]} & \mathbf{P}^{4[-3]} \\ \mathbf{P}^{2[1]} & \mathbf{P}^{3[1]} & \mathbf{P}^{4[1]} \\ \mathbf{P}^{2[3]} & \mathbf{P}^{3[3]} & \mathbf{P}^{4[3]} \end{vmatrix}, \\ D_1 &\equiv \begin{vmatrix} \mathbf{P}^{2[-3]} & \mathbf{P}^{3[-3]} & \mathbf{P}^{4[-3]} \\ \mathbf{P}^{2[-1]} & \mathbf{P}^{3[-1]} & \mathbf{P}^{4[-1]} \\ \mathbf{P}^{2[3]} & \mathbf{P}^{3[3]} & \mathbf{P}^{4[3]} \end{vmatrix}, \quad D_3 \equiv \begin{vmatrix} \mathbf{P}^{2[-3]} & \mathbf{P}^{3[-3]} & \mathbf{P}^{4[-3]} \\ \mathbf{P}^{2[-1]} & \mathbf{P}^{3[-1]} & \mathbf{P}^{4[-1]} \\ \mathbf{P}^{2[1]} & \mathbf{P}^{3[1]} & \mathbf{P}^{4[1]} \end{vmatrix}, \\ D &= \begin{vmatrix} \mathbf{P}^{1[-3]} & \mathbf{P}^{2[-3]} & \mathbf{P}^{3[-3]} & \mathbf{P}^{4[-3]} \\ \mathbf{P}^{1[-1]} & \mathbf{P}^{2[-1]} & \mathbf{P}^{3[-1]} & \mathbf{P}^{4[-1]} \\ \mathbf{P}^{1[1]} & \mathbf{P}^{2[1]} & \mathbf{P}^{3[1]} & \mathbf{P}^{4[1]} \\ \mathbf{P}^{1[3]} & \mathbf{P}^{2[3]} & \mathbf{P}^{3[3]} & \mathbf{P}^{4[3]} \end{vmatrix}. \end{aligned} \tag{A.25}$$

Notice that, using $\mathbf{Q}_i = \frac{Q_{1|i}^+ - Q_{1|i}^-}{\mathbf{P}_1}$, the equation gives an expression for $Q_{1|i}$ in terms of $\mathbf{P}$ and $\mathbf{Q}_i$,

$$\begin{aligned} Q_{1|i} \;=\; & \begin{vmatrix} \mathbf{P}^{1[-3]} & \mathbf{P}^{2[-3]} & \mathbf{P}^{3[-3]} & \mathbf{P}^{4[-3]} \\ \mathbf{P}^{1[-1]} & \mathbf{P}^{2[-1]} & \mathbf{P}^{3[-1]} & \mathbf{P}^{4[-1]} \\ \mathbf{P}^{1[1]} & \mathbf{P}^{2[1]} & \mathbf{P}^{3[1]} & \mathbf{P}^{4[1]} \\ \mathbf{P}^{1[3]} & \mathbf{P}^{2[3]} & \mathbf{P}^{3[3]} & \mathbf{P}^{4[3]} \end{vmatrix}^{-1} \left(\begin{vmatrix} \mathbf{Q}_i^{[-3]} & \mathbf{P}^{2[-3]} & \mathbf{P}^{3[-3]} & \mathbf{P}^{4[-3]} \\ \mathbf{Q}_i^{[-1]} & \mathbf{P}^{2[-1]} & \mathbf{P}^{3[-1]} & \mathbf{P}^{4[-1]} \\ \mathbf{Q}_i^{[1]} & \mathbf{P}^{2[1]} & \mathbf{P}^{3[1]} & \mathbf{P}^{4[1]} \\ \mathbf{Q}_i^{[3]} & \mathbf{P}^{2[3]} & \mathbf{P}^{3[3]} & \mathbf{P}^{4[3]} \end{vmatrix} \right. \\ & \left. - \mathbf{P}_a^{[1]}\mathbf{P}^{a[3]} \begin{vmatrix} \mathbf{P}^{2[-3]} & \mathbf{P}^{3[-3]} & \mathbf{P}^{4[-3]} \\ \mathbf{P}^{2[-1]} & \mathbf{P}^{3[-1]} & \mathbf{P}^{4[-1]} \\ \mathbf{P}^{2[1]} & \mathbf{P}^{3[1]} & \mathbf{P}^{4[1]} \end{vmatrix} \mathbf{Q}_i^{[1]} - \mathbf{P}_a^{[-1]}\mathbf{P}^{a[-3]} \begin{vmatrix} \mathbf{P}^{2[-1]} & \mathbf{P}^{3[-1]} & \mathbf{P}^{4[-1]} \\ \mathbf{P}^{2[1]} & \mathbf{P}^{3[1]} & \mathbf{P}^{4[1]} \\ \mathbf{P}^{2[3]} & \mathbf{P}^{3[3]} & \mathbf{P}^{4[3]} \end{vmatrix} \mathbf{Q}_i^{[-1]} \right) \end{aligned} \tag{A.26}$$

In this way one can avoid the constant ambiguity arising in (4.26).

A.5 The LLL-algorithm

We here describe how the LLL-algorithm [144] is applied to a very simple example, following the discussion in [145]. The basic idea behind the method is to find a vector in a given basis that minimises the Euclidean length.

The contribution $\mathcal{P}_2^{\text{rat}}(S)$ to the reciprocity function $\mathcal{P}(S)$ for twist-2 operators has transcendentality 3 and can thus be expressed in the four-dimensional basis of binomial sums with transcendentality 3,

$$\mathcal{P}_2^{\text{rat}}(S) = d_3\mathbb{S}_3(S) + d_{2,1}\mathbb{S}_{2,1}(S) + d_{1,2}\mathbb{S}_{1,2}(S) + d_{1,1,1}\mathbb{S}_{1,1,1}(S)\,. \tag{A.27}$$

We will try to obtain the four coefficients d from just three values of $\mathcal{P}_2^{\text{rat}}$ at $S = 2, 4, 6$. This gives us an underdetermined system:

$$\frac{3}{4}d_3 + \frac{9}{4}d_{2,1} + \frac{15}{4}d_{1,2} + \frac{21}{4}d_{1,1,1} = 12 \tag{A.28}$$

$$\frac{865}{864}d_3 + \frac{2035}{864}d_{2,1} + \frac{4885}{864}d_{1,2} + \frac{11095}{864}d_{1,1,1} = \frac{475}{18} \tag{A.29}$$

$$\frac{39151}{36000}d_3 + \frac{28567}{12000}d_{2,1} + \frac{246911}{36000}d_{1,2} + \frac{734461}{36000}d_{1,1,1} = \frac{16121}{450} \tag{A.30}$$

We can multiply these equations by the greatest appearing denominator, divide by the greatest common divisor, and package them into a 3×5 matrix,

$$\begin{pmatrix} 1 & 3 & 5 & 7 & -16 \\ 173 & 407 & 977 & 2219 & -4560 \\ 799 & 1749 & 5039 & 14989 & -26320 \end{pmatrix}. \tag{A.31}$$

Next, we combine the transpose of this matrix multiplied by a very large number, e.g. 10^{10}, with a 5×5 identity matrix,

$$\begin{pmatrix} 1 & 0 & 0 & 0 & 0 & 10000000000 & 1730000000000 & 7990000000000 \\ 0 & 1 & 0 & 0 & 0 & 30000000000 & 4070000000000 & 17490000000000 \\ 0 & 0 & 1 & 0 & 0 & 50000000000 & 9770000000000 & 50390000000000 \\ 0 & 0 & 0 & 1 & 0 & 70000000000 & 22190000000000 & 149890000000000 \\ 0 & 0 & 0 & 0 & 1 & -160000000000 & -45600000000000 & -263200000000000 \end{pmatrix}. \tag{A.32}$$

The LLL-algorithm, which in `Mathematica` is implemented in the function `LatticeReduce`, is now applied to this matrix. The result is

$$\begin{pmatrix} 0 & -8 & 8 & 0 & 1 & 0 & 0 & 0 \\ 38 & -8 & -1 & 1 & 1 & 0 & 0 & 0 \\ 5 & -3 & -2 & -1 & -1 & -50000000000 & 310000000000 & 10000000000 \\ 8 & -13 & -8 & -5 & -5 & -260000000000 & -180000000000 & -20000000000 \\ -15 & 4 & 1 & 0 & 0 & 20000000000 & 100000000000 & 500000000000 \end{pmatrix}. \tag{A.33}$$

The rows with zeros in the last three columns correspond to possible solutions to our underdetermined problem. They are ordered after the corresponding norm, so the upper row is the likely candidate. Indeed the upper row translates to

$$-8\mathbb{S}_{2,1} + 8\mathbb{S}_{1,2} = \mathcal{P}_2^{\text{rat}}, \tag{A.34}$$

which matches the result found from direct matching in section 7.1.3.

Appendix B

Special functions

This appendix collects the definitions and relevant properties of the special functions that arise in the perturbative treatment of the Quantum Spectral Curve. The sections about ζ-values and η-functions are heavily based on section 2 of [109], and we refer to this paper and references therein for a more complete discussion of the properties of these functions.

B.1 Zeta-values

Definition

The *Euler-Zagier sums* or *multiple zeta values* (MZV) are defined by the infinite sum

$$\zeta_{a_1,\ldots,a_k} = \sum_{0<n_1<\ldots<n_k<\infty} \frac{1}{n_1^{a_1}\cdots n_k^{a_k}}. \tag{B.1}$$

k is called the *depth* of the sum, while $w = \sum_{i=1}^{k} a_i$ is called *transcendentality* or *weight*. A ζ-value is called *irreducible* if it cannot be written in terms of ζ-values of lower depth or transcendentality.

B.1.1 Algebraic relations

ζ-values satisfy two important types of algebraic relations.

Stuffle relations

The stuffle product, $\star$, takes two ordered multi-indices and stuffles them in all possible ways, i.e. combines them without altering the respective ordering, but possibly adding indices from the two multi-indices. For example,

$$\begin{aligned} (a)\star(b) &= \{(a,b),(a+b),(b,a)\} \\ (a_1,a_2)\star(b) &= \{(a_1,a_2,b),(a_1,a_2+b),(a_1,b,a_2),(a_1+b,a_2),(b,a_1,a_2)\}. \end{aligned} \tag{B.2}$$

The ζ-values satisfy the *stuffle algebra*, $\zeta_A\zeta_B = \sum_{C\in A\star B}\zeta_C \equiv \zeta_A\star\zeta_B$, where a capital letter denotes a multi-index. For example, the product of two single-indexed ζ-values satisfies

$$\zeta_a\zeta_b = \zeta_a\star\zeta_b = \zeta_{a,b}+\zeta_{b,a}+\zeta_{a+b}\,, \tag{B.3}$$

which can be seen by spitting the summation on the left-hand side: $\sum_{n,m}\frac{1}{n^a m^b} = \sum_{n<m}\frac{1}{n^a m^b} + \sum_{n>m}\frac{1}{n^a m^b} + \sum_{n=m}\frac{1}{n^a m^b}$.

Shuffle relations

The shuffle product, $\sqcup\!\sqcup$, takes two ordered multi-indices and shuffles them in all possible ways, i.e. combines them without altering the respective ordering. For example,

$$\begin{aligned}(a)\sqcup\!\sqcup(b) &= \{(a,b),(b,a)\} \\ (a_1,a_2)\sqcup\!\sqcup(b) &= \{(a_1,a_2,b),(a_1,b,a_2),(b,a_1,a_2)\}\,.\end{aligned} \tag{B.4}$$

The ζ-values satisfy *shuffle relations*. However, these relations are more transparent in a different notation:

$$\zeta_{a,b,\ldots} = \hat{\zeta}_{\underbrace{1,0,\ldots,0}_{a},\underbrace{1,0,\ldots,0}_{b},1,0,\ldots} \tag{B.5}$$

Then $\hat{\zeta}_A$ satisfy the *shuffle algebra*, $\hat{\zeta}_A\hat{\zeta}_B = \sum_{C\in A\sqcup\!\sqcup B}\hat{\zeta}_C \equiv \hat{\zeta}_A\sqcup\!\sqcup\hat{\zeta}_B$. For example

$$\zeta_1\zeta_2 = \hat{\zeta}_1\hat{\zeta}_{1,0} = \hat{\zeta}_1\sqcup\!\sqcup\hat{\zeta}_{1,0} = 2\hat{\zeta}_{1,1,0}+\hat{\zeta}_{1,0,1} = 2\zeta_{1,2}+\zeta_{2,1}\,. \tag{B.6}$$

The shuffle relations can be derived explicitly using the Feynman representation,

$$\zeta_{a_1+1,a_2+1,\ldots,a_k+1} = \int_0^\infty \mathrm{d}\mu_1\int_{t_1}^\infty \mathrm{d}\mu_2\ldots\int_{t_{k-1}}^\infty \mathrm{d}\mu_k\,(t_1-t_2)^{a_1}\ldots(t_{k-1}-t_k)^{a_{k-1}}t_k^{a_k}, \tag{B.7}$$

where $\mathrm{d}\mu_i \equiv \frac{\mathrm{d}t_i}{a_i!(e^{t_i}-1)}$. For example,

$$\begin{aligned}\zeta_1\zeta_2 &= \int_0^\infty \mathrm{d}\mu_1\int_0^\infty \mathrm{d}\mu_2 t_2 \\ &= \int_0^\infty \mathrm{d}\mu_1\int_0^{t_1} \mathrm{d}\mu_2 t_2 + \int_0^\infty \mathrm{d}\mu_1\int_{t_1}^\infty \mathrm{d}\mu_2 t_2 \\ &= \int_0^\infty \mathrm{d}\mu_2\int_{t_2}^\infty \mathrm{d}\mu_1 t_2 + \int_0^\infty \mathrm{d}\mu_1\int_{t_1}^\infty \mathrm{d}\mu_2 t_2 \\ &= \int_0^\infty \mathrm{d}\mu_2\int_{t_2}^\infty \mathrm{d}\mu_1 (t_2-t_1) + \int_0^\infty \mathrm{d}\mu_2\int_{t_2}^\infty \mathrm{d}\mu_1 t_1 + \int_0^\infty \mathrm{d}\mu_1\int_{t_1}^\infty \mathrm{d}\mu_2 t_2 \\ &= 2\zeta_{1,2}+\zeta_{2,1}.\end{aligned} \tag{B.8}$$

Irreducible multiple zeta values

Since the stuffle and shuffle algebras provide two different ways to write a product of ζ-values as a linear combination of other ζ-values with the same total transcendentality, i.e. $\zeta_I \zeta_J = \sum c_{IJ}^K \zeta_K = \sum d_{IJ}^K \zeta_K$, we see that $\sum (c_{IJ}^K - d_{IJ}^K)\zeta_K = 0$, so all ζ-values are not linearly independent.

The stuffle and shuffle relations can be combined to yield identities such as $\zeta_{1,2} = \zeta_3$. According to the *diophantine conjecture* [157], all possible algebraic relations between ζ-values arise from the shuffle and stuffle algebras, which means that the total transcendentality is always preserved in such relations.

A possible choice for the basis of the number field spanned by the ζ-values is to pick the values with lowest depth and highest rightmost labels out of those that are linearly dependent. Table B.1 lists this basis up to transcendentality 15.

w	1	2	3	5	7	8	9	10	11	12	13	14	15
MZV	ζ_1	ζ_2	ζ_3	ζ_5	ζ_7	$\zeta_{2,6}$	ζ_9	$\zeta_{2,8}$	ζ_{11} $\zeta_{1,2,8}$	$\zeta_{2,10}$ $\zeta_{1,1,2,8}$	ζ_{13} $\zeta_{1,2,10}$ $\zeta_{1,3,9}$	$\zeta_{2,12}$ $\zeta_{4,10}$ $\zeta_{1,1,2,10}$	ζ_{15} $\zeta_{1,2,12}$ $\zeta_{1,3,11}$ $\zeta_{1,1,1,2,10}$

Table B.1: A possible basis of irreducible MZVs up to transcendentality $w = 15$. The ancillary files of [1] at arxiv.org contains a file with explicit replacement rules to reduce an expression to this basis.

Single-valued MZVs

The *single-valued multiple zeta-values* [129] are special combinations of MZVs that are expected to appear in quantum field theory results. The ones appearing in the perturbative results of chapter 6 are

$$\begin{aligned}
Z_{11}^{(2)} &= -\zeta_{3,5,3} + \zeta_3\,\zeta_{3,5}\,, \\
Z_{13}^{(2)} &= -\zeta_{5,3,5} + 11\,\zeta_5\,\zeta_{3,5} + 5\,\zeta_5\,\zeta_8\,, \\
Z_{13}^{(3)} &= -\zeta_{3,7,3} + \zeta_3\,\zeta_{3,7} + 12\,\zeta_5\,\zeta_{3,5} + 6\,\zeta_5\,\zeta_8\,, \\
Z_{15}^{(2)} &= \zeta_{3,7,5} - \zeta_5\,\zeta_{3,7} - 3\,\zeta_5\,\zeta_{10} + 21\,\zeta_9\,\zeta_6 + \frac{175}{2}\,\zeta_{11}\,\zeta_4 + \frac{637}{2}\,\zeta_{13}\,\zeta_2\,, \\
Z_{15}^{(3)} &= -\zeta_{3,9,3} + \zeta_3\,\zeta_{3,9} + 12\,\zeta_5\,\zeta_{3,7} + 30\,\zeta_7\,\zeta_{3,5} + 6\,\zeta_5\,\zeta_{10} + 15\,\zeta_7\,\zeta_8\,.
\end{aligned} \tag{B.9}$$

B.1.2 Twisted generalisation

In the fully twisted QSC, a twisted generalisation of the MZVs appears:

$$\zeta_{a_1,\ldots,a_k}^{\mathsf{x}_1,\ldots,\mathsf{x}_k} \equiv \sum_{1\le n_1<\ldots<n_k<\infty} \frac{\mathsf{x}_1^{n_1}\cdots\mathsf{x}_k^{n_k}}{n_1^{a_1}\cdots n_k^{a_2}}\,. \tag{B.10}$$

B.2 Harmonic and binomial sums

This appendix discusses the harmonic and binomial sums that appear in the analytic structure of the anomalous dimension of solution series discussed in chapter 7. The following discussion is heavily based on [142].

B.2.1 Harmonic sums, S

Definition

Harmonic sums are defined through

$$\mathbf{S}_a(S) \equiv \sum_{j=1}^{S} \frac{\text{sign}(a)^j}{j^{|a|}}\,, \qquad \mathbf{S}_{a_1,a_2,\ldots,a_n}(S) \equiv \sum_{j=1}^{S} \frac{\text{sign}(a_1)^j}{j^{|a_1|}} \mathbf{S}_{a_2,\ldots,a_n}(j)\,. \tag{B.11}$$

The transcendentality of a harmonic sum $\mathbf{S}_{a_1,\ldots,a_n}$ is defined as $w = \sum_{j=1}^{n} |a_j|$.

Algebraic relations and basis of given transcendentality

Harmonic sums satisfy algebraic relations similar to the stuffle relations, e.g.

$$\mathbf{S}_a \mathbf{S}_b = \mathbf{S}_{a,b} + \mathbf{S}_{b,a} - \mathbf{S}_{\text{sign}(ab)(|a|+|b|)}\,, \tag{B.12}$$

where the argument of the harmonic sums are the same. This type of relations allows one to linearise products of harmonic sums. All multi-indexed harmonic sums of a given transcendentality form a basis for any possible expression of that transcendentality.

An algorithm to generate the relations of the type (B.12), i.e. to write $\mathbf{S}_{a_1,a_2,\ldots,a_m}\mathbf{S}_{b_1,b_2,\ldots,b_n}$ in the linear basis, was given in [142] and can be summarised in the following way:

- Start from the expression $\mathbf{S}^{(1)}_{a_1,a_2,\ldots,a_m}\mathbf{S}^{(2)}_{b_1,b_2,\ldots,b_n}\mathbf{S}^{(3)}_{\emptyset}$.
- Recursively move indices to $\mathbf{S}^{(3)}$ via the replacement rule

$$\begin{aligned}\mathbf{S}^{(1)}_{a_1,a_2,\ldots,a_m}\mathbf{S}^{(2)}_{b_1,b_2,\ldots,b_n}\mathbf{S}^{(3)}_{c_1,c_2,\ldots,c_k} \;\to\; &+\mathbf{S}^{(1)}_{a_1,a_2,\ldots,a_m}\mathbf{S}^{(2)}_{b_2,\ldots,b_n}\mathbf{S}^{(3)}_{c_1,c_2,\ldots,c_k,b_1} \\ &+\mathbf{S}^{(1)}_{a_2,\ldots,a_m}\mathbf{S}^{(2)}_{b_1,b_2,\ldots,b_n}\mathbf{S}^{(3)}_{c_1,c_2,\ldots,c_k,a_1} \\ &-\mathbf{S}^{(1)}_{a_2,\ldots,a_m}\mathbf{S}^{(2)}_{b_2,\ldots,b_n}\mathbf{S}^{(3)}_{c_1,c_2,\ldots,c_k,\text{sign}(a_1b_1)(|a_1|+|b_1|)}\end{aligned} \tag{B.13}$$

  until either $\mathbf{S}^{(1)}$ or $\mathbf{S}^{(2)}$ runs out of indices.

- Replace bilinear terms via ($i \in \{1,2\}$)

$$\mathbf{S}^{(i)}_{a_1,a_2,\ldots,a_m}\mathbf{S}^{(3)}_{c_1,c_2,\ldots,c_k} \;\to\; \mathbf{S}_{c_1,c_2,\ldots,c_k,a_1,a_2,\ldots,a_m}\,. \tag{B.14}$$

For example, to express the product $\mathbf{S}_1\mathbf{S}_2$ the procedure yields

$$\mathbf{S}^{(1)}_1\mathbf{S}^{(2)}_2\mathbf{S}^{(3)}_{\emptyset} \;\to\; \mathbf{S}^{(1)}_1\mathbf{S}^{(3)}_2 + \mathbf{S}^{(2)}_2\mathbf{S}^{(3)}_1 - \mathbf{S}^{(3)}_3 \;\to\; \mathbf{S}_{1,2} + \mathbf{S}_{2,1} - \mathbf{S}_3\,, \tag{B.15}$$

so $\mathbf{S}_1\mathbf{S}_2 = \mathbf{S}_{1,2} + \mathbf{S}_{2,1} - \mathbf{S}_3$.

Analytic continuation

For simplicity, we here describe the case $\mathbf{S}_{a>0}$. The generalisation to negative and multiple indices can be done along the same lines. The analytic continuation to non-integer S is obtained by the trick

$$\mathbf{S}_a(S) = \sum_{j=1}^{S} \frac{1}{j^a} = \sum_{j=1}^{\infty} \left(\frac{1}{j^a} - \frac{1}{(j+S)^a} \right) = \zeta_a - \sum_{j=1}^{\infty} \frac{1}{(j+S)^a} \,. \tag{B.16}$$

Derivatives

The derivative of a harmonic sum with respect to its argument can be found by considering the analytic continuation (B.16):

$$\frac{\mathrm{d}}{\mathrm{d}S}\mathbf{S}_a(S) = a \sum_{j=1}^{\infty} \frac{1}{(j+S)^{a+1}} = a \left(\sum_{j=1}^{\infty} \frac{1}{j^{a+1}} - \sum_{j=1}^{S} \frac{1}{j^{a+1}} \right) = a\big(\zeta_{a+1} - \mathbf{S}_{a+1}(S)\big) \,. \tag{B.17}$$

Power expansion

To more generally do a power expansion around a positive integer S_0, we can again use (B.16). For example,

$$\begin{aligned}
\mathbf{S}_a(S_0+w) &= \zeta_a - \sum_{j=1}^{\infty} \frac{1}{(j+S_0+w)^a} \\
&= \zeta_a - \sum_{j=1}^{\infty} \sum_{k=0}^{\infty} \frac{(\text{-}1)^k [a]_k}{k!(j+S_0)^{a+k}} w^k \\
&= \zeta_a + \sum_{k}^{\infty} \frac{(\text{-}1)^k [a]_k}{k!} \left(\mathbf{S}_{a+k}(S_0) - \zeta_{a+k} \right) w^k \\
&= \mathbf{S}_a(S_0) - a \left(\mathbf{S}_{a+1}(S_0) - \zeta_{a+1} \right) w + \frac{a(a+1)}{2} \left(\mathbf{S}_{a+2}(S_0) - \zeta_{a+2} \right) w^2 + \mathcal{O}(w^3) \,.
\end{aligned} \tag{B.18}$$

Behaviour at negative integer arguments

It is clear from (B.16) that $\mathbf{S}$ has poles at negative integer arguments. In the BFKL and double logarithmic limits, we need to expand around such points. Consider the argument $S = S_0 + w$ where $S_0 \in \mathbb{Z}_-$. We then get

$$\begin{aligned}
\mathbf{S}_a(S_0+w) &= \zeta_a - \sum_{j=1}^{-S_0-1} \frac{1}{(-j+w)^a} - \frac{1}{w^a} - \sum_{j=1}^{\infty} \frac{1}{(j+w)^a} \qquad \text{(B.19)}\\
&= \zeta_a - \frac{1}{w^a} - \sum_{j=1}^{-S_0-1} \sum_{k=0}^{\infty} \frac{(\text{-}1)^k [a]_k}{k!(\text{-}j)^{a+k}} w^k - \sum_{j=1}^{\infty} \sum_{k=0}^{\infty} \frac{(\text{-}1)^k [a]_k}{k! j^{a+k}} w^k \\
&= \zeta_a - \frac{1}{w^a} - \sum_{k=0}^{\infty} \frac{[a]_k}{k!} \Big((\text{-}1)^a \mathbf{S}_{a+k}(-S_0-1) + (\text{-}1)^k \zeta_{a+k} \Big) w^k \\
&= -\frac{1}{w^a} - (\text{-}1)^a \mathbf{S}_a(-S_0-1) - w\, a\big((\text{-}1)^a \mathbf{S}_{a+1}(-S_0-1) - \zeta_{a+1}\big) + \mathcal{O}(w^2)\,.
\end{aligned}$$

B.2.2 Binomial sums, $\mathbb{S}$

Definition

The *binomial sums* are defined in terms of the harmonic sums (B.11) via

$$\mathbb{S}_{a_1,\ldots,a_n}(N) = (-1)^N \sum_{j=1}^{N} (-1)^j \binom{N}{j} \binom{N+j}{j} \mathbf{S}_{a_1,\ldots,a_n}(j)\,. \qquad \text{(B.20)}$$

Basis of given transcendentality

As for the harmonic sums, the binomial sums satisfy algebraic relations that make it possible to write any term of a given transcendentality in a linearised basis.

Relations between harmonic and binomial sums with same argument

Binomial sums can be reexpressed in terms of harmonic sums with the same argument. In practice, an easy way to find these relations is to simply match the sums at a large enough set of fixed values. For the lowest transcendentalities, the relations are

$$\begin{aligned}
\mathbb{S}_1 &= 2\mathbf{S}_1 && \text{(B.21a)}\\
\mathbb{S}_2 &= -2\mathbf{S}_{\text{-}2} && \text{(B.21b)}\\
\mathbb{S}_{1,1} &= -2\mathbf{S}_2 + 4\mathbf{S}_{1,1} && \text{(B.21c)}\\
\mathbb{S}_3 &= 2\mathbf{S}_{\text{-}3} - 4\mathbf{S}_{\text{-}2,1} && \text{(B.21d)}\\
\mathbb{S}_{2,1} &= 2\mathbf{S}_3 && \text{(B.21e)}\\
\mathbb{S}_{1,2} &= 2\mathbf{S}_{\text{-}3} - 4\mathbf{S}_{1,\text{-}2} && \text{(B.21f)}\\
\mathbb{S}_{1,1,1} &= 2\mathbf{S}_3 - 4\mathbf{S}_{1,2} - 4\mathbf{S}_{2,1} + 8\mathbf{S}_{1,1,1}\,. && \text{(B.21g)}
\end{aligned}$$

B.3 Eta-functions

In this appendix, we discuss the aspects of Hurwitz η-functions relevant for the perturbative solution algorithms of the QSC. The section is simply a summary of the discussion in [109], to which we refer for further details.

Definition

The multiple Hurwitz η-functions are defined as

$$\eta_{k_1,k_2,\ldots,k_n}(u) \equiv \sum_{0\leq j_1<\ldots<j_n}^{\infty} \frac{1}{(u+\mathbb{i}j_1)^{k_1}\cdots(u+\mathbb{i}j_n)^{k_n}}. \tag{B.22}$$

Note that they can be defined iteratively through

$$\eta_{k,K} \equiv \sum_{j=0}^{\infty} \frac{\eta_K^{[2+2n]}}{(u+\mathbb{i}j)^k}\,. \tag{B.23}$$

It follows from the definition that the η-functions satisfy the relation

$$\eta_{k,K} - \eta_{k,K}^{[2]} = \frac{\eta_K^{[2]}}{u^k}, \tag{B.24}$$

which can be used to uniformise the shifts in expressions. The single-indexed η-functions are related to the polygamma function, $\psi^{(k)}$, via

$$\eta_k(u) = \frac{\mathbb{i}^k}{(k-1)!}\psi^{(k-1)}(-\mathbb{i}u)\,. \tag{B.25}$$

Algebraic relations

The η-functions satisfy stuffle relations the stuffle algebra $\eta_J\eta_K = \sum_{I\in J\star K}\eta_I$, e.g.

$$\eta_{k_1}\eta_{k_2} = \eta_{k_1,k_2} + \eta_{k_2,k_1} + \eta_{k_1+k_2} \tag{B.26a}$$

$$\eta_{k_1}\eta_{k_2,k_3} = \eta_{k_1,k_2,k_3} + \eta_{k_2,k_1,k_3} + \eta_{k_2,k_3,k_1} + \eta_{k_1+k_2,k_3} + \eta_{k_2,k_1+k_3}\,. \tag{B.26b}$$

The η-functions are linearly independent as they satisfy no other relations of this kind, i.e.

$$\sum_K c_K\eta_K = 0 \quad\Rightarrow\quad c_K = 0\,. \tag{B.27}$$

The stuffle-relations can be used to linearise any expression in η-functions.

Power expansion at $u = 0$

The power expansion of η-functions at $u = 0$ is one of the main operations in the perturbative algorithms described in chapter 6. The expansion contains MZVs, and for a single-indexed η-function it has the structure

$$\eta_k = \frac{1}{u^k} + (\text{-}\mathbb{i})^k\sum_{j=0}^{\infty}\frac{\mathbb{i}^j[k]_j}{j!}u^j\zeta_{k+j}\,, \tag{B.28}$$

where $[k]_j$ is the Pochhammer symbol. In the multi-indexed case, the expansion is

$$\begin{aligned}\eta_{k_1,k_2,k_3,\dots} &= \frac{1}{u^{k_1}}(\text{-}\mathbb{i})^{k_2+k_3+\dots}\sum_{j_2,j_3,\dots=0}^{\infty}\frac{\mathbb{i}^{j_2+j_3+\dots}[k_2]_{j_2}[k_3]_{j_3}\cdots}{j_2!j_3!\cdots}u^{j_2+j_3+\dots}\zeta_{k_2+j_2,k_3+j_3,\dots}\\ &+(\text{-}\mathbb{i})^{k_1+k_2+\dots}\sum_{j_1,j_2,\dots=0}^{\infty}\frac{\mathbb{i}^{j_1+j_2+\dots}[k_1]_{j_1}[k_2]_{j_2}\cdots}{j_1!j_2!\cdots}u^{j_1+j_2+\dots}\zeta_{k_1+j_1,k_2+j_2,\dots}\,. \quad \text{(B.29)}\end{aligned}$$

B.3.1 Periodic functions

To parametrise $\mathbb{i}$-periodic functions with at most constant asymptotics and poles only at $\mathbb{i}\mathbb{Z}$, we use the functions

$$\mathcal{P}_k(u) \equiv \sum_{n=-\infty}^{\infty}\frac{1}{(u+\mathbb{i}n)^k} = \eta_k + \bar{\eta}_k^{[-2]}\,. \quad \text{(B.30)}$$

Relation to trigonometric functions

The $\mathbb{i}$-periodic functions $\mathcal{P}_k$ are related to $\coth(\pi u) = \frac{\cosh(\pi u)}{\sinh(\pi u)}$, through e.g.

$$\begin{aligned}\mathcal{P}_1 &= \pi\coth(\pi u)\\ \mathcal{P}_2 &= \pi^2\left(\coth^2(\pi u)-1\right)\\ \mathcal{P}_3 &= \pi^3\left(\coth^3(\pi u)-\coth(\pi u)\right)\,. \quad \text{(B.31)}\end{aligned}$$

The equality for $\mathcal{P}_1$ follows from the observation that both expressions have matching periodicity, poles and residues. All other relations can be derived by taking derivatives of the first, using that $\frac{\mathrm{d}}{\mathrm{d}u}\mathcal{P}_k = -k\mathcal{P}_{k+1}$. Note that $\mathcal{P}_k \sim e^{-2\pi u}$ at $u\to\infty$ for $k>1$.

Power expansion at $u=0$

The power expansion of $\mathcal{P}_k$ at $u=0$ is

$$\mathcal{P}_k = \frac{1}{u^k} + (\text{-}\mathbb{i})^k\sum_{j=0}^{\infty}\frac{\mathbb{i}^j[k]_j}{j!}\left(1-(-1)^{k+j}\right)\zeta_{k+j}u^j\,, \quad \text{(B.32)}$$

which only contains the transcendental numbers $\zeta_{2n}\sim\zeta_2^n\sim\pi^{2n}$.

B.3.2 Twisted generalisation

In the fully twisted QSC, and in the Q-operators of non-compact spin chains, we encounter a twisted generalisation of the η-functions:

$$\eta^{\mathsf{x}_1,\dots,\mathsf{x}_n}_{a_1,\dots,a_n}(u) \equiv \sum_{0\le k_1<\dots<k_n\le\infty}\frac{\mathsf{x}_1^{k_1}\cdots\mathsf{x}_n^{k_n}}{(u+\mathbb{i}k_1)^{a_1}\cdots(u+\mathbb{i}k_n)^{a_n}}\,. \quad \text{(B.33)}$$

Note that the sum is only well-defined when the twists x_i are phases. Products of twisted η-functions again satisfy stuffle relations that always make it possible to linearise expressions, e.g.

$$\eta^{\mathsf{x}_1}_{a_1}\eta^{\mathsf{x}_2}_{a_2} = \eta^{\mathsf{x}_1\mathsf{x}_2}_{a_1+a_2} + \eta^{\mathsf{x}_1,\mathsf{x}_2}_{a_1,a_2} + \eta^{\mathsf{x}_2,\mathsf{x}_1}_{a_2,a_1}\,. \quad \text{(B.34)}$$

Generalised Lerch transcendents

When working with Q-operators, we prefer to make the change of variables $z = \mathbb{i}u - \frac{1}{2}$. This makes it natural to work with the generalised Lerch transcendents defined by

$$\Phi^{\mathsf{x}_1,\mathsf{x}_2,\ldots,\mathsf{x}_n}_{a_1,a_2,\ldots,a_n}(z) = \sum_{0\le k_1<k_2<\ldots<k_n}^{\infty} \frac{\mathsf{x}_1^{k_1}\mathsf{x}_2^{k_2}\cdots\mathsf{x}_n^{k_n}}{(z+k_1)^{a_1}(z+k_2)^{a_2}\cdots(z+k_n)^{a_n}}\,. \tag{B.35}$$

These functions are equivalent to the twisted η-functions (B.33),

$$\Phi^{\mathsf{x}_1,\mathsf{x}_2,\ldots,\mathsf{x}_n}_{a_1,a_2,\ldots,a_n}(z) = \mathbb{i}^n \eta^{\mathsf{x}_1,\mathsf{x}_2,\ldots,\mathsf{x}_n}_{a_1,a_2,\ldots,a_n}(\mathbb{i}z)\,, \tag{B.36}$$

and they similarly satisfy stuffle relations, e.g.

$$\Phi^{\mathsf{x}_1}_{a_1}\Phi^{\mathsf{x}_2}_{a_2} = \Phi^{\mathsf{x}_1,\mathsf{x}_2}_{a_1,a_2} + \Phi^{\mathsf{x}_1\mathsf{x}_2}_{a_1+a_2} + \Phi^{\mathsf{x}_2,\mathsf{x}_1}_{a_2,a_1}\,. \tag{B.37}$$

It follows from the definition (B.35) that the generalised Lerch transcendents satisfy the identity

$$\Phi^{\mathsf{x},\mathsf{x}_1,\ldots,\mathsf{x}_n}_{a,a_1,\ldots,a_n}(z) = \frac{\mathsf{x}_1\cdots\mathsf{x}_n}{z^a}\Phi^{\mathsf{x}_1,\ldots,\mathsf{x}_n}_{a_1,\ldots,a_n}(z+1) + \mathsf{x}\mathsf{x}_1\cdots\mathsf{x}_n\Phi^{\mathsf{x},\mathsf{x}_1,\ldots,\mathsf{x}_n}_{a,a_1,\ldots,a_n}(z+1)\,. \tag{B.38}$$

Power expansion at $z = 0$

The power expansion of the generalised Lerch transcendents at $z = 0$ has the form

$$\begin{aligned}
\Phi^{\mathsf{x}}_{a} &= \frac{1}{z^a} + \sum_{j=0}^{\infty}\frac{(-1)^j[a]_j}{j!}u^j\zeta^{\mathsf{x}}_{a+j}\,, \qquad (B.39)\\
\Phi^{\mathsf{x}_1,\mathsf{x}_2,\ldots}_{a_1,a_2,\ldots} &= \frac{1}{z^{a_1}}\sum_{j_2,j_3,\ldots=0}^{\infty}\frac{(-1)^{j_2+j_3+\cdots}[a_2]_{j_2}[a_3]_{j_3}\cdots}{j_2!j_3!\cdots}u^{j_2+j_3+\cdots}\zeta^{\mathsf{x}_2,\mathsf{x}_3,\ldots}_{a_2+j_2,a_3+j_3,\ldots}\\
&\quad + \sum_{j_1,j_2,\ldots=0}^{\infty}\frac{(-1)^{j_1+j_2+\cdots}[a_1]_{j_1}[a_2]_{j_2}\cdots}{j_1!j_2!\cdots}u^{j_1+j_2+\cdots}\zeta^{\mathsf{x}_1,\mathsf{x}_2,\ldots}_{a_1+j_1,a_2+j_2,\ldots}\,.
\end{aligned}$$

B.4 Pochhammer, Gamma, Beta and Hypergeometric functions

This section collects a number of definitions and identities for Pochhammer symbols, Gamma functions, Beta functions and Hypergeometric functions that are used in the thesis. See e.g. [158] for more details.

B.4.1 Gamma functions and the rising Pochhammer symbol

For $n \in \mathbb{N}_+$ the Gamma function and the rising Pochhammer symbol satisfy

$$[z]_n \equiv \frac{\Gamma(z+n)}{\Gamma(z)} = z(z+1)\cdots(z+n-1) \tag{B.40a}$$

$$[z-n+1]_n = (-1)^n[-z]_n \tag{B.40b}$$

$$[z]_{-n} \equiv \frac{\Gamma(z-n)}{\Gamma(z)} = \frac{1}{[z-n]_n} = \frac{(-1)^n}{[1-z]_n} \tag{B.40c}$$

$$[z]_{n+m} = [z]_n[z+n]_m\,. \tag{B.40d}$$

One can do the following partial fraction decomposition:

$$\frac{1}{[z]_k} = \sum_{j=0}^{k-1} \frac{(\text{-}1)^j}{(z+j)j!(k-1-j)!}\,. \tag{B.41}$$

Appearance in oscillator products

For oscillators satisfying $[\mathbf{a}, \mathbf{a}^\dagger] = \mathbf{a}\mathbf{a}^\dagger - \mathbf{a}^\dagger\mathbf{a} = 1$ the following reorderings can be made:

$$(\mathbf{a}^\dagger)^k\mathbf{a}^k = \frac{\Gamma(\mathbf{N_a}+1)}{\Gamma(\mathbf{N_a}-k+1)} = [\mathbf{N_a}-k+1]_k \tag{B.42}$$

$$\mathbf{a}^k(\mathbf{a}^\dagger)^k = \frac{\Gamma(\mathbf{N_a}+1+k)}{\Gamma(\mathbf{N_a}+1)} = [\mathbf{N_a}+1]_k\,. \tag{B.43}$$

B.4.2 Beta function

For $\mathrm{Re}\,(x) > 0$ and $\mathrm{Re}\,(y) > 0$, the Beta function is defined by

$$\mathrm{B}(x,y) = \int_0^\infty \mathrm{d}t\; t^{x-1}(1-t)^{y-1} = \frac{\Gamma(x)\Gamma(y)}{\Gamma(x+y)}\,. \tag{B.44}$$

B.4.3 Hypergeometric functions

The generalised Hypergeometric function is defined by

$${}_pF_q\left(\begin{matrix}a_1,\ldots a_p\\ b_1,\ldots,b_q\end{matrix};z\right) \equiv \sum_{n=0}^{\infty} \frac{[a_1]_n\cdots[a_p]_n}{[b_1]_n\cdots[b_q]_n}\frac{z^n}{n!}\,. \tag{B.45}$$

Euler transform

The function ${}_2F_1$ satisfies the relation

$$ {}_2F_1\left(\begin{matrix}a,b\\c\end{matrix};z\right) \;=\; (1-z)^{c-a-b}\,{}_2F_1\left(\begin{matrix}c-a,c-b\\c\end{matrix};z\right)\,. \tag{B.46} $$

Euler integral transform

For $c\in\mathbb{N}_+$,

$$ {}_{p+1}F_{q+1}\left(\begin{matrix}a_1,\ldots a_p,c\\b_1,\ldots,b_q,d\end{matrix};z\right) \;=\; \frac{\Gamma(d)}{\Gamma(c)\Gamma(d-c)}\int_0^1 \mathrm{d}t\; t^{c-1}(1-t)^{d-c-1}\,{}_pF_q\left(\begin{matrix}a_1,\ldots a_p\\b_1,\ldots,b_q\end{matrix};tz\right)\,. \tag{B.47} $$

Relation for ${}_3F_2$

The function ${}_3F_2$ satisfies the relation

$$ {}_3F_2\left(\begin{matrix}a,b,c\\d,e\end{matrix};1\right) = \frac{\Gamma(e)\Gamma(d+e-a-b-c)}{\Gamma(e-a)\Gamma(d+e-b-c)}\,{}_3F_2\left(\begin{matrix}a,d-b,d-c\\d,d+e-b-c\end{matrix};1\right)\,. \tag{B.48} $$

Appendix C

Discrete calculus

This appendix collects the technical details related to solving finite-difference equations and evaluating auxiliary space traces for Q-operators.

C.1 The Ψ-operation

The Ψ-operation plays a role in several chapters of the thesis, and it is one of the main operations in the perturbative algorithms of chapter 6.

Definition

The Ψ operation is defined as the inverse of the difference operator $\nabla(f) = f - f^{[2]}$, and is unique up to the addition of an $\mathbb{i}$-periodic function $\mathcal{P}$, which needs to be fixed from boundary conditions, i.e.

$$\Psi(f - f^{[2]}) = f + \mathcal{P}\,. \tag{C.1}$$

It can be represented by the infinite sum $\Psi(f) = \sum_{k=0}^{\infty} f^{[2k]}$ when this sum is convergent.

In this appendix we explain how to compute the action of the Ψ-operator (C.1) on the algebra of functions encountered in the perturbative solution of the QSC. It will be clear that this class of functions is closed with respect to the action of Ψ.

C.1.1 Action on basis of functions appearing in the QSC

First note that any rational function of the form $\frac{\sum_a b_a u^a}{\prod_{n,m}(u+in)^m}$ can be rewritten as a sum of a polynomial and shifted inverse powers, $\sum c_a u^a + \sum_{n,m} \frac{d_{n,m}}{(u+in)^m}$. The expressions encountered in the perturbative solution of the QSC can then be split in four classes of functions of the spectral parameter: monomials, shifted inverse powers, products of monomials and η-functions, and products of inverse powers and η-functions. Note that $\mathbb{i}$-periodic functions $\mathcal{P}_a$ (B.30) are treated as constants by Ψ, i.e. $\Psi(\mathcal{P}_a\, f) = \mathcal{P}_a\, \Psi(f)$.

Monomials

Applying Ψ to a polynomial $p(u) = \sum_{a=0}^{n} c_a u^a$ results in a polynomial of one order higher, $f(u) = \Psi(p(u))$, found from solving the equation

$$f(u) - f(u + \mathbb{i}) = p(u)\,. \tag{C.2}$$

In practice, one can compute and store only the action on monomials $\Psi(u^a)$.

Shifted inverse powers

By the definition of the η-function (B.22), the action of Ψ on a shifted inverse power is

$$\Psi\left(\frac{1}{(u+\mathbb{i}n)^a}\right) = \sum_{m=0}^{\infty} \frac{1}{(u+\mathbb{i}n+\mathbb{i}m)^a} = \eta_a^{[2n]}\,. \tag{C.3}$$

For $a \geq 2$ the sum is convergent, while for $a = 1$ we regularise the logarithmically divergent sum by postulating that it is equal to $\eta_1^{[2n]}$, which is defined as $\eta_1(u) \equiv \mathbb{i}\psi(-\mathbb{i}u)$ [109], where ψ is the digamma function.

Terms of the form $\frac{\eta}{(u+\mathbb{i}n)^a}$

To handle products of η-functions and shifted inverse powers, we use the representation $\Psi(f) \equiv \sum_{n=0}^{\infty} f^{[2n]}$ when the sum is convergent. Therefore

$$\Psi\left(\frac{\eta_A^{[2n+2]}}{(u+\mathbb{i}n)^a}\right) = \eta_{a,A}^{[2n]}\,. \tag{C.4}$$

The logarithmically divergent sums are always regularised so as to satisfy (C.4).

When an expression of the kind $\Psi\left(\frac{\eta_A^{[2n]}}{(u+\mathbb{i}m)^a}\right)$ is encountered, the strategy is to shift the η-function using the relation (B.24) until the produced terms have the form (C.4) or the η-function runs out of indices.

Terms of the form $u^a\eta$

Products of monomials and η-functions are handled using the relation

$$\nabla\left(\Psi(u^a)\eta_{b,A}^{[2n]}\right) = u^a\eta_{b,A}^{[2n]} + \Psi(u^a)^{[2]}\frac{1}{(u+\mathbb{i}n)^b}\eta_A^{[2+2n]}\,, \tag{C.5}$$

which leads to

$$\Psi(u^a\eta_{b,A}^{[2n]}) \;=\; \Psi(u^a)\eta_{b,A}^{[2n]} - \Psi\left(\Psi(u^a)^{[2]}\frac{1}{(u+\mathbb{i}n)^b}\eta_A^{[2+2n]}\right)\,. \tag{C.6}$$

The last relation is applied repeatedly until the produced terms are products of shifted inverse powers and η-functions, or the η-function runs out of indices.

C.1.2 Action on twisted basis of functions

The action on the twisted basis of functions appearing in the Q-operator construction proceeds in complete analogy with the untwisted case. We here give the action on the basis of generalised Lerch transcendents and the redefined spectral parameter $z = \mathbb{i}u - \frac{1}{2}$, on which we define Ψ through $\Psi(f(z) - f(z+1)) = f(z) + \mathcal{P}$. This means that Ψ can be represented as $\Psi(f(z)) = \sum_{k=0}^{\infty} f(z+k)$ when the sum is convergent. The encountered functions can be split into four classes exactly as above.

Monomials, $\mathsf{x}^z z^a$

For $\mathsf{x} \neq 1$, $\Psi(\mathsf{x}^z z^a)$ is another polynomial with an overall exponential factor of the form $p(z) = \mathsf{x}^z(c_a z^a + ... + c_0)$ satisfying the constraint $p(z) - p(z+1) = \mathsf{x}^z z^a$. This constraint fixes $p(z)$ completely. In the case $\mathsf{x} = 1$, the polynomial is of degree $a+1$ instead.

Shifted inverse powers

From the definition of the generalised Lerch transcendent (B.35) we have

$$\Psi\left(\frac{\mathsf{x}^z}{(z+m)^a}\right) = \mathsf{x}^z \Phi_a^{\mathsf{x}}(z+m)\,. \tag{C.7}$$

Terms of the form $\frac{\mathsf{x}^z \Phi}{(z+m)^a}$

Note that

$$\Psi\left(\frac{\mathsf{x}^z \Phi^{\mathsf{x}_1,\mathsf{x}_2,\ldots,\mathsf{x}_n}_{a_1,a_2,\ldots,a_n}(z+1)}{z^a}\right) = \mathsf{x}^z \Phi^{\mathsf{x},\mathsf{x}_1,\mathsf{x}_2,\ldots,\mathsf{x}_n}_{a,a_1,a_2,\ldots,a_n}(z)\,. \tag{C.8}$$

To evaluate $\Psi\left(\frac{\mathsf{x}^z \Phi^{\mathsf{x}_1,\mathsf{x}_2,\ldots,\mathsf{x}_n}_{a_1,a_2,\ldots,a_n}}{(z+m)^a}\right)$, use (B.38) to align the shifts and then use (C.8).

Terms of the form $\mathsf{x}^z z^a \Phi$

To evaluate products of monomials and generalised Lerch transcendents, one can, as in (C.6), use the finite difference analog of partial integration,

$$\Psi\left(f\left(g - g^{[2]}\right)\right) = fg - \Psi\left(g^{[2]}\left(f - f^{[2]}\right)\right)\,. \tag{C.9}$$

To evaluate $\Psi(\mathsf{x}^z z^a \Phi^{\mathsf{x}_1,\mathsf{x}_2,\ldots,\mathsf{x}_n}_{a_1,a_2,\ldots,a_n})$, set $f = (\mathsf{x}_1 \cdots \mathsf{x}_n)^z \Phi^{\mathsf{x}_1,\mathsf{x}_2,\ldots,\mathsf{x}_n}_{a_1,a_2,\ldots,a_n}$ and $g - g^{[2]} = \left(\frac{\mathsf{x}}{\mathsf{x}_1 \cdots \mathsf{x}_n}\right)^z z^a$. This can be used recursively until no terms of this type are present.

C.2 Evaluating auxiliary space traces

We encounter the following three expressions in the normalised supertraces (8.20). By $\widehat{\mathrm{str}}_{ab}$ we refer to the normalised supertrace over the factor space in which the oscillator $\boldsymbol{\xi}_{ab}$ acts.

Monomials

Using the same argument as in section 2.3.3, the trace over a monomial is

$$\widehat{\mathrm{str}}_{ab}\,\mathbf{N}_{ab}^{k}=\begin{cases}\dfrac{\sum_{n=0}^{k}\left\langle {k \atop n}\right\rangle\left(\frac{\mathsf{x}_a}{\mathsf{x}_b}\right)^{n+1-\delta_{k,0}}}{\left(1-\frac{\mathsf{x}_a}{\mathsf{x}_b}\right)^{k}} & \text{bosonic}\\[2ex] \left(\dfrac{\mathsf{x}_a}{\mathsf{x}_a-\mathsf{x}_b}\right)^{1-\delta_{k,0}} & \text{fermionic}\end{cases}, \tag{C.10}$$

where $\left\langle {k \atop n}\right\rangle$ are the Eulerian numbers defined by

$$\left\langle {k \atop n}\right\rangle=\sum_{j=0}^{n+1}(-1)^{j}\binom{k+1}{j}(n-j+1)^{k}\,. \tag{C.11}$$

Negative powers

From the definition of the Lerch transcendent (C.7), we have

$$\widehat{\mathrm{str}}_{ab}\,\frac{1}{(\mathbf{N}_{ab}+r)^{\ell}}=\begin{cases}\frac{\mathsf{x}_b-\mathsf{x}_a}{\mathsf{x}_b}\,\Phi_{\ell-m}^{\frac{\mathsf{x}_a}{\mathsf{x}_b}}(r) & \text{bosonic}\\[2ex] \frac{1}{\mathsf{x}_b-\mathsf{x}_a}\left(\frac{\mathsf{x}_b}{r^{\ell}}-\frac{\mathsf{x}_a}{(r+1)^{\ell}}\right) & \text{fermionic}\end{cases}. \tag{C.12}$$

Monomial times Lerch transcendent

The trace over a product of a monomial and a Lerch transcendent is

$$\begin{aligned}&\widehat{\mathrm{str}}_{ab}\,\mathbf{N}_{ab}^{k}\Phi_{\ell}^{\mathsf{x}}(\mathbf{N}_{ab}+r)\\ &=\begin{cases}\frac{\mathsf{x}_b-\mathsf{x}_a}{\mathsf{x}_b}\left\{\frac{\delta_{k,0}+\sum_{t=1}^{k}\left\langle {k \atop t-1}\right\rangle\left(\frac{\mathsf{x}_a/\mathsf{x}_b}{\mathsf{x}}\right)^{t}}{\left(1-\frac{\mathsf{x}_a/\mathsf{x}_b}{\mathsf{x}}\right)^{k+1}}\Phi_{\ell}^{\mathsf{x}}(r)-\frac{1}{\mathsf{x}}\sum_{s=0}^{k}\binom{k}{s}\frac{\delta_{s,k}+\sum_{t=1}^{k-s}\left\langle {k-s \atop t-1}\right\rangle\left(\frac{\mathsf{x}_a/\mathsf{x}_b}{\mathsf{x}}\right)^{t}}{\left(1-\frac{\mathsf{x}_a/\mathsf{x}_b}{\mathsf{x}}\right)^{k-s+1}}\right.\\ \qquad\left.\times\left[\left(\sum_{j=0}^{s}\binom{s}{j}(1-r)^{s-j}\Phi_{\ell-j}^{\mathsf{x}_a/\mathsf{x}_b}(r-1)\right)-\delta_{s,0}\frac{1}{(r-1)^{\ell}}\right]\right\} & \text{bosonic}\\[2ex] \frac{1}{\mathsf{x}_b-\mathsf{x}_a}\Big(\mathsf{x}_b\delta_{k,0}\Phi_{\ell}^{\mathsf{x}}(r)-\mathsf{x}_a\Phi_{\ell}^{\mathsf{x}}(r+1)\Big) & \text{fermionic}\end{cases}\end{aligned}. \tag{C.13}$$

Proof To show this formula in the bosonic case, one can use a "partial summation" trick. Denote $f=f(j)$, $f^{+}=f(j+1)$, and $\Delta(f)\equiv f(j)-f(j+1)$. Observe that

$$\Delta(fg)=f^{+}\Delta(g)+g\Delta(f)\,. \tag{C.14}$$

Now sum over j to get ($\Sigma = \sum_{j=0}^{\infty}$)

$$\Sigma(g\Delta(f)) = fg|_{j=0} - \Sigma(f^{+}\Delta(g))\,. \tag{C.15}$$

To evaluate the expression

$$\sum_{j=0}^{\infty} \mathsf{y}^{j} j^{k} \Phi_{l}^{\mathsf{x}}(r+j)\,, \tag{C.16}$$

identify $g = \mathsf{x}^{j}\Phi_{l}^{\mathsf{x}}(r+j)$ and $\Delta(f) = (\frac{\mathsf{y}}{\mathsf{x}})^{j} j^{k}$. We then have $\Delta(g) = \frac{\mathsf{x}^{j}}{(r+j)^{l}}$, and we need to find f, which solves the equation

$$f(j) - f(j+1) = \left(\frac{\mathsf{y}}{\mathsf{x}}\right)^{j} j^{k}\,. \tag{C.17}$$

The solution to this equation has the structure

$$f(j) = \left(\frac{\mathsf{y}}{\mathsf{x}}\right)^{j} \sum_{s=0}^{k} \frac{(-1)^{k+1-s}\binom{k}{s} j^{s}}{(\frac{\mathsf{y}}{\mathsf{x}}-1)^{k+1-s}} \left(\delta_{s,k} + \sum_{t=1}^{k-s} \left\langle {k-s \atop t-1} \right\rangle \left(\frac{\mathsf{y}}{\mathsf{x}}\right)^{t}\right)\,. \tag{C.18}$$

Then

$$fg|_{j=0} = \Phi_{l}^{\mathsf{x}}(r) \frac{(-1)^{k+1}}{(\frac{\mathsf{y}}{\mathsf{x}}-1)^{k+1}} \left(\delta_{k,0} + \sum_{t=1}^{k} \left\langle {k \atop t-1} \right\rangle \left(\frac{\mathsf{y}}{\mathsf{x}}\right)^{t}\right)\,, \tag{C.19}$$

and (C.16) evaluates to

$$\Sigma(f^{+}\Delta(g)) \;=\; \frac{\mathsf{y}}{\mathsf{x}} \sum_{j=0}^{\infty} \frac{\mathsf{y}^{j}}{(r+j)^{l}} \sum_{s=0}^{k} \frac{(-1)^{k+1-s}\binom{k}{s}(j+1)^{s}}{(\frac{\mathsf{y}}{\mathsf{x}}-1)^{k+1-s}} \left(\delta_{s,k} + \sum_{t=1}^{k-s} \left\langle {k-s \atop t-1} \right\rangle \left(\frac{\mathsf{y}}{\mathsf{x}}\right)^{t}\right)\,. \tag{C.20}$$

Bibliography

[1] C. Marboe, D. Volin, Quantum spectral curve as a tool for a perturbative quantum field theory, Nucl. Phys. B899 (2015) 810–847. arXiv:1411.4758, doi:10.1016/j.nuclphysb.2015.08.021.

[2] C. Marboe, V. Velizhanin, D. Volin, Six-loop anomalous dimension of twist-two operators in planar $\mathcal{N} = 4$ SYM theory, JHEP 07 (2015) 084. arXiv:1412.4762, doi:10.1007/JHEP07(2015)084.

[3] C. Marboe, V. Velizhanin, Twist-2 at seven loops in planar $\mathcal{N} = 4$ SYM theory: full result and analytic properties, JHEP 11 (2016) 013. arXiv:1607.06047, doi:10.1007/JHEP11(2016)013.

[4] C. Marboe, D. Volin, Fast analytic solver of rational Bethe equations, J. Phys. A50 (20) (2017) 204002. arXiv:1608.06504, doi:10.1088/1751-8121/aa6b88.

[5] C. Marboe, D. Volin, The full spectrum of AdS5/CFT4 I: Representation theory and one-loop Q-system. arXiv:1701.03704.

[6] R. Frassek, C. Marboe, D. Meidinger, Evaluation of the operatorial Q-system for non-compact super spin chains, JHEP 09 (2017) 018. arXiv:1706.02320, doi:10.1007/JHEP09(2017)018.

[7] C. Marboe, D. Volin, The full spectrum of planar $\mathrm{AdS}_5/\mathrm{CFT}_4$ II, work in progress.

[8] F. Gliozzi, J. Scherk, D. I. Olive, Supersymmetry, Supergravity Theories and the Dual Spinor Model, Nucl. Phys. B122 (1977) 253–290. doi:10.1016/0550-3213(77)90206-1. • L. Brink, J. H. Schwarz, J. Scherk, Supersymmetric Yang-Mills Theories, Nucl. Phys. B121 (1977) 77–92. doi:10.1016/0550-3213(77)90328-5.

[9] S. Mandelstam, Light Cone Superspace and the Ultraviolet Finiteness of the N=4 Model, Nucl. Phys. B213 (1983) 149–168. doi:10.1016/0550-3213(83)90179-7. • L. Brink, O. Lindgren, B. E. W. Nilsson, The Ultraviolet Finiteness of the N=4 Yang-Mills Theory, Phys. Lett. B123 (1983) 323. doi:10.1016/0370-2693(83)91210-8.

[10] P. Di Francesco, P. Mathieu, D. Senechal, Conformal Field Theory, Graduate Texts in Contemporary Physics, Springer-Verlag, New York, 1997. doi:10.1007/978-1-4612-2256-9. URL http://www-spires.fnal.gov/spires/find/books/www?cl=QC174.52.C66D5::1997

[11] J. A. Minahan, Review of AdS/CFT Integrability, Chapter I.1: Spin Chains in N=4 Super Yang-Mills, Lett. Math. Phys. 99 (2012) 33–58. arXiv:1012.3983, doi:10.1007/s11005-011-0522-9.

[12] J. M. Maldacena, The large N limit of superconformal field theories and supergravity, Adv. Theor. Math. Phys. 2 (1998) 231–252. arXiv:hep-th/9711200. • S. S. Gubser, I. R. Klebanov, A. M. Polyakov, Gauge theory correlators from non-critical string theory, Phys. Lett. B428 (1998) 105–114. arXiv:hep-th/9802109, doi:10.1016/S0370-2693(98)00377-3. • E. Witten, Anti-de Sitter space and holography, Adv. Theor. Math. Phys. 2 (1998) 253–291. arXiv:hep-th/9802150.

[13] J. A. Minahan, K. Zarembo, The Bethe-ansatz for N = 4 super Yang-Mills, JHEP 03 (2003) 013. arXiv:hep-th/0212208.

[14] N. Gromov, V. Kazakov, S. Leurent, D. Volin, Quantum spectral curve for AdS_5/CFT_4, Phys.Rev.Lett. 112 (2014) 011602. arXiv:1305.1939, doi:10.1103/PhysRevLett.112.011602.

[15] N. Gromov, V. Kazakov, S. Leurent, D. Volin, Quantum spectral curve for arbitrary state/operator in AdS_5/CFT_4, JHEP 09 (2015) 187. arXiv:1405.4857, doi:10.1007/JHEP09(2015)187.

[16] V. Kac, Lie superalgebras, Advances in Mathematics 26 (1) (1977) 8 – 96. doi:http://dx.doi.org/10.1016/0001-8708(77)90017-2.
URL http://www.sciencedirect.com/science/article/pii/0001870877900172

[17] V. Kazakov, A. Sorin, A. Zabrodin, Supersymmetric Bethe ansatz and Baxter equations from discrete Hirota dynamics, Nucl. Phys. B790 (2008) 345–413. arXiv:hep-th/0703147, doi:10.1016/j.nuclphysb.2007.06.025.

[18] Z. Tsuboi, Analytic Bethe ansatz and functional equations associated with any simple root systems of the Lie superalgebra sl(r+1|s+1), Physica A252 (1998) 565–585. arXiv:0911.5387, doi:10.1016/S0378-4371(97)00625-0.

[19] I. Bars, M. Gunaydin, Unitary Representations of Noncompact Supergroups, Commun. Math. Phys. 91 (1983) 31. doi:10.1007/BF01206048. • M. Gunaydin, N. Marcus, The Spectrum of the S^5 Compactification of the Chiral $N = 2, D = 10$ Supergravity and the Unitary Supermultiplets of $U(2, 2/4)$, Class. Quant. Grav. 2 (1985) L11.

[20] N. Beisert, The complete one-loop dilatation operator of N = 4 super Yang-Mills theory, Nucl. Phys. B676 (2004) 3–42. arXiv:hep-th/0307015, doi:10.1016/j.nuclphysb.2003.10.019.

[21] N. Beisert, The dilatation operator of N = 4 super Yang-Mills theory and integrability, Phys. Rept. 405 (2005) 1–202. arXiv:hep-th/0407277, doi:10.1016/j.physrep.2004.09.007.

[22] I. Schur, Über die rationalen Darstellungen der allgemeinen linearen Gruppe, Sitzungsberichte Akad. Berlin 1927. • H. Weyl, The Classical Groups. Their Invariants and Representations, Princeton University Press, 1939.

[23] W. Fulton, J. Harris, Representation Theory: A First Course, Graduate Texts in Mathematics, Springer New York, 1991.
URL https://books.google.ie/books?id=6GUH8ARxhp8C

[24] N. Gromov, V. Kazakov, Z. Tsuboi, PSU(2,2|4) Character of Quasiclassical AdS/CFT, JHEP 07 (2010) 097. arXiv:1002.3981, doi:10.1007/JHEP07(2010)097.

[25] D. Volin, String hypothesis for gl(n|m) spin chains: a particle/hole democracy, Lett.Math.Phys. 102 (2012) 1–29. arXiv:1012.3454, doi:10.1007/s11005-012-0570-9.

[26] Z. Tsuboi, Wronskian solutions of the T, Q and Y-systems related to infinite dimensional unitarizable modules of the general linear superalgebra $gl(M|N)$, Nucl.Phys. B870 (2013) 92–137. arXiv:1109.5524, doi:10.1016/j.nuclphysb.2013.01.007.

[27] D. Volin, M. Gunaydin, Schwinger oscillators and classification of unitary representations of $su(N, M|K)$, to appear.

[28] G. Polya, R. C. Read, Combinatorial Enumeration of Groups, Graphs and Chemical Compounds, Springer Verlag, New York, 1987. • A. M. Polyakov, Gauge fields and space-time, Int. J. Mod. Phys. A17S1 (2002) 119–136. arXiv:hep-th/0110196, doi:10.1142/S0217751X02013071.

[29] M. Bianchi, J. F. Morales, H. Samtleben, On stringy AdS(5) x S**5 and higher spin holography, JHEP 07 (2003) 062. arXiv:hep-th/0305052, doi:10.1088/1126-6708/2003/07/062.

[30] V. K. Dobrev, V. B. Petkova, All Positive Energy Unitary Irreducible Representations of Extended Conformal Supersymmetry, Phys. Lett. B162 (1985) 127–132. doi:10.1016/0370-2693(85)91073-1. • V. K. Dobrev, V. B. Petkova, On the group theoretical approach to extended conformal supersymmetry: classification of multiplets, Lett. Math. Phys. 9 (1985) 287–298. doi:10.1007/BF00397755.

[31] L. Andrianopoli, S. Ferrara, On short and long SU(2,2/4) multiplets in the AdS / CFT correspondence, Lett. Math. Phys. 48 (1999) 145–161. arXiv:hep-th/9812067, doi:10.1023/A:1007550823624. • L. Andrianopoli, S. Ferrara, E. Sokatchev, B. Zupnik, Shortening of primary operators in N extended SCFT(4) and harmonic superspace analyticity, Adv. Theor. Math. Phys. 4 (2000) 1149–1197. arXiv:hep-th/9912007. • F. A. Dolan, H. Osborn, On short and semi-short representations for four-dimensional superconformal symmetry, Annals Phys. 307 (2003) 41–89. arXiv:hep-th/0209056, doi:10.1016/S0003-4916(03)00074-5.

[32] N. Beisert, M. Staudacher, The N=4 SYM integrable super spin chain, Nucl. Phys. B670 (2003) 439–463. arXiv:hep-th/0307042, doi:10.1016/j.nuclphysb.2003.08.015.

[33] N. Beisert, The su(2—3) dynamic spin chain, Nucl. Phys. B682 (2004) 487–520. arXiv:hep-th/0310252, doi:10.1016/j.nuclphysb.2003.12.032.

[34] N. Beisert, M. Bianchi, J. F. Morales, H. Samtleben, On the spectrum of AdS/CFT beyond supergravity, JHEP 02 (2004) 001. arXiv:hep-th/0310292.

[35] H. Bethe, On the theory of metals. 1. Eigenvalues and eigenfunctions for the linear atomic chain, Z. Phys. 71 (1931) 205–226.

[36] L. D. Faddeev, How Algebraic Bethe Ansatz works for integrable model, arXiv:hep-th/9605187.

[37] R. I. Nepomechie, A Spin chain primer, Int. J. Mod. Phys. B13 (1999) 2973–2986. arXiv:hep-th/9810032, doi:10.1142/S0217979299002800.

[38] M. Staudacher, Review of AdS/CFT Integrability, Chapter III.1: Bethe Ansätze and the R-Matrix Formalism, Lett. Math. Phys. 99 (2012) 191–208. arXiv:1012.3990, doi:10.1007/s11005-011-0530-9.

[39] R. J. Baxter, Partition function of the eight vertex lattice model, Annals Phys. 70 (1972) 193–228, [Annals Phys.281,187(2000)]. doi:10.1016/0003-4916(72)90335-1.

[40] V. V. Bazhanov, T. Lukowski, C. Meneghelli, M. Staudacher, A Shortcut to the Q-Operator, J.Stat.Mech. 1011 (2010) P11002. arXiv:1005.3261, doi:10.1088/1742-5468/2010/11/P11002.

[41] V. V. Bazhanov, R. Frassek, T. Lukowski, C. Meneghelli, M. Staudacher, Baxter Q-Operators and Representations of Yangians, Nucl.Phys. B850 (2011) 148–174. arXiv:1010.3699, doi:10.1016/j.nuclphysb.2011.04.006.

[42] V. Kazakov, S. Leurent, D. Volin, T-system on T-hook: Grassmannian Solution and Twisted Quantum Spectral Curve, JHEP 12 (2016) 044. arXiv:1510.02100, doi:10.1007/JHEP12(2016)044.

[43] P. P. Kulish, N. Y. Reshetikhin, Diagonalization of Gl(N) invariant transfer matrices and quantum N wave system (Lee model), J. Phys. A16 (1983) L591–L596.

[44] P. P. Kulish, Integrable graded magnets, J. Sov. Math. 35 (1986) 2648–2662, [Zap. Nauchn. Semin.145,140(1985)]. doi:10.1007/BF01083770.

[45] E. Ragoucy, G. Satta, Analytical Bethe Ansatz for closed and open $gl(M|N)$ super-spin chains in arbitrary representations and for any Dynkin diagram, JHEP 09 (2007) 001. arXiv:0706.3327, doi:10.1088/1126-6708/2007/09/001.

[46] R. Frassek, T. Lukowski, C. Meneghelli, M. Staudacher, Oscillator Construction of su(n|m) Q-Operators, Nucl.Phys. B850 (2011) 175–198. arXiv:1012.6021, doi:10.1016/j.nuclphysb.2011.04.008.

[47] R. Frassek, T. Lukowski, C. Meneghelli, M. Staudacher, Baxter Operators and Hamiltonians for 'nearly all' Integrable Closed $\mathfrak{gl}(n)$ Spin Chains, Nucl. Phys. B874 (2013) 620–646. arXiv:1112.3600, doi:10.1016/j.nuclphysb.2013.06.006.

[48] V. Kazakov, S. Leurent, Z. Tsuboi, Baxter's Q-operators and operatorial Backlund flow for quantum (super)-spin chains, Commun.Math.Phys. 311 (2012) 787–814. arXiv:1010.4022, doi:10.1007/s00220-012-1428-9.

[49] R. Frassek, T. Lukowski, C. Meneghelli, M. Staudacher, unpublished. • R. Frassek, Q-operators, Yangian invariance and the quantum inverse scattering method, Ph.D. thesis, Durham U., Dept. of Math. (2014). arXiv:1412.3339.
URL https://inspirehep.net/record/1333697/files/arXiv:1412.3339.pdf

[50] N. Beisert, C. Ahn, L. F. Alday, Z. Bajnok, J. M. Drummond, et al., Review of AdS/CFT Integrability: An Overview, Lett.Math.Phys. 99 (2012) 3–32. arXiv:1012.3982, doi:10.1007/s11005-011-0529-2.

[51] L. N. Lipatov, Asymptotic behavior of multicolor QCD at high energies in connection with exactly solvable spin models, JETP Lett. 59 (1994) 596–599, [Pisma Zh. Eksp. Teor. Fiz.59,571(1994)]. arXiv:hep-th/9311037.

[52] L. Faddeev, G. Korchemsky, High-energy QCD as a completely integrable model, Phys.Lett. B342 (1995) 311–322. arXiv:hep-th/9404173, doi:10.1016/0370-2693(94)01363-H.

[53] V. M. Braun, S. E. Derkachov, A. N. Manashov, Integrability of three-particle evolution equations in QCD, Phys. Rev. Lett. 81 (1998) 2020–2023. arXiv:hep-ph/9805225, doi:10.1103/PhysRevLett.81.2020.

[54] N. Beisert, C. Kristjansen, M. Staudacher, The dilatation operator of N = 4 super Yang-Mills theory, Nucl. Phys. B664 (2003) 131–184. arXiv:hep-th/0303060, doi:10.1016/S0550-3213(03)00406-1.

[55] C. Sieg, Superspace calculation of the three-loop dilatation operator of N=4 SYM theory, Phys. Rev. D84 (2011) 045014. arXiv:1008.3351, doi:10.1103/PhysRevD.84.045014.

[56] B. I. Zwiebel, N=4 SYM to two loops: Compact expressions for the non-compact symmetry algebra of the su(1,1—2) sector, JHEP 02 (2006) 055. arXiv:hep-th/0511109, doi:10.1088/1126-6708/2006/02/055.

[57] F. Fiamberti, A. Santambrogio, C. Sieg, D. Zanon, Wrapping at four loops in N=4 SYM, Phys.Lett. B666 (2008) 100–105. arXiv:0712.3522, doi:10.1016/j.physletb.2008.06.061. • V. Velizhanin, The four-loop anomalous dimension of the Konishi operator in N=4 supersymmetric Yang-Mills theory, JETP Lett. 89 (2009) 6–9. arXiv:0808.3832, doi:10.1134/S0021364009010020.

[58] B. Eden, P. Heslop, G. P. Korchemsky, V. A. Smirnov, E. Sokatchev, Five-loop Konishi in N=4 SYM, Nucl.Phys. B862 (2012) 123–166. arXiv:1202.5733, doi:10.1016/j.nuclphysb.2012.04.015.

[59] R. R. Metsaev, A. A. Tseytlin, Type IIB superstring action in AdS(5) x S(5) background, Nucl. Phys. B533 (1998) 109–126. arXiv:hep-th/9805028, doi:10.1016/S0550-3213(98)00570-7.

[60] I. Bena, J. Polchinski, R. Roiban, Hidden symmetries of the AdS(5) x S**5 superstring, Phys. Rev. D69 (2004) 046002. arXiv:hep-th/0305116, doi:10.1103/PhysRevD.69.046002.

[61] V. A. Kazakov, A. Marshakov, J. A. Minahan, K. Zarembo, Classical / quantum integrability in AdS/CFT, JHEP 05 (2004) 024. arXiv:hep-th/0402207.

[62] V. Kazakov, K. Zarembo, Classical / quantum integrability in non-compact sector of AdS/CFT, JHEP 0410 (2004) 060. arXiv:hep-th/0410105, doi:10.1088/1126-6708/2004/10/060. • N. Beisert, V. A. Kazakov, K. Sakai, Algebraic curve for the SO(6) sector of AdS/CFT, Commun. Math. Phys. 263 (2006) 611–657. arXiv:hep-th/0410253,

doi:10.1007/s00220-005-1528-x. • S. Schafer-Nameki, The Algebraic curve of 1-loop planar N=4 SYM, Nucl. Phys. B714 (2005) 3–29. arXiv:hep-th/0412254, doi:10.1016/j.nuclphysb.2005.02.034. • N. Beisert, V. Kazakov, K. Sakai, K. Zarembo, Complete spectrum of long operators in N=4 SYM at one loop, JHEP 0507 (2005) 030. arXiv:hep-th/0503200, doi:10.1088/1126-6708/2005/07/030. • N. Beisert, V. A. Kazakov, K. Sakai, K. Zarembo, The algebraic curve of classical superstrings on $AdS_5 \times S^5$, Commun. Math. Phys. 263 (2006) 659–710. arXiv:hep-th/0502226, doi:10.1007/s00220-006-1529-4.

[63] S. Schafer-Nameki, Review of AdS/CFT Integrability, Chapter II.4: The Spectral Curve, Lett. Math. Phys. 99 (2012) 169–190. arXiv:1012.3989, doi:10.1007/s11005-011-0525-6.

[64] N. Gromov, P. Vieira, The $AdS_5 \times S^5$ superstring quantum spectrum from the algebraic curve, Nucl. Phys. B789 (2008) 175–208. arXiv:hep-th/0703191, doi:10.1016/j.nuclphysb.2007.07.032.

[65] A. B. Zamolodchikov, A. B. Zamolodchikov, Factorized S-matrices in two dimensions as the exact solutions of certain relativistic quantum field models, Annals Phys. 120 (1979) 253–291. doi:10.1016/0003-4916(79)90391-9.

[66] P. Dorey, Exact S matrices, in: Conformal field theories and integrable models. Proceedings, Eotvos Graduate Course, Budapest, Hungary, August 13-18, 1996, 1996, pp. 85–125. arXiv:hep-th/9810026.

[67] M. Staudacher, The factorized S-matrix of CFT/AdS, JHEP 05 (2005) 054. arXiv:hep-th/0412188.

[68] N. Beisert, The $su(2|2)$ dynamic S-matrix, Adv. Theor. Math. Phys. 12 (2008) 945. arXiv:hep-th/0511082.

[69] N. Beisert, The Analytic Bethe Ansatz for a Chain with Centrally Extended $su(2|2)$ Symmetry, J. Stat. Mech. 0701 (2007) P017. arXiv:nlin/0610017.

[70] G. Arutyunov, S. Frolov, M. Zamaklar, The Zamolodchikov-Faddeev algebra for AdS(5) x S**5 superstring, JHEP 04 (2007) 002. arXiv:hep-th/0612229.

[71] A. Santambrogio, D. Zanon, Exact anomalous dimensions of N = 4 Yang-Mills operators with large R charge, Phys. Lett. B545 (2002) 425–429. arXiv:hep-th/0206079, doi:10.1016/S0370-2693(02)02627-8.

[72] R. A. Janik, The $AdS_5 x S^5$ superstring worldsheet S-matrix and crossing symmetry, Phys. Rev. D73 (2006) 086006. arXiv:hep-th/0603038, doi:10.1103/PhysRevD.73.086006.

[73] N. Beisert, R. Hernandez, E. Lopez, A crossing-symmetric phase for AdS(5) x S^5 strings, JHEP 11 (2006) 070. arXiv:hep-th/0609044.

[74] N. Beisert, B. Eden, M. Staudacher, Transcendentality and Crossing, J.Stat.Mech. 0701 (2007) P01021. arXiv:hep-th/0610251, doi:10.1088/1742-5468/2007/01/P01021.

[75] G. Arutyunov, S. Frolov, The Dressing Factor and Crossing Equations, Journal of Physics A: Mathematical and Theoretical 42 (42) (2009) 425401. arXiv:0904.4575.

URL http://stacks.iop.org/1751-8121/42/i=42/a=425401 • D. Volin, Minimal solution of the AdS/CFT crossing equation, J.Phys. A42 (2009) 372001. arXiv:0904.4929, doi:10.1088/1751-8113/42/37/372001.

[76] P. Vieira, D. Volin, Review of AdS/CFT Integrability, Chapter III.3: The Dressing factor, Lett.Math.Phys. 99 (2012) 231–253. arXiv:1012.3992, doi:10.1007/s11005-011-0482-0.

[77] N. Beisert, M. Staudacher, Long-range $PSU(2,2|4)$ Bethe Ansätze for gauge theory and strings, Nucl. Phys. B727 (2005) 1–62. arXiv:hep-th/0504190, doi:10.1016/j.nuclphysb.2005.06.038.

[78] M. Luscher, Volume Dependence of the Energy Spectrum in Massive Quantum Field Theories. 1. Stable Particle States, Commun. Math. Phys. 104 (1986) 177. doi:10.1007/BF01211589.

[79] J. Ambjorn, R. A. Janik, C. Kristjansen, Wrapping interactions and a new source of corrections to the spin-chain / string duality, Nucl. Phys. B736 (2006) 288–301. arXiv:hep-th/0510171, doi:10.1016/j.nuclphysb.2005.12.007.

[80] Z. Bajnok, R. A. Janik, Four-loop perturbative Konishi from strings and finite size effects for multiparticle states, Nucl. Phys. B807 (2009) 625–650. arXiv:0807.0399, doi:10.1016/j.nuclphysb.2008.08.020.

[81] Z. Bajnok, A. Hegedus, R. A. Janik, T. Lukowski, Five loop Konishi from AdS/CFT, Nucl.Phys. B827 (2010) 426–456. arXiv:0906.4062, doi:10.1016/j.nuclphysb.2009.10.015.

[82] Z. Bajnok, R. A. Janik, T. Lukowski, Four loop twist two, BFKL, wrapping and strings, Nucl. Phys. B816 (2009) 376–398. arXiv:0811.4448, doi:10.1016/j.nuclphysb.2009.02.005.

[83] T. Lukowski, A. Rej, V. N. Velizhanin, Five-Loop Anomalous Dimension of Twist-Two Operators, Nucl. Phys. B831 (2010) 105–132. arXiv:0912.1624, doi:10.1016/j.nuclphysb.2010.01.008.

[84] Z. Bajnok, R. A. Janik, Six and seven loop Konishi from Luscher corrections, JHEP 1211 (2012) 002. arXiv:1209.0791, doi:10.1007/JHEP11(2012)002.

[85] D. Bombardelli, A next-to-leading Luscher formula, JHEP 1401 (2014) 037. arXiv:1309.4083, doi:10.1007/JHEP01(2014)037.

[86] C.-N. Yang, C. P. Yang, Thermodynamics of a one-dimensional system of bosons with repulsive delta-function interaction, J. Math. Phys. 10 (1969) 1115–1122.

[87] A. B. Zamolodchikov, Thermodynamic Bethe Ansatz in relativistic models. Scaling three state Potts and Lee-Yang models, Nucl. Phys. B342 (1990) 695–720. doi:10.1016/0550-3213(90)90333-9.

[88] P. Dorey, R. Tateo, Excited states by analytic continuation of TBA equations, Nucl. Phys. B482 (1996) 639–659. arXiv:hep-th/9607167, doi:10.1016/S0550-3213(96)00516-0.

[89] Z. Bajnok, Review of AdS/CFT Integrability, Chapter III.6: Thermodynamic Bethe Ansatz, Letters in Mathematical Physics 99 (2010) 299–320, 10.1007/s11005-011-0512-y. arXiv:1012.3995.
URL http://dx.doi.org/10.1007/s11005-011-0512-y

[90] S. J. van Tongeren, Introduction to the thermodynamic Bethe ansatz[J. Phys.A49,no.32,323005(2016)]. arXiv:1606.02951, doi:10.1088/1751-8113/49/32/323005.

[91] G. Arutyunov, S. Frolov, On String S-matrix, Bound States and TBA, JHEP 12 (2007) 024. arXiv:0710.1568, doi:10.1088/1126-6708/2007/12/024.

[92] G. Arutyunov, S. Frolov, String hypothesis for the AdS_5xS^5 mirror, JHEP 03 (2009) 152. arXiv:0901.1417, doi:10.1088/1126-6708/2009/03/152.

[93] N. Gromov, V. Kazakov, P. Vieira, Exact Spectrum of Anomalous Dimensions of Planar N=4 Supersymmetric Yang-Mills Theory, Phys. Rev. Lett. 103 (2009) 131601. arXiv:0901.3753, doi:10.1103/PhysRevLett.103.131601.

[94] D. Bombardelli, D. Fioravanti, R. Tateo, Thermodynamic Bethe Ansatz for planar AdS/CFT: A Proposal, J.Phys. A42 (2009) 375401. arXiv:0902.3930, doi:10.1088/1751-8113/42/37/375401.

[95] N. Gromov, V. Kazakov, A. Kozak, P. Vieira, Exact Spectrum of Anomalous Dimensions of Planar N = 4 Supersymmetric Yang-Mills Theory: TBA and excited states, Lett.Math.Phys. 91 (2010) 265–287. arXiv:0902.4458, doi:10.1007/s11005-010-0374-8.

[96] G. Arutyunov, S. Frolov, Thermodynamic Bethe Ansatz for the AdS_5xS^5 Mirror Model, JHEP 05 (2009) 068. arXiv:0903.0141, doi:10.1088/1126-6708/2009/05/068.

[97] G. Arutyunov, S. Frolov, R. Suzuki, Exploring the mirror TBA, JHEP 05 (2010) 031. arXiv:0911.2224, doi:10.1007/JHEP05(2010)031.

[98] N. Gromov, V. Kazakov, P. Vieira, Exact Spectrum of Planar $\mathcal{N} = 4$ Supersymmetric Yang-Mills Theory: Konishi Dimension at Any Coupling, Phys. Rev. Lett. 104 (2010) 211601. arXiv:0906.4240, doi:10.1103/PhysRevLett.104.211601.

[99] S. Frolov, Konishi operator at intermediate coupling, J. Phys. A44 (2011) 065401. arXiv:1006.5032, doi:10.1088/1751-8113/44/6/065401.

[100] S. Frolov, Scaling dimensions from the mirror TBA, J.Phys. A45 (2012) 305402. arXiv:1201.2317, doi:10.1088/1751-8113/45/30/305402.

[101] G. Arutyunov, S. Frolov, R. Suzuki, Five-loop Konishi from the Mirror TBA, JHEP 04 (2010) 069. arXiv:1002.1711, doi:10.1007/JHEP04(2010)069. • J. Balog, A. Hegedus, 5-loop Konishi from linearized TBA and the XXX magnet, JHEP 06 (2010) 080. arXiv:1002.4142, doi:10.1007/JHEP06(2010)080.

[102] S. Frolov, R. Suzuki, Temperature quantization from the TBA equations, Phys.Lett. B679 (2009) 60–64. arXiv:0906.0499, doi:10.1016/j.physletb.2009.06.069.

[103] A. Cavaglià, D. Fioravanti, R. Tateo, Extended Y-system for the AdS_5/CFT_4 correspondence, Nucl. Phys. B843 (2011) 302–343. arXiv:1005.3016, doi:10.1016/j.nuclphysb.2010.09.015.

[104] R. Hirota, Discrete analogue of a generalized toda equation, Journal of the Physical Society of Japan 50 (11) (1981) 3785–3791. doi:10.1143/JPSJ.50.3785.
URL http://dx.doi.org/10.1143/JPSJ.50.3785

[105] N. Gromov, V. Kazakov, P. Vieira, Finite volume spectrum of 2d field theories from hirota dynamics, JHEP 2009 (12) (2008) 060. arXiv:0812.5091.

[106] N. Gromov, V. Kazakov, S. Leurent, D. Volin, Solving the AdS/CFT Y-system, JHEP 1207 (2012) 023. arXiv:1110.0562, doi:10.1007/JHEP07(2012)023.

[107] J. Balog, A. Hegedus, Hybrid-NLIE for the AdS/CFT spectral problem, JHEP 1208 (2012) 022. arXiv:1202.3244, doi:10.1007/JHEP08(2012)022.

[108] S. Leurent, D. Serban, D. Volin, Six-loop Konishi anomalous dimension from the Y-system, Phys.Rev.Lett. 109 (2012) 241601. arXiv:1209.0749, doi:10.1103/PhysRevLett.109.241601.

[109] S. Leurent, D. Volin, Multiple zeta functions and double wrapping in planar $N = 4$ SYM, Nucl.Phys. B875 (2013) 757–789. arXiv:1302.1135, doi:10.1016/j.nuclphysb.2013.07.020.

[110] N. Gromov, V. Kazakov, S. Leurent, Z. Tsuboi, Wronskian Solution for AdS/CFT Y-system, JHEP 1101 (2011) 155. arXiv:1010.2720, doi:10.1007/JHEP01(2011)155. • A. Hegedus, Discrete Hirota dynamics for AdS/CFT, Nuclear Physics B 825 (3) (2009) 341 – 365. arXiv:0906.2546, doi:10.1016/j.nuclphysb.2009.09.012.
URL http://www.sciencedirect.com/science/article/pii/S0550321309004854

[111] N. Gromov, F. Levkovich-Maslyuk, G. Sizov, S. Valatka, Quantum spectral curve at work: from small spin to strong coupling in $\mathcal{N} = 4$ SYM, JHEP 07 (2014) 156. arXiv:1402.0871, doi:10.1007/JHEP07(2014)156.

[112] M. Alfimov, N. Gromov, V. Kazakov, QCD Pomeron from AdS/CFT Quantum Spectral Curve, JHEP 07 (2015) 164. arXiv:1408.2530, doi:10.1007/JHEP07(2015)164.

[113] N. Gromov, F. Levkovich-Maslyuk, G. Sizov, Pomeron Eigenvalue at Three Loops in $\mathcal{N} = 4$ Supersymmetric Yang-Mills Theory, Phys. Rev. Lett. 115 (25) (2015) 251601. arXiv:1507.04010, doi:10.1103/PhysRevLett.115.251601.

[114] N. Gromov, F. Levkovich-Maslyuk, G. Sizov, Quantum Spectral Curve and the Numerical Solution of the Spectral Problem in AdS5/CFT4, JHEP 06 (2016) 036. arXiv:1504.06640, doi:10.1007/JHEP06(2016)036.

[115] A. Hegedus, J. Konczer, Strong coupling results in the AdS_5 /CF T_4 correspondence from the numerical solution of the quantum spectral curve, JHEP 08 (2016) 061. arXiv:1604.02346, doi:10.1007/JHEP08(2016)061.

[116] N. Gromov, V. Kazakov, G. Korchemsky, S. Negro, G. Sizov, Integrability of Conformal Fishnet Theory. arXiv:1706.04167.

[117] R. Klabbers, S. J. van Tongeren, Quantum Spectral Curve for the eta-deformed AdS_5xS^5 superstring. arXiv:1708.02894.

[118] N. Gromov, F. Levkovich-Maslyuk, Quantum Spectral Curve for a cusped Wilson line in $\mathcal{N} = 4$ SYM, JHEP 04 (2016) 134. arXiv:1510.02098, doi:10.1007/JHEP04(2016)134.

[119] N. Gromov, F. Levkovich-Maslyuk, Quark-anti-quark potential in $\mathcal{N} = 4$ SYM, JHEP 12 (2016) 122. arXiv:1601.05679, doi:10.1007/JHEP12(2016)122.

[120] A. Cavaglià, D. Fioravanti, N. Gromov, R. Tateo, The Quantum Spectral Curve of the ABJM theoryarXiv:1403.1859. • D. Bombardelli, A. Cavaglià, D. Fioravanti, N. Gromov, R. Tateo, The full Quantum Spectral Curve for AdS_4/CFT_3arXiv:1701.00473.

[121] N. Gromov, G. Sizov, Exact Slope and Interpolating Functions in N=6 Supersymmetric Chern-Simons Theory, Phys. Rev. Lett. 113 (12) (2014) 121601. arXiv:1403.1894, doi:10.1103/PhysRevLett.113.121601.

[122] A. Cavaglià, N. Gromov, F. Levkovich-Maslyuk, On the Exact Interpolating Function in ABJ Theory, JHEP 12 (2016) 086. arXiv:1605.04888, doi:10.1007/JHEP12(2016)086.

[123] L. Anselmetti, D. Bombardelli, A. Cavaglià, R. Tateo, 12 loops and triple wrapping in ABJM theory from integrability, JHEP 10 (2015) 117. arXiv:1506.09089, doi:10.1007/JHEP10(2015)117.

[124] Z. Tsuboi, Analytic Bethe ansatz and functional equations for Lie superalgebra sl(r+1|s+1), J. Phys. A30 (1997) 7975–7991. arXiv:0911.5386, doi:10.1088/0305-4470/30/22/031.

[125] Z. Tsuboi, Solutions of the T-system and Baxter equations for supersymmetric spin chains, Nucl.Phys. B826 (2010) 399–455. arXiv:0906.2039, doi:10.1016/j.nuclphysb.2009.08.009.

[126] R. I. Nepomechie, C. Wang, Twisting singular solutions of Bethe's equations, J. Phys. A47 (50) (2014) 505004. arXiv:1409.7382, doi:10.1088/1751-8113/47/50/505004.

[127] W. Hao, R. I. Nepomechie, A. J. Sommese, Completeness of solutions of Bethe's equations, Phys. Rev. E88 (5) (2013) 052113. arXiv:1308.4645, doi:10.1103/PhysRevE.88.052113.

[128] G. P. Pronko, Y. G. Stroganov, Bethe Equations "on the Wrong Side of Equator", J. Phys. A32 (1999) 2333–2340. arXiv:hep-th/9808153, doi:10.1088/0305-4470/32/12/007.

[129] F. Brown, Single-valued Motivic Periods and Multiple Zeta Values, SIGMA 2 (2014) e25. arXiv:1309.5309, doi:10.1017/fms.2014.18. • O. Schnetz, Graphical functions and single-valued multiple polylogarithms, Commun. Num. Theor. Phys. 08 (2014) 589–675. arXiv:1302.6445, doi:10.4310/CNTP.2014.v8.n4.a1.

[130] G. Arutyunov, S. Frolov, A. Sfondrini, Exceptional Operators in N=4 super Yang-Mills, JHEP 1209 (2012) 006. arXiv:1205.6660, doi:10.1007/JHEP09(2012)006.

[131] D. J. Broadhurst, D. Kreimer, Knots and numbers in Phi**4 theory to 7 loops and beyond, Int.J.Mod.Phys. C6 (1995) 519–524. arXiv:hep-ph/9504352, doi:10.1142/S012918319500037X.

[132] J. Blumlein, D. Broadhurst, J. Vermaseren, The Multiple Zeta Value Data Mine, Comput.Phys.Commun. 181 (2010) 582–625. arXiv:0907.2557, doi:10.1016/j.cpc.2009.11.007.

[133] G. Korchemsky, Bethe ansatz for QCD pomeron, Nucl.Phys. B443 (1995) 255–304. arXiv:hep-ph/9501232, doi:10.1016/0550-3213(95)00099-E. • B. Eden, M. Staudacher, Integrability and transcendentality, J. Stat. Mech. 0611 (2006) P014. arXiv:hep-th/0603157.

[134] M. Beccaria, Anomalous dimensions at twist-3 in the sl(2) sector of N=4 SYM, JHEP 0706 (2007) 044. arXiv:0704.3570, doi:10.1088/1126-6708/2007/06/044.

[135] A. V. Kotikov, L. N. Lipatov, A. Rej, M. Staudacher, V. N. Velizhanin, Dressing and Wrapping, J. Stat. Mech. 0710 (2007) P10003. arXiv:0704.3586, doi:10.1088/1742-5468/2007/10/P10003.

[136] A. V. Kotikov, L. N. Lipatov, V. N. Velizhanin, Anomalous dimensions of Wilson operators in N=4 SYM theory, Phys. Lett. B557 (2003) 114–120. arXiv:hep-ph/0301021, doi:10.1016/S0370-2693(03)00184-9.

[137] A. V. Kotikov, L. N. Lipatov, A. I. Onishchenko, V. N. Velizhanin, Three-loop universal anomalous dimension of the Wilson operators in N = 4 SUSY Yang-Mills model, Phys. Lett. B595 (2004) 521–529. arXiv:hep-th/0404092, doi:10.1016/j.physletb.2004.05.078.

[138] A. V. Kotikov, A. Rej, S. Zieme, Analytic three-loop Solutions for N=4 SYM Twist Operators, Nucl. Phys. B813 (2009) 460–483. arXiv:0810.0691, doi:10.1016/j.nuclphysb.2008.12.022.

[139] M. Beccaria, A. V. Belitsky, A. V. Kotikov, S. Zieme, Analytic solution of the multiloop Baxter equation, Nucl. Phys. B827 (2010) 565–606. arXiv:0908.0520, doi:10.1016/j.nuclphysb.2009.10.030.

[140] M. Beccaria, V. Forini, T. Lukowski, S. Zieme, Twist-three at five loops, Bethe Ansatz and wrapping, JHEP 03 (2009) 129. arXiv:0901.4864, doi:10.1088/1126-6708/2009/03/129. • V. N. Velizhanin, Six-Loop Anomalous Dimension of Twist-Three Operators in N=4 SYM, JHEP 11 (2010) 129. arXiv:1003.4717, doi:10.1007/JHEP11(2010)129.

[141] A. Kotikov, L. Lipatov, DGLAP and BFKL equations in the N=4 supersymmetric gauge theory, Nucl.Phys. B661 (2003) 19–61. arXiv:hep-ph/0208220, doi:10.1016/S0550-3213(03)00264-5.

[142] J. A. M. Vermaseren, Harmonic sums, Mellin transforms and integrals, Int. J. Mod. Phys. A14 (1999) 2037–2076. arXiv:hep-ph/9806280, doi:10.1142/S0217751X99001032.

[143] Yu. L. Dokshitzer, G. Marchesini, G. P. Salam, Revisiting parton evolution and the large-x limit, Phys. Lett. B634 (2006) 504–507. arXiv:hep-ph/0511302, doi:10.1016/j.physletb.2006.02.023. • Yu. L. Dokshitzer, G. Marchesini, N=4 SUSY Yang-Mills: three loops made simple(r), Phys. Lett. B646 (2007) 189–201. arXiv:hep-th/0612248, doi:10.1016/j.physletb.2007.01.016. • B. Basso, G. P. Korchemsky, Anomalous dimensions of high-spin operators beyond the leading order, Nucl. Phys. B775 (2007) 1–30. arXiv:hep-th/0612247, doi:10.1016/j.nuclphysb.2007.03.044.

[144] A. K. Lenstra, H. W. Lenstra, L. Lovász, Factoring polynomials with rational coefficients, Mathematische Annalen 261 (4) (1982) 515–534. doi:10.1007/BF01457454.
URL http://dx.doi.org/10.1007/BF01457454

[145] V. Velizhanin, Twist-2 at five loops: Wrapping corrections without wrapping computations, JHEP 1406 (2014) 108. arXiv:1311.6953, doi:10.1007/JHEP06(2014)108.

[146] L. N. Lipatov, Reggeization of the Vector Meson and the Vacuum Singularity in Nonabelian Gauge Theories, Sov. J. Nucl. Phys. 23 (1976) 338–345, [Yad. Fiz.23,642(1976)]. • E. A. Kuraev, L. N. Lipatov, V. S. Fadin, The Pomeranchuk Singularity in Nonabelian Gauge Theories, Sov. Phys. JETP 45 (1977) 199–204, [Zh. Eksp. Teor. Fiz.72,377(1977)]. • I. I. Balitsky, L. N. Lipatov, The Pomeranchuk Singularity in Quantum Chromodynamics, Sov. J. Nucl. Phys. 28 (1978) 822–829, [Yad. Fiz.28,1597(1978)].

[147] V. G. Gorshkov, V. N. Gribov, L. N. Lipatov, G. V. Frolov, Double logarithmic asymptotics of quantum electrodynamics, Phys. Lett. 22 (1966) 671–673. doi:10.1016/0031-9163(66)90701-3. • R. Kirschner, L. n. Lipatov, Double Logarithmic Asymptotics and Regge Singularities of Quark Amplitudes with Flavor Exchange, Nucl. Phys. B213 (1983) 122–148. doi:10.1016/0550-3213(83)90178-5.

[148] V. N. Velizhanin, Double-logs, Gribov-Lipatov reciprocity and wrapping, JHEP 08 (2011) 092. arXiv:1104.4100, doi:10.1007/JHEP08(2011)092.

[149] M. Albrech, D. Cadé, X. Pujol, D. Stehlé, fplll-4.0, a floating-point lll implementation.
URL https://github.com/dstehle/fplll

[150] O. Lunin, J. M. Maldacena, Deforming field theories with U(1) x U(1) global symmetry and their gravity duals, JHEP 05 (2005) 033. arXiv:hep-th/0502086, doi:10.1088/1126-6708/2005/05/033. • S. Frolov, Lax pair for strings in Lunin-Maldacena background, JHEP 05 (2005) 069. arXiv:hep-th/0503201.

[151] B. Basso, S. Komatsu, P. Vieira, Structure Constants and Integrable Bootstrap in Planar N=4 SYM Theory. arXiv:1505.06745.

[152] T. Fleury, S. Komatsu, Hexagonalization of Correlation Functions. , JHEP 01 (2017) 130. arXiv:1611.05577, doi:10.1007/JHEP01(2017)130. • B. Eden, A. Sfondrini, Tessellating cushions: four-point functions in N=4 SYM. arXiv:1611.05436. • B. Basso, F. Coronado, S. Komatsu, H. T. Lam, P. Vieira, D.-l. Zhong, Asymptotic Four Point Functions. arXiv:1701.04462.

[153] M. de Leeuw, C. Kristjansen, K. Zarembo, One-point Functions in Defect CFT and Integrability, JHEP 08 (2015) 098. arXiv:1506.06958, doi:10.1007/JHEP08(2015)098.

[154] I. Buhl-Mortensen, M. de Leeuw, A. C. Ipsen, C. Kristjansen, M. Wilhelm, Asymptotic one-point functions in AdS/dCFT. arXiv:1704.07386.

[155] O. Gurdogan, V. Kazakov, New Integrable 4D Quantum Field Theories from Strongly Deformed Planar $\mathcal{N} = 4$ Supersymmetric Yang-Mills Theory, Phys. Rev. Lett. 117 (20) (2016) 201602, [Addendum: Phys. Rev. Lett.117,no.25,259903(2016)]. arXiv:1512.06704, doi:10.1103/PhysRevLett.117.201602,10.1103/PhysRevLett.117.259903.

[156] R. Borsato, O. Ohlsson Sax, A. Sfondrini, B. Stefanski, The complete $AdS_3\times S^3\times T^4$ worldsheet S matrix, JHEP 10 (2014) 66. arXiv:1406.0453, doi:10.1007/JHEP10(2014)066. • R. Borsato, O. Ohlsson Sax, A. Sfondrini, B. Stefanski, The $AdS_3 \times S^3 \times S^3 \times S^1$ worldsheet S matrix, J. Phys. A48 (41) (2015) 415401. arXiv:1506.00218, doi:10.1088/1751-8113/48/41/415401.

[157] M. E. Hoffman, The algebra of multiple harmonic series, Journal of Algebra 194 (2) (1997) 477 – 495. doi:http://dx.doi.org/10.1006/jabr.1997.7127.
URL http://www.sciencedirect.com/science/article/pii/S0021869397971271

[158] M. Abramowitz, I. A. Stegun, Handbook of Mathematical Functions with Formulas, Graphs, and Mathematical Tables, ninth dover printing, tenth gpo printing Edition, Dover, New York, 1964.